Technische Universität München
TUM School of Medicine and Health

Exploiting the ubiquitin system to identify novel vulnerabilities in B-cell malignancies and lung adenocarcinoma

Tobias Ronard Schulze, M.Sc.

Vollständiger Abdruck der von der TUM School of Medicine and Health der Technischen Universität München zur Erlangung eines

Doctor of Philosophy (Ph.D.)

genehmigten Dissertation.

Vorsitz:	Prof. Dr. Angelika Harbauer
Betreuer:	Prof. Dr. Florian Bassermann

Prüfende der Dissertation:

1. apl. Prof. Dr. Robert A. J. Oostendorp
2. Prof. Dr. Daniel Krappmann

Die Dissertation wurde am 31.03.2024 bei der TUM School of Medicine and Health der Technischen Universität München eingereicht und durch die TUM School of Medicine and Health am 31.05.2024 angenommen.

Content

Abbreviations

Short	Name
°C	Degree Celsius
AA	Amino acid
ABC	Activated B-cell-like
ACN	Acetonitrile
AID	Activation-induced cytidine deaminase
ALK	Anaplastic lymphoma kinase
AML	Acute myeloid leukemia
APC/C	Anaphase-promoting complex
APCs	Antigen presenting cells
APEX	Engineered Ascorbate Peroxidase
ATCC	American Type Culture Collection
ATM	Serine-protein kinase ATM
BCL2	Apoptosis regulator Bcl-2
BCMA	B-cell maturation antigen
BCR	B-cell receptor
BioID	Biotin identification
BRAF	B-Raf proto-oncogene
BrdU	Bromodeoxyuridine
C-terminal	Carboxy terminal
CAR	Chimeric Antigen Receptors
CBL	Casitas B linage lymphoma-b
CCND1	G1/S-specific cycline-D1
CDC20	Cell division cycle protein 20
CDK1/2	Cyclin-dependent kinase 1/2
CDK2	Cyclin-dependent kinase 2
CDKN2A	Cyclin Dependent Kinase Inhibitor 2A
cDNA	Complementary DNA
CHX	Cycloheximide
CMP	Counts per million
CRISPR	Clustered regularly interspaced short palindromic repeats
CRL	Cullin-RING ligase
CRL3	Cullin Ring E3 ligase
Ctrl	Control
Cul3	Cullin-3
Cul4A/B	Cullin4A/B
DAG1	Dystroglycan 1
DCAF7	DDB1- and CUL4-associated factor 7
DDB1	Damage Specific DNA Binding Protein 1
DHRS4	Dehydrogenase/Reductase (SDR family) Member 4
DiGLY	Lysine-ϵ-Glycine-Glycine ubiquitin remnant motif
DLBCL	Diffuse Large B-cell Lymphoma
DMEM	Dulbecco’s Modified Eagle’s Medium

DMSO	Dimethyl sulfoxide
DNA	Deoxyribonulceic acid
dNTP	2'-deoxynucleoside-5'-triphosphate
dsDNA	Double-stranded DNA
DSMZ	Deutsche Sammlung von Mikroorganismen und Zellkulturen
DUBs	Deubiquitylating enzymes
DYRK1A	Dual specific tyrosine-phosphorylation-regulated kinase 1A
DYRK1B	Dual specific tyrosine-phosphorylation-regulated kinase 1B
E. coli	Escherichia coli
ECL	Enhanced chemiluminescence solution
EGFR	Epidermal growth factor receptor
ERAD	Endoplasmic-reticulum-associated protein degradation
EV	Empty vector
FA	Formic acid
FBS	Fetal Bovine Serum
FDA	Food and drug administration
FDC	Follicular dendritic cells
FLAG-IPs	FLAG immunoprecipitations
fw	Forward
GAPDH	Glyceraldehyde 3-phosphate dehydrogenase
GCB	Germinal center B-cell like
gDNA	Genomic DNA
GFP	Green fluorescence reporter
GSEA	Gene set enrichment analysis
h, hrs	Hour, hours
HECT	E6-AP carboxyl terminus domain
HEK293T	Human embryonic kidney cells
HRP	Horse radish peroxidase
IAP	Inhibitor of apoptosis
IBR	In-between RINGs
IF	Immunofluorescence
Ig	Immunoglobulin
IgH	Immunoglobulin heavy chain
IgL	Immunoglobulin light chain
IL	Interleukin
IL-6	Interleukin-6
IMiDs	Immunomodulatory imide drugs
IP	Immunoprecipitation
IRS1	Insulin receptor substrate 1
kDa	Kilo Dalton
KLHL14	Kelch-like protein 14
KRAS	KRAS proto-oncogene
KRAS	KRAS proto-oncogene
LFQ	Label-free quantification
LuAD	Lung adenocarcinoma

Lys or K	Lysine
M	Molar
M1	Mono-ubiquitylation
MCL	Mantel cell lymphoma
MDM2	E3 ubiquitin-protein ligase Mdm2
MGUS	Monoclonal gammopathy of undetermined significance
min	Minute
MM	Multiple myeloma
mM	Millimolar
MOI	Multiplicity of infection
mRNA	Messenger RNA
MW	Molecular weight
MYC	Myc proto-oncogene protein
N-terminal	Amino terminal
NF-κB	Nuclear factor kappa-light-chainenhancer of activated B cells
NGS	Next-generation sequencing
NHL	Non-Hodgkin´s lymphoma
nM	Nanomolar
Notch1	Neurogenic locus notch homologue protein 1
NSCLC	Non-small-cell lung cancers
NT	Non-targeting
NUDCD3	NudC domain-containing protein 3
OCI AML3	Acute myeloid lymphoma cell line
Oligo	Oligonucleotide
OS	Overall survival
p53	Cellular tumor antigen p53
PBS	Phosphate buffered saline
PCR	Polymerase chain reaction
Pen/Strep	Penicillin-streptomycin
PFA	Paraformaldehyde
PI	Proteasome inhibitors
Polybrene	Hexadimethrine bromide
PROTACs	Proteolysis-targeting chimeras
qPCR	Quantitative PCR
RAG1	Recombination-activating gene 1
RAG2	Recombination-activating gene 2
RBR	RING-between RING-RING
RBX1	RING finger protein RING-Box1
RFP	Red fluorescence reporter
RING	Really interesting new gene domain
RLDs	Regulators of chromosome condensation 1 (RCC1)-like domains
RNA	Ribonucleic acid
ROS1	Proto-oncogene tyrosine-protein kinase ROS
rpm	Revolution per minute
RPMI	Roswell Park Memorial Institute

RT	Room temperature
rv	Reverse
SCENITH	Single Cell Energetic Metabolism by Profiling Translation inhibition
SCF	SKP, cullin, F-box containing complex
SCLC	Small-cell lung cancer
SDS	Sodium dodecyl sulfate
SDS-PAGE	SDS-polyacrylamide gel electrophoresis
sec	Second
sgNT	Non-targeting shRNA
sgPOLR2	SgRNA targeting polymerase 2
sgRNA	Single-guide RNA
shRNA	Short-hairpin RNA
siRNA	Small interfering RNA
SKP2	(Choi et al., 2018). S-phase kinase-associated protein 2
SMM	Smoldering myeloma
SUMO	Small ubiquitin-related modifier
SUMO	Small ubiquitin-related modifier
TAP	tandem affinity purification
TCA	Trichloroacetic acid

1 Summary

Protein ubiquitylation is a post-translational modification that regulates protein function, turnover, and homeostasis and therefore plays a critical role in healthy cell and cancer biology. In many cancers, aberrations in the ubiquitin system lead to an imbalance and either the accumulation of oncoproteins that drive tumor development or the loss of tumor suppressor proteins that inhibit tumorigenesis. In recent years, drugs targeting the ubiquitin system, such as small molecule inhibitors of the proteasome, compounds specifically targeting E1, E2, E3 ligases or DUBs, and targeted protein degradation using proteolysis-targeting chimera (PROTAC) have been developed, and while proteasome inhibitors are already used in the clinic, E3/DUB inhibitors and PROTACs are in early clinical trials (Bekes et al., 2022; Deng et al., 2020). This highlights the importance of better understanding the role of the ubiquitin system in cancer and identifying new targets within this system to develop even better treatment approaches. Therefore, we set out to discover novel vulnerabilities within the ubiquitin-proteasome system in two highly heterogeneous cancer entities.

B-cell-derived malignancies account for approximately 95% of lymphomas and arise from B-cells at various stages of development and activation (Thandra, Barsouk, Saginala, Padala, et al., 2021). While entities such as multiple myeloma (MM) and mantel cell lymphoma (MCL) are considered incurable, diffuse large B-cell lymphoma (DLBCL) can be successfully treated with immuno-chemotherapy. Analyzing patient data, we discovered that the Cullin-3 (Cul3) ubiquitin ligase Kelch-like protein 14 (KLHL14) is significantly downregulated in MM and MCL patients. Overexpression of KLHL14 in MM, MCL, DLBCL, and other cancers resulted in a significant dropout of B-cell lymphoma cells but no other cancer cell lines, confirming a tumor-suppressive role of the E3 ubiquitin ligase, specifically in B-cell malignancies. Interactome screens coupled with mass spectrometry identified NudC domain-containing protein 3 (NUDCD3) as a potential ubiquitylated substrate of KLHL14. Altering NUDCD3 protein abundance in B-cell lymphoma cell lines resulted in growth disadvantages, making the KLHL14-NUDCD3 axis an interesting target for new treatment approaches.

Lung adenocarcinoma (LuAD) is the most common subtype of lung cancer, with one of the highest cancer-related death rates expected to increase in the future and a high demand for new druggable targets (American Cancer Society, 2023). We performed a CRISPR-Cas9-based dropout screen with guide RNAs targeting only the ubiquitin system to find novel vulnerabilities within this system. Here, we identified the E3 ubiquitin ligase DDB1- and Cul4-associated factor 7 (DCAF7) as a cancer-dependent gene. Depletion of DCAF7 not only in LuAD cells but also in other cancer entities resulted in the loss of these cells, suggesting an oncogenic role of DCAF7 that is not restricted to a specific cancer entity. We demonstrated that DCAF7 forms ubiquitin ligase complexes with Cullin4A/B (Cul4A/B) and Damage Specific DNA Binding Protein 1 (DDB1), where it serves as a substrate recruiting subunit. By performing a functional proteomic Lysine-ϵ-Glycine-Glycine ubiquitin remnant motif (DiGLY) screen in addition to tandem affinity purification (TAP) screen coupled with mass spectrometry, we discovered several potential interactors and protein substrates of DCAF7 that will help us understand its molecular function in the future.

Taken together, using two different screening approaches, we identified two different E3 ubiquitin ligases: DCAF7, which is a potential oncogene in lung cancer and many other cancers, and KLHL14, which acts as a tumor suppressor specifically in B-cell malignancies. For the latter, we discovered NUDCD3 as its potential ubiquitylated substrate and interactor. DCAF7 and KLHL14 are novel susceptibilities and represent potential targets for new anti-cancer therapeutics.

2 Introduction

2.1 The Ubiquitin-Proteasome system

2.1.1 Protein ubiquitylation

In 2004, the Nobel Prize in chemistry was awarded to A. Ciechanover A. Hershko and I. Rose for the discovery of ubiquitin-mediated protein degradation (Giles, 2004). This discovery led to the exploration of cellular proteolysis as a central field of research in biology. The Ubiquitin Proteasome System (UPS) is one of the major pathways for protein degradation in cells. It plays a crucial role in regulating various cellular functions such as quality control, cell-cycle progression/division, DNA repair, cell differentiation and regulation of membrane receptors endocytosis and trafficking (Nandi et al., 2006). Due to this essential role in maintaining protein homeostasis, UPS dysfunction is associated with a variety of human diseases including neurodegenerative disease and cancer (Deng et al., 2020; Schmidt et al., 2021). The development of new drugs that precisely target UPS components or the proteasome is therefore at the center of the efforts of research laboratories and pharmaceutical companies.

Ubiquitin is a small protein consisting of 76 amino acids (AA) with a molecular mass of 8.6 kDa. It is highly conserved throughout evolution and present in all eukaryotic cells (Zuin et al., 2014). Ubiquitylation of proteins is a post-translational modification, and the molecular basis for this reaction is the attachment of ubiquitin molecules to target proteins. The process consists of a three-step enzymatic cascade involving ubiquitin-activating enzymes (E1s), ubiquitin-conjugating enzymes (E2s), and ubiquitin ligases (E3s) (Figure 1)(Komander & Rape, 2012). Notably, the attachment of ubiquitin to a substrate can have many other consequences besides protein degradation by the 26S proteasome, including protein delocalization, enhancement or prevention of protein interactions, and alteration of protein activity (Haglund & Dikic, 2005).

The first step in the ubiquitylation cascade can be carried out by a total of two known human E1 enzymes (UBA1 and UBA6) (Deng et al., 2020). First, a ubiquitin monomer is activated by an E1 enzyme. This is a two-step, ATP-dependent reaction. The E1 enzyme catalyzes the acyl-adenylation of the C-terminus of the ubiquitin protein by binding ATP. AMP is released and ubiquitin is transferred to an active cysteine residue of the E1 enzyme, resulting in a thioester bond between the E1 cysteine sulfhydryl group and the C-terminal carboxyl group of the ubiquitin (Schulman & Harper, 2009).

The following conjugation reaction involves the E2 and E1 enzymes. While most eukaryotic organisms have 16-35 E2 enzymes, humans have ~40 (Stewart et al., 2016). An E2 enzyme binds to both the E1 enzyme and the activated ubiquitin, and through a catalyzed trans(thio)esterification reaction, the activated ubiquitin is transferred to the E2 enzyme (Valimberti et al., 2015).

The final step in the enzyme cascade is a ligation step catalyzed by an E3 ubiquitin ligase resulting in the attachment of ubiquitin to a substrate protein. The E3 ligase possesses substrate specificity and identifies its protein substrate through a variety of different degrons (short amino acid sequences) or chemical motifs on the substrate (Ravid & Hochstrasser, 2008). In most cases, ubiquitin is bound to the lysine residues (K) of the substrate protein, forming an isopeptide bond between the ε-amino group of the substrate and the free carboxyl group of the ubiquitin backbone (Hershko & Ciechanover, 1998). This can also occur at the N-terminal methionine of the substrate protein (K. T. Nguyen et al., 2022). E3 ligases have either

a ‘homologous to the ‘E6-AP carboxyl terminus domain’ (HECT), the ‘really interesting new gene domain’ (RING), RING-between RING-RING (RBR), or the U-box domain. E3 ligases with the RING or U-box domain facilitate the direct transfer of ubiquitin from E2 to substrate. HECT and RBR domain E3s form a thioester intermediate and temporarily bind ubiquitin before transferring it to the chosen substrate protein (Figure 3a)(Berndsen & Wolberger, 2014).

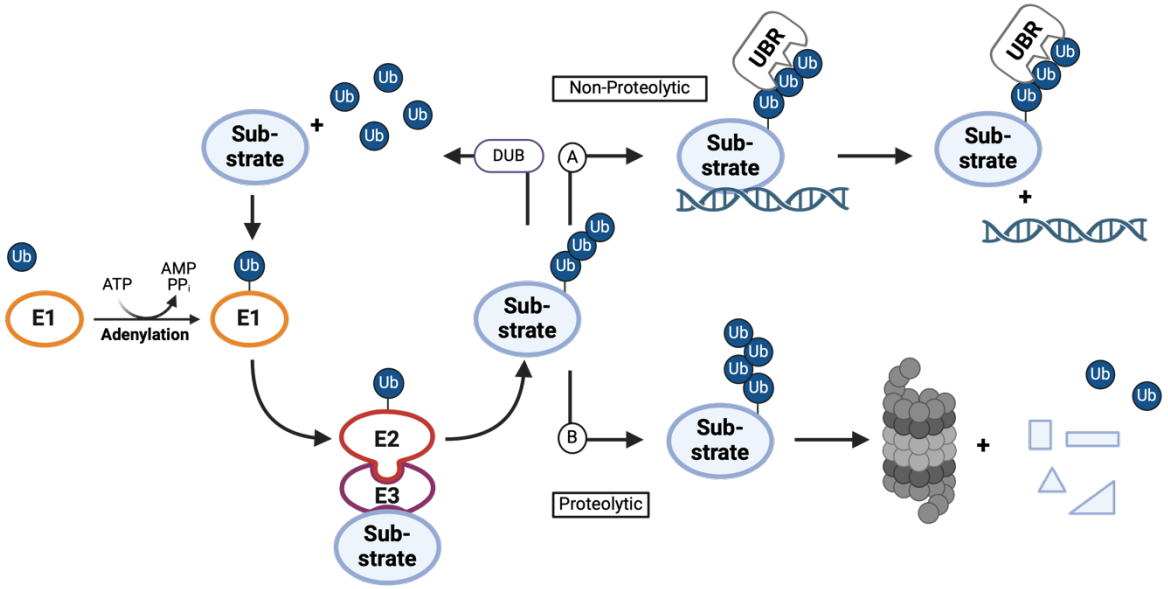

Figure 1 The enzymatic ubiquitylation cascade. Ubiquitin (Ub, dark blue) is activated in an ATP-dependent reaction and covalently bound to the ubiquitin-activating enzyme (E1, orange) through a thioester bond. The ubiquitin is then transferred to the ubiquitin-conjugating enzyme (E2, red), which in turn interacts with a E3 ubiquitin ligase (E3, purple), which facilitates the transfer of ubiquitin to a lysine residue on a substrate protein (light blue) or to a pre-attached ubiquitin molecule. Ubiquitylation of substrates results in either degradation by the proteolytic pathway (B) or altered signaling and trafficking functions by the non-proteolytic pathway (A). This depends on the type of ubiquitin chain attached to the substrate protein. In the non-proteolytic pathway, Ub-binding domains (UBDs) recognize the ubiquitin moieties and mediate the specific function of the ubiquitylated substrate, which includes DNA repair, immune response, and cell cycle regulation. K48 and K11 ubiquitin chains trigger the proteolytic response where the substrate protein is degraded by the proteasome (gray molecular structure). Alternatively, deubiquitylating enzymes (DUBs) can cleave the ubiquitin chains and recycle the ubiquitin molecules. The figure was generated using Biorender.

There are multiple different ubiquitylation modifications that can lead to different cellular outcomes within the UPS. Mono-ubiquitylation (M1) is when only a single ubiquitin molecule is attached to a substrate, which can regulate endocytosis and histone modification of this substrate (Hicke, 2001). The ubiquitin protein itself has a total of seven lysine residues, which can be attached to other ubiquitin molecules. Isopeptide bonds between the carboxy terminus of an already attached ubiquitin protein and the ε-amino group of a lysine of another ubiquitin monomer result in the formation of polyubiquitin chains. Different types of polyubiquitin chains with different functions can form depending on the exact lysine residue of the poly ubiquitylation (Figure 2)(Dammer et al., 2011). The two most studied chain types are K48 and K63. While K48-linked ubiquitylation primarily targets proteins for 26S proteasome-mediated degradation, K63-linked chains are involved in autophagy, cytokine signaling, and DNA damage repair (Komander, 2009). Less studied K6-linkages and K27-linkages have also been implicated in the DNA damage response, while K-11 linkages have also been shown to mark substrates for proteasomal degradation (Swatek & Komander, 2016). In addition to the eight major ubiquitin chain types that perform different physiological functions (M1, K6, K11, K27, K29, K33, K48, K63), heterotypic chains with multiple types of ubiquitin linkages have been reported (French et al., 2021; Tracz & Bialek, 2021).

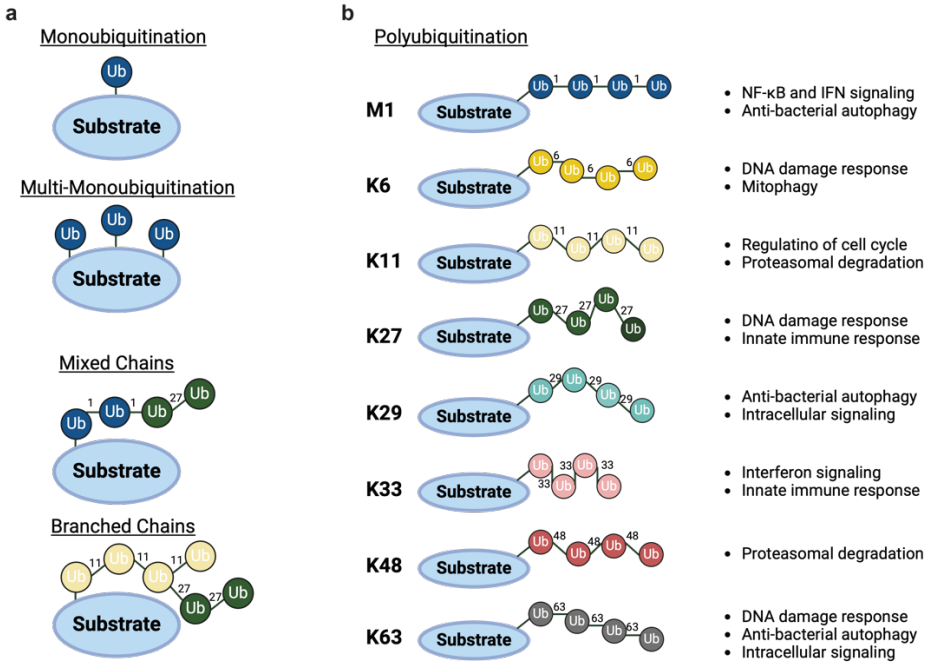

Figure 2 Different ubiquitin chain types serve specific functions. (a) Illustration of monoubiquitylation, multi-monoubiquitylation, mixed linkage type ubiquitylation of M1 and K27, and branched chain of K11 and K27. **(b)** Various ubiquitin chains including M1, K6, K11, K27, K29, K33, K48, K63 and their functions (right side). The figure was generated using Biorender and adapted from (Chen et al., 2022).

While there are other mechanisms for protein degradation, such as lysosomal degradation (specific organelles with protease-filled acidic compartments), UPS-mediated protein degradation is one of the most important processes in eukaryotes (Bard et al., 2018). This reaction involves proteasomes that destroy ubiquitin-labeled proteins by breaking peptide bonds. The process allows cells to control the levels of certain proteins and to degrade damaged and misfolded proteins (Livneh et al., 2016). The 26S proteasome consists of three subunits, one 20S core protein subunit, and two 19S regulatory cap subunits with a total molecular mass of 2000 kDa (Voges et al., 1999). The catalytic core of the proteasome is a hollow structure and is responsible for the degradation of incoming proteins. Peptide proteolysis is carried out by the β-subunits of the 20S core particle through a threonine-dependent nucleophilic attack (Cascio et al., 2001). To broaden the range of peptides generated, eukaryotes have three different catalytic active β-subunits. While the active site of the β5 subunit predominantly cleaves after hydrophobic residues, the active sites of the β1 and β2 subunits target acidic and basic residues (Kunjappu & Hochstrasser, 2014). The cleaved peptides (usually 7-9 residues long) are then further degraded by cytoplasmic proteases (Chen et al., 2016). A 19S regulatory cap subunit is attached to each end of the 20S core particle. These are equipped with ATPase active sites and ubiquitin-binding sites that direct the ubiquitylated proteins into the core of the 26S proteasome (Dong et al., 2019).

2.1.2 Ubiquitin-E3 ligases

The hierarchical structure within the E1-E2-E3 enzyme cascade allows for very precise regulation of the ubiquitylation process. This refined and complex ubiquitylation network is further fine-tuned because a single E3 ligase can target a large number of proteins, while multiple E3 ligases can also ubiquitinate a single protein (Timms et al., 2023). E3s are the most diverse group of enzymes within the ubiquitylation pathway because they are responsible for substrate specificity. With over 600 E3s encoded in the human genome, they are divided into

four families based on the mechanism by which they transfer ubiquitin to their substrate and their specificity: HECT, RING finger, U-box, and RBR type (Figure 3a) (Yang et al., 2021).

The RING finger E3 ligases are the most prominent and abundant family and are characterized by a zinc-binding RING domain. During the final step of the ubiquitylation cascade, RING E3 ligases do not form an E3-ubiquitin intermediate. However, the RING domain acts as a scaffold that binds the E2 conjugation enzyme and directly transfers the ubiquitin from the E2 enzyme to the specific protein substrate (Metzger et al., 2014). There are more than 600 RING-type E3 ligases, so they can be subdivided into two groups: multi-subunit E3 ligases and monomeric RING-finger E3 ligases. The E3 ubiquitin-protein ligase Mdm2 (MDM2) is a monomeric RING E3 ligase, that can auto-ubiquitinate itself (Kim et al., 2020). Cullin-RING E3 ligases are typical multi-subunit E3s assembled on one of six Cullin scaffold proteins, linked to a RING box protein at the N-terminus and an adaptor protein together with a substrate receptor at the C-terminus (Figure 3b) (Budhidarmo et al., 2012). The SCF E3 ligase complex (S phase kinase-associated protein 1-Cullin1 F-box protein) is the largest and best characterized Cullin-RING multi-subunit E3 (Nakayama & Nakayama, 2006). The C-terminus of CUL1 binds to the RING domain protein RBX1 and facilitates the recruitment of the E2 enzyme. The N-terminus of CUL1 attaches to SKP1, which serves as an adaptor for binding to a specific F-box protein (Jin et al., 2004). The F-box protein is responsible for the recognizing and binding of the substrate protein through various substrate binding domains such as leucine-rich repeats (referred to as FBXLs), WD40 domains (referred to as FBXWs) and other domains (FBXOs) (Jin et al., 2004). While SCF-type ligases most commonly produce K48 ubiquitin chains, several F-box proteins have recently been reported to facilitate non-proteolytic K63 ubiquitylation (Bassermann et al., 2014; Zhang, Yang, et al., 2017). RING finger E3 ligases can be regulated by various modifications such as phosphorylation, neddylation, and auto ubiquitylation (Enchev et al., 2015).

In contrast to RING finger E3 ligases, HECT E3 ligases transfer ubiquitin to the substrate protein via a two-step reaction. First, ubiquitin is transferred to a catalytic cysteine residue of the HECT E3 domain and then transferred from the E3 to the target substrate (Metzger et al., 2012). This catalytic function of the HECT domain is carried out by its C-terminal region, while the N-terminal part of the ligase is responsible for substrate specificity (Rotin & Kumar, 2009). Human HECT E3 ligases can be divided into three subfamilies based on their N-terminal extension: The HERC family, characterized by one or more regulators of chromosome condensation 1 (RCC1)-like domains (RLDs) that function as GTPase Ran regulators and interact with chromatin through histones H2A and H2B. The Nedd4 family, with tryptophan-tryptophan and C2 domains, which target proteins to phospholipids. And a group of other HECTs with diverse domains (Weber et al., 2019). HECT E3 ligases can be regulated by inhibiting catalytic activity through intramolecular interactions (Sluimer & Distel, 2018).

Like HECT E3 ligases, RING-between RING-RING E3 ligases also transfer ubiquitin to a catalytic cysteine on the E3 first before transferring ubiquitin to the substrate protein. RBR E3 ligases are a RING-HECT hybrid E3 ligase, consisting of RING1, RING2, and a central in-between RINGs (IBR) domain (Spratt et al., 2014). While the RING2 domain contains the catalytic cysteine, RING1 recruits the E2-bound ubiquitin. The IBR domain has a similar structure to the RING2 domain without the catalytic cysteine (Walden & Rittinger, 2018). Like HECT E3s, RBR E3 ligases can be held in an autoinhibited state by intramolecular interactions to regulate the E3 activity.

Similar to RING E3s, U-box E3 ligases can transfer the ubiquitin directly to the protein substrate without an intermediate step. Ubiquitin-loaded E2 enzymes interact with the C-

terminal U-box domain of the U-box E3 ligase for the ubiquitin transfer process (Hatakeyama & Nakayama, 2003).

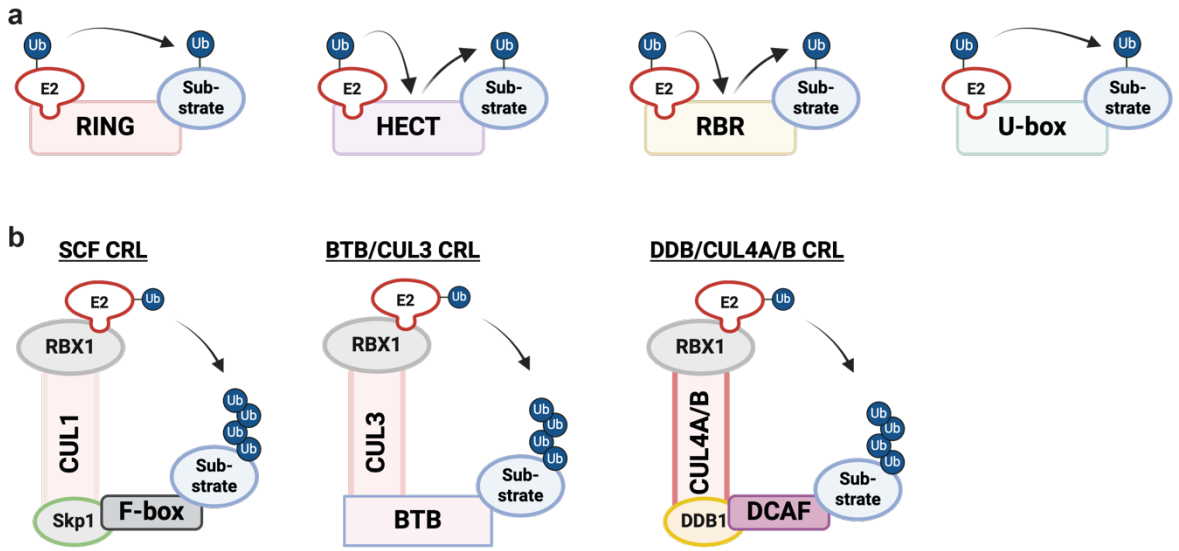

Figure 3 Four major families of E3 ubiquitin ligases. (a) Model structure of the four major human ubiquitin E3 ligases. U-box and RING E3 ligases do not form an E3 ubiquitin intermediate but transfer ubiquitin molecules directly to the bound substrate. HECT and RBR E3 ligases transfer ubiquitin to cysteine on the E3 before transferring it to the substrate protein. **(b)** Model of Cullin-RING E3 ligases (Cul1, Cul3, Cul4A/B). To form Cullin-RING E3 ligases, the respective Cullin proteins recruit receptor proteins (F-box, DCAF7), adaptor proteins (Skp1, BTB, DDB1), and the RING protein RBX1/2. Formed Cullin-RING ligases (CRL) catalyze ubiquitin transfer from E2 to substrate. The figure was generated with Biorender and adapted from (Diaz et al., 2022).

2.1.3 Deubiquitylating enzymes (DUBs)

DUBs are proteases that reverse the action of ubiquitin E3 ligases by cleaving the isopeptide bond between the substrate protein and ubiquitin. The interplay between E3 ubiquitin enzymes and DUBs allows for a fast and highly balanced protein regulation. However, the role of DUBs extends beyond that of ubiquitin E3 ligase antagonists. A critical function of DUBs is to recycle and generate free ubiquitin, thereby creating a pool of available ubiquitin for use by other enzymes. In addition, DUBs can also cleave ubiquitin-like proteins such as small ubiquitin-related modifier (SUMO) or NEDD8 and their substrate proteins (Wing, 2003).

The human genome encodes over 90 deubiquitylating enzymes, which can be divided into two major classes: cysteine proteases and metalloproteases. These can be further categorized into ubiquitin-specific proteases (USPs), Machado-Josephin domain proteases, ubiquitin C-terminal hydrolases, Jab1/Mov34/Mpr1 Pad1 N-terminal+ and ovarian tumor proteases (Nijman et al., 2005). To catalyze the hydrolysis of ubiquitin bonds, all DUBs have an active site cysteine residue accompanied by a histidine and an asparagine or aspartate (catalytic tirade) (Cotto-Rios et al., 2012). Most DUBs are cysteine proteases that are active or inactive depending on whether the cysteine contains an inactive thiol or a reactive thiolate group (Ronau et al., 2016). Once active, the cysteine residue triggers a nucleophilic attack on the isopeptide bond that binds ubiquitin to the lysine residue of the substrate protein or other ubiquitin proteins, leading to a thioester intermediate between the cysteine of ubiquitin and the DUB. Subsequently, the histidine and asparagine/aspartate of the catalytic triad catalyze the hydrolysis of the intermediate and subsequently the released ubiquitin is recycled (Snyder & Silva, 2021). While many of the USP DUBs can cleave many different ubiquitin chain types but have a substrate specificity, DUBs from the ovarian tumor protease family mostly cleave a

specific ubiquitin chain type and have no substrate specificity (Mevissen et al., 2013; Mevissen & Komander, 2017).

DUBs play essential roles in many cellular processes, including the cell cycle, where ubiquitin-specific processing proteases target cell cycle proteins such as cyclin-dependent kinase 2 (CDK2), cyclin A, and KRAS to regulate cell cycle progression and the G1/S transition (Ducker & Shaw, 2021). In addition, DUBs regulate the DNA damage repair machinery by interacting with MDM2, which ubiquitinates cellular tumor antigen p53 (p53) for degradation (Khoronenkova et al., 2012). DUBs also regulate translation by targeting ribosome ubiquitylation (Kapadia & Gartenhaus, 2019).

Because DUBs play critical roles in many cellular processes, they are also involved in the development and progression of many diseases. In neurodegenerative diseases, DUBs modulate processes such as neuroinflammation and protein secretion. They also regulate the stability of proteins such as Tau and amyloid beta protein, which are known for their pathogenic potential (B. Liu et al., 2022). In many cancers like lung, liver, and colon, DUBs such as ubiquitin carboxyl-terminal hydrolase 14 (USP14), 21 (USP21), and 28 (USP28) are overexpressed, which deubiquitinates oncogenes such as MEK2, c-MYC and Notch1 (neurogenic locus notch homolog protein 1), stabilizing them and increasing cancer proliferation, survival and migration (J. Liu et al., 2022). Recently the DUB OTUD6B has been identified as an oncogene that drives G1/S-transition and therefore regulates multiple myeloma progression (Paulmann et al., 2022). Since DUBs play critical roles in many cellular processes, they are tightly regulated through regulation of their transcription and translation rates or though post translational modifications such as phosphorylation (Sahtoe & Sixma, 2015).

The first DUB inhibitor targeting multiple myeloma by simultaneously inhibiting USP14 and ubiquitin carboxyl-terminal hydrolase isozyme L5 (UCHL5) entered clinical trials in 2015. But to date more than 50 DUB inhibitors have been identified, several of which are in clinical trials (Lai et al., 2020). DUB inhibitors like CT1073 and CT1113, that simultaneously inhibit USP25 and USP28, show broad-spectrum anti-cancer activity (Peng et al., 2022). But a significant difficulty in developing DUB inhibitors is the similarity between their catalytic and substrate binding domains, which means that broad-spectrum inhibitors could block multiple DUBs and thus affect different cellular processes (Schauer et al., 2020). Therefore, the focus today is on non-competitive inhibitors of DUBs.

2.1.4 The Ubiquitin-Proteasome system in cancer

The UPS is essential for protein degradation and non-proteolytic signaling in several cellular processes, including cell cycle control, DNA damage repair, transcriptional regulation, and protein localization (Nandi et al., 2006). Thus, ubiquitylation mediates both the quantity and quality of various proteins and ensures cellular homeostasis (Komander & Rape, 2012). The Hallmarks of Cancer by D. Hanahan and B. Weinberg describe the complex, multi-step process of gradual transformation from healthy cells into cancer cells. Malignant transformation occurs through reprogramming of cellular signaling networks, leading to increased cell survival and proliferation, invasion, metastasis, and immune evasion (Hanahan & Weinberg, 2000). Because the UPS is involved in almost all cellular processes by precisely regulating the activity and abundance of proteins, it acts as a checkpoint in many of these signaling pathways (Bassermann & Pagano, 2010; Duan & Pagano, 2021). Consequently, the UPS, particularly E3 ligases and their substrate proteins, are often deregulated by genetic or post-translational alterations in human cancers (Bassermann et al., 2014; Shi & Grossman, 2010). Mutations in

E3 ligases can lead to insufficient ubiquitylation of proto-oncogenes or rapid degradation of tumor suppressors, thus contribute to cancer development (Figure 4) (Deng et al., 2020).

Mutations in E3 ligase complexes are present in most hallmarks of cancer (Duan & Pagano, 2021). One example of E3s that upregulate cell proliferation is the E3 ubiquitin ligase Casitas B linage lymphoma-b (CBL) family. They target multiple receptors, such as the epidermal growth factor receptor (EGFR), leading to its degradation (Kales et al., 2010). Mutations in CBL can inhibit their E3 activity and the ubiquitylation of substrates, leading to increased proliferation via enhanced EGFR abundance (Peschard & Park, 2003). In human DLBCL, the Cullin-RING E3 ligase (CRL3) substrate receptor Kelch-like protein 6 is frequently mutated (Choi et al., 2019). This inhibits its interaction with Cul3 and, thus, its E3 ligase activity, stabilizing the substrate ro-quin-2 and promoting tumor cell growth (Choi et al., 2018). S-phase kinase-associated protein 2 (SKP2) is the substrate recognition domain of the SKP, Cullin, F-box containing complex (SCF) complex and is often overexpressed in a variety of human cancers (Gstaiger et al., 2001). It is an example of an E3 ligase complex with pre-oncogene function. When overexpressed, SKP2 leads to increased ubiquitylation and degradation of p27, resulting in overactivation of cyclin-dependent kinase 1/2 (CDK1/2) and increased cell cycle progression (Cai et al., 2020).

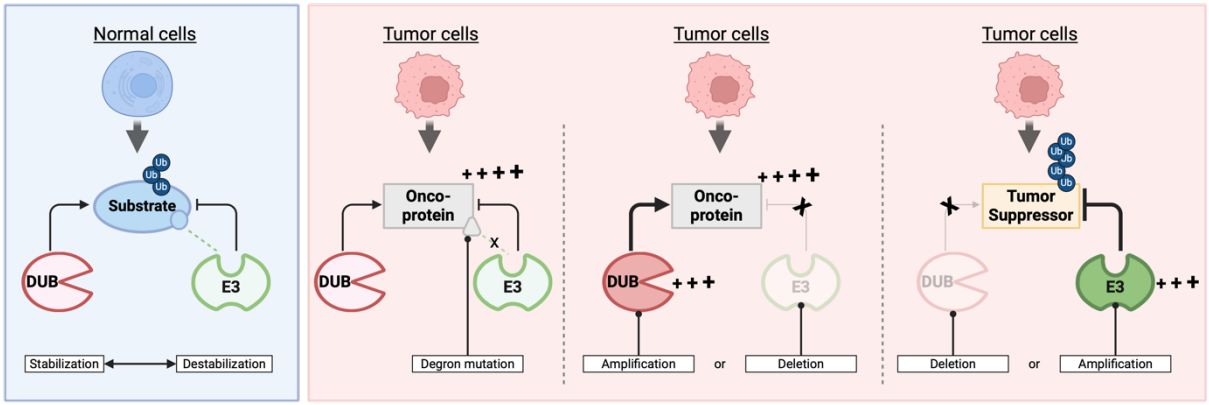

Figure 4 The role of E3 ligases and DUBs in cancer development. The balance between DUBs and E3 ligases is critical for maintaining protein abundance and homeostasis in healthy cells (blue). Cancer cells often have mutations in the UPS, leading to an increased amounts of oncoproteins or a decreased amounts of tumor suppressors (red). Cancer cells may carry mutations in the degrons of oncogenes that render E3 ligases unable to recognize and ubiquitinate their target proteins. Alternatively, tumor cells may harbor deletion mutations in E3 ligase genes or have amplified DUB genes that have oncoproteins as substrates, both result in decreased ubiquitylation of relevant oncoproteins and thus promote tumorigenesis. Conversely, tumor cells often have amplifications of E3 ligases that target tumor suppressors or deletions in DUBs that typically target these suppressors. This can lead to increased degradation of such proteins and further drive tumorigenesis. The figure was generated with Biorender.

The essential functions of the UPS in controlling cellular processes at multiple levels and their important role in cancer development make them promising targets for novel drugs and new therapeutic strategies (Senft et al., 2018). E3 ligases and deubiquitylating enzymes (DUBs) have the highest substrate specificity among the UPS, making them the most intesting targets (Huang & Dixit, 2016). The best-studied effect of protein ubiquitylation is the substrate degradation by the proteasome, making proteasome inhibitors (PI) such as Carfilzomib or Bortezomib a comprehensive drug option in various cancer entities. Both Carfilzomib and Bortezomib target the β5 subunit of the core proteasome. They are part of the standard treatment regime for most hematological malignancies, with high response rates especially in multiple myeloma (Nunes & Annunziata, 2017). However, since proteasome inhibitors have the disadvantage of causing severe side effects via non-specific inhibition of the proteasome protein degradation process, small molecular E3 inhibitors are another therapeutic strategy (Wu et al., 2020). They can either limit E3 substrate interaction or inhibit the activity of the E3

ligase. Small molecules (Nutlins, MI-219, and RITA) targeting the RING-type MDM2 ligase complex have been tested in clinical trials and have been shown to disrupt MDM2 interaction with p53, resulting in cancer cell cycle arrest and apoptosis (Issaeva et al., 2004; Shen & Maki, 2011; Zheng et al., 2010). Another example is the SKP2 inhibitor C1, which disrupts the interaction with p27, thereby inhibiting the Skp2-mediated degradation of p27 (Rodriguez et al., 2020). The disadvantages of small molecules is that they are highly toxic, can also trigger resistance, and are often not effective against mutated proteins (He et al., 2021). As a result of research into small molecule inhibitors, proteolysis-targeting chimeras (PROTACs) and compounds that act as molecular glues have recently emerged (An & Fu, 2018). PROTACs are dual-function molecules consisting of two separate ligands covalently attached to a linker. One ligand can bind to the protein of interest, while the other can bind to a specific E3 ligase. The protein of interest is then ubiquitinated by the bound E3 ligase and degraded by the proteasome (Bekes et al., 2022). PROTACs have been designed for more than 50 proteins identified as potential drug targets (He et al., 2022). So far, the E3 ligases MDM2, inhibitor of apoptosis (IAP), cereblon, and von Hippel-Lindau (VHL) have been frequently selected for PROTAC development (Girardini et al., 2019; Zhang et al., 2020). ARV-110, which targets the androgen receptor, is the first PROTAC to enter the clinic (T. T. Nguyen et al., 2022). While PROTACs show high selectivity and specificity, they also have drawbacks such as toxicities, poor tissue permeability, and degradation of unwanted proteins (An & Fu, 2018). A similar strategy of inducing a neo-interaction between a protein of interest and a specific E3 ligase is utilized by molecular glues. These are natural substances, such as plant hormones, or synthetic compounds, such as immunomodulatory imide drugs (IMiDs) (Schreiber, 2021). Like PROTACs, the molecular glues create a proximity between the target and E3 ligase, resulting in ubiquitylation of the substrate, followed by proteasomal degradation (Sasso et al., 2023). The main advantages over PROTACs are that molecular glues use non-bivalent small molecules and do not demand high affinity for the E3 and neo-substrate (Li et al., 2022).

2.1.5 Kelch-like protein 14

Kelch-like protein 14 is encoded on chromosome 18q12.1 and belongs to a larger family of Kelch-like proteins that can function as a subunit of the Cullin-RING ubiquitin ligase complex. In contrast to SCF/CRL1, they contain a Cullin-3 as a molecular scaffold and are not dependent on SKP1 for substrate binding (Figure 3b). SKP1 is replaced by a BTB domain that acts as a substrate-specific adaptor and is attached to Cullin-3. Kelch-like proteins are characterized by a series of repeats known as Kelch motifs that form a beta-propeller structure involved in substrate recognition. In addition to the six carboxy-terminal Kelch-like motifs, KLHL14 contains a BACK domain and an amino-terminal BTB domain, both of which facilitate binding to the Cullin-3 subunit of the Cullin-RING ubiquitin ligase complex (Dhanoa et al., 2013; Shi et al., 2019). KLHL14 is predominantly expressed in the human spleen and thyroid, with an exceptionally high level of expression in B-cells, suggesting a potential role of KLHL14 in B-cell development (Li et al., 2018).

KLHL14 was initially discovered as an interactor of TorsinA implicated in the pathophysiology of Torsion dystonia (an autosomal dominant disorder with painful muscle contractions) independently of the ubiquitin system (Giles et al., 2009). Studies have shown that KLHL14 mRNA is highly expressed in GABA pre-interneurons and corticospinal neurons in mice, suggesting further UPS-independent functions of KLHL14 (Sahni, Shnider, et al., 2021; Zhang, Weinrich, et al., 2017). Nevertheless, KLHL14 has been identified as a Cullin-3 substrate adaptor and has been implicated in the progression of several cancers. Bioinformatic

studies based on GEPIA datasets have revealed that KLHL14 expression levels are elevated in ovarian and endometrial cancers, which is associated with poorer prognosis (Chen et al., 2020; Wang et al., 2022). Recent findings suggest that KLHL14 may be an important diagnostic biomarker, as it is hypomethylated in endometrial cancer (Wu et al., 2017). While mice with homozygous deletion of KLHL14 exhibit embryonic lethality, heterozygous deletion of KLHL14 inhibits the proliferation of innate-like B-cell population B-1b-cells, which respond to T-cell-independent antigens and mediate long-lasting IgM memory to infection. At the same time, heterozygous deletion of KLHL14 promotes the development of innate-like B-cell population B-1a cells, which are the primary producers of poly-reactive IgM antibodies. (Li et al., 2018). In another study, elevated KLHl14 expression was detected in amniotic epithelial cells during epithelial-mesenchymal transition (Di Lollo et al., 2020). Although KLHL14 is highly expressed in B-cells, genetic studies have identified frequent mutations in KLHL14, rendering it inactive in diffuse large B-cell lymphoma (Schmitz et al., 2018). In a follow-up study, KLHL14 was found to ubiquitylate the B-cell receptor (BCR), tagging it for proteasomal degradation and therefore inhibiting BCR-driven NF-κB signaling (Choi et al., 2020). This suggests a tumor suppressor function of KLHL14 by regulating B-cell receptor-dependent NF-κB signaling in DLBCL. Despite the growing evidence for a critical function of KLHL14 in DLBCL and the UPS, further research is needed to understand the entire molecular mechanism.

2.1.6 DDB1-Cul4 associated factor 7

DCAF7, known as WD repeat and SOCS box-containing protein 7 (WDSB7), is encoded on chromosome 17q23.3. and has seven tryptophan-aspartate dipeptide repeats that form a β-propeller shape (WD40 domain) (Stirnimann et al., 2010). It is a member of the DCAF family of Cullin-RING ubiquitin ligases. In contrast to SCF/CRL1 and Cullin-3 discussed above, they contain Cullin-4A and Cullin-4B as their molecular backbone and do not rely on SKP1 to bind the substrate adaptor (Figure 3b) (Jackson & Xiong, 2009). Instead, the N-terminus of the Cul4A/B backbone binds to DDB1. The C-terminus of the Cul4A/B scaffold is attached to the RING finger protein RING-Box1 (RBX1), which is responsible for binding the E2 enzyme. DDB1 binds a specific substrate receptor protein, such as DCAF7, which can recognize and bind the ligase-specific substrates. This Cul4 ligase complex transfers the E2-bound ubiquitin to the bound substrate protein (Lee & Zhou, 2007).

Structurally, all DCAF proteins have a WD40 domain consisting of at least four WD repeats that fold into a beta-sheet and form a β-propeller-like structure (Stirnimann et al., 2010). Although most DCAFs have been shown to function as substrate receptor proteins in the CRL4 complex and the so-called WDXR amino acid motif is responsible for the interaction with DDB1, not all function as substrate receptor proteins (Angers et al., 2006). In addition, post-translational modifications of DCAFs are sometimes necessary for substrate recruitment (Jin et al., 2006). It has been published that DCAF7 plays a role outside of ubiquitylation and can form a complex with the dual specific tyrosine-phosphorylation-regulated kinase 1A and 1B (DYRK1A, DYRK1B), which phosphorylates RNA polymerase II and promotes myogenesis (Yu et al., 2019). Dysfunction of DYRK1A is associated with neurodevelopmental disorders, and the DCAF7/DYRK1A complex is required for craniofacial development and proper growth and suppresses irregular cell growth and transformation (Miyata & Nishida, 2023; Yousefelahiyeh et al., 2018). Both DYRK1A and DYRK1B share a DCAF7 binding domain, and comparing 4 DYRK1A proteomic studies, three detected DCAF7, further confirming an interaction between these two complexes (Ananthapadmanabhan et al., 2023). Another paper reported that overexpression or knockdown of DCAF7 results in UPS independent up- or

downregulation of both interactors DYRK1A and DYRK1B, which affects the transition from proliferation to differentiation in C2C12 cells (Yousefelahiyeh et al., 2018). In addition, a BioID (Biotin identification) approach (proximity-based interactome using a biotin ligase) identified insulin receptor substrate 1 (IRS1) as a DCAF7 interactor that regulates cell proliferation by controlling cell cycle arrest at G2 (Frendo-Cumbo et al., 2022).

Recently, DCAF7-Cul4B-mediated ubiquitylation was shown to regulate MEN1 protein expression in pancreatic neuroendocrine tumors. MEN1 is a tumor suppressor and one of the most mutated genes in this entity. Downregulation of DCAF7 inhibited tumor growth in pancreatic neuroendocrine tumors (Xu et al., 2023). In addition, DCAF7 appears to play a broader role in DNA repair pathways, as DNA Ligase I is a potential substrate of DCAF7, and a study links DCAF7 to the protein expression levels of the nucleotide excision repair subunits of the ERCC1-ERCC4 endonuclease complex (Kawara et al., 2019; Peng et al., 2016). However, further research is needed to understand the molecular mechanisms and substrate interactions of DCAF7 that appear to be involved in the tumorigenesis of various cancers.

2.2 Development and heterogenicity of B-cell malignancies

2.2.1 B-cell development

B lymphocytes belong to the adaptive immune system and play a key role in humoral immunity. In humans, B-cells make up 15% of all lymphocytes and are the primary antibody (immunoglobulin (Ig)) producing cells (Cooper, 2015). Antibodies are proteins that can either be secreted or act as a B-cell receptor on the plasma membrane of the B-cell. Antibodies can recognize and directly neutralize pathogens using pathogen-specific antigens, highlighting the importance of highly diverse but also pathogen-specific BCR pools (Hoffman et al., 2016). In addition, B-cells serve as antigen presenting cells (APCs) to T-cells, secrete cytokines to modulate the immune response, and can provide long-term immunity through specific memory B-cells (Rastogi et al., 2022).

B lymphocytes arise from hematopoietic stem cells in the bone marrow, and differentiate into multipotent progenitor cells and common lymphoid progenitor cells (Cobaleda et al., 2007). To fully develop into naïve B-cells, they undergo a rigorous maturation and selection process to prevent self-reactivity (Figure 5)(Wardemann et al., 2003). Immunoglobulin heavy and light chain gene segments (variable V, diversity D, joining J) are rearranged during this process. Hence, the pro-B-cells evolve from pro-cell to pre-B-cell to naïve B-cell. This V(D)J recombination is facilitated by specific recombinase enzymes based on somatic recombination (Roth, 2014). The enzymes splice the variable, joining and sometimes diversity gene segments so that each B-cell can produce a unique BCR with a specific affinity for antigens. This process begins with the activation of the V(D)J recombinase by the recombination-activating gene 1 and gene 2 (RAG1, RAG2), which then binds to a specific signaling sequence (RSS) adjacent to a V(D)J-coding gene segment (Schatz & Swanson, 2011). The recombinase induces a single-strand break and hairpin formation, leading to the generation of the recombination center (Curry et al., 2005). Several proteins are then involved in opening the hairpin, which allows the terminal deoxynucleotidyl transferase (TdT) to randomly add non-template nucleotides to the coding-end (Schatz & Ji, 2011). After exonucleases removed bases and DNA polymerases made the two ends compatible for joining, the coding ends are ligated together by DNA ligase IV (Helmink & Sleckman, 2012; van Gent & van der Burg, 2007). This process is called non-homologous end joining, and after the successful formation of pre-B-cell receptors, proliferation/expansion of the pre-B-cell is

triggered by the tyrosine kinase SYK (Cornall et al., 2000). The V(D)J recombinase machinery is downregulated and successful recombined VL and JL gene segments are paired with the heavy chain, resulting in a highly variable paratope (Fernandez-Quintero et al., 2020). The resulting immunoglobulins can recognize antigens to which the organism has never been exposed, allowing the adaptive immune system to respond to emerging pathogens.

To prevent self-reactivity of these newly produced BCRs, B-cells in the bone marrow undergo two types of selection. Positive selection is antigen-independent and ensures the correct formation and function of the cell surface BCRs of the B-cell (Nemazee, 2017). BCRs that cannot bind to their ligand or cannot sustain signaling are arrested in their development. The second process is negative selection, which aims to prevent autoimmunity by mature B-cells responding to the body's own antigens (Sandel & Monroe, 1999). The BCRs of B-cells are exposed to self-antigens, and those that bind too strongly are either clonally deleted, the BCR is edited, they become inactive, or the signal is ignored, and development into mature B-cells continues (Nemazee, 2017).

In the final development step, the B-cells migrate to secondary lymphoid organs, such as the lymph nodes or spleen, where they await activation. There are two independent pathways of B-cell activation in the lymphoid organs. T-cell-dependent activation is based on helper T-cells presenting antigens on their T-cell receptor to the B-cell's BCR (Parker, 1993). In addition to the antigen, T-cells also express co-stimulatory factors required for B-cell activation, such as CD40 and IL-4 (Frauwirth & Thompson, 2002). The cell-cell interaction triggers the formation of a germinal center where the activated B-cells undergo proliferation, antibody class switching, and affinity maturation, increasing the antibody's affinity to the presented antigen (Kuppers, 2005). The enzyme activation-induced cytidine deaminase (AID) is responsible for the affinity maturation process by randomly mutating parts of the variable regions (V_H and V_L) of the immunoglobulin (Sheppard et al., 2018). It is also active in Ig class switching, remodeling the constant region of the IgH gene locus so that IgD or IgM becomes either IgE, IgG, or IgA (Chaudhuri et al., 2003). This can alter the effector function of the rearranged antibodies. Finally, the B-cells differentiate into either memory B-cells, which persist in the organism and respond rapidly to renewed exposure to the antigen, or plasma cells, which are effector cells that produce and secrete large quantities of the antibodies to directly neutralize the pathogen (Calame, 2001; Kurosaki et al., 2015). Specific polysaccharides and unmethylated CpG DNA can activate B-cells independently of T-cells (Vos et al., 2000). This is known as T-cell-independent activation, in which the B-cells receive their co-stimulatory factors by cross-linking of multiple BCRs or Toll-like receptors (Allman et al., 2019). In contrast to T-cell-mediated activation, no germinal center is formed, but the BCRs can undergo Ig class switching. T-cell-independent activated B-cells develop into short-lived plasma blasts or long-lived plasma cells (Hoyer et al., 2004).

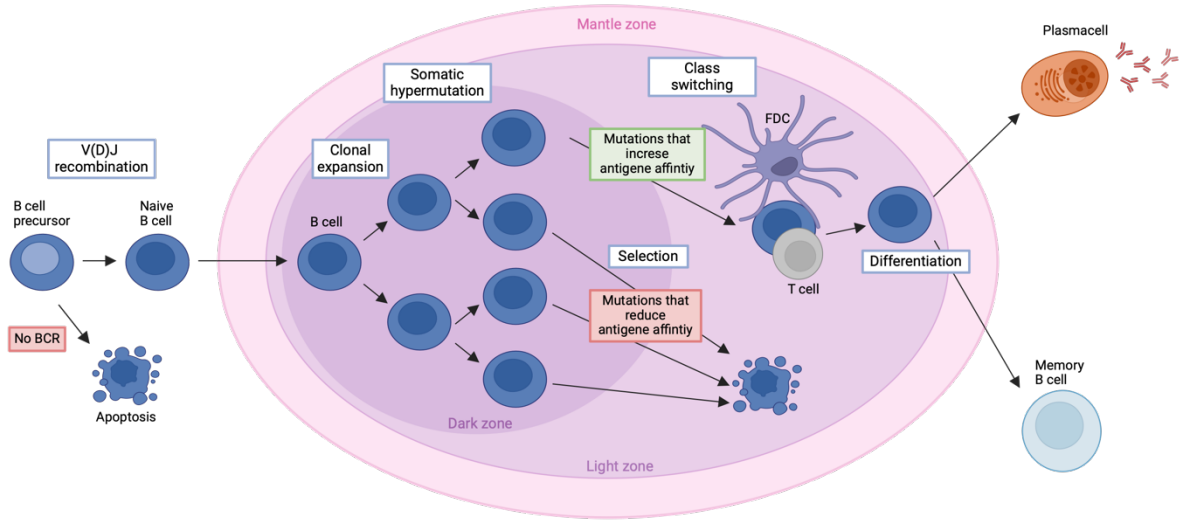

Figure 5 B-cell development. Naïve B-cells that have undergone V(D)J recombination and produce a B-cell receptor enter the germinal center upon antigen activation to fully differentiate and develop. B-cells undergo clonal expansion and somatic hypermutations in the dark zone of the germinal center, introducing diversity into the V(D)J region of the immunoglobulin. B-cells that acquire deleterious mutations that reduce antigen affinity undergo apoptosis. B-cells that acquire beneficial mutations that increase BCR affinity are positively selected by T-cells and follicular dendritic cells (FDCs). Positively selected B-cells can undergo class switching in the light zone of the germinal center and ultimately differentiate into either plasma cells or memory B-cells. Figure generated with Biorender and adapted from (Kuppers, 2005).

2.2.2 B-cell derived malignancies

In the Western world, about 20 new non-Hodgkin´s lymphoma (NHL) cases are diagnosed per 100,000 people yearly (Thandra, Barsouk, Saginala, Padala, et al., 2021). Approximately 95% of NHL cases are of B-cell origin, while the remaining cases are T-cell related (Thandra, Barsouk, Saginala, Padala, et al., 2021). The World Health Organization distinguishes about 15 types of B-cell lymphomas based, in part, on differentiation markers on the cell surface and distinct gene expression patterns (Swerdlow et al., 2016). During B-cell development and maturation, the cells exhibit extreme genomic instability during V(D)J recombination, affinity maturation, and class switching, combined with clonal expansion. This ensures a high diversity of B-cells and high-affinity antibodies but also results in a high risk of malignant transformation (Kuppers, 2005). Hallmarks of many B-cell lymphomas are genetic mutations or chromosomal translocations of immunoglobulin loci that activate oncogenes or silence tumor suppressors (Kuppers & Dalla-Favera, 2001). For example, more than 90% of follicular lymphomas have the t(14;18) translocation, also known as BCL2-IgH (Rabkin et al., 2008). The apoptosis regulator Bcl-2 (BCL2) gene is translocated to the IgH transcriptional enhancer, resulting in constitutive overexpression of the anti-apoptotic protein BCL2. In addition to translocations, somatic hypermutations in genes such as Myc proto-oncogene protein (MYC) or cyclin dependent kinase inhibitor 2A (CDKN2A) can cause genetic mutations that drive malignant transformation in B-cells (Khodabakhshi et al., 2012). Further, impaired BCR signaling is a key feature of many B-cell lymphomas, which can lead to increased proliferation and survival (Niemann & Wiestner, 2013). Depending on their classification, the different types of B-cell lymphoma show distinct clinical symptoms and require different treatment approaches.

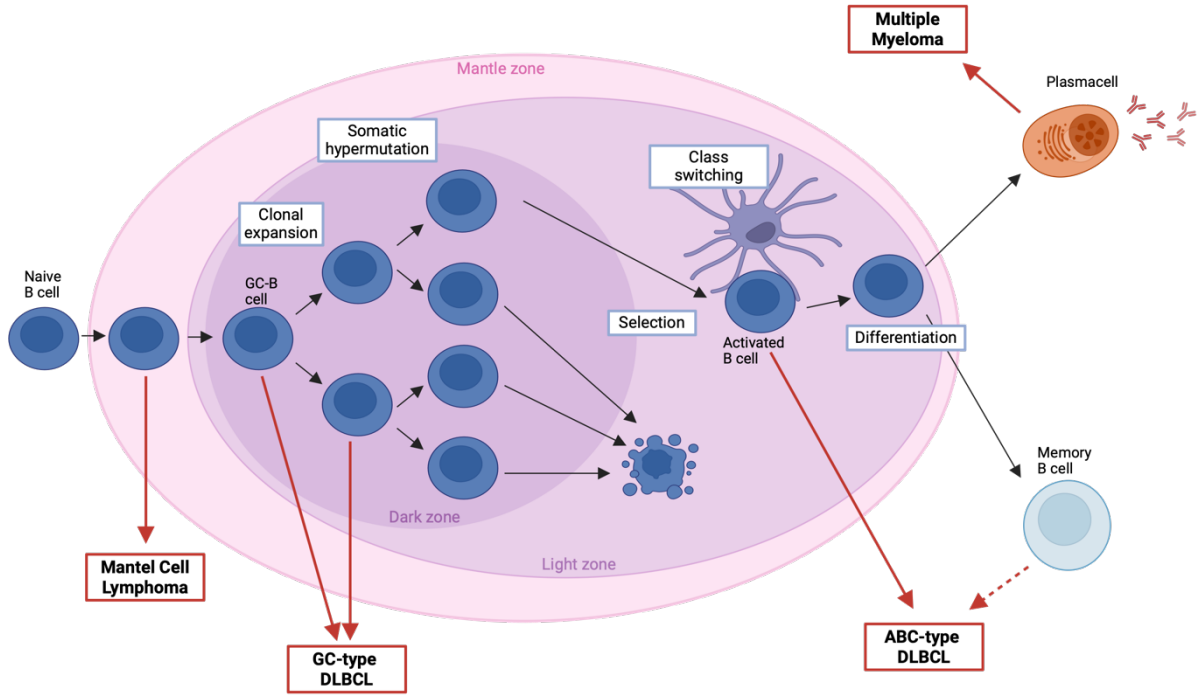

Figure 6 Cellular origins of MCL, DLBCL and Multiple Myeloma. The origin of human B-cell malignancies such as Mantel cell lymphoma, diffuse large B-cell lymphoma, and multiple myeloma can be traced to specific stages of B-cell development based on their distinct molecular features and gene expression profiles. MCL arises from a specific subset of B-cells found in the maternal zone prior to clonal expansion and somatic hypermutation. The cellular origin of germinal center B-cell-like DLBCL (GC-type DLBCL) is from B-cells that are part of the germinal center response during differentiation. Activated B-cell-like DLBCL (ABC-type DLBCL) originates from post-germinal center-activated B-cells that are in a later stage of differentiation. MM arises from terminally differentiated plasma cells that have left the germinal center and are homing through the bone marrow. Figure generated with Biorender and adapted from (Koues et al., 2015).

2.2.3 Multiple Myeloma

According to the American Cancer Society, 35,730 adults in the United States will be diagnosed with multiple myeloma in 2023 (American Cancer Society., 2023). The 5-year relative survival rate in the US is approximately 58%, and although the disease is considered treatable, no cure has been found (American Cancer Society., 2023). The exact cause of MM remains unknown, but risk factors include family history, advancing age, obesity, and radiation exposure. The symptoms of MM can be diverse, but patients most commonly suffer from hypercalcemia, renal and kidney failure, anemia, and bone pain/lesions (CRAB-criteria). MM accounts for about 10% of all lymphomas and is a multi-stage disease deriving from B-cells that have left the germinal center and become plasma cells (Figure 6)(Kuppers, 2005). Initial genetic and epigenetic changes lead to the development of monoclonal gammopathy of undetermined significance (MGUS) characterized by increased numbers of plasma cells (< 10% clonal plasma cells and <3g/dL M-Protein in serum) (Kyle & Rajkumar, 2009). From here, the disease progresses to smoldering myeloma (SMM) (10%-60% clonal plasma cells and >3g/dL M-Protein), in which malignant plasma cells produce abnormal antibodies and further genetic alterations lead to highly proliferative multiple myeloma (presence of end-organ or tissue damage) (Heider et al., 2021; Kyle & Rajkumar, 2009). The proliferating MM cells replace hematopoietic stem cells and cause anemia in patients, while the imbalance between osteoblasts and osteoclasts by cytokine release triggers bone lesions and hypercalcemia (Oyajobi, 2007). Impaired renal function is caused by the increased number of

immunoglobulins and free light chains circulating in the patient's blood. When these tumor cells enter the peripheral blood, plasma cell leukemia has manifested (Kumar et al., 2017).

The initiating events in the pathogenesis of MM are usually primary translocations. In most cases, the IgH gene locus q32 on chromosome 14 is translocated upstream of various oncogenes such as cyclin D1 on 11q13 or D3 on 6p21, c-MAF on 16q23 or the fibroblast growth factor receptor 3 on 4p16.3. (Heider et al., 2021; Puertas et al., 2023). The translocated IgH enhancer leads to increased expression of these oncogenes and initiates the progression of multiple myeloma from plasma precursor cells to MGUS (Kuehl & Bergsagel, 2002). These initiating events occur most likely at an early stage during plasma cell development, when double strand DNA breaks are introduced for immunoglobulin class switch recombination. As the disease progresses, secondary translocations, somatic mutations and chromosomal gains, and losses occur in the maligning B-cells (Fonseca et al., 2003). These secondary genetic aberrations occur independent of the DNA remodeling processes and at different rates depending on the type of the primary translocation during B-cell maturation (Rajkumar et al., 2013). In approximately 50% of cases, a monoallelic deletion of chromosome 13 is observed during disease progression towards MM (Rajkumar & Kumar, 2016). Other common deletions are seen on chromosomes 1p and 17p, while associated genetic mutations are found in G1/S-specific cycline-D1 (CCND1), serine-protein kinase ATM (ATM), B-RAF proto-oncogene (BRAF), TP53-binding protein 1 (TP53) and KRAS proto-oncogene (KRAS) (Weaver & Tariman, 2017).

As with many cancers, the tumor microenvironment plays a pivotal role, and with MM, the bone microenvironment is essential for disease development and progression (Lemaire et al., 2011). MM cells often interact not only with the extracellular matrix but also with bone marrow stromal and endothelial cells and osteoblasts (Garcia-Ortiz et al., 2021). This affects the persistence of MM and can trigger the release of cytokines (Interleukin-6 (IL-6), vascular endothelial growth factors (VEGFs), tumor necrosis factor-alpha (TNF-alpha)) that promote cell proliferation and survival (Oranger et al., 2013).

MM diagnosis includes a combination of laboratory tests, clinical imaging, and evaluations in combination with a bone marrow biopsy. Blood and urine samples are tested for the presence of paraprotein (M protein or monoclonal protein) produced by the tumor clone, anemia, kidney function, and high calcium levels (Cook & Macdonald, 2007). In addition, a bone marrow biopsy from the hip bone is performed to estimate the amount of plasma cells in the bone marrow, and X-ray scans are performed to detect bone damage and diagnose MM. To facilitate the diagnosis of MM and define three risk groups, the revised International Staging System was published in 2015 (Palumbo et al., 2015). Stage I patients have $\beta 2M < 3.5$ mg/L, albumin ≥ 3.5 g/dL, normal cytogenetics, and no elevated LDH. Stage II patients are not classified under Stage I or Stage III. Stage III patients have $\beta 2M \geq 5.5$ mg/L and either elevated LDH or high-risk cytogenetics [t(4,14), t(14,16), and/or del(17p)] (Costa & Usmani, 2020; Palumbo et al., 2015).

Treatment of MM is based on either a triple or quadruple therapy, which includes combinations of monoclonal antibodies (e.g., Daratumumab), immunomodulatory agents (e.g., Lenalidomide), steroids (e.g., Dexamethasone), and proteasome inhibitors (e.g., Bortezomib or Carfilzomib) (Rajkumar, 2012). This is followed by high-dose chemotherapy (e.g., Melphalan or Doxorubicin) and autologous stem cell transplantation for younger patients (Parrondo et al., 2020). Nevertheless, patients often relapse, and MM frequently develops drug resistance due to further genetic mutations and clonal evolution (Stalker & Mark, 2022). Promising new treatment approaches are immune cell therapy such as CAR-T-cell therapy, where genetically

engineered patient T-cells express chimeric antigen receptors (CAR) directed against myeloma cell surface proteins or antibodies couple T-cell specific CD3 to these surface markers. For example, the B-cell maturation antigen (BCMA) is expressed on MM cells and can be targeted by CAR-T-cells, leading to the destruction of the MM cells (Roex et al., 2020). Several CAR-T-cell therapies for MM are currently in clinical trials and two have been approved by the Food and Drug Administration (FDA) for the treatment of relapsed patients with refractory multiple myeloma Idecabtagene-Vicleucel (Ide-Cel, bb2121) and Ciltacabtagene Autoleucel (Cilta-cel) (Holstein, 2023; Sharma et al., 2022). Nevertheless, MM remains incurable, meaning that patients with MM will relapse in the end, thus highlighting the importance of understanding the pathogenesis and finding new druggable targets (San-Miguel et al., 2023).

2.2.4 Diffuse Large B-cell Lymphoma

DLBCL represents a malignancy of large B-cells that accounts for a third of all NHLs, making it the most common NHL subtype (Swerdlow et al., 2016). It is estimated that more than 25,000 DLBCL cases are diagnosed yearly in the USA, with DLBCL patients having a 5-year relative survival rate of 47.9% (Chihara et al., 2022). The exact cause of DLBCL is unknown but the risk factors for developing DLBCL include family history, radiation exposure, advanced age and weakened immune system. DLBCL develops primarily in the lymph nodes and therefore the most common symptom in DLBCL patients is lymph node swelling (Sethi & Haq, 2021). In some DLBCL cases, organs other than the lymph nodes are the starting point of the disease, leading to organ-specific symptoms. Notably, DLBCL is pictured as a single entity but the mutational landscapes, molecular characteristics, and signaling pathways in DLBCL are very heterogeneous from patient to patient.

Although there are several subtypes of DLBCL, the two most common are the germinal center B-cell-like (GCB) and activated-B-cell-like (ABC) types (Chapuy et al., 2018). GCB-type DLBCL arises form germinal center stage B-cells with high expression of CD10, BCL-6 and GCET1 genes (Figure 6)(Rosenwald & Staudt, 2003). They often harbor chromosomal translocation in the transcription factor BCL2 gene and the MYC gene transcription factor (Clipson et al., 2015). Gain-of-function mutations in the EZH2 gene, a histone-lysine N-methyltransferase that inhibits lymphocyte maturation, are also common (Beguelin et al., 2013). ABC type DLBCL develops from B-cells that have already passed the clonal expansion stage of the germinal center and have high expression of CD44 and MUM1/IRF4 (Figure 6)(Frick et al., 2011). Genetic alterations in the ABC subtype are often found in the CD79A, CD79B, and MYD88 genes, leading to a constant BCR signaling and activation of the NF-κB pathway (Kraan et al., 2013). In approximately 10% of cases, a mutation is found in CARD11 leading to NF-κB activation and signaling independent of BCR stimulation (Lenz et al., 2008). Loss-of-function mutations are found in the A20, PRDM1, and SPIB genes, which inhibit plasma cell differentiation (Testoni et al., 2015). GCB-type DLBCL has a more favorable prognosis and generally responds better to chemotherapy than ABC DLBCL.

Despite the differences in the pathophysiological mechanisms and prognosis, the standard treatment for ABC- and GCB-type DLCBL is similar and consists of a combinatory treatment of different chemotherapeutic agents (R-CHOP), Rituximab (monoclonal anti-CD20-antibody), Cyclophosphamide, Prednisone, Doxorubicin, and Vincristine with the addition of Etoposide in younger patients (Cabanillas & Shah, 2017). The distinct genetic mutations and dysregulated signaling pathways in GBC (mutations in RZH2, BCL2, and hyperactive PI3K/AKT/mTOR and JAK/STAT signaling) and ABC (mutations in MYD88, CD79A, CD79B,

and increased BCR/NFKB signaling) are being investigated as potential new targets for personalized therapy. For example, CUDC-907, a PI3K and histone deacetylase inhibitor, is in clinical trials for refectory GBC DLBCL with MYC gene alterations (Oki et al., 2017). GSK525762, an inhibitor of MYC gene expression, is in clinical trials for treating DLBCLs with translocations in MYC, BCL6, and BCL2 (Martin-Romano et al., 2020). Combination therapy with MCL-1 inhibitors or BCL-XL inhibitors (S63845, A1331852) in addition to Venetoclax is being tested to counteract tumor resistance due to increased expression of anti-apoptotic proteins of the BCL-2 family such as BCL-XI (Zhu et al., 2024). The dependence of ABC type DLBCL on NF-κB signaling has also been the target of novel therapeutic approaches. Unfortunately, the anticipated additional effect of proteasome inhibitors such as Bortezomib in combination with R-CHOP has not shown significant results (Dunleavy et al., 2009). However, small molecular inhibitors such as Ibrutinib (Bruton's tyrosine kinase inhibitor), which specifically block the NF-κB pathway, have shown success in combination with R-CHOP (Younes et al., 2019). Like MM, CAR-T therapies are currently being investigated for refractory patients who have received an autologous stem cell transplant.

2.2.5 Mantel cell lymphoma

Mantel cell lymphoma is another subtype of B-cell lymphoma originating from CD5-positive antigen-naïve pre-germinal center B-cells located in the mantel zone around the germinal center (Figure 6)(Bertoni & Ponzoni, 2007). It is a rare form of NHL, accounting for only 5-7% of cases, and is diagnosed in approximately one out of 200,000 individuals annually (Lynch et al., 2024). The likelihood of developing MCL increases with age, with the median age of onset being between 60-70 years of age. Typical symptoms are non-specific lymphadenopathy combined with B symptoms such as night sweats, fevers, and chills (Armitage & Longo, 2022). At the time of diagnosis, 80% of the patients have an advanced form of MCL in which secondary organs such as the bone marrow or gastrointestinal tract are affected (Armitage & Longo, 2022).

Like DLBCL and MM, the development of MCL is triggered by an accumulation of genetic mutations in B-cells. However, the exact factors that cause the genetic alterations are not yet known. One feature of MCL is the specific chromosomal translocation t(11;114)(q13;q32), which causes the CCND1 locus to be juxtaposed to the IgH gene locus, resulting in overexpression of Cyclin D1 (Li et al., 1999; Yin & Luthra, 2013). Cyclin D1 is a cell cycle regulator whose constitutive expression contributes to abnormal cell proliferation and chromosomal instability. Mutations in genes such as ATM (43,5%), TP53 (26,8%), and CDKN2A (23,9%) were also found frequently in patients, which further contribute to early clonal expansion and resistance mechanisms of MCL (Hill et al., 2020). The t(11;14) translocation is an important diagnostic marker in addition to lymph node biopsies, blood tests, and imaging studies (Yin & Luthra, 2013).

Similar to DLBCL, chemotherapy regimens including CHOP (Cyclophosphamide, Doxorubicin, Vincristine, pPednisone) and newer proteasomal inhibitory drugs like Bortezomib and Ibrutinib are the current treatment of choice (Kumar et al., 2022). However, as with DLBCL and MM, research needs to identify new potential targets and explore new treatment options, with understanding the molecular biology of MCL, DLCBL, and MM being key factors.

2.3. Development and heterogenicity of lung cancer

2.3.1 Lung cancer epidemiology

Lung cancer is one of the most diagnosed and deadliest cancers in the world (American Cancer Society, 2023). Current estimations suggest that there will be more than 200,000 new cases of lung cancer and more than 100,000 cancer deaths in the US in 2024 (American Cancer Society, 2023). A major difficulty with lung cancer is that patients with early-stage lung cancer often lack clear symptoms and most of the time the cancer is only detected by medical imaging. During later stages of the disease most patients develop respiratory symptoms such as cough and chest pain. But even then, specific symptoms can vary depending on the size and location of the tumor in the lung (Ruano-Ravina et al., 2020). Lung cancer is prone to metastasize and about one-third of patients experience symptoms because the cancer has spread to areas outside the lungs (Xing et al., 2019). A common diagnostic tool to confirm and classify lung cancer is a biopsy of the suspected tissue.

There are two distinct subtypes of lung cancer: 15% of cases are small-cell lung cancer (SCLC), and 85% are non-small-cell lung cancers (NSCLC) (Thai et al., 2021). The latter can be further divided into three histological subtypes: Squamous cell carcinoma (30%), Large-cell carcinoma (15%) and, LuAD accounting for 40% of NSCLC cases (Figure 7)(Chen & Dhahbi, 2021; Thai et al., 2021). Lung cancer develops by genetic alteration in the DNA of lung cells. Tobacco smoking accounts for 80%- 90% of lung cancer cases and is the major cause of lung cancer (Walser et al., 2008). Other factors that contribute to lung cancer development are excessive exposure to toxic chemicals (asbestos or volatile organic compounds) and chronic lung disease (Schabath & Cote, 2019). But just like with other cancers, these driver mutations can also sometimes occur randomly and trigger lung cancer development.

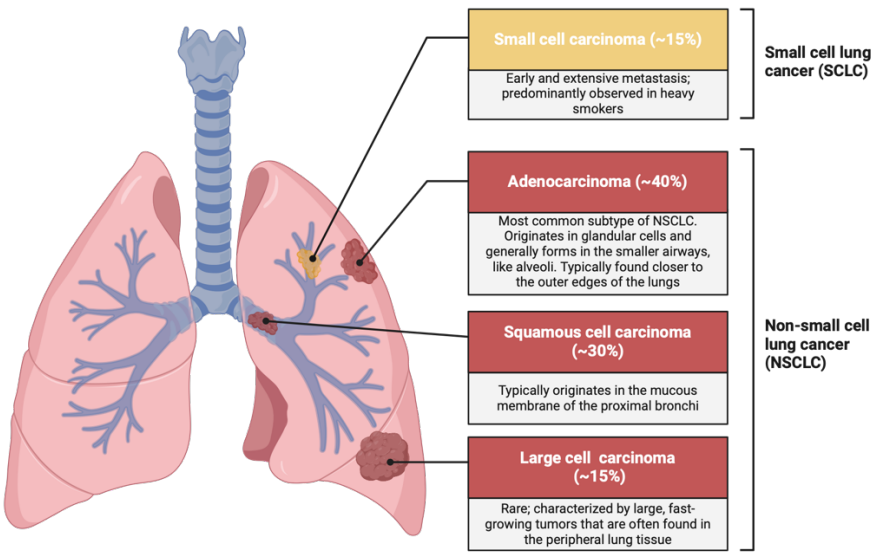

Figure 7 Classification of lung cancer. Visualization of the origin of small cell lung cancer in yellow and non-small cell lung cancer in red. SLCLC is a very aggressive form of lung cancer and originates from neuroendocrine cells (Visualized in yellow). NSCLC is subdivided into three distinct forms of lung cancer (Visualized in red). Adenocarcinoma originates from the glandular epithelial cells in the peripheral areas of the lung. Squamous cell carcinoma develops from the squamous epithelial cells lining the airways in the lung. Large cell carcinoma arises from the epithelial cells of the lung and is characterized by large, undifferentiated cells. Figure generated with Biorender and adapted from (Cheung & Nguyen, 2015).

2.3.2 Lung Adenocarcinoma

LuAD is the most common form of lung cancer and originates in the glandular cells of the lung that produce mucus and other fluids. LuAD has one of the highest mutational loads, as smoking and toxin exposure are strong mutagenic factors (Yang et al., 2002). The mutational profiles and signaling pathways involved in LuAD are highly heterogeneous from patient to patient. A relatively common somatic mutation in LuAD is in the TP53 gene (46% of cases). TP53 is one of the most important human tumor suppressors and involved in multiple different cellular processes. Therefore, it is considered “the guardian of the genome,” and often mutated in many different cancers (Lane, 1992). Somatic mutations in EGFR are found in 32% of LuAD cases, especially in non-smokers. Mutated EGFR is constantly activated and results in uncontrolled cell proliferation (Bethune et al., 2010). Somatic mutations commonly found in smokers are in the proto-oncogene KRAS (32% of cases). KRAS is then permanently active, and this results in uncontrolled signaling of the RAS/MAPK pathway, leading to increase cell proliferation (Herbst et al., 2018; Reck et al., 2021). Notably, in LuAD patients mutations in KRAS and EGFR are mutually exclusive (Suda et al., 2010). In some LuAD cases TERT, MDM2, and MYC genes are amplified, or CDKN2A and BRAF are mutated (Shi et al., 2022). Chromosomal rearrangements in membrane tyrosine kinase receptors such as anaplastic lymphoma kinase (ALK) and proto-oncogene tyrosine-protein kinase ROS (ROS1) are also found to a lesser extent in LuAD patients (Song et al., 2017).

Staging of LuAD is an important aspect of the initial diagnosis and selection of the best treatment strategy. Therefore, the TNM system is used for LuAD, which considers three factors: Tumor size and extent (T), Nodal involvement (N), and whether the cancer has metastasized (M) (Lababede & Meziane, 2018). Based on this classification, the following stages are distinguished: Stage I: The cancer is small and limited to the lung. Stage II: The cancer is larger or has spread to nearby lymph nodes. Stage III: The cancer has spread to lymph nodes in the center of the chest. Stage IV: The cancer has spread to distant body parts (Myers & Wallen, 2024). In the early stages (I, II, and IIIA) of LuAD, the best treatment approach is surgical removal of the tumor by lobectomy or pneumonectomy with adjuvant radiation therapy after surgery (Myers & Wallen, 2024). Systemic treatment with platinum-based doublet chemotherapy, for example Cisplatin, is commonly used in advanced stages (IV) unresectable tumors, or also as adjuvant therapy following surgery to eliminate residual cancer cells (Bodor et al., 2018).

LuAD have become the poster child for patient-based targeted therapy using tyrosine kinase inhibitors for LuADs with specific molecular profiles. Gefitinib is a clinically approved first-generation tyrosine kinase inhibitor. An example for a clinically approved second-generation inhibitor is Dacomitinib and Osimertinib is a third-generation inhibitor. Most of the tyrosine kinase inhibitors are more effective than chemotherapy in patients with EGFR mutations (Johnson et al., 2022). LuAD patients harboring a BRAF V600 mutation can be treated with Dabrafenib (Odogwu et al., 2018). Crizotinib is approved by the FDA as a first-line therapy in LuAD patients that have a translocation in the ROS1 or ALK gene (Chuang & Neal, 2015). In addition, patients that do not have these targetable mutations can be treated with immune checkpoint inhibitors. A very prominent example for an approved immunotherapy is the PD-1 inhibitor Pembrolizumab (Gandhi et al., 2018). This drug is used as first-line treatment for patients who have a high PD-L1 expression in their tumors. It binds to the PD-1 receptor and blocks it from binding to ligands that would deactivate the immune cell, therefore restoring T-cell-mediated antitumor immunity. Additionally, Pembrolizumab is an approved treatment in combination with platinum-based chemotherapy for LuAD patients independent of PD-L1 expression levels, (Verschueren et al., 2023).

However, tumors can acquire additional mutations in these targeted tyrosine kinase receptors or downstream signaling mediators and develop resistance to many of the discussed therapies (Ashrafi et al., 2022). In addition, a significant number of LuAD patients lack identifiable mutations in the described oncogenic drivers. Together, this underscores the necessity of getting a better understanding of the molecular pathogenesis of this disease.

3 Aim of this study

3.1 KLHL14 in B-cell malignancies

B-cell malignancies account for 95% of lymphomas and arise from B-cells at various stages of development. Depending on the specific subtype of B-cell malignancy different genetic alterations lead to uncontrolled proliferation and failed terminal differentiation (Thandra, Barsouk, Saginala, Padala, et al., 2021). Immune chemotherapy can cure some of the B-cell malignancies like DLBCL in 50% of cases, but entities such as MCL and MM remain incurable. This emphasizes the need for new therapeutic targets and a better understanding of the molecular pathogenies of the disease (Kuppers, 2005; Poletto et al., 2022; Pu et al., 2022).

The UPS is one of the major players that regulates protein abundance and aberrations of the UPS have been implicated in the pathophysiology of several malignancies (Deng et al., 2020). B-cell lymphomas often exhibit mutations in UPS-related genes, such as chronic activation of NF-κB signaling (Choi et al., 2020) and approved treatments that target the UPS include Carfilzomib and Bortezomib (Nunes & Annunziata, 2017). Despite these available proteasomal inhibitors, most B-cell lymphomas develop resistance to the therapy due to additional mutations (Hill et al., 2020; Stalker & Mark, 2022). Together, this suggests that aberrant UPS functioning drives B-cell lymphomas and further highlights the need to better understand the role of UPSs in these malignancies and to identify novel E3-ligase-substrate pairs as potential drug targets (Choi & Busino, 2019; Di Costanzo et al., 2020; Suh et al., 2013).

This study aimed to (I) identify novel UPS members involved in B-cell lymphomas, focusing on MM, MCL, and DLBCL patient samples and data; (II) characterize the molecular function and phenotype of the novel UPS members in these entities; (III) and identify and characterize disease-relevant ubiquitylated substrates using mass spectrometry-based screens.

3.2 DCAF7 in Lung Adenocarcinoma

Lung cancer is the leading cause of cancer-related death globally, with 1.8 million deaths in 2023 and an estimated increase to 2.9 million deaths in 2040 (Ferlay et al., 2021). LuAD is the most common subtype of lung cancer and oncogenic driver mutations that are involved in disease initiation and progression are highly heterogeneous between patients (de Sousa & Carvalho, 2018). Furthermore, not all driver mutations and underlying pathways have been discovered; of those that have, only a small proportion are targetable with current drugs. In addition, the development of drug resistance is a common feature in LuAD (Ashrafi et al., 2022).

All this underscores the urgency of identifying new drug targets by better understanding the pathophysiological mechanisms that play key roles in LuAD. Dysregulation of the UPS has been implicated in the pathophysiology and maintenance of several cancers (Fhu & Ali, 2021; LaPlante & Zhang, 2021; Rohondia et al., 2020). In addition, as previously described, anticancer drugs targeting protein degradation by the UPS through inhibiting the proteasome have been approved by the FDA in B-cell lymphomas (Takahashi et al., 2017).

Therefore, this study aimed to (I) discover novel vulnerabilities within the UPS in LuAD by analyzing a CRISPR Cas-9 dropout screen for E3 ligase complexes; (II) characterize the molecular function and pathways of these vulnerabilities in LuAD; (III) and find interaction partners and ubiquitylated substrates of E3 ligases by proteome and interactome screens based on mass spectrometry.

4 Material and methods

4.1 Material

4.1.1 Devices and Instruments

Device	Supplier
Accuri C6 plus	BD Biosciences
Aqualine water bath	Lauda-Brinkmann
Axiovert 40 CFL with HBO50	Carl Zeiss
BioSAFE SC-smart CHRONOS 220	Cryotherm
BransonSonifier 250	Heinemann
Centrifuge 5417R with rotor F453011	Eppendorf
Centrifuge 5424 with rotor FA452411	Eppendorf
ChemiDoc MP Imaging System	Bio-Rad Laboratories
Concentrator plus	Eppendorf
Curix 60	Agfa
ENVAIReco safe Comfort Sterilwerkbänke	ENVAIR
FACS Aria Fusion	BD Biosciences
FACS BD ISR II	BD Biosciences
Fridges and freezers	Liebherr
Gel IX IMAGER 20	INTAS
GloMax Discover Multimode Microplate Reader	Promega
HERAcell 150i CO2 incubator	ThermoFisher Scientific
HERAfreeze	ThermoFisher Scientific
HERASafe KS safety cabinet	ThermoFisher Scientific
HypercassetteTM	Amersham Biosciences
Innova 40 shaker for bacteria	New Brunswick Scientific
Invitrogen Chamber for Ready Gels	Invitrogen
LTQ Orbitrap Velos mass spectrometer	Thermo Fisher Scientific
Magnetic Themo Stirrer RCT Basic	IKA Laboratory Equipment
Mastercycler nexus	Eppendorf
Mini-PROTEAN Tetra Cell SDS Electrophoresis System	Bio-Rad Laboratories
Mini-Sub® Cell GT system for agarose gel electrophoresis	Bio-Rad Laboratories
Multifuge 3SR+	ThermoFisher Scientific
NanoPhotometer	Implen
Neubauer Chamber	Marienfeld
Novex Mini Cell System for precast NuPAGE gels	ThermoFisher Scientific
Orbitrap Eclipse Tribrid Tribrid Mass Spectrometer	ThermoFisher Scientific
Orbitrap Fusion Lumos Tribrid Mass Spectrometer	ThermoFisher Scientific
peqSTAR Thermocycler	Peqlab Biotechnology
Pipetman Neo	Gilson
Polymax 1040 Platform Shaker	Heidolph Instruments

PowerPac Basic Power Supply	Bio-Rad Laboratories
PowerPac HC Power Supply	Bio-Rad Laboratories
Precision balance 572-37	Kern & Son
QuantStudioTM 5 Real-Time-PCR machine	ThermoFisher Scientific
Quintix Analytical Balance	Sartorius
Rotina 380R centrifuge	Hettich
RS-VA 10 Vortexer	Phoenix Instrument
Scanner V850 Pro	Epson
SevenCompact pH/Ion pH-meter	Mettler-Toledo
SP8 Confocal Microscope	Leica Microsystems
Thermo block MBT250	Kleinfeld Labortechnik
Thermomixer Compact	Eppendorf
Tube Rotator	Fröbel Labortechnik
Tumbling Roller Mixer RM5	Neolab

4.1.2 Consumables

Consumable	**Supplier**
3mm CHR paper (Whatman)	GE Healthcare
Biodyne™ B Nylon Membrane	Thermo Fisher Scientific
Cell culture flasks	Greiner Bio-One
Cell culture plates	Biochrom/Falcon/Techno Plastic Products
Cell scraper	Sarstedt
CL-XPosure™ Films	Thermo Fisher Scientific
Cryo tubes	Sarstedt
Glass Cover slips for microscope slides	Sarstedt
Hypodermic needles	Braun
Immobilon-P PVDF transfer membrane	Millipore
Insulin syringes Microfine Plus 29G	BD Biosciences
MicroAmp Fast 96-Well Reaction Plate	Applied Biosystems
MicroAmp Optical Adhesive Film	Applied Biosystems
PCR Tubes	VWR
Pierce Protein Concentrators PES 10K MWCO	ThermoFisher Scientific
Pipette tips	Sarstedt
Reagent reservoirs	VWR
SafeSeal tubes	Sarstedt
Serological pipettes	Greiner Bio-One
Syringe filters	TPP/Biochrom
Syringes	Braun
UVette routine pack	Eppendorf
x-well chamber slides on PCA detachable	Sarstedt

4.1.3 Chemicals and Reagents

Chemical/reagent	**Supplier**

16 % Formaldehyde, mehtanol free	Thermo Fisher Scientific
2-Chloracetamide (CAA)	Sigma-Aldrich
2-Propanol	Carl Roth
3-(N-morpholino)propanesulfonic acid (MOPS)	Sigma-Aldrich
3x FLAG Peptide	Sigma-Aldrich
4-Methylmorpholine	Sigma-Aldrich
5- Bromo-2′-deoxyuridine (BrdU)	Sigma-Aldrich
Acetic acid glacial	Carl Roth
Acetone	Carl Roth
Acetonitrile (ACN)	Sigma-Aldrich
Agarose NEEO	Carl Roth
Albumin Fraction V (BSA)	Carl Roth
Ammonium persulfate (APS)	Sigma-Aldrich
Ampicillin sodium salt	Sigma-Aldrich
Anti-FLAG M2 Affinity Gel	Sigma-Aldrich
Anti-HA-Agarose	Sigma-Aldrich
Aprotinin from bovine lung	Sigma-Aldrich
Aqua ad injectabilia, sterile	B. Braun Melsungen
Bacto Agar	BD Diagnostics
Bacto Tryptone	BD Diagnostics
Bacto Yeast Extract	BD Diagnostics
BES buffered saline	Sigma-Aldrich
Beta-Glycerolphosphate disodium salt hydrate (G-2-P)	Sigma-Aldrich
Beta-Mercaptoethanol	Sigma-Aldrich
Blasticidin S HCl	Thermo Fisher Scientific
Boric acid	Sigma-Aldrich
Bortezomib	Janssen-Cilag
Brilliant Blue R 250	Carl Roth
Bromphenol Blue	Sigma-Aldrich
Calcium chloride dihydrate	Sigma-Aldrich.
CellTrace FarRed	Thermofisher
CS&T Beads	BD Biosciences
Cycloheximide (CHX)	Sigma-Aldrich
Deoxycholic acid sodium salt	Sigma-Aldrich
Di-Sodium hydrogene phosphate dihydrate	Merck
Dimethyl pimelimidate (DMP)	Sigma-Aldrich
Dimethylsulfoxid (DMSO)	Carl Roth
Disodium Phosphate	Carl-Roth
DL-Dithiothreitol	Sigma-Aldrich
DNA Loading Dye (6x)	Thermo Fisher Scientific
DNA Stain Clear G	SERVA Electrophoresis
dNTP Mix, 10 mM each	Thermo Fisher Scientific
Dodecylsulfate-Na-salt (in pellets, SDS))	SERVA
Doxycyline Monohydrat	Sigma-Aldrich

era-Mag SpeedBead Carboxylate-modified Magnetic particles B	Cytiva
Ethanol	Merck
Ethylene-bis(oxyethylenenitrilo)tetraacetic acid (EGTA)	Sigma-Aldrich
Ethylenediaminetetraacetic acid (EDTA)	Sigma-Aldrich
FACS Clean	BD Biosciences
FACS Flow	BD Biosciences
FACS Rinse	BD Biosciences
Fluoride ion solution (NaF)	Sigma-Aldrich
Formaldehyde (16 % w/v) (PFA)	ThermoFisher Scientific
Formic acid (FA)	Merck
Gelatin from cold water fish skin	Sigma-Aldrich
Gibco™ Trypan Blue Solution, 0.4%	Thermo Fisher Scientific
Glucose	Sigma-Aldrich
Glutathione Sepharose 4B	GE Healthcare
Glycerol	Sigma-Aldrich
Glycin	Carl Roth
Hexadimethrine bromide (polybrene)	Sigma-Aldrich
Hexanucleotide Mix, 10x conc.	Roche
Hoechst3342	Sigma-Aldrich
Hydrochloric acid 32%	Carl Roth
Hydrochloric acid fuming 37%	Carl Roth
IL6	Peprotech
Imidazole	Sigma-Aldrich
Leupeptin	Sigma-Aldrich
Lipofectamine 2000 Reagent	Thermo Fischer Scientific
Lipofectamine RNAiMAX Reagent	Thermo Fischer Scientific
Liproxstatin-1	MedChem Express
Live/dead Fixable Dead Cell Stain APC-coupled	ThermoFisher Scientific
Magnesium chloride anhydrous	Sigma-Aldrich
Magnesium sulfate anhydrous	Sigma-Aldrich
Methanol	J. T. Baker
MG132	Tocris
N-(2-Hydroxyethyl)piperazine-N`-2-ethane sulfonic acid (HEPES)	SERVA
N-p-Tosyl-L-phenylalanine chloromethyl ketone (TPCK)	Sigma-Aldrich
N,N,N`,N``-tetramethyl-ethylenediamine (TEMED)	Sigma-Aldrich
Ni-NTA Agarose	Qiagen
Nonidet P-40 substitute (10%)	Roche
NuPAGE MES SDS Running buffer (20x)	Thermo Fisher Scientific
Nα-Tosyl-L-lysine chloromethyl ketone hydrochloride (TLCK)	Sigma-Aldrich
Okadaic Acid Prorocentrum sp.	Calbiochem

PBS Dulbecco, powder	Biochrom
Penicillin-Streptomycin (10.000 U/mL)	Thermo Fisher Scientific
Phalloidin-iFluor 647 Conjugate	AAT Bioquest
Phenylmethanesulfonylfluoride solution (PMSF)	Sigma-Aldrich
PI/RNase staining buffer	BD Pharmingen
Poly-D-Lysin hydrobromide	Sigma-Aldrich
Poly-L-Lysin solutuon 0.1%	Sigma-Aldrich
Ponceau S solution	Sigma-Aldrich
Potassium chloride	Sigma-Aldrich
PowerUPTM SYBRTM Green Master Mix	ThermoFisher Scientific
ProLong™ Diamond Antifade Mountant	Thermo Fisher Scientific
Propidium iodide	Sigma-Aldrich
Protein G Agarose, Fast Flow	Sigma-Aldrich
Protein G Sepharose 4 Fast Flow	GE Healthcare
Puromycin	Thermo Fisher Scientific
RNaseOUT Recombinant Ribonuclease Inhibitor	Thermo Fisher Scientific
Rotiphorese NF-Acrylamide/Bis-solution 40% (29:1)	Carl Roth
Saponin	Sigma-Aldrich
Sera-Mag SpeedBead Carboxylate-modified Magnetic particles A	Cytiva
Sheath Additive	BD Biosciences
Skim Milk Power	Sigma-Aldrich
SOC Medium	New England Biolabs
Sodium acetate	Merck
Sodium azide	Merck
Sodium carbonate	Merck
Sodium chloride	Carl Roth
Sodium dihydrogen phosphate monohydrate	Merck
Sodium fluoride	Sigma-Aldrich
Sodium hydroxide solution 45%	Carl Roth
Sodium orthovanadate	Sigma-Aldrich
Sodium phosphate dibasic	Sigma-Aldrich
Sodium tetraborate decahydrate (Borax)	Sigma-Aldrich
Sodium thiosulfate pentahydrate	Sigma-Aldrich
Strep-Tactin Superflow	IBA Lifesciences
Succores	Sigma-Aldrich
SuperSignal West Femto Maximum Sensitivity Substrate	Thermo Fisher Scientific
SuperSignal West Pico Chemiluminescent Substrate	Thermo Fisher Scientific
TMT10plex	Thermo Fisher Scientific
Trichloroacetic acid solution (TCA)	Sigma-Aldrich
Trifluoroacetic acid (TFA)	Sigma-Aldrich
Tris	Carl Roth
Tris Buffered Saline (10x)	Sigma-Aldrich

Triton X-100	Sigma-Aldrich
Trypsin inhibitor from soybean	Sigma-Aldrich
Trypsin-EDTA (0.5%), no phenol red	Thermo Fisher Scientific
Tween 20	Sigma-Aldrich

4.1.4 Commercial Kits

Kit	Supplier
DC Protein Assay	Bio-Rad
DNeasy Blood & Tissue Kit	Qiagen
GeneJET Gel Extraction Kit	Thermo Fisher Scientific
In-FusionR HD Cloning Kit	Takara Bio USA
innuPREP RNA Mini Kit	Innuscreen GmbH
NucleoBond Xtra Midi	MACHEREY-NAGEL
peqGOLD Plasmid Miniprep Kit	Peqlab
Pierce BCA Protein Assay	Thermo Fisher Scientific
Pierce™ Silver staining kit	Thermo Fisher Scientific
PTMScan Ubiquitin Remnant motif (K-e-GG) Kit	Cell Signaling Technology
QIAquick PCR Purification Kit	Qiagen
QIAshredder	Qiagen
Rapid DNA Dephos & Ligation Kit	Roche
RNase-Free DNase Set	Qiagen
RNeasy Mini Kit	Qiagen

4.1.5 Enzymes

Enzyme	Manufacturer
AgeI (BshTI)	Thermo Fisher Scientific
BamHI	Thermo Fisher. Scientific
BclI	Thermo Fisher. Scientific
DpnI	Thermo Fisher Scientific
EcoRI	Thermo Fisher Scientific
HindIII	Thermo Fisher Scientific
HpaI	Thermo Fisher Scientific
NheI	Thermo Fisher Scientific
NotI	Thermo Fisher Scientific
Q5 DNA-polymerase	New England Biolabs
SalI	Thermo Fisher Scientific
XbaI	Thermo Fisher Scientific
XhoI	Thermo Fisher Scientific
XmaI	Thermo Fisher Scientific

4.1.6 Oligonucleotides

Oligonucleotide	Sequence (5'-3')	Vector
Cloning Oligonucelotides		
DCAF7_NheI_fw	CCGGCTAGCATGTCCCTGC	pcDNA3.0
DCAF7_XhoI_rv	CCGCTCGAGCTACACTCTGA	pcDNA3.0
DCAF7_BclI_fw	CCGTGATCAATGTCCCTGC	pcDNA3.0
DCAF7_BclI_fw_2	CCGTGATCAATGTCCCTGCACGGCAAA	pcDNA3.0 /pcDNA-FLAG
DCAF7_NheI_fw_2	CCGGCTAGCATGTCCCTGCACGGCAAA	pHIV
DCAF7_XhoI_rv_2	CCGCTCGAGCTACACTCTGAGTATCTCC	pHIV
DCAF7_NheI_FLAG_FW	GCC GCT AGC GCC ACC ATG GAC TAC AAA GAC GAT GAC GAC AAG TCC CTG CAC GGC AA	pHIV
DCAF7_HindIII_RV	CCC AAG CTT CTA CAC TCT GAG TAT CTC	pcDNA3.1 /pcDNA-FLAG
DCAF7_HindIII_FLG_Rv	CCC AAG CTT CTA CTT GTC GTC ATC GTC TTT GTA GTC CAC TCT GAG TAT CTC	pcDNA3.1 /pcDNA-FLAG
DCAF7 _NheI_Fw	GCT AGC GCC ACC ATG TCC CTG CAC GGC AA	pcDNA3.1 /pcDNA-FLAG
DCAF7_HpaI_FLAG_FW	CCC GTT AAC GCC ACC ATG GAC TAC AAA GAC GAT GAC GAC AAG TCC CTG CAC GGC AA	pcDNA3.1 /pcDNA-FLAG
DCAF7_XmaI_RV	CCC GGG CTA CAC TCT GAG TAT CTC	pHIV
DCAF7_XmaI_FLAG_Rv	CCC CCC GGG CTA CTT GTC GTC ATC GTC TTT GTA GTC CAC TCT GAG TAT CTC	pHIV
DCAF7 _HpaI_Fw	GTT AAC GCC ACC ATG TCC CTG CAC GGC A	pHIV
KLHL14_NheI_FWD	GCC GCTAGC TCCAGATCCGGGGACAGG	pHIV
KLHL14_SalI_RV	GCCGTCGACTTATTTGTTGTATGGTAC	pcDNA3.1 /pcDNA-FLAG
KLHL14_XbaI_FWD	GCCTCTAGAGCCACCATGTCCAGATCCGGG	pcDNA3.1 /pcDNA-FLAG
KLHL14_BamHI_RV	GCCGGATCCTTATTTGTTGTA	pHIV
KLHL14_XbaI_FLAG_FWD	GCCTCTAGAGCCACCATGGACTACAAAGACGATGACGACAAGTCCAGATCCGGG	pHIV
KLHL14_AgeI_FWD	GCCACCGGTGCCACCATGTCCAGATCCGGGGACAGGA	pHIV

KLHL14_MluI_RV	GCCACGCGTTTATTTGTTGTATGGTAC	pTRIPZ
KLHL14_AgeI_FLAG_FWD	GCCACCGGTGCCACCATGGACTACAAAGACGATGACGACAAGTCCAGATCCGGGGA	pTRIPZ
KLHL14_SalI_del_KELCH6_RV	GCCGTCGACTTAGCTGTCATCAAGCACTGCAC	pTRIPZ
KLHL14_SalI_del_KELCH5-6_RV	GCCGTCGACTTAGCGATCATTCATTACA	pcDNA3.1
KLHL14_SalI_del_KELCH4-6_RV	GCCGTCGACTTACCCATTGTGCA	pcDNA3.1
KLHL14_SalI_del_KELCH3-6_RV	GCCGTCGACTTACTTGTCCAACCGA	pcDNA3.1
KLHL14_SalI_del_KELCH2-6_RV	GCCGTCGACTTAGTTTTCCACCTC	pcDNA3.1
KLHL14_SalI_del_KELCH_RV	GCCGTCGACTTATTTCTTGTTAGAGCGAATT	pcDNA3.1
KLHL14_del_BTB_C-term_FWD	GCAGCTGTTTGACACGGTGGAGGA	pcDNA3.1
KLHL14_del_BTB_N-term_RV	TCCTCCACCGTGTCAAACAGCTGCTTC	pcDNA3.1
KLHL14_del_BTB_BACK_C-term_FWD	GAAGCAGCTGTTTTCAGTGGATTTCA	pcDNA3.1
KLHL14_del_BTB_BACK_N-term_RV	TGAAATCCACTGAAAACAGCTGCTTC	pcDNA3.1
NUDCD3_pHIV_XbaINFlag_FW	GCC TCT AGA GCC ACC ATG GAC TAC AAA GAC GAT GAC GAC AAG GAG ACA GGG GCG	pcDNA3.1
NUDCD3_pHIV_BamHI_RV	GCC GGA TCC TTA AAA CTG CAC AGC CCC CGG GGA	pHIV
NUDCD3_pHIV_XbaI_FW	GCC TCT AGA GCC ACC ATG GAG ACA GGG GCG	pHIV
NUDCD3_pHIV_BamHICFLG_RV	GCC GGA TCC CTA CTT GTC GTC ATC GTC TTT GTA GTC TTA AAA CTG CAC AGC CCC CGG GGA	pHIV
NUDCD3_pHIV_XbaINMyc_FW	GCCTCTAGAGCCACCATGGAACAGAAACTGATCTCTGAAGAAGACCTGGAGACAGGGGCG	pHIV
NUDCD3_pHIV_BamHIMYC_RV	GCCGGATCCCTACAGGTCTTCTTCAGAGATCAGTTTCTGTTCTTAAAACTGCACAGCCCCCGGGGA	pHIV
		pHIV
shRNA sequences		
shCTRL	CCTAAGGTTAAGTCGCCCTCG	
shDCAF7_1	GCTGAAGGAGAGATCAACAAT	
shDCAF7_2	GCTGGAGTGTTTGCTAAACAA	
shDCAF7_3	GTTCAGCTTGTTGGTTTAGAT	
shNUDCD3_1	CCTGAGAAAGACTTGTCATTT	
shNUDCD3_2	TGAGCAAGGTGGGCGAGTATT	

shNUDCD3_3	CCCAGCAAATTGGGATCACAT	
Sequencng Primer		
pTRIPZ_Seq_rv	GCGGGCCGCTGTCCTGAG	
pTRIPZ_Seq_fw	GTCGAGGTAGGCGTGT	
pHIV seq_FWD	TGG AAT TTG CCC TTT TTG AG	
pHIV seq_RV	AGG AAC TGC TTC CTT CAC GA	
pcDNA3_for	GGCTAACTAGAGAACCCACTG	
pcDNA3_rev	GGCAACTAGAAGGCACAGTC	
qPCR Primer		
qPCR control RPLP0_Fw	GCACTGGAAGTCCAACTACTTC	
qPCR control RPLP0_RV	TGAGGTCCTCCTTGGTGAACAC	
qPCR_DCAF7_fw	AGGGATCCACATGAGCTTTG	
qPCR_DCAF7_rv	CAGCTTCGTGGAGGAGTACA	
sgRNA sequences		
sgDCAF7_1	GCATGTCGTATCAATGCTTG	
sgDCAF7_2	TTCATCGCGTAGACTGTCCA	
sgNT	ACGGAGGCTAAGCGTCGCAA	
sgPOLR2I	GAACCGCATTCTGCTCTACG	
siRNA		
siNT pool	DHARMACON (D-001810-10)	
siDCAF7 pool	DHARMACON (L-019999-00-0005)	

4.1.7 Bacteria

Bacteria strain	**Supplier**
NEB 5-alpha competent *E. coli*	New England Biolabs

4.1.8 Standards

Standard	**Supplier**
GeneRuler 1 kb DNA Ladder	Thermo Fisher Scientific
PageRuler Plus Prestained Protein Ladder	Thermo Fisher Scientific

4.1.9 Plasmids

Plasmid	**Origin**
DCAF7 N-FLAG in pCDNA 3.1 (+) Zeo	V. Wagner

lentiGuide GFP DCAF7 gRNA_3	V. Wagner
lentiGuide GFP DCAF7 gRNA_4	V. Wagner
pcDNA - N-FLAG-NUDCD3	T. Schulze
pcDNA 3.1 DCAF7	V. Wagner
pcDNA Flag A	F. Bassermann
pcDNA3 (N)Flag-DCAF7	V. Wagner
pcDNA3 (N)Flag-Strep-DCAF7	V. Wagner
pcDNA3 (N)HA-DCAF7	V. Wagner
pCDNA3.1 Myc-KLHL14	R. Spallek,
pcDNA3.1-(+) zeo	Thermo Fisher Scientific
pcDNA3.1-N-FLAG	Prof. F. Bassermann
pcDNA3.1-N-FLAG-KLHL14	R. Spallek,
pcDNA3.1-N-FLAG-KLHL14_deltaBTB	R. Spallek,
pcDNA3.1-N-FLAG-KLHL14_deltaKELCH	R. Spallek,
pHIV eGFP (N) Flag DCAF7	V. Wagner
pHIV eGFP (N) Flag Empty Vector	V. Wagner
pHIV eGFP (N)SF-TAP DCAF7	V. Wagner
pHIV EGFP NUDCD3	T. Schulze
pHIV EGFP NUDCD3 N-FLAG Tag	T. Schulze
pHIV EGFP NUDCD3 N-MYC Tag	T. Schulze
pHIV puro (N) SF-TAP DCAF7	V. Wagner
pHIV-EGFP-KLHL14	R. Spallek,
pHIV-EGFP-N-FLAG-KLHL14	R. Spallek,
pHIV-EGFP-N-FLAG-KLHL14_deltaBTB	R. Spallek,
pHIV-EGFP-N-FLAG-KLHL14_deltaKELCH	R. Spallek,
pLKO dsRed sh_scramble	M. Heider, AG Bassermann
pLKO dsRed shDCAF7_1	V. Wagner
pLKO dsRed shDCAF7_2	V. Wagner
pLKO dsRed shDCAF7_3	V. Wagner
pLKO dsRed shNUDCD3 _1	T. Schulze
pLKO dsRed shNUDCD3 _2	T. Schulze
pLKO dsRed shNUDCD3 _3	T. Schulze
plko-puro shDCAF7_1	V. Wagner
plko-puro shDCAF7_2	V. Wagner
plko-puro shDCAF7_3	V. Wagner
pLKO.1 TRC cloning vector	Addgene (#10878), D. Root
pLKO.1-Puro-sh_scramble	Addgene (#1864), D. Sabatini
pMD2.G	Addgene (#12259), D. Trono
pMSCV	Clontech
pRK5_HA_ubi_K11 only	R. Spallek,
pRK5_HA_ubi_K27 only	R. Spallek,
pRK5_HA_ubi_K29 only	R. Spallek,
pRK5_HA_ubi_K6 only	R. Spallek,
pRK5_HA_ubi_WT	M. Heider, AG Bassermann
pRK5-HA Ubi K63 only	R. Spallek,

pRK5-HA_EV	M. Heider, AG Bassermann
pRK5-HA_ubi_K33 only	R. Spallek,
pRK5-HA-Ubiquitin-WT	Addgene (#17608), T. Dawson
pRKS-HA ubi K48 only	R. Spallek,
psPAX2	Addgene (#12260), D. Trono
pTRIPZ	Thermo Fisher Scientific
pTRIPZ-KLHL14	R. Spallek,
pTRIPZ-N-FLAG-KLHL14	R. Spallek,
pTRIPZ-RFP_only	R. Spallek,

4.1.10 Antibodies

Antibody (clone)	**Species**	**Dilution**	**Supplier**
a/ß-tubulin	Rabbit	1:1000 (WB), 1:400 (IF)	Cell Signaling Technology (#2148)
AKT	Rabbit	1:1000 (WB)	Cell Signaling Technology (#9272)
anti-mouse IgG Alexa Fluor 488	Goat	1:1000 (IF)	Invitrogen (#A11001)
anti-mouse IgG Alexa Fluor 594	Goat	1:1000 (IF)	Invitrogen (#A11005)
anti-rabbit IgG Alexa Fluor 488	Goat	1:1000 (IF)	Invitrogen (#A11008)
anti-rabbit IgG Alexa Fluor 594	Goat	1:1000 (IF)	Invitrogen (#A11012)
ATF4	Rabbit	1:1000 (WB)	Cell Signaling Technology (#11815)
BUB3	Rabbit	1:1000 (WB)	Abcam (#AB4180-100)
Caspase 3	Rabbit	1:1000 (WB)	Cell Signaling Technology (#9662S)
CDC20	Rabbit	1:1000 (WB)	Cell Signaling Technology (#4823S)
Centrin-3 (SS12)	Mouse	1:1000 (WB), 1:400 (IF)	Santa Cruz Biotechnology (#sc-100933)
Cleaved Caspase-3 (Asp175)	Rabbit	1:1000 (WB)	Cell Signaling Technology (#9664S)
Cul3	Rabbit	1:1000 (WB)	Cell Signaling Technology (#2759)
Cul3	Rabbit	1:1000 (WB)	Proteintech (#11107-1-AP)
Cul3	Mouse	1:1000 (WB)	Sigma (#Sag4200180)
Cul4A	Rabbit	1:1000 (WB)	Betyl (#A300-739A)
Cyclin A (H-432)	Mouse	1:1000 (WB)	Santa Cruz Biotechnology (#sc-751)
Cyclin B1	Rabbit	1:500 (WB)	Cell Signaling Technology (#4138)
Cyclin D1 (G124-326)	Mouse	1:500 (WB)	BD Biosciences (#554180)
Cyclin E (HE12)	Mouse	1:1000 (WB)	Santa Cruz Biotechnology (#sc-247)
DAG1	Rabbit	1:1000 (WB)	Proteintech (#11017-1-Ap)

DDB1	Rabbit	1:1000 (WB)	Betyl (#A300-462A)
DHRS4	Rabbit	1:1000 (WB)	Proteintech (#15279-1-AP)
ECL anti-mouse IgG, HRP-linked	Sheep	1:30.000 (WB)	GE Healthcare (#NA931)
ECL anti-rabbit IgG, HRP-linked	Doneky	1:30.000 (WB)	GE Healthcare (#NA934)
ERK1/2	Mouse	1:1000 (WB)	Santa Cruz (#sc-514302)
FLAG	Rabbit	1:1000 (WB), 1:800 (IF)	Sigma-Aldrich (#F7425)
FLAG-M2	Mouse	1:1000 (WB), 1:800 (IF)	Sigma (#F3165)
GAPDH	Mouse	1:1000 (WB)	Santa Cruz (#sc-47724)
HA	Rabbit	1:1000 (WB)	Cell Signaling Technology (#3724)
KLHL14	Rabbit	1:1000 (WB), 1:100 (IF)	Proteintech (#16693-1-AP)
LC3A/B	Rabbit	1:1000 (WB)	Cell Signaling Technology (#12741S)
mTOR	Rabbit	1:1000 (WB)	Cell Signaling Technology (#2972S)
Myc-Tag	Rabbit	1:1000 (WB)	Millipore (#06-549)
NRF2	Mouse	1:1000 (WB)	Santa Cruz (#sc-365949)
NUDCD3	Rabbit	1:1000 (WB)	Proteintech (#11764-1-AP)
NUDCD3 (H-10)	Mouse	1:1000 (WB)	Santa Cruz Biotechnology (#sc-514016)
p-AKT (Thr308)	Rabbit	1:1000 (WB)	Cell Signaling Technology (#4056S)
p-ERK1/2	Rabbit	1:1000 (WB)	Cell Signaling Technology (#9101S)
p-Histon H2A.X (S139)	Mouse	1:1000 (WB)	Santa Cruz Biotechnology (#sc-517348)
p-Histone H3 (S10)	Rabbit	1:1000 (WB)	Cell Signaling Technology (#9701)
p-mTOR (Ser2448)	Rabbit	1:1000 (WB)	Cell Signaling Technology (#2971S)
p-p53 (S15)	Rabbit	1:1000 (WB)	Cell Signaling Technology (#9284)
p-p70 S6 Kinase (Thr389)	Rabbit	1:1000 (WB)	Cell Signaling Technology (#9234S)
p14ARF	Mouse	1:1000 (WB)	Santa Cruz Biotechnology (#sc-53639)
p21-WAF1 (EA10)	Mouse	1:1000 (WB)	Calbiochem (#0p64)
p27 (G173-524)	Mouse	1:500 (WB)	BD Biosciences (#554069)
p53	Rabbit	1:1000 (WB)	Cell Signaling Technology (#9282)
p62	Rabbit	1:1000 (WB)	Cell Signaling Technology (#5114S)
p70 S6 Kinase	Rabbit	1:1000 (WB)	Cell Signaling Technology (#9202)
PARP-1	Mouse	1:1000 (WB)	Santa Cruz (#sc-8007)
PLK1 (PL6/PL2)	mouse	1:500 (WB)	Thermo Fisher Scientific (#33-1700)

ß-actin (AC-15)	Mouse	1:5000 (WB)	Sigma-Aldrich (#A-1978)
Vinculin	Mouse	1:1000 (WB)	Santa Cruz (#sc-73614)
WDR68 / DCAF7	Rabbit	1:1000 (WB), 1:100 (IF)	Abcam (#AB138490)
XBP1	Mouse	1:1000 (WB)	Santa Cruz (#sc-8015)

4.1.11 Cell lines

Cell line	Entity	Supplier
OCI-LY7	DLBCL	DSMZ (ACC-688)
A549	Epithelial like LC	ATCC (CRM-CCL-185)
AMO-1	MM	DSMZ (ACC-538)
Granta-519	MCL	Gift of Prof. M. Dreyling
H929	MM	DSMZ (ACC-163)
HCC-44	LuAD	DSMZ (ACC 534)
HCC827	LuAD	ATCC (CRL-2868)
HEK293T	Embryonic kidney	ATCC (CRL-3216)
HL-60	AML	DSMZ (ACC 3)
IMR-90	Lung fibroblast	Gift of Dr. F. Bassermann
INA-6	MM	DSMZ(ACC 862)
Jeko	MCL	DSMZ (ACC 553)
JJN3	MM	DSMZ (ACC-541)
JVM2	MCL	DSMZ (ACC 12)
KMS12BM	MM	DSMZ (ACC-551)
L363	MM	DSMZ (ACC-49)
LP-1	MM	DSMZ (ACC-41)
MHH-PreB1	DLBCL	DSMZ (ACC 354)
MM1.S	MM	ATCC (CRL-2974)
MOLM-13	AML	DSMZ (ACC 554)
MV4-11	AML	DSMZ (ACC 102)
NCI-H1417	SCLC	ATCC (CRL-5869)
NCI-H1437	LuAD	ATCC (CRL-5872)
NCI-H1650	LuAD	ATCC (CRL-5883)
NCI-H1703	LuSC	ATCC (CRL-5889)
NCI-H1975	LuAD	ATCC (CRL-5908)
NCI-H2087	LuAD	ATCC (CRL-5922)
NCI-H2228	LuAD	ATCC (CRL-5935)

NCI-H23	LuAD	ATCC (CRL-5800)
NCI-H460	LCLC	ATCC (HTB-177)
NCI-H520	LuSC	ATCC (HTB-182)
NCI-H661	LCLC	ATCC (HTB-183)
NCI-H748	SCLC	ATCC (CRL-5841)
Oci-AML3	AML	DSMZ (ACC 582)
Oci-LY3	DLBCL	DSMZ (ACC 761)
OPM2	MM	Gift of Prof. U. Keller
OVCAR-3	ovarian carcinom	ATCC (HTB-161)
Rec1	MCL	DSMZ (ACC 584)
RPMI8226	MM	DSMZ (ACC-402)
SCLC-21H	SCLC	DSMZ (ACC 372)
Sp49	MCL	Gift of Dr. F. Bassermann
SU-DHL-10	DLBCL	DSMZ (ACC-576)
TMD8	DLBCL	Gift of Prof. D. Krappmann
U266	MM	DSMZ (ACC-9)
Z138	MCL	ATCC (CRL-3001)

4.1.12 Cell culture medium and supplements

Product	**Supplier**
Dulbecco's Modified Eagle's Medium (DMEM)	Life Technologies
Fetal Bovine Serum (FBS) superior	Biochrom Merck
Newborn Calf Serum (NCS)	Biochrom Merck
Horse Serum	Gibco
Interleukin 6 (IL-6), human	Thermo Fisher Scientific
Iscove's Modified Dulbecco's Medium (IMDM)	Life Technologies
Opti-MEM I, reduced serum medium	Life Technologies
Phosphate buffered saline (PBS), 10X, sterile	Life Technologies
Penicillin/ Streptomycin (100X)	Life Technologies
RPMI 1640 GlutaMAX medium	Life Technologies
Trypan Blue Stain (0,4%)	Life Technologies
Trypsin-EDTA (10X) solution	Biochrom Merck

4.1.13 Solutions and buffers

Borax buffer

100 mM Borax (pH 8.8)

Coomassie destaining solution

45% methanol (v/v)

10% acetic acid (v/v)

Coomassie staining solution

45% methanol (v/v)
10% acetic acid (v/v)
0.25% Brilliant Blue R-250 (w/v)

DiGLY blocking buffer

200 mM ethanolamine (PH 8.0)

DiGLY elution buffer

0.15% trifluoroacetic acid (v/v)

FACS Buffer

1x PBS
3% FBS

Freezing medium

90% FBS (heat inactivated)
10% DMSO

IF Blocking Buffer

PBS (1x)
0.25% gelatin from cold water fish skin
0.01% Saponin

IF Permeabilization Buffer

0.1% Triton-X
PBS (1x)

IF Staining Buffer

PBS (1x)
0.5% BSA
0.01% saponin

Inhibitors in WB Lysis Buffers

1 µg/mL aprotinin
1 mM DTT
10 mM G-2-P
1 µg/mL leupeptin
0.1 mM PMSF
0.1 mM Na_3VO_4
10 µg/mL soybean trypsin inhibitor 5 µg/mL TLCK
10 µg/mL TPCK

Laemmli Buffer (5x)

300 mM Tris (pH 6.8)
10% SDS
5% β-mercaptoethanol
0.05% bromphenolblue
50% glycerol

Luria-Bertani (LB) medium (1×)

1% Bacto Tryptone
0.5% Bacto Yeast Extract
170 mM NaCl

LB-agar plates

1.5% Bacto Agar
LB medium

Lysis Buffer (150 mM NaCl)

50 mM Tris (pH 7.5)
150 mM NaCl
0.1% NP40
5 mM EDTA
5 mM MgCl2
5% Glycerol

Lysis Buffer (250 mM NaCl)

50 mM Tris (pH 7.5)
250 mM NaCl
0.1% Triton X-100
1 mM EDTA
50 mM NaF

SDS Running Buffer (10×)

250 mM Tris (pH 7.5)
1.92 M glycine
1% SDS

Separating gel buffer

1.5 M TRIS (pH 8.8)

Sep-Pak Solvent A

0.1% formic acid (v/v)

Sep-Pal Solvent B

0.1% formic acid (v/v)
50% acetonitrile (v/v)

Stacking gel buffer

0.5 M TRIS (pH 6.8

StageTip Solvent A

0.1% formic acid (v/v)

StageTip Solvent B

0.1% formic acid (v/v)
60% acetonitrile (v/v)

Stripping Buffer

62.5 mM Tris (pH 6.8)
2% SDS
0.867% β-mercaptoethanol

Transfer Buffer (10x)

48 mM Tris (pH 7.5)
20% methanol
39 mM glycine

Washing Buffer

PBS (1×)

0.1% Tween 20

4.1.14 Software and databases

Software/database	Usage	Supplier
Adobe Illustrator	Generation of figures	Adobe
Basic local alignment search tool	Cloning	NCBI
cBioPortal	Databank research	Memorial Sloan Kettering Cancer Center
CellQuest Pro	Flow cytomtery analysis	BD Biosciences
CRAPome	Mass spectrometry analysis	University of Michigan and Samuel Lunenfeld Research Institute Toronto
DepMap	Databank research	Broad Institute
FlowJo Single Cell Analysis Software v10.10	Flow cytomtery analysis	Tree Star
Gene Expression Omnibus	Databank research	NCBI
GeneCardsSuite	Databank research	Weizmann Institute of Science
Grammarly/OpenAI	Spelling/proofreading	Grammarly/OpenAI
GPP Web Portal	Databank research and sh/sgRNA design	Broad Institute
Image Studio lite	Immunoblot analysis	LI-COR Biosciences
ImageJ	Immunoblot analysis	W.S. Rasband, U.S. National Institute of Health
IMARIS Viewer	IF analysis	Oxford Instruments
Immgen database	Databank research	Immunological Genome Project
Kmplot	Databank research	(Gyorffy, 2024)
Oncomine	Databank research	Thermo Fisher Scientific
Prism	Generation of figures	Graph Pad Software
Serial Cloner	Cloning	Open Source
SnapGene	Cloning	GSL Biotech LLC
The human protein atlas	Databank research	The human protein atlas consortium
TNMplot	Databank research	(Bartha & Gyorffy, 2021)
UniProt	Databank research	UniProt Consortium

4.2 Methods

4.2.1 Molecular biology

4.2.1.1 Molecular cloning

Expression vectors tools commonly used in molecular biology to alter the expression of specific genes within target cells. Expression vectors are mostly circular double-stranded DNA (dsDNA) molecules. They can be engineered using various molecular cloning techniques. For gene overexpression specific inserts (complementary DNA (cDNA)) are cloned into the vector. For gene knockout or knockdown single guide RNA (sgRNA) sequence or short hairpin RNA (shRNA) sequence are cloned into the expression vector. These inserts can either be synthesized or amplified from template DNA using the polymerase chain reaction (PCR). Both the insert and the plasmid are cut with bacterial restriction enzymes and then joined together

by an enzymatic ligation reaction to form an intact plasmid. This construct is then amplified in bacteria. Modifying the primers used in this method, can introduce various modifications into the DNA sequences, such as point mutations or deletions of larger regions within a gene of interest.

4.2.1.2 Polymerase chain reaction

PCR is a rapid *in vitro* method for amplifying specific DNA sequences, and in this study, it was primarily used to amplify cDNA. Forward and reverse primers that are homologous to the cDNA of the target gene and contain a restriction enzyme site were designed. The PCR was performed using a Q5 polymerase-based system set up according to the manufacturer's guidelines.

The annealing temperature for each PCR cycle was adjusted to the specific needs of each primer pair and was set 10 degrees Celsius (°C) below the respective melting temperature. The duration of the extension phase was adjusted based on the size of the expected PCR product and the extension rate of the NEB Q5 polymerase (20-30 sec/kb).

The general steps of the PCR reaction are detailed below. The PCR products were subjected to agarose gel electrophoresis and gel purification to confirm the correct size of the PCR product.

Reagent/compound Amount	Reagent/compound Amount
DNA-Template	20-100 ng
Forward primer (Fw) (10 µM)	2.5 µL
Reverse primer (Rv) (10 µM)	2.5 µL
dNTPs (10 mM)	1 µL
Q5-Reaction Buffer (5x)	10 µL
Q5 High GC Enhancer (5x)	10 µL
Q5-High-Fidelity Polymerase	0.5 µL
Nuclease free dH2O	To 50 µL

Program step	Temperature	Time	Repetitions
Initial Denaturation	98°C	3 min	
Denaturation	98°C	20 sec	30 Cycles
Annealing	X	30 sec	30 Cycles
Elongation	72°C	X	30 Cycles
Final Elongation	72°C	3 min	
Storage	8°C	∞	

4.2.1.3 Agarose Gel Electrophoresis and Gel Purification

After PCR or restriction enzyme digestion was completed, the DNA was separated in an electric field according to its size. This process is called gel electrophoresis. Agarose at a concentration of 1.2% (w/v) was dissolved in TAE buffer by heating. The solution was allowed to cool for 2 minutes and mixed with 3 µL DNA Stain Clear G per 100 µL agarose. The still liquid agarose solution was poured into a gel chamber with a comb inserted and solidified at room temperature (RT). The gel was then transferred to a gel running chamber and covered

with TAE buffer. PCR or restriction enzyme digest products were mixed with 6x DNA loading dye and loaded onto the gel next to a 1kb DNA ladder. Samples were run at 100V for 45 minutes. Afterwards, the DNA was visualized under ultraviolet (UV) light. If desired, specific DNA segments were cut out from the gel with a scalpel and purified using the GeneJet Gel Extraction Kit according to the manufacturer's protocol.

4.2.1.4 Restriction Digestion and Ligation of DNA

A fundamental concept in molecular cloning is the precise cutting or digestion of DNA using bacterial enzymes, followed by the joining or ligation of this DNA to another segment, such as an expression vector. These restriction enzymes can target specific DNA motifs and produce either blunt ends from a clean cut across both DNA strands or sticky ends characterized by 3' or 5' overhangs. Depending on the DNA end sequence, these cut DNA fragments can be joined together by another enzymatic reaction called ligation. To perform a restriction digest, 0.4-4 µg of gel-purified DNA (plasmid and/or insert) was combined with 0.5 µL of a selected restriction enzyme, digestion buffer, and water to a total volume of 30 µL. The digestion reaction was incubated at 37°C for 1 hour for most restriction enzymes unless otherwise specified by the manufacturer. The Rapid DNA Dephos & Ligation Kit was used to ligate DNA fragments and plasmids using 40 ng of digested plasmid (4:1 ratio) according to the manufacturer's instructions.

4.2.1.5 Annealing and ligation of short hairpin RNA (shRNA) and single guide RNA (sgRNA) oligonucleotides

Oligonucleotides for shRNA or sgRNA constructs were designed via the GPP web portal (BroadInstitute) and ordered Eurofins Genomics in Ebersberg, Germany. Next, 1 µL of forward and reverse oligonucleotides (100 µM) were added to 48 µL of buffer G. This mixture was heated to 95°C for 5 minutes in boiling water and cooled to RT over several hours to allow the complement oligos to anneal. Simultaneously the desired cloning vector was digested as described above. Next, 2 µL of the annealed oligonucleotides were added to 50 ng of the digested cloning vector (pLenti CRISPR GFP or pLKO.1 DsRed and pLKO.1 Tet puro plasmid). The Rapid DNA Dephos & Ligation Kit was used to ligate DNA fragments and plasmids according to the manufacturer's protocol. After the ligation reaction, the plasmid was transformed into chemically competent NEB 5-alpha E. coli bacteria (described in section 4.2.1.6).

4.2.1.6 Bacterial Transformation

Introducing DNA/plasmids into competent bacteria for amplification or insert verification is called bacterial transformation. For this process, 15 µL of NEB® 5-alpha Competent E. coli was added to 1.5 µL of the ligation mixture and incubated on ice for 20 minutes. Next, the mixture underwent a heat shock for 45-second at 45°C on a heat block. This allows the DNA/plasmids to enter the bacterial cells. Afterwards, the mixture was incubated on ice for 2 minutes. The mixture was then supplemented with 200 µL of SOC medium and incubated at 37°C for 20 minutes at 500 rpm. LB agar plates were prepared with the corresponding antibiotics and the mixture was plated on the LB agar plates (100 µg/mL ampicillin or 50 µg/mL kanamycin). To let positively transformed bacterial colonies grow, the plates were incubated overnight at 37°C. For further amplification bacterial colonies were picked and incubated overnight at 37°C and 250 rpm in LB medium containing the corresponding antibiotics.

4.2.1.7 Extraction of plasmid DNA from bacteria

Plasmid extraction from bacterial samples was performed using two different commercial kits, depending on the sample volume. The peqGOLD Plasmid Miniprep Kit was used for samples up to 5 mL, while the NucleoBond® Xtra Midi Kit was used for larger volumes, up to 200 mL of overnight cultures, following the manufacturer's instructions. For long-term storage of positively transformed bacteria, 300 µL glycerol was mixed with 700 µL bacterial culture and stored at -80°C. After molecular cloning to identify bacterial colonies containing the correct plasmid, the extracted plasmids were analyzed by test digestion and subsequent sequencing by Eurofins Genomics in Ebersberg, Germany, with either promoter or gene-specific primers.

4.2.1.8 RNA Isolation from Eukaryotic Cells

Cell pellets were harvested and quickly frozen before the RNA was isolated. The cell pellets were homogenized with QIAshredder spin columns to extract as much RNA as possible. Next the Qiagen RNeasy Mini Kit was used according to the manufacturer's instructions to isolate the RNA. The samples were treated with 0.5 µL DNase I buffer and incubated at 37°C for 30 minutes to digest genomic DNA. Next, EDTA was added to reach a final concentration of 5 mM. The reaction was stopped by heat-inactivation at 75°C for 10 minutes. The RNA concentration in the final eluates was determined spectrophotometrically. The samples were stored in RNase-free water at -80°C.

4.2.1.9 Reverse Transcription

The SuperScript III Reverse Transcriptase Kit from ThermoFisher Scientific was used to convert RNA into cDNA. Therefore, a mixture of 1 µg RNA, 1 µL of random hexamer primers in a total of 17.5 µL of dH2O was incubated at 70°C for 5 minutes. Afterwards, the mixture was placed on ice for 5 minutes. Next, 6 µL 5X reverse transcriptase buffer, 3 µL DTT, 0.5 µL RNase Out, 1 µL 100 mM mixed dNTPs, and 1 µL SuperScript III reverse transcriptase (ThermoFisher Scientific) was added. The mixture was incubated at 42°C for 60 minutes and subsequently heat-inactivated at 95°C for 5 minutes. The cDNA was stored at -20°C for future use.

4.2.1.10 Quantitative PCR

Quantitative PCR (qPCR) was used to analyze the expression levels of specific target genes and performed on a QuantStudioTM 5 Real-Time PCR machine. The samples were prepared following the instructions of the PowerUPTM SYBRTM Green Master Mix manufacturer's protocol. The primer-BLAST platform of NCBI was used to design qPCR primer for our genes of interest. Reverse transcribed cDNA samples were diluted to get 4 ng/uL of cDNA in H2O. For the experimental setup 96-well plates were used and 2 µL of cDNA sample was added in triplicates to the plate. Next, 10 µL LightCycler 480 SYBR Green I Master Mix (Applied Biosystems), 6.8 µL water, and 1.2 µL primer mix (including both forward and reverse primers at 10mM each) was added to each well containing cDNA sample. For the measueremnt the plate was sealed with a foil, briefly centrifuged, and loaded into the QuantStudioTM 5 Real-Time PCR instrument. In this study we ran 40 amplification cycles. For

the analyzis the samples were normalized to the expression of the housekeeping gene ribosomal protein large subunit P0 (RPLP0).

4.2.2 Cell culture and cell-based assays

4.2.2.1 Culture of eukaryotic cells

All cell lines in this study were cultured in a humidified incubator at 37°C and 5% CO2. The medium for cell culturing was always supplemented with 1% penicillin/streptomycin (Pen/Strep) and GlutaMax unless otherwise noted. Additionally, medium was supplemented with serum (FBS or FCS) in different concentrations. Before using the serum in cell culture, it was heat-inactivated at 65°C for 60 minutes. The table below shows every cell line used in this study with the respective medium.

Suspension cells were cultured in flasks until they reached densities of 1-10 x10^5 cells/mL. They were split every two days at a ratio of 1:4 to 1:10, depending on the cell line and the individual growth rate.

Adherent cells were cultured in treated cell culture plates and split at 80% confluency. To split the cells, they were once washed with phosphate buffer saline (PBS) and incubated at 37°C for 3-10 minutes with trypsin until all cells detached from the plate. Complete growth medium was added to stop the trypsin reaction. To remove the trypsin the cells were centrifuged at 1200 rpm for 4 minutes and subsequently resuspended in fresh growth medium. Depending on the cell line and the growing conditions 1/2-1/10 of the cell suspension was seeded on a new plate and cultured at 37°C and 5% CO2.

Some experience required an exact cell number. Therefore, cells were harvested as described above and diluted 1:2 in trypan blue. Subsequently, the cells were counted with a Neubauer counting chamber. The respective cell numbers were seeded onto a new culture dish with warm complete growth medium.

Cell line	Type	Culture Medium
TMD8	DLBCL-ABC	RPMI1640 + 15% FBS
OCI-Ly3	DLBCL-ABC	RPMI1640 + 20% FBS
SU-DHL-10	DLBCL-GBC	RPMI1640 + 10% FBS
OCI-Ly7	DLBCL-GBC	IMDM + 20% FBS
MHH PreB1	DLBCL-	RPMI1640 + 15% FBS
NCI-H1437	NSCLC-LuAD	RPMI1640 + 10% FBS
NCI-H1792	NSCLC-LuAD	RPMI1640 + 10% FBS
NCI-H23	NSCLC-LuAD	RPMI1640 + 10% FBS
HCC-44	NSCLC-LuAD	RPMI1640 + 10% FBS
HCC827	NSCLC-LuAD	RPMI1640 + 10% FBS

NCI-H2228	NSCLC-LuAD	RPMI1640 + 10% FBS
NCI-H1650	NSCLC-LuAD	RPMI1640 + 10% FBS
NCI-H1975	NSCLC-LuAD	RPMI1640 + 10% FBS
NCI-H520	NSCLC-LuAD	RPMI1640 + 10% FBS
NCI-H1703	NSCLC-LuAD	RPMI1640 + 10% FBS
A549	NSCLC-Epithelial	DMEM + 10% FBS
NCI-H748	SCLC	RPMI1640 + 10% FBS
NCI-H1417	SCLC	RPMI1640 + 10% FBS
OCI-AML3	AML	MEM alpha + 10% FBS
MV4-11	AML	IMDM + 10% FBS
MOLM-13	AML	RPMI1640 + 10% FBS
THP-1	AML	RPMI1640 + 10% FBS
Jeko1	MCL	RPMI1640 + 15% FBS
Z138	MCL	IMDM + 10% Horse Serum
Granta	MCL	RPMI1640 + 15% FBS
JVM2	MCL	RPMI1640 + 15% FBS
Rec1	MCL	RPMI1640 + 15% FBS
Mino	MCL	RPMI1640 + 15% FBS
SP49	MCL	IMDM + 10% FBS
OPM2	MM	RPMI1640 + 15% FBS
LP1	MM	IMDM + 20% FBS
RPMI	MM	RPMI1640 + 10% FBS
JJN3	MM	DMEM 40%, IMDM 40% + 10% FBS
U266	MM	RPMI1640 + 10% FBS
L363	MM	RPMI1640 + 15% FBS
Amo1	MM	RPMI1640 + 20% FBS

H929	MM	RPMI1640 + 15% FBS 1mM Sodium Pyruvate + 50uM ßMercaptoethanol
INA6	MM	RPMI1640 + 20% FBS 10ng/mL IL-6
KMS12BM	MM	RPMI1640 + 20% FBS
MM1.S	MM	RPMI1640 + 20% FBS

4.2.2.2 Freezing and Thawing Cells

For each freezing process fresh freezing medium was prepared. To heat inactivated FBS by adding dimethyl sulfoxide (DMSO) was added to reach a concentration of 10%. Next, cells were harvested and counted as described before (4.2.2.1). Depending on the cell line 1-10x10^6 cells were resuspended in the fresh freezing medium and transferred to cryotubes. Freezing container were prepared by adding isopropanol to ensure a gradual cooling rate of 1°C per minute later. The cryotubes were added to the freezing container and stored at -80°C for 24 hours. Next, the frozen cells were transferred to liquid nitrogen for long-term storage.

During the cell-thawing process it is important to quickly wash out the toxic DMSO. The frozen cryotubes were quickly added to a water bath at 37°C. After 30 seconds the cells were diluted in the appropriate growth medium and centrifuged to remove the DMSO. Afterwards the cells were added to fresh growth medium and cultured.

4.2.2.3 Cell Harvesting

Supernatants from cultured adherent cells were discarded, and cells were detached from the culture plates by scraping them into ice-cold PBS. Confluent cells were transferred by pipetting from the culture flask to a falcon tube. The harvested cells were spun down at 1200 rpm for 4 minutes and washed in PBS once. The supernatant was discarded, and the cell pellets were lysed for further experiments. Alternatively, the cell pellets were stored at -80°C for later use, depending on the experiment.

4.2.2.4 Calcium Phosphate DNA Transfection

Calcium phosphate method is a common assay to transiently transfect HEK293T cells with desired plasmids. One day before the transfection, HEK293T cells were harvested and counted. In a 10 cm dish 3.5x10^6 cells were seeded and cultured overnight. On the next day 10 µg DNA was diluted in 450 µL sterile dH2O and 50 µL 2.5 M CaCl2 was added. The DNA CaCL2 mixture was carefully mixed and incubated at RT for 5 minutes. Next, the mixture was vortexed continuously while 500 µL BES buffer was added dropwise. The mixture was incubated at RT for 25 minutes and subsequently added to the plated HEK293T cells. After 24 hours incubation at 37°C in 5% CO2 the medium was changes or the cells were directly harvested.

4.2.2.5 Lipofectamine 2000 DNA Transfection

Lipofectamine 2000 is another transfection method that was also used for all adherent cell lines in this study. Lipofectamine 2000 was used according to the manufacturer's instructions. Similar to the calcium phosphate method, the cells were harvested and counted one day before the Lipofectamine transfection. Depending on the cell line, the appropriate amount of cells was seeded into a new dish to get 70-80% confluency on the next day. The growth medium of the cells was changed to Pen/Strep-free medium on the next day. In two separate tubes the DNA and Lipofectamine 2000 reagent were mixed with serum free Opti-MEM medium and incubated for 5 minutes. The concentration of the DNA and the amount of the Lipofectamine was adjusted according to the amount of transfected cells. The DNA-Opti-MEM mixture was added to the Lipofectamine-Opti-MEM mixture and carefully mixed. The mixture was incubated at RT for 25 minutes and afterwards added carefully to the cells. The cell culture plate was moved carefully to distribute the DNA-Lipofectamine mixture and incubated for up to four hours in the incubator incubated at 37°C in 5% CO2. Afterwards the medium was changed to complete growth medium.

4.2.2.6 Transient transfection of cells with siRNA

To test antibody specificity or knockdown a specific gene of interest, siRNA transfection was performed according to the protocol provided by the manufacturer of the Lipofectamine RNAiMAX reagent. The cells were harvested and counted one day before the Lipofectamine RNAiMAX transfection. Depending on the cell line, the appropriate number of cells was seeded into a new dish to get 70-80% confluency on the next day. The growth medium of the cells was changed to Pen/Strep-free medium on the next day. In two separate tubes the siRNA and Lipofectamine RNAiMAX reagent were mixed with serum free Opti-MEM medium and incubated for 5 minutes. The siRNA-Opti-MEM mixture was added to the Lipofectamine-Opti-MEM mixture and carefully mixed. The mixture was incubated at RT for 25 minutes and afterwards added carefully to the cells. The cell culture plate was moved carefully to distribute the siRNA-Lipofectamine mixture and incubated for up to four hours in the incubator incubated at 37°C in 5% CO2. Afterwards the medium was changed to complete growth medium.

4.2.2.7 Production of Lentiviral Particles and Viral Transduction of Cells

Lentiviral particles were used for a stable integration of the desired DNA/plasmid sequence into the cell genome. HEK293T cells were transfected with 15 µg packaging plasmid (psPAX2), 5 µg envelope plasmid (pMD2.G), and 20 µg transgene plasmid using the calcium phosphate method described in 4.2.2.4. After 24 hours of incubation at 37°C and 5% CO2, the medium was changed to 7-10 mL of serum-free OptiMEM. After another 24 hours of incubation at 37°C and 5% CO2, the medium containing lentiviral particles was filtered through a 0.45 µm filter and either used immediately for infection/transduction or stored at -80°C.

For transduction of adherent cells, the cells were counted and seeded into appropriate culture dishes (50-70% confluency). Next, viral supernatant was added while the cells were still in suspension. The amount of viral supernatant was adjusted based on cell number and desired infection rate. 8 µg/µL Polybrene was added to increase transduction efficiency. After 24 hours of incubation at 37°C and 5% CO2, the medium was discarded, and the cells were washed twice with PBS and transferred to new dishes containing fresh culture medium.

For suspension cell lines, 1x10^6 cells per well were seeded in a 6-well plate with growth medium. The amount of viral supernatant was adjusted based on cell number and

desired infection rate and added to the cells. 8 µg/µL Polybrene was added to increase transduction efficiency. Depending on the cell line, the plate was centrifuged at 300-700g for 45-60 minutes and incubated at 37°C and 5% CO2 for 24 hours. On the next day, the medium was discarded, and the cells were washed twice with PBS and transferred to a new flask containing fresh culture medium.

Some constructs in this study included an antibiotic resistance cassette to select transduced cells. Depending on the resistance, cells were treated with either puromycin (1-4 µg/mL) or blasticidin (10 µg/mL) 48 hours after transduction. Cells were selected for 1-2 weeks, and transgene expression was confirmed by immunoblotting.

4.2.2.8 Doxycycline treatment for transgene expression

A doxycycline-inducible system allows the expression of a transgene at a desired time after doxycycline treatment. In this study, the system was used for the timed overexpression of plasmids. By viral transduction (described 4.2.2.7), the plasmid containing the transgene of interest was stably incorporated into the cells of interest. After selecting cells for positive transduction, doxycycline (1 µg/mL) was added to the medium to induce transgene expression. Doxycycline treatment was refreshed every 48 hours.

4.2.2.9 Cycloheximide Treatment for Protein Stability Assays

Cycloheximide (CHX) inhibits eukaryotic ribosomes, inhibiting translation and, thus, new protein synthesis. This allows the analysis of protein stability and turnover. CHX was dissolved in 100% ethanol to produce a 100 mg/mL stock solution. CHX was made fresh before each experiment. 200 µg/mL CHX was added to the cell medium for various time periods up to 12 hours. To determine whether the observed protein degradation was proteasome-dependent, 10 µM proteasome inhibitor MG132 was used as a control in one condition.

4.2.2.10 Flow Cytometry

Flow cytometry is a method for sorting and analyzing cells using a laser to characterize them at the single-cell level. In a thin liquid stream, individual cells move past laser beams for excitation and appropriate detector modules for emission signals. This allows the physical characterization of cells by size and granularity, along with fluorescent signals from expressed fluorochromes or fluorochrome-coupled antibodies.

Data from the study were acquired using a BD LSRII or FACS Accuri C6 plus and analyzed using FlowJo v10.10 software.

4.2.2.11 Flow Cytometry of GFP or RFP Transduced Cells

Cells were analyzed by flow cytometry for the dropout screens, and to determine the viral transduction efficiency of cells infected with viral vectors containing GFP or RFP. The cells were collected from the culture at the indicated time points and washed with 2 mL PBS. Next, the cells were resuspended in PBS and analyzed by flow cytometry. The expression of dsRed and GFP was detected in the FL-2 (PE) and FL-1 (FITC) channels, respectively, and the data were further analyzed using FlowJo v10.10 software.

4.2.2.12 Live/dead Staining

ThermoFisher Scientific's live/dead stain coupled to APC that binds to amines on the cell surface or inside of dying cells. The dye can only enter cells and bind to amines intracellularly when the cell membrane is damaged during cell death. This increases the fluorescence intensity compared to when the dye can only intact with amins on the plasma membrane. The APC fluorophore was linked to the live/dead dye for multiplexing.

For the experiment, cells were harvested, counted, and washed with PBS before being resuspended in the live/dead dye (1:1000 in PBS) and incubated on ice for 15 minutes. The samples were then washed twice with PBS and analyzed by Flow cytometric analyses.

4.2.2.13 Cell Tracer Analysis

ThermoFisher Scientific's CellTracer Far Red Cell Proliferation kit is an amine-reactive fluorescence-coupled cytoplasmic dye. The dye dilutes progressively as cells divide, altering its fluorescence signal intensity. The change of fluorescence signal over time allows to detect cells that are progressing slower through the cell cycle.

For the experiment, cells were counted, and equal amounts were stained with the CellTracer Far Red Cell Proliferation kit (1 µM staining solution) according to the manufacturers protocol. The cells were incubated for 20 minutes in a water bath at 37°C. Afterwards, cells were spun down, washed in PBS once, and cultured. Each day the cells were analyzed by flow cytometry.

4.2.2.14 Cell Cycle Analysis

The cellular DNA content can be measured by the DNA-intercalating fluorescent dye Propidium Iodide. Cells in the G0/G1 phase have a DNA content of 2N. Cells in the G2/M phase have double the amount of DNA (4N). Therefore, cells in the G2/M phase exhibit significantly higher fluorescence levels when stained with Propidium Iodide. than cells in the G0/G1 phase. Cells undergo DNA replication in preparation for cell division during the synthesis (S) phase of the cell cycle, resulting in an intermediate level of DNA and the intensity of the Propidium Iodide signal is between the intensity of cells in G1 and G2/M phase.

In this study, BD Pharmingen's Propidium Iodide/RNase Staining Buffer was used according to the manufacturer's protocol. In some experiments, the S phase population was further resolved by treating cells with Bromodeoxyuridine (BrdU). BrdU incorporates during the S-phase of DNA replication. For the experiment, BrdU was incubated with the cells for 45 minutes at 37°C in 5% CO2. Next, the cells were harvested and fixed in 80% ice-cold ethanol. Afterwards Propidium Iodide /RNase staining was performed for 15 minutes at RT. The BrdU was visualized by a specific anti-BrdU antibody conjugated to FITC. The cells were analyzed by flow cytometry. The relative number of cells in each cell cycle phase was determined using the Watson (Pragmatic) model in FlowJo software.

4.2.2.15 Immunofluorescence (IF)

Fluorochrome-coupled antibodies combined with immunofluorescence microscopy is a popular method for visualizing the localization of proteins within their subcellular compartments. Adherent cells were collected, counted, seeded at the desired density in an 8-well chamber slide, and cultured for 24 hours. For suspension cells, the coverslip was coated with 150 µL poly-D-lysin for 1 hour at RT, followed by a single wash with ddH2O. The

suspension cells were also counted and resuspended in HBSS before being plated onto the treated coverslips and incubated for 1 hour at 37°C in 5% CO2.

After seeding the cells onto the coverslip, the medium was removed, and the cells were fixed with 4% Paraformaldehyde (PFA) in PBS for 10 minutes at RT. After one wash with PBS, the cells were permeabilized with 0.1% Triton-X in PBS for 3 minutes at RT. After three consecutive washes with PBS, the cells were incubated with IF-blocking buffer (0.25% gelatin from cold water fish skin, 0.01 saponin in PBS) for 1 hour at RT to prevent unspecific antibody binding. The primary antibodies were then diluted in IF staining buffer (0.5% BSA, 0.01% saponin in PBS) at the recommended dilutions and incubated on the slide overnight at 4°C. The slide was then washed three times with PBS and incubated with the appropriate fluorochrome-conjugated secondary antibodies for one hour at RT in the dark. After three more washes with PBS, the nuclei were stained with 1 µg/mL Hoechst 33342 for 15 minutes. After removing the chamber, the slide was washed once with ddH2O. Lastly, a mounting medium was added to the slide, and a glass coverslip was placed on top before conducting confocal microscopy.

4.2.3 CRISPR-Cas9 screen and analyzes

4.2.3.1 CRISPR-Cas9 screen

A CRISPR-Cas9 screen is a genome-wide, high-throughput approach to study gene function and interaction effects. This screen is using the CRISPR-Cas9 system to introduce targeted genetic modifications. Our CRISPR-Cas9 screen was conducted be V.Wagner. Three LuAD cell lines, previously stably transduced with a Cas9 expression construct, were used for this screen. Prior to the CRISPR-Cas9 screen, these cell lines were selected for Cas-9 expression by blasticidin treatment for two weeks. Lentiviral particles were generated from a pooled sgRNA library as described in 4.2.2.7. The Cas-9 LuAD cells were then transduced at a multiplicity of infection (MOI) of 0.15-0.2 to reduce the occurrence of double transduction events. To get a 1000x coverage of the sgRNA library of 3200 sgRNAs, 3.2 million sorted cells were washed with PBS, harvested, and the cell pellet was stored at -80°C to serve as the day 4 sample. An additional 3.2 million sorted cells were re-cultured in fresh medium for 14 days. The cells were split during this time to prevent overgrowth, but the 1000-fold coverage was maintained. On day 14, 3.2 million sorted cells were again collected and stored at -80°C to serve as the day 18 sample.

To measure the abundance of sgRNAs at the different time points, genomic DNA was extracted from the frozen samples using the DNeasy Blood and Tissue Kit according to the manufacturer's instructions. To increase the DNA yield, the samples spin columns were eluted twice, once with 30 µL and then with 20 µL. PCR amplification of the sgRNA locus was performed with the addition of adaptors and barcodes to facilitate Illumina-based sequencing and multiplexing of the samples. PCR amplification was performed at 1000x coverage. The amount of genomic DNA required was calculated:

$$required\ gDNA = library\ size\ (number\ of\ sgRNAs)\ x\ coverage\ x\ 10\ pg\ (DNA\ per\ cell)$$

Reagent	*Amount*
Q5-reaction buffer (5x)	*10 µL*
Forward primer (10 µM) P50X	*2.5 µL*
Reverse primer (10 µM) P70X	*2.5 µL*
dNTPs (10mM)	*1 µL*

GC Enhancer	*10 µL*
Genomic DNA	*3.5 µg*
Q5 High Fidelity Polymerase	*0.5 µL*
Nuclease-free dH2O	*To 50 µL*

35 µg of genomic DNA was used and divided into 10 separate PCR reactions, each containing 3.5 µg of gDNA, which resulted in a diversification of mutations occurring during the amplification process. Different combinations of barcoded PCR primers were used to multiplex the samples:

NCI-H23 day 4 (sgRNA_NGS-P504, sgRNA_NGS-P704), NCI-H23 day 18 (sgRNA_NGS-P504, sgRNA_NGS-P705)

NCI-H1437 day 4 (sgRNA_NGS-P501, sgRNA_NGS-P701), NCI-H1437 day 18 (sgRNA_NGS-P502, sgRNA_NGS-P702)

HCC-44 day 4 (sgRNA_NGS-P502, sgRNA_NGS-P703), HCC-44 day 18 (sgRNA_NGS-P503, sgRNA_NGS-P704),

After PCR, the products were purified using the QIAquick PCR Purification Kit (Qiagen) according to the manufacturer's protocol. PCR products were pooled for each sample and cell line. Agarose gel electrophoresis was performed on the samples to confirm successful amplification by the appearance of a distinct 281 bp band (barcoded and amplified sgRNA locus).

Program step	*Temperature*	*Time*
Initial Denaturation	*98°C*	*2 min*
Cycles: 30		
Denaturation	*98°C*	*20 sec*
Annealing	*60°C*	*45 sec*
Elongation	*72°C*	*45 sec*
Final Elongation	*72°C*	*5 min*

4.2.3.2 Illumina MiSeq sequencing

After the PCR reaction, the samples were sequenced using Illumina MiSeq technology. DNA concentration was measured for each barcoded sample for multiplexing. The samples were compared to Illumina DNA standards from the KAPA library quantification kit (Kapa Biosystems) using qPCR. An aliquot of each sample was diluted 1:1000, 1:10,000, and 1:100,000 and measured alongside the DNA standard in technical triplicate. The reaction mix for qPCR was prepared: (0.9 µL library qPCR primers (RP7_fw and FP5_rv, 10 mM each), 2 µL template, 4.6 µL dH2O and 7.5 µL LightCycler 480 SYBR Green I Master Mix). The qPCR reaction was set up as described above. The DNA concentration of each sample was measured, and samples were diluted and pooled to a total of 50 µL of 4 nM library. To verify the correct concentration of the library, a agarose gel was run. The pooled multiplexed sample was sequenced by R. Oellinger (Department of Internal Medicine II, Klinikum rechts der Isar, Munich, Germany) on a MiSeq Illumina using the MiSeq Reagent Kit v2. A total of 6 pmol of the library was used for sequencing, and 4 µL of the library was combined with 1 µL of Illumina PhiX control. The web tool of the CRISPRAnalyzeR pipeline (J. Winter et al., 2017) was used to map the sequencing reads to the library reference file.

4.2.4 Protein biochemistry

4.2.4.1 Cell Lysis

Cell lysis by cell membrane disruption is a method to analyze the protein content or protein-protein interactions of a cell population. Collected cell pellets were lysed in a specific lysis buffer containing protease and phosphatase inhibitors to avoid degradation or alteration of post-translational modifications. Unless otherwise specified, ice-cold 150 nM NaCl lysis buffer supplemented with DTT and protease (PMSK, TLCK, TPCK, PIN) and phosphatase (Nava, glycerol-2-phosphate) inhibitors was used. Cell pellets were thoroughly resuspended in lysis buffer, incubated on ice for 20 minutes, and DNA/membrane debris were removed by centrifugation at 14,000 rpm at 4°C for 20 minutes. The supernatants were then transferred to new tubes on ice, and protein concentrations of the supernatants were measured by the Lowry method using a Bio-Rad DC protein assay according to the manufacturer's protocol. Protein samples were denatured by adding Laemmli buffer and boiled at 95°C for 5 minutes. Proteins were then analyzed by SDS gel electrophoresis or stored at -20°C.

4.2.4.2 SDS polyacrylamide gel electrophoresis

SDS-polyacrylamide gel electrophoresis (SDS-PAGE) allows the separation of proteins according to their mass. Denatured proteins are coated with negatively charged SDS. This allowed them to move through a polyacrylamide gel at a mass-specific rate, independent of their intrinsic charge when an electric field is applied. The percentage of acrylamide in a gel was chosen according to the molecular weight of the proteins of interest. The polyacrylamide gels were run using the Mini-PROTEAN® Tetra Electrophoresis System. The gels consisted of a separating gel (375 mM Tris pH 8.8, 10% SDS, 10% APS, acrylamide) and a stacking gel (125 mM Tris pH 6.8, 10% SDS, 10% APS, 4.4% acrylamide). Adding 5 µL TEMED per 5 mL stacking and 4 µL TEMED per 10 mL separating gel, initiated polymerization. After polymerization, 20-25 µg of denatured protein sample was loaded into the pockets of a gel built in a running buffer-filled chamber next to a protein ladder and resolved at 80-120 V. After electrophoresis, gels were incubated in Coomassie or silver stain to visualize proteins in the gel or transferred to a membrane for immunoblot analysis.

4.2.4.3 Coomassie- and Silver-staining

After SDS-PAGE, Coomassie or silver staining can visualize proteins directly on an acrylamide gel by. Both techniques stain proteins according to the charge in their amino acid chains. Coomassie interacts with positive amine groups through van der Waals interactions and can visualize proteins ≥50 ng and is therefore the less sensitive stain. Acrylamide gels were incubated in a Coomassie staining solution for at least 1 hour while shaking. Access dye was washed out with a Coomassie de-staining solution. Silver staining reduces silver ions to elemental silver through negatively charged residues and can detect proteins down to 1 ng. The Thermo Scientific Pierce Silver Staining Kit was used for silver staining according to the manufacturer's instructions.

4.2.4.4 Immunoblot Analysis (Western Blot)

Proteins can be identified by the Western blot method. Proteins previously separated by SDS-PAGE were bound to polyvinylidene fluoride (PVDF) membranes by hydrophobic and

polar interactions and visualized with specific antibodies. The PVDF membrane was activated in methanol for at least 1 minute and blotted together with the gel containing the proteins in a wet Mini Trans-Blot cell from Bio-Rad. Using ice-cold transfer buffer, the blotting process was performed at 0.250 A for 90 minutes. Next, the membrane was stained with Ponceau solution, which reversibly stains all membrane-bound proteins. The Ponceau was washed out with H2O and the membrane was blocked in either 5% milk or 5% BSA in PBS-T for 45 minutes at RT. Afterwards, the membrane was incubated overnight on a roller mixer with the appropriate primary antibodies diluted in either 5% milk or 5% BSA in PBS-T. The next day, the membrane was washed five times for 10 minutes each with PBS-T. Afterwards, the membrane was incubated for two hours at RT with a secondary antibody conjugated to horseradish peroxidase (HRP) directed against the species of the primary antibody for chemiluminescent detection. After two hours the membrane was washed again five times for 10 minutes each with PBS-T. To visualize the proteins, the membrane was incubated with enhanced chemiluminescence solution (ECL), and proteins were detected using Bio-Rad's ChemiDoc Imaging Systems.

4.2.4.5 Stripping of membranes

The PVDF membrane was stripped of the previously used antibodies to re-analyze the PVDF membrane and stain it with a different primary antibody. Therefore, the membrane was incubated with stripping buffer (0.5 M NaOH) for 5 minutes and washed twice with PBS-T for 10 minutes. The membrane was blocked with either 5% milk or 5% BSA in PBS-T for 50 minutes and incubated with new primary antibodies overnight.

4.2.4.6 Immunoprecipitation

Immunoprecipitation is a technique to isolate and purify a specific protein of interest from a cell lysate using an antibody that binds specifically to that protein. These specific antibodies are usually coupled to agarose gel by a covalent bond, which allows sedimentation of bound proteins by centrifugation. In this study, immunoprecipitation of FLAG-tagged proteins was performed from whole cell extracts using standard 150 mM lysis buffer unless noted otherwise. To reduce unspecific protein binding to the FLAG-M2 agarose gel, the cell lysate was incubated with empty agarose gel for 15 minutes at 4°C on a rotating wheel for preclearance. The mixture was then centrifuged at 200 rcf for 3 minutes, and the supernatant was transferred to new tubes without disturbing the empty agarose gel. FLAG-M2 agarose gel was thawed, washed twice in lysis buffer, and blocked with 1% BSA in PBS on a rotating wheel for 30-60 minutes at 4°C. The gel was then washed three times with lysis buffer, and one gel volume of lysis buffer was added to obtain a 1:1 ratio. The clarified lysate was incubated with the blocked FLAG-M2 agarose gel on a rotating wheel for 90 minutes at 4°C. The mixture was centrifuged at 200 rcf for 3 minutes and the supernatant was discarded. Next the FLAG-M2 agarose gel was washed five times with lysis buffer. After the last washing step, all liquid was removed from the beads, 40 µL of 2x Laemmli buffer was added, and the mixture was incubated at 95°C for 10 minutes to elute bound proteins. Finally, samples of WCE and IPs were analyzed using SDS-PAGE and immunoblot.

4.2.4.7 *In-vivo*-ubiquitylation assay

An *in-vivo*-ubiquitylation assay allows the analysis of the ubiquitylation status of a protein under specific conditions in a cellular context. HEK293T cells were seeded on 6 cm dishes and cultured for 24 hours. The next day, the cells were transfected with plasmids

encoding 1-3 µg FLAG-tagged substrate candidate, 1-2.5 µg E3 ligase of interest or controls, and 0.3-1 µg HA-tagged ubiquitin or one of its variants using the Lipofectamine 2000 method (4.2.2.5). After 24 hours of incubation, 10 µM MG132 was added to the cells for three hours to accumulate proteins that get degraded by the proteasome. Cells were harvested, and cell pellets were lysed in 100 µL ice-cold 250 mM NaCl lysis buffer supplemented with protease and phosphatase inhibitors. After 20 minutes of incubation on ice, the lysates were centrifuged, and the supernatants were transferred to a new tube. The samples were denatured by adding 1% SDS (v/v), 6 mM EDTA, 0.1%NP-40, and heating to 95°C for 10 minutes, followed by 2 minutes cool down at RT. Next, the samples were diluted with 900 µL of 250 mM NaCl lysis buffer supplemented with 1% Triton X-100 (Sigma) and incubated on ice for 15 minutes. Finally, FLAG-Immunoprecipitation was performed as described in 4.2.4.6.

4.2.4.8 Mass Spectrometry

Mass spectrometry is a method for measuring the mass-to-charge ratio of ions, which can be used to identify and quantify proteins. FLAG-IP, followed by mass spectrometry, was used to identify the interaction partners of DCAF7 and KLHL14. KLHL14 was cloned into a doxycycline-inducible vector pTRIPZ and transduced into MM1.S cells together with an empty vector control. These cells were then either left asynchronous or arrested in mitosis by a sequential thymidine and nocodazole treatment for 25 hours, and transgene expression was induced for 18 hours prior to sample collection and mass spectrometry.

For DCAF7 samples, HEK293T cells were transiently transfected with plasmids encoding SF-DCAF7 or SF-EV. All samples were generated in triplicates, and cells were harvested and frozen at -80°C until FLAG purification. For DCAF7 and KLHL14 samples, cell lysis was performed using 150 mM standard lysis buffer. FLAG IP was performed as described in 4.2.4.6. DCAF7 samples were eluted with 3xFLAG peptide. Therefore, the proteins bound to the gel were washed once with TBS, followed by elution with 5x the dry gel volume of 200 µg/mL 3xFLAG peptide in TBS. The mixture was then incubated on a rotating wheel for 30 minutes at 4°C. An additional TBS wash was included after each elution step to maximize protein yield.

KLHL14 samples were eluted with acidified glycine. For this purpose, the gel was washed with 0.2 M glycine (pH 7.0), followed by three sequential 5-minute elution steps at RT using 2.5 times the bead bed volume of 0.2 M glycine (pH 3.5)/HCl. The eluates from each sample were pooled and neutralized with 50 µL TRIS (pH 6.0)/HCl.

For both KLHL14 and DCAF7 purification, the eluted proteins were precipitated by adding 20% (v/v) trichloroacetic acid (TCA) and incubated overnight at 4°C. The next day, the proteins were centrifuged at 20,000 rcf and 4°C for 30 minutes, followed by a wash step with 100% ice-cold acetone. After drying the proteins in a vacuum concentrator, the samples were resuspended in LDS buffer (NuPAGE), reduced with DTT, and alkylated with chloroacetamide (CAA). 50% of the HEK293T purification was then loaded onto a 4-12% BIS-TRIS NuPAGE gel and stained with Coomassie. All samples were sent for analysis either to the Department of Proteomics and Bioanalytics at TUM or to the Bavarian Center for Biomolecular Mass Spectrometry at the University Hospital Rechts der Isar.

4.2.4.9 Mass Spectrometry Analysis

KLHL14 samples were processed and analyzed by Jana Zecha (Department of Proteomics and Bioanalytics, TUM) and DCAF7 by Piero Giansant of BayBioMS@MRI. Briefly, dried proteins were reconstituted, reduced with dithiothreitol (DTT), and alkylated with chloroacetamide (CAA). Half of each sample was loaded for electrophoresis on a 4-12% BIS-TRIS NuPAGE gel, followed by in-gel trypsin digestion. This digestion resulted in tryptic peptides. The peptides were then extracted, dried, and reconstituted in a buffer containing 0.1% formic acid (FA). Samples were analyzed using a Dionex Ultimate 3000 UHPLC+ system or nano LC-MS/MS on an Eksigent NanoLC-ultra 1D+ system. Both systems were connected to a Q Exactive HF mass spectrometer (Thermo Fisher Scientific). MaxQuant was used to identify and quantify peptides and proteins in the samples. MS2 spectra were searched against the human reference proteome, which contains common contaminants. Differences in sample preparation are described below:

Purified protein	DCAF7	KLHL14	KLHL14
Type of purification	Strep-FLAG/TAP	Single FLAG	Single FLAG
Cell/sample preparation by	V. Wagner	R. Spallek	R.Spakkel
Cell type, number, treatment	$2x10^9$ HEK293T	$5x10^8$ MM1.S cells	$5x10^8$ mitotic MM1.S cells
Analysis type	Interactome	Interactome	Interactome
Type of Gel	Short gel	Short gel	Short gel
Replicates per sample	3	3	3
MaxQuant Verison	v2.0.3.0	v1.6.3.2	v1.6.3.3
Operator	Piero Giansanti	Piero Giansanti	Julia Mergner

4.2.4.10 DiGLY Proteomics

DiGLY proteomics is a specialized method to identify and analyze proteins modified by ubiquitylation by detecting di-glycine remnants on lysine residues after trypsin digestion. Here, it was used to detect proteins with reduced ubiquitylation after DCAF7 knockdown. NCI-H1437 and HCC-44 cells were lentivirally transduced with shRNAs targeting DCAF7 or non-targeting control shRNAs. The transduction rate was 95-100%, and the experiment was performed in three biological replicates. After 48 hours post-transduction, the cells were harvested, washed twice with PBS, and stored at -80°C. Whole cell extracts were prepared by lysing the pellets in SDS lysis buffer and subsequently boiling them at 95°C for 5 minutes. Protein concentrations were determined using the Pierce BCA Protein Assay Kit according to the manufacturer's protocol. Next, 2 µg of protein from each sample was mixed with 100 µL of SpeedBeads magnetic carboxylate-modified particles in a 1:1 mixture of A and B beads. To precipitate the proteins on the beads 100% Ethanol was added to the samples to achieve a final concentration of 70% Ethanol. After two washing steps, once with 80% ethanol and once with acetonitrile

(ACN), the proteins were reduced with 10 mM TCEP and alkylated with 50 mM chloracetamide (CAA) for 45 minutes at 37°C. After adding of 40 µg trypsin, the mixture was incubated at 37°C for 16 hours, and the digestion was stopped by adding of FA at 0.5% the next day.

Sep-Pakt tC18 cartridges were prepared with ACN and solvent B (0.1% FA, 50% ACN in ddH2O) and equilibrated twice with solvent A (0.1% FA in ddH2O). Next, the acidified peptides were loaded onto the cartridges to desalt the samples. The peptides were washed twice with solvent A and then eluted twice with solvent B. After measuring the peptide concentration with a Nanodrop, 50 µg of peptides per sample were set aside, frozen at -80°C, and dried in a Speed Vac for whole proteome analysis. A separate aliquot of 450 µg peptides was also frozen at -80°C and dried for DiGLY enrichment.

All DiGLY enrichment steps were performed on ice, and all bead centrifugation steps were performed at 2000 rcf at 4°C. Beads from the PTM Scan Ubiquitin Remnant Motif (K - e - GG) Kit were washed with borax buffer and cross-linked with 20 mm dimethyl pimelidimate in borax buffer. Next, the beads were washed with DiGLY blocking buffer and incubated overnight at 4°C on a rotating wheel. After resuspension in Immuno-Affinity Purification buffer, the beads were divided into nine tubes for DiGLY immunoprecipitation. The peptides were then reconstituted in Immuno-Affinity Purification buffer and added to the tubes containing the beads, followed by incubation at 4°C for one hour on a rotating wheel. Afterwards, the samples were washed twice with ice-cold PBS and resuspended in 50 µL of 100 mM HEPES (pH 8.5) for TMT labeling.

TMT labeling was performed carefully to minimize TMT hydrolysis and ensure efficient labeling. Each sample was labeled with a different TMT channel. For this step, 200 µg TMT reagent was dissolved in 5 µL anhydrous ACN, and 2.5 µL was added to the beads. The mixture was incubated for 10 minutes at 25°C while shaking. The reaction was quenched with 2 µl of 5% hydroxylamine (v/v), and the incubation step was repeated for 5 minutes under the same conditions. Next, the beads were washed with PBS and resuspended in 120 µL PBS, and a 5 µL aliquot was stored at -20°C to evaluate labeling efficiency. All samples from one cell line were pooled and washed twice with PBS. Afterwards, 100 µL DiGLY elution buffer was added to the peptides, and they were incubated at RT for 5 minutes while shaking for the eluting of the peptides. We used self-packed StageTips to desalt the eluted peptides. First, the StageTips were treated with ACN and StageTip Solvent B; next, StageTip Solvent A was used to equilibrate the StageTip. Then, the sample peptides were acidified with 1% (v/v) FA and loaded onto the equilibrated StageTip. To optimize this process and get as many desalted peptides as possible, the flowthrough was reloaded onto the StageTip, washed with Solvent A again, and eluted with 40 µL of Solvent B. The peptides were frozen at -80°C and dried in a Speed Vac.

The peptides assigned to the whole proteome analysis were prepared for TMT labeling. They were diluted in 10 µL of 100 mM HEPES (pH 8.5). The TMT labeling procedure was similar to what was previously described, but only 50 µg of TMT reagent was used per sample, and the incubation time with TMT reagent was extended to 1 hour. The labeled peptides from each cell line were pooled and desalted using Sep-Pak tC18 cartridges. Dr. Y. Chang (Chair of Proteomics and Bioanalytics at TUM) then fractionated 50 µg of the labeled pooled peptides and loaded them onto StageTips, and eluted them in a series of increasing ACN concentrations (5%, 7.5%, 10%, 12.5%, 15%, 17.5%, 50%). The 5% and 50% ACN fractions were combined, as were the 17.5% ACN fraction and the first flow from sample loading. The fractions were frozen at -80°C and dried in a speed vac.

The fractionated whole proteome samples were reconstituted in 0.1% FA, and each was measured with a 60 min linear gradient MS3 acquisition on a Fusion Lumos Tribrid mass spectrometer. The DiGLY-enriched pooled sample for each cell line was reconstituted in 0.1% FA and analyzed using a 100-min linear gradient MS3 acquisition on the Fusion Lumos Tribrid mass spectrometer. Again, MaxQuant was used to identify and quantify peptides and proteins in the samples. MS2 spectra were searched against the human reference proteome. Perseus was used for further analysis. For both the total proteome and the DiGLY-enriched samples, each TMT channel was normalized to the median intensity of that channel. The mass spectrometric analysis of the data was performed by Dr. Y Chang.

4.2.4.11 Statistical Analysis

All quantified experiments were performed in at least three independent biological replicates (triplicates). Immunoblot analyses that were not quantified typically reflect results from at least two independent experiments. Statistical analysis was performed by log-rank (Mantel-Cox) test, Pearson's correlation or linear regression, paired or unpaired two-tailed Student's t-test, or one-way ANOVA, depending on the data. GraphPad Prism software was used for this purpose. Error bars in the figures represent the mean ± standard deviation (S.D.). The p-values are indicated in the figure legends when a statistically significant difference was found: 0.1234 (ns), 0.0332 (*), 0,0021 (**), 0.0002(***), <0.0001(****).

5 Results

This study was conducted as a joint effort within the research group led by Prof. Dr. F. Bassermann at the Klinikum Rechts der Isar at TUM, with support from collaborators at various institutions and colleagues within our group. We have included relevant data obtained by other researchers from our group or the collaborators at other institutes to ensure a comprehensive understanding of the project. The contributions of each participant are recognized in the text and figure captions.

Furthermore, I started my PhD working on the LuAD-DCAF7 project but, after two years, shifted focus to the B-cell malignancies-KLHL14 project due to more promising results.

5.1 Results KLHL14

5.1.1 KLHL14 expression is decreased in patients with multiple myeloma, mantel cell lymphoma, and diffuse large B-cell lymphoma

The ubiquitin-proteasome system plays a critical role in controlling protein abundance, and aberrations in the UPS are often associated with many different malignancies. B-cell-derived cancers such as multiple myeloma, mantel cell lymphoma, and diffuse large B-cell lymphoma frequently harbor mutations in genes related to the UPS that can lead to persistent NF-κB signaling and drive unchecked proliferation and survival. In addition, some of these diseases show a high response rate to proteasome inhibitors, which together highlights the central role of the UPS in these cancer entities. Nevertheless, they remain largely incurable, presenting the urgent need for new targets for therapeutic intervention. To discover novel potential targets within the UPS, we obtained patient data from our collaborator T. Haferlach and analyzed the RNA expression levels for up and downregulated proteins of the UPS. RNAseq data from 263 multiple myeloma and 76 mantel cell patients was provided, and one of the most downregulated UPS proteins in both entities compared to 64 healthy control donor samples was the poorly characterized subunit of the Cullin-RING ubiquitin E3 ligase complex KLHL14 (Figure 8 a, b).

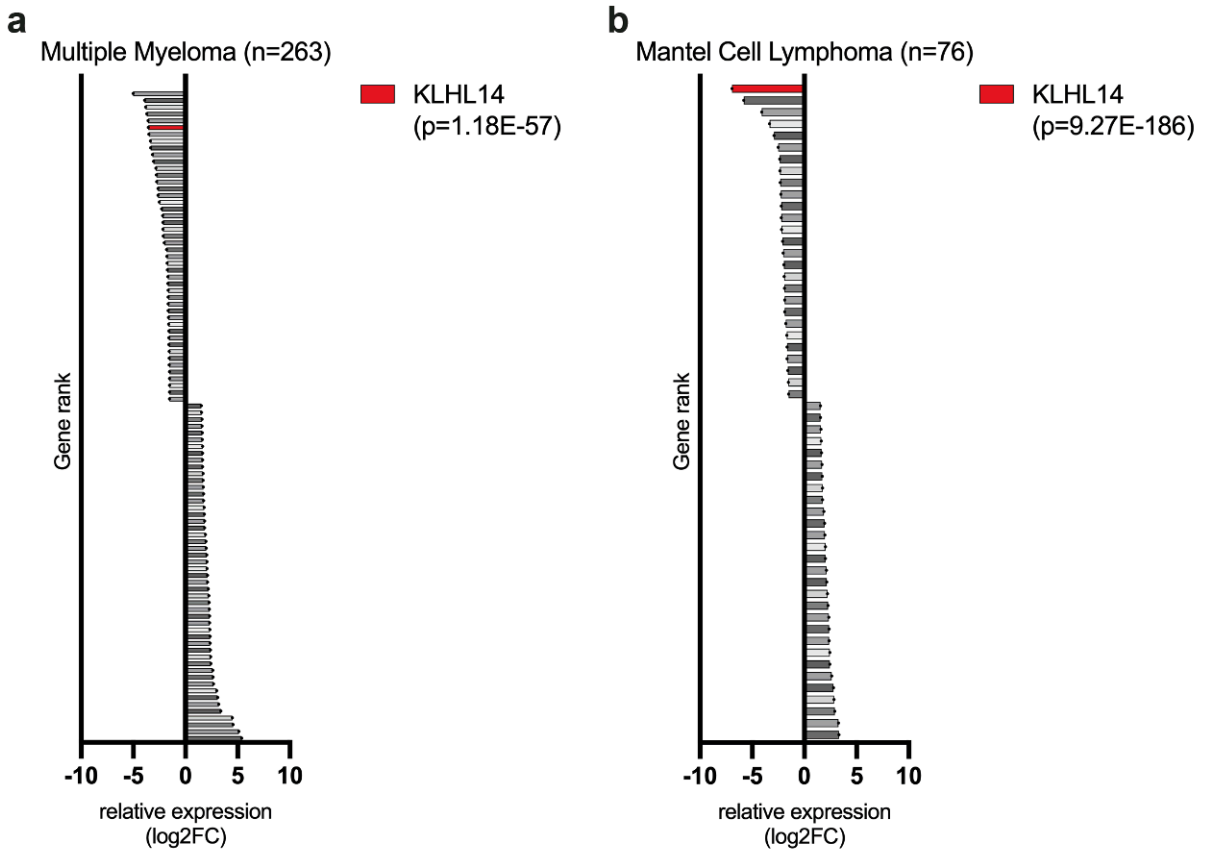

Figure 8 KLHL14 mRNA levels are significantly downregulated in MM and MCL patient samples. Relative mRNA expression of significantly up and downregulated ($p < 0.05$) UPS genes. 263 MM **(a)** and 76 MCL **(b)** patient samples were compared with bone marrowl samples of 64 healthy control donors. Log2 fold changes of RNA expression levels were plotted according to gene rank. KLHL14 is highlighted in red. The data was contributed by T. Haferlach, MLL Munich.

To verify this patient-based observation, we analyzed two different publicly available data sets (GSE16558, GSE59000) and compared the mRNA expression levels of KLHL14 between healthy plasma cells and MM cells. Multiple myeloma patients (n=60) showed significantly lower KLHL14 mRNA expression compared to healthy plasma cells (n=5) in the first dataset (Figure 9a). KLHL14 mRNA expression also decreased significantly in patients during MM disease progression from healthy plasma cells to MGUS and SMM (Figure 9b). In addition, analyzing the overall patient survival in multiple myeloma patients of the CoMMpass dataset revealed that those with low KLHL14 expression had a worse overall survival than those patients with high KLHL14 expression (Figure 9c). Taken together, the decreased expression of KLHL14 mRNA in MM and MCL patients and the correlation of high KLHL14 expression with better overall survival suggest a tumor-suppressive role of KLHL14 in B-cell malignancies.

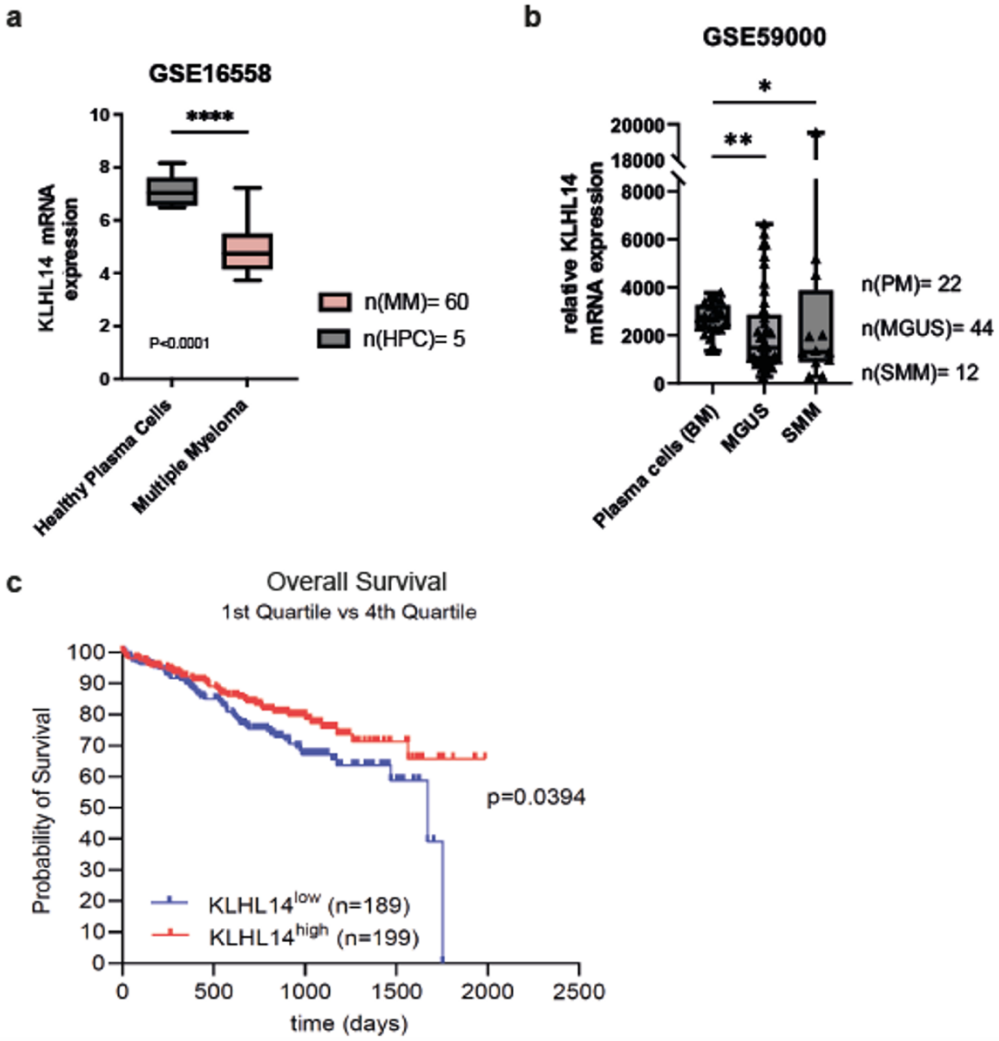

Figure 9 KLHL14 mRNA levels are significantly downregulated in MM samples from different datasets. (a) Relative KLHL14 mRNA expression levels in patients from data set GSE16558 of 5 healthy plasma cell donors and 60 MM patients. **** P <0.0001, by Student's t-test. **(b)** Relative KLHL14 mRNA expression levels in patients from data set GSE59000 from 22 healthy plasma cell donors, 44 MGUS patients, and 12 SMM patients. ** P < 0.01, * P < 0.1 by Student's t-test. **(c)** Overall survival (OS) of MM patients. MM patients with high KLHL14 expression are shown in red, and patients with low KLHL14 expression are shown in blue. Data were obtained from the CoMMpass dataset.

To confirm the findings from the publicly available databases on a protein level and to select the optimal cell line systems for further investigation of KLHL14, a large panel of cell lines was analyzed for KLHL14 protein expression. Whole cell extracts (WCEs) from MM, DLBCL, acute myeloid leukemia (AML), MCL, and NSCLC were immunoblotted for KLHL14 expression (Figure 10a-d). The DLBCL cell line TMD8, known for high KLHL14 protein levels (Choi et al., 2020), was used as a reference in each cell line panel. As our data analysis of mRNA expression levels suggested, MM cells exhibited a low KLHL14 expression compared to TMD8. The only out layer was the cell lines KMS12BM, which showed higher levels of KLHL14 protein expression compared to other MM cells (Figure 10a). Similarly, all AML and NSCLC cell lines had almost no detectable KLHL14 protein expression (Figure 10b, c). Ovarian cancer cell lines have been published to have higher KLHL14 expression (Chen et al., 2020), which was confirmed by our immunoblot that also showed increased KLHL14 protein levels in OVCAR3. DLBCL also has higher KLHL14 expression but has been highlighted as a hot spot for mutant forms of KLHL14 (Choi et al., 2020). Most of the MCL cell lines showed

moderate KLHL14 protein expression (Figure 10d). Combining the results of KLHL14 mRNA expression levels in MM and MCL patients with the protein expression levels of KLHL14 in our cell panels confirmed the low abundance of KLHL14 protein in most cancer cell lines, adding to the suggested tumor suppressor phenotype of KLHL14.

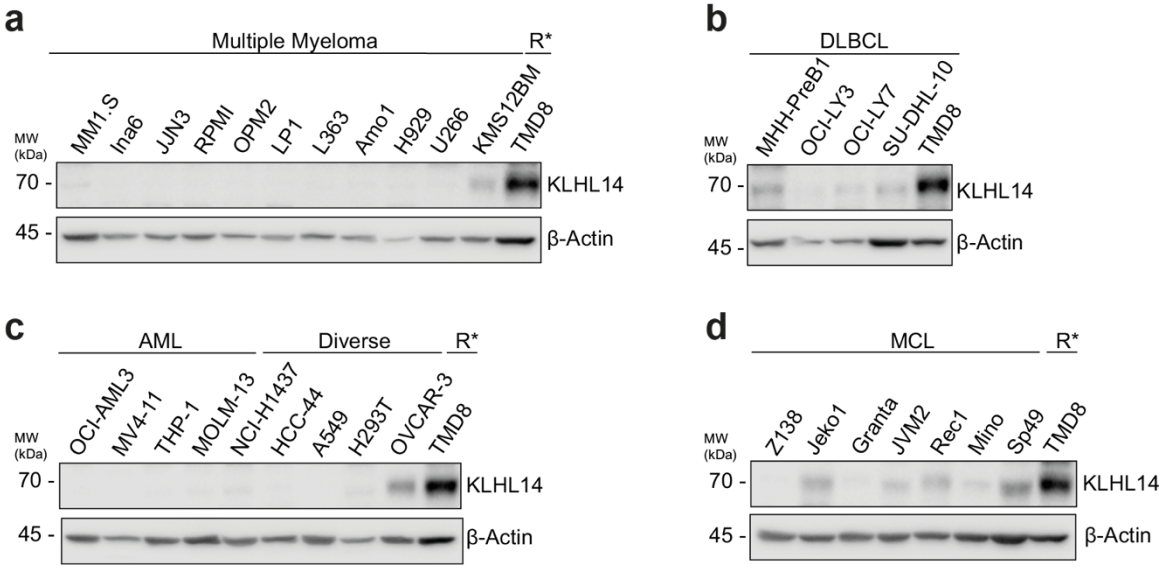

Figure 10 Low KLHL14 protein expression in MM, AML, and MCL cell lines indicates tumor suppressor function. Immunoblot analysis of whole cell extracts from cell lines **(a)** MM, **(b)** DLBCL, **(c)** AML/Diverse, and **(d)** MCL. TMD8 (R*) was used as a reference for KLHL14 protein expression. The indicated antibodies were used, loading control: β-actin.

5.1.2 KLHL14 overexpression leads to reduced proliferation in B-cell malignancies

To confirm the proposed tumor suppressor function of KLHL14, we transduced MM, MCL, DLBCL, AML, and NSCLC cell lines with lentiviral particles containing a vector encoding for either a KLHL14 overexpression construct or an empty vector in combination with a green fluorescence reporter (GFP). Transduction efficiency ranged from 10-80% depending on the cell line. The ratio of transduced cells (GFP-positive) to non-transduced wild type cells (GFP-negative) was measured by flow cytometry over a 14-day time course. Confirming the tumor suppressor function of KLHL14 in B-cell malignancies, cells with the overexpressing construct dropped out over time, while the ratio of empty vector transduced cells to wild type remained the same over time (Figure 11a). Interestingly, this dropout of KLHL14 overexpressing cells was only observed in MM, MCL, and DLBCL cell lines and not in AML and NSCLC cell lines. This suggests a very specific tumor suppressive function of KLHL14 only in B-cell derived malignancies. Immunoblot analysis of samples collected at the same time points as the dropout assay confirmed the decrease in KLHL14 protein expression only in MM (MM1.S), MCL (Z-138), and DLBCL (OCI-LY3) cell lines over time (Figure 11b). KLHL14 protein levels remained unchanged in AML (HL60) and NSCLC (A549) cells, recapitulating the observed results of the flow cytometry-based dropout assay (Figure 11b).

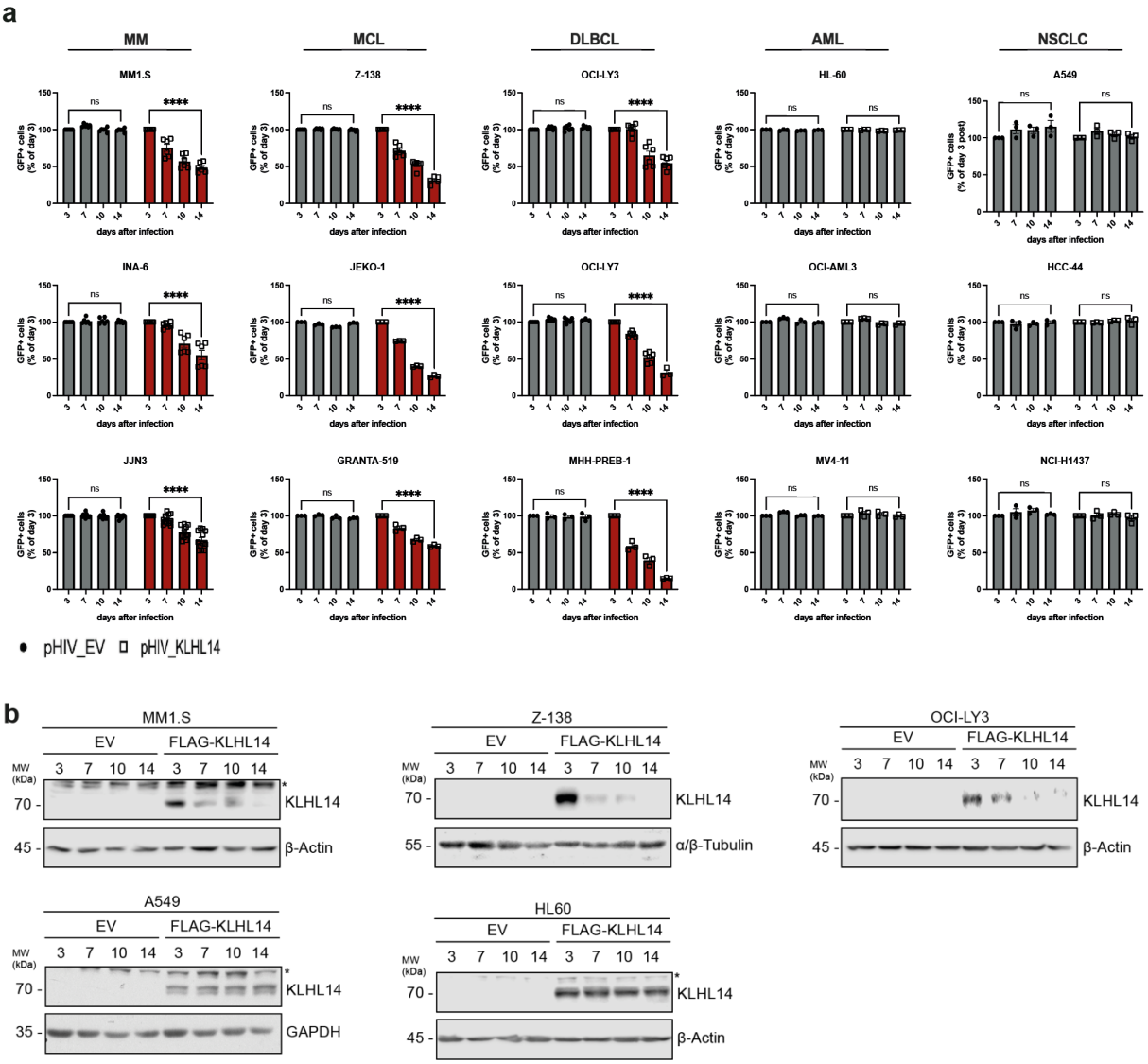

Figure 11 Overexpression of KLHL14 in B-cell malignancies leads to a dropout phenotype of cells. (a) A competitive growth assay was performed with different MM, MCL, DLBCL, AML, and NSCLC cell lines. Cells were transduced with lentiviral particles containing FLAG-KLHL14-GFP (in red) or empty-vector-GFP (in grey). Transduction efficiency was between 10-80%. The ratio of cells positively transduced (GFP+ positive) to non-transduced (GFP negative) was measured by flow cytometry over a 14-day time course. Data were normalized to day 3. Statistical tests were performed by 2way ANOVA: 0.1234 (ns), 0.0332 (*), 0,0021 (**), 0.0002(***), <0.0001(****). (MHH-PREB1, OCI-AML3, and the NSCLC dropouts were performed by R. Spallek) **(b)** Immunoblot analysis of WCE collected from cells at the same timepoints as in a. The indicated antibodies were used, loading control: β-actin, GAPDH, and α/β-tubulin (Immunoblot of A549 was conducted by R. Spallek).

5.1.3 Full-length KLHL14 is required to exert the observed tumor suppressor function

KLHL14 is a subunit of the Cullin-RING ubiquitin ligase complex consisting of a BTB domain, acting as a substrate-specific adaptor, a BACK domain involved in Cul3 binding, and six Kelch motifs responsible for substrate recognition. Mutation of any of these essential regions could inhibit the protein function of KLHL14 in MM, MCL and DLBCL and therefore its tumor suppressive phenotype. To validate this hypothesis, we generated deletion mutants of the Flag-tagged KLHL14 protein, either missing the BTB or Kelch domains (Figure 12a). The expression of these mutated KLHL14 variants was confirmed by lentiviral transduction of MM1.S cells. Immunoblotting for the different KLHL14 versions using a FLAG antibody confirmed successful protein expression (Figure 12b). To address the question if those mutant

KLHL14 versions would also lead to a dropout phenotype in cells, we performed a similar dropout assay as in Figure 11 but included cells lentivirally transduced with deltaBTB and deltaKelch domain variants of KLHL14 in addition to the empty vector and full-length KLHL14. Again, measuring the ratio of transduced to non-transduced cells by flow cytometry showed that the ratio of cells overexpressing the full-length KLHL14 dropped over time, but cells overexpressing the deltaBTB or deltaKelch domain variants of KLHL14 did not dropout of the mixed population (Figure 12c). This confirmed that KLHL14 requires an intact Kelch and BTB domain to exert its tumor suppressor function.

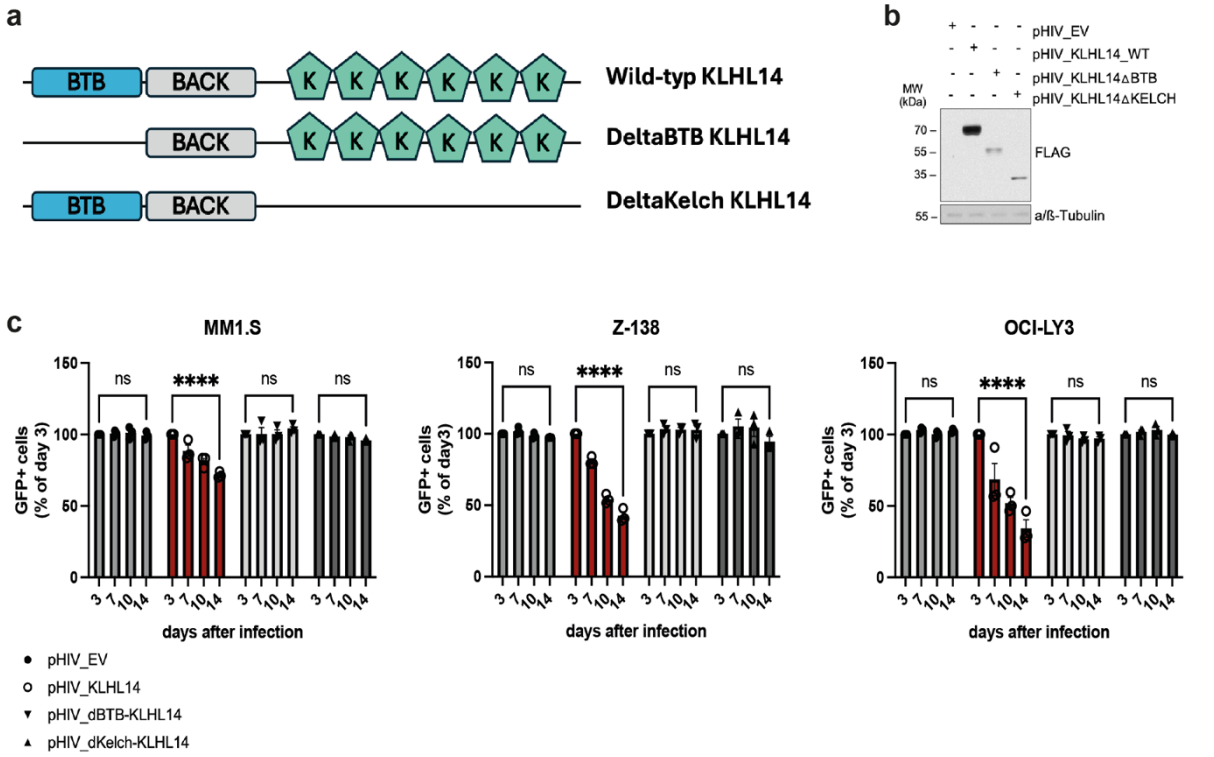

Figure 12 Intact BTB and Kelch domains are necessary for KLHL14 tumor suppressive function. **(a)** Diagram of KLHL14 wild type and the cloned deletion mutants. K = Kelch fold domains. **(b)** Immunoblot analysis of WCE from MM1.S cells, three days post-infection with lentiviral particles containing empty vector (EV), wild type (WT) FLAG-tagged KLHL14, or different mutated versions of FLAG-tagged KLHL14. Loading control: α/β-tubulin **(c)** Competitive growth assay of MM1.S, Z-138, and OCI-LY3. Cells were transduced with lentiviral particles containing FLAG-KLHL14 (in red), empty vector (in grey), deltaBTB-KLHL14 (in light gray), or deltaKelch-KLHL14 (in dark gray) in combination with a GFP reporter. Transduction efficiency ranged from 20-80%. The ratio of positive (GFP+) to negative (GFP negative) transduced cells was measured by flow cytometry over the 14-day time course. Data were normalized to day 3. Statistical tests were performed by 2way ANOVA: 0.1234 (ns), 0.0332 (*), 0,0021 (**), 0.0002(***), <0.0001(****). (KLHL14 mutant design and cloning, as well as the dropout assay in MM1.S were performed by R. Spallek).

5.1.4 Doxycycline-induced KLHL14 overexpression system confirms dropout phenotype in cells

Lentiviral transduction for constitutive overexpression of proteins was a useful tool for the dropout assays where we aimed for transduction efficiencies between 10-80%. Reaching 100% transduction efficiency with these lentiviral particles in the MM, MCL, and DLBCL cell lines was impossible. This made further studies of the KLHL14 overexpression phenotype difficult. The variability in transduction rates and virus production, as well as the presence of a mixed culture of both transduced and non-transduced cells, can interfere with the investigation of the molecular mechanisms involved in the dropout of KLHL14-overexpressing cells.

To address this issue, a doxycycline-inducible expression system was used for future experiments. The pTRIPZ vector system was modified by removing only the miRNA site from an empty vector, leaving the red fluorescence reporter (RFP) intact, or replacing both the miRNA and RFP sites with FLAG-KLHL14. MM1.S, Z-138, and OCI-LY3 cells were lentivirally transduced with these vectors and selected for vector expression using puromycin, resulting in a pure, stable cell line overexpressing either an empty vector with RFP or FLAG-KLHL14 after doxycycline treatment. Immunoblot analysis confirmed a significant increase in KLHL14 expression upon doxycycline induction in all three cell lines (Figure 13a).

To determine whether the stable cell lines show a similar dropout phenotype, we combined the same number of cells expressing the EV-RFP and FLAG-KLHL14 and induced transgene expression by doxycycline. Over a period of 20 days, we compared the ratio of EV-RFP to FLAG-KLHL14 expressing cells by flow cytometry. Analyzing the ratio of the EV-RFP to FLAG-KLHL14 expressing cells showed a significant drop of MM1.S, Z-138, and OCI-LY3 cells expressing KLHL14 compared to the empty vector over the time course (Figure 13b). This confirmed that doxycycline-induced KLHL14 overexpression also leads to a dropout of the population in the competitive growth assay and that this system can be used to investigate the underlying molecular mechanisms of the observed dropout.

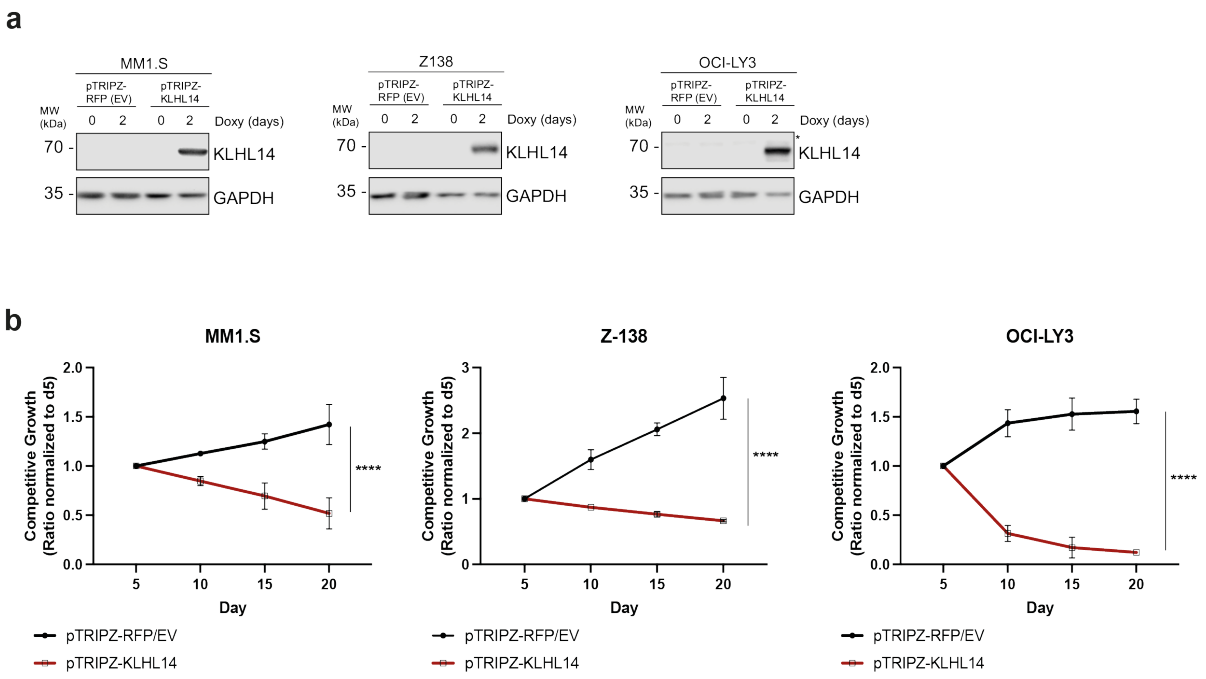

Figure 13 Doxycycline pTRIPZ system leads to dropout upon induction of KLHL14 overexpression. (a) Immunoblot analysis of WCE from MM1.S, OCI-LY3, and Z-138 cells stably expressing pTRIPZ-EV(RFP) or pTRIPZ-KLHL14. Cells were harvested at the indicated timepoints after treatment with doxycycline (1 µg/mL). The indicated antibodies were used, loading control: GAPDH. **(b)** Competitive growth dropout assay of MM1.S, Z-138, and OCI-LY3 cells stably expressing pTRIPZ-EV(RFP) or pTRIPZ-KLHL14. Cells were seeded together each at $0.5x10^6$ cells/mL and treated with doxycycline (1 µg/mL) for 20 consecutive days. The ratio of pTRIPZ-EV(RFP) to pTRIPZ-KLHL14 expressing cells was measured by flow cytometry at the indicated time points post infection. The ratio was normalized to day 5. Statistical tests were performed by 2way ANOVA: 0.1234 (ns), 0.0332 (*), 0,0021 (**), 0.0002(***), <0.0001(****).

5.1.5 KLHL14 localizes to distinct foci near the nucleus

The observed dropout phenotype of KLHL14-overexpressing cells could be attributed to a variety of molecular mechanisms, including the induction of apoptosis or another form of cell death, changes in the cell cycle, or metabolic alterations. As a basis for understanding

KLHL14's role as a tumor suppressor in B-cell malignancies, we investigated its subcellular localization to pinpoint its molecular function and potential substrates within this entity. We conducted immunofluorescence (IF) staining of wild type MHH-PREB-1 and OVCAR-3 cells since both have higher KLHL14 expression levels according to our cell panel (Figure 10b, c). For this purpose, cells were attached to poly-D-lysine-coated slides, fixed with 4% paraformaldehyde (PFA), and stained with a KLHL14-specific antibody in addition to DNA staining (Hoechst33258) and F-actin (Phalloidin), followed by confocal microscopy (LEICA-SF8). In these wild type cells, KLHL14 was localized in and around the nucleus, but most notably in punctual foci in close proximity to the nucleus (green dots indicated by white arrow) (Figure 14). There were usually one to two very bright foci per cell that appeared to be at a distinct localization, but there were also cells without any of these foci structures.

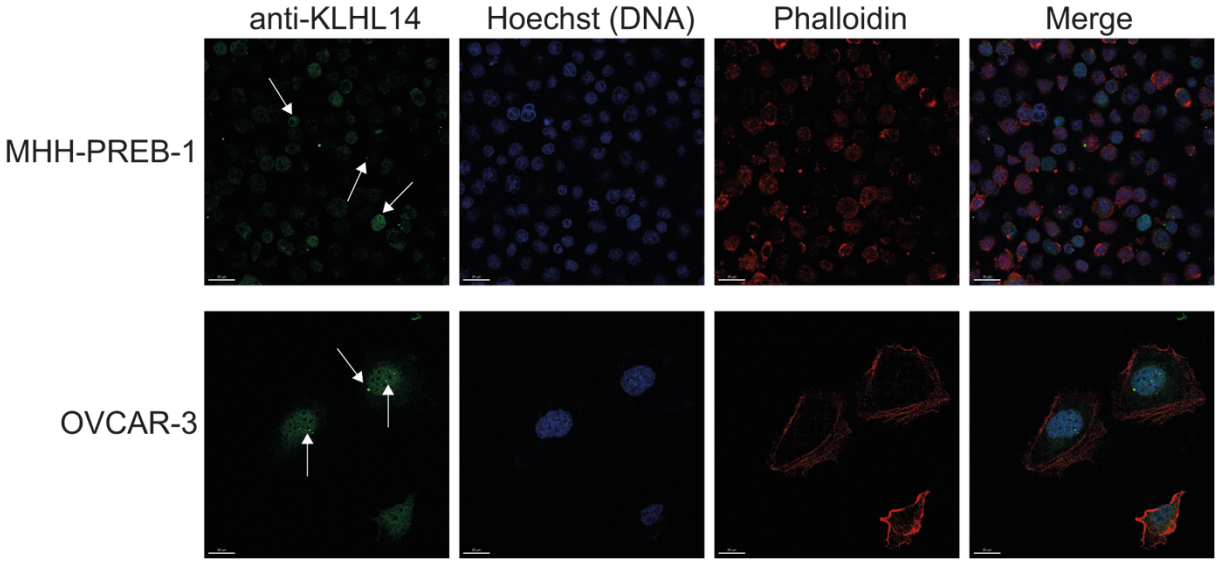

Figure 14 KLHL14 is localizes to distinct foci in and around the nucleus in wild type MHH-PREB-1 and OVCAR-3 cells. Representative immunofluorescence images of cells mounted on poly-D-lysine coated slides, fixed with 4% PFA and stained with corresponding antibodies. Images were captured with a LEICA-SF8 confocal microscope. The scale bar represents 20 µm. MHH-PREB-1 and OVCAR-3 cells stained with endogenous KLHL14 antibody (green) and the corresponding Alexa-Fluor-448 conjugated secondary antibody. F-actin was stained with Phalloidin (red), and the DNA was stained with Hoechst33258 (blue).

This initial observation was confirmed by further IF staining of MM1.S cells stably expressing pTRIPZ-EV or pTRIPZ-KLHL14. Here, the cells were treated with doxycycline for 24 hours for transgene expression prior to fixation and staining. Staining of the MM1.S cells with the KLHL14 antibody also showed clear foci-like dots in both samples but significantly more and brighter dots in the pTRIPZ-KLHL14 expressing cells (Figure 15a). Staining of the same cells with an anti-FLAG IF antibody revealed the same foci-like dots of KLHL14 within the cell in the pTRIPZ-KLHL14 expressing cells compared to no such structures in the pTRIPZ-EV expressing cells (Figure 15b).

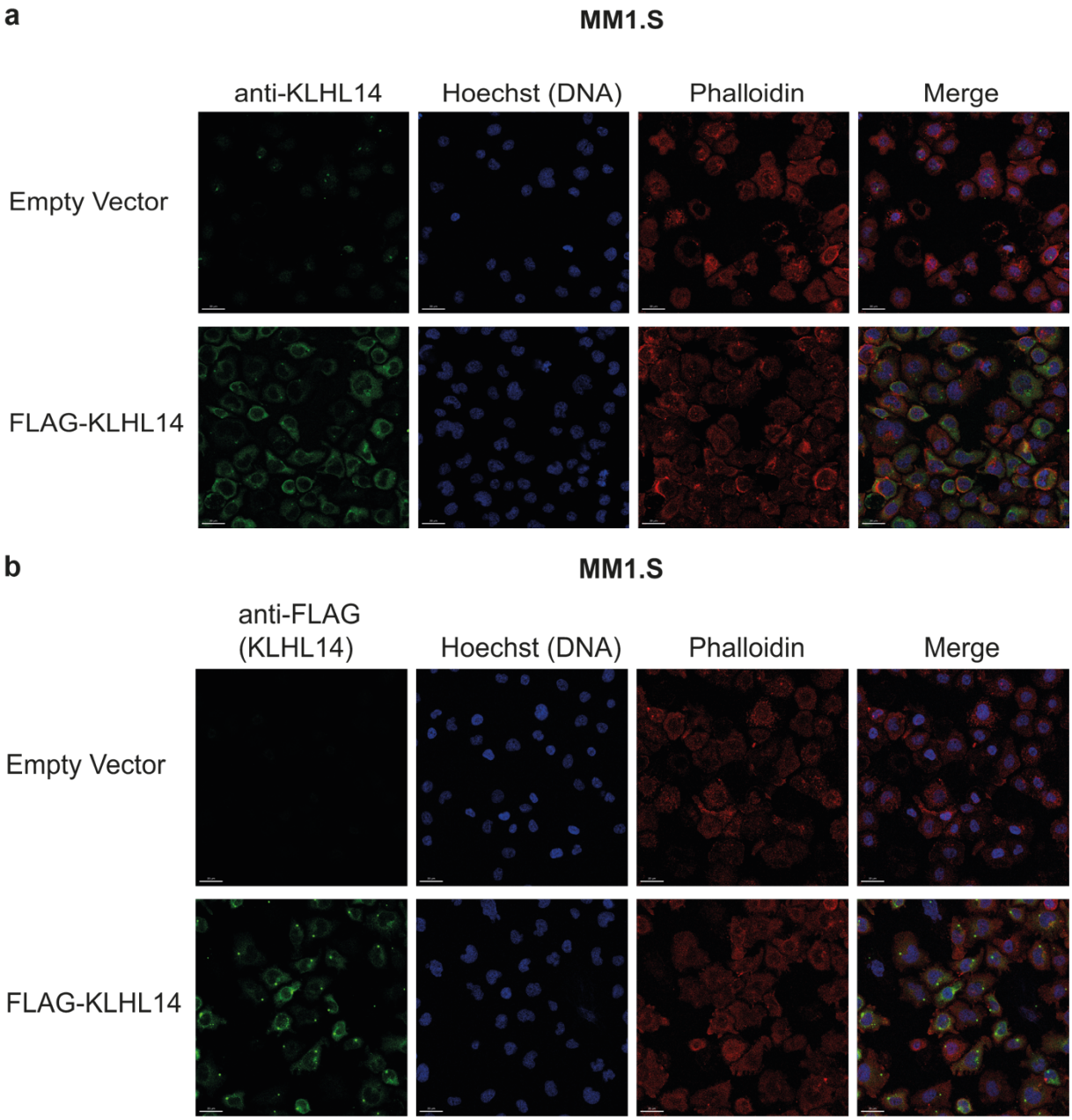

Figure 15 KLHL14 localizes to distinct foci in and around the nucleus of MM1.S cells overexpressing KLHL14. Representative immunofluorescence images of cells mounted on poly-D-lysine coated slides, fixed with 4% PFA and stained with corresponding antibodies. Images were captured with a LEICA-SF8 confocal microscope. The scale bar represents 20 µm. **(a, b)** MM1.S cells stably expressing pTRIPZ-EV or pTRIPZ-KLHL14 were treated with doxycycline (1 µg/mL) for 24 hours before fixation. They were stained with either **(a)** endogenous KLHL14 antibody (green) or **(b)** anti-FLAG (KLHL14 green) and the corresponding Alexa-Fluor-448 conjugated secondary antibody. F-actin was stained with Phalloidin (red), and the DNA was stained with Hoechst33258.

This foci-like structure resembled a centrosomal localization, which could mean an involvement of KLHL14 in the function of microtubule organizing centers and cell cycle regulation. To investigate this hypothesis, we co-stained MM1.S cells stably expressing pTRIPZ-EV or pTRIPZ-KLHL14 with an anti-FLAG and an anti-CENTRIN-3 antibody after doxycycline-induced transgene expression. Despite the similarity, no co-localization between KLHL14 and CENTRIN-3 was found in these cells (Figure 16).

We concluded that KLHL14 is predominantly localized as foci-like structures in and around the nucleus in cells. However, these KLHL14-specific foci-like structures do not co-

localize with centrin-3, therefore not suggesting a direct function of KLHl14 in centrosome biology.

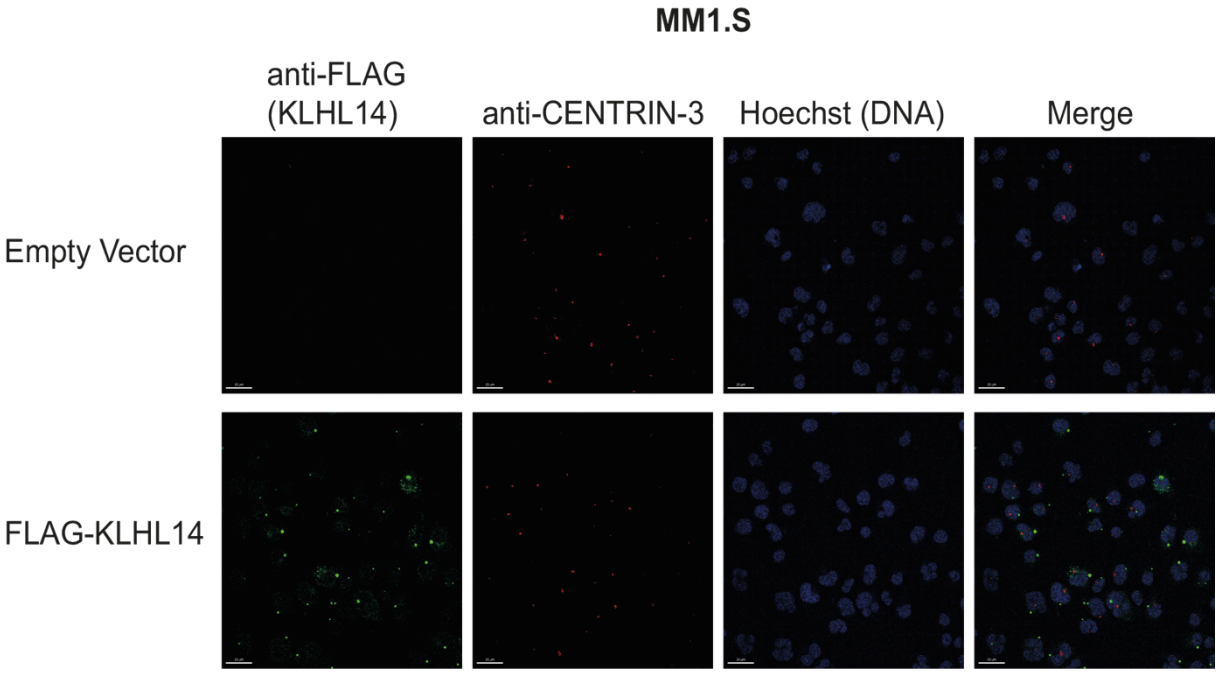

Figure 16 KLHL14-foci do not co-localize with CENTRIN-3 in MM1.S cells. Representative immunofluorescence images of cells mounted on poly-D-lysine coated slides, fixed with 4% PFA and stained with corresponding antibodies. Images were captured with a LEICA-SF8 confocal microscope. The scale bar represents 20 µm. The same cells from figure 15 were stained with anti-FLAG antibody (green) and anti-CENTRIN-3 antibody (red) and the corresponding Alexa-Fluor-448 and -594 conjugated secondary antibodies. The DNA was stained with Hoechst33258 (blue).

5.1.6 KLHL14 overexpression does not lead to increased cell death

To test the hypothesis that increased cell death is induced by KLHL14 expression and leads to the observed dropout phenotype, we performed a Live/Dead assay using flow cytometry. The assay is based on an APC-conjugated dye that binds to amines on the cell surface of intact cells as well as to amines inside of dying cells. Interactions on the cell surface of healthy cells result in a lower fluorescence signal than when the dye can additionally interact with amines inside of a dying cell. This allows live and dead cells to be distinguished based on the fluorescence intensity. The total amount of dead cells of MM1.S, OCI-LY3, and Z-138 cells stably expressing pTRIPZ-EV or pTRIPZ-KLHL14 was measured without doxycycline and one, three, and seven days under doxycycline treatment. No significant increase in dead cells was observed with KLHL14 expression in any of the cell lines (Figure 17a). Generally, the maximum percentage of dead cells never reached more than 10 % on any given day, strongly suggesting that KLHL14 overexpression does not cause cell death.

In addition, we analyzed the whole cell extracts of these cells at corresponding time points to the Live/Dead assay by immunoblotting. Comparison of protein levels between the cells expressing either pTRIPZ-EV or pTRIPZ-KLHL14 showed no significant and consistent increase in apoptosis indicators such as cleaved caspase3 under doxycycline-induced KLHL14 overexpression in all three cell lines (Figure 17b). Also, no significant and consistent elevated levels of DNA damage proteins such as phospho-Histone H3, phospho-H2A.X, or cleaved PARP-1 were detected in cells overexpressing KLHL14 compared to the empty vector (Figure 17b). Given the minimal evidence of increased cell death, with no significant increase of dead cells in the live/dead flow cytometry analysis and no significant and consistent

upregulation of cell death or DNA damage markers in all three cell lines, we concluded that the dropout phenotype was not primarily due to increased cell death or DNA damage resulting from KLHL14 overexpression.

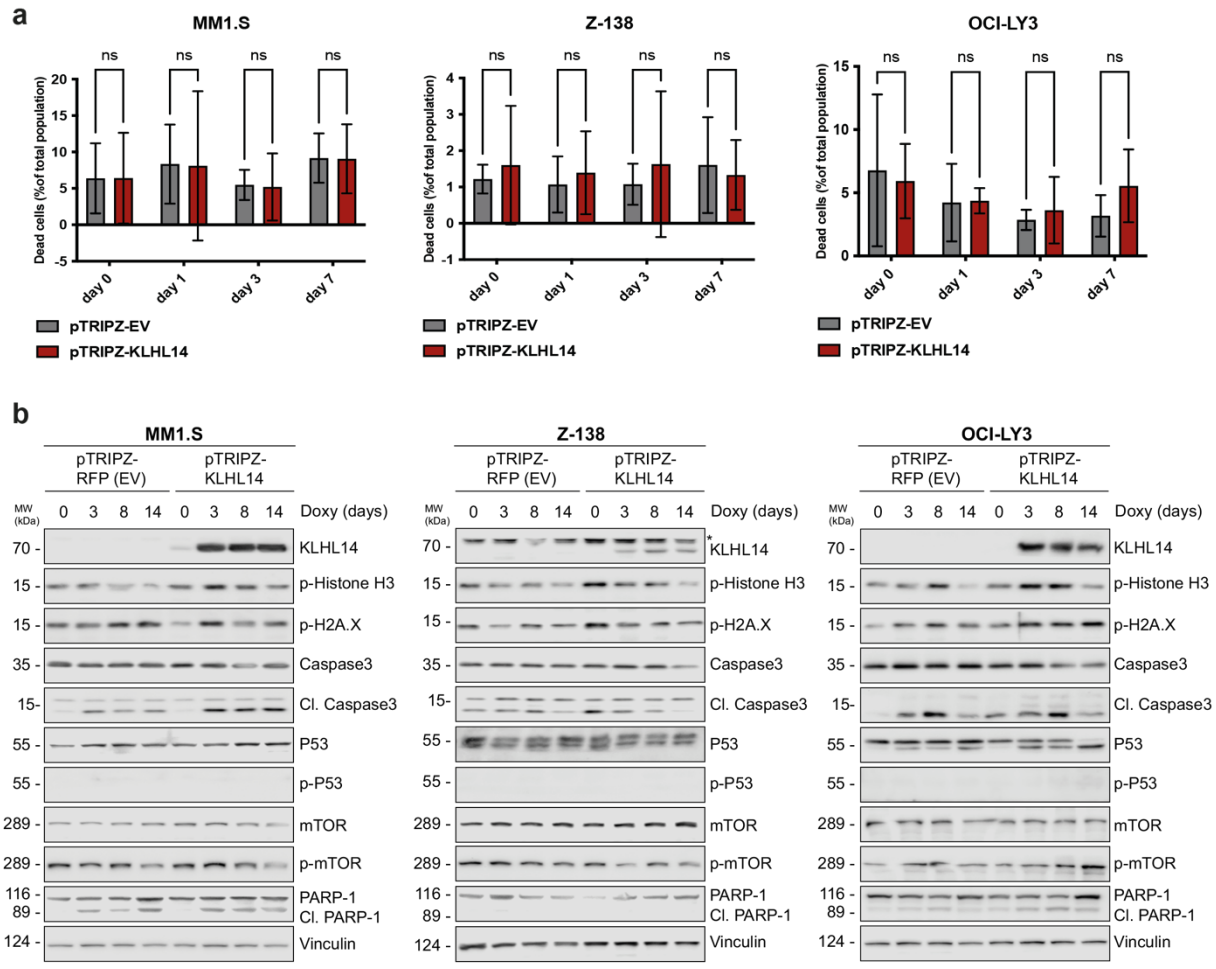

Figure 17 Cell death or DNA damage is not the cause for cell dropout upon KLHL14 overexpression. MM1.S, OCI-LY3, and Z-138 cells stably expressing pTRIPZ-EV or pTRIPZ-KLHL14 were treated with doxycycline (1 µg/mL) for 14 consecutive days. **(a)** Live/dead APC assay with MM1.S, OCI-LY3, and Z-138 cells at indicated time points post doxycycline treatment. Cells were stained with APC-coupled dye, and the signal intensity was measured by flow cytometry. The total amount (%) of dead cells in the corresponding culture is depicted. Statistical tests were performed by 2way ANOVA: 0.1234 (ns), 0.0332 (*), 0,0021 (**), 0.0002(***), <0.0001(****). **(b)** Representative immunoblot analysis of these MM1.S, OCI-LY3, and Z-138 cells from one of the Live/dead APC assays to confirm KLHL14 overexpression as well as DNA damage and cell death marker expression levels. Samples were harvested at the indicated time points, and WCEs were analyzed by immunoblot using the indicated antibodies. Loading control: Vinculin.

5.1.7 KLHL14 overexpression does not result in significant changes in cell cycle progression

Besides cell death, cell cycle progression is critical for cell proliferation and survival. Therefore, we analyzed whether the increased KLHL14 expression leads to changes in the underlying molecular processes of cell cycle progression. Cell cycle impairments can lead to an arrest in a specific cell cycle phase or an extension of the total cycle duration. Cell cycle profiles of MM1.S, OCI-LY3, and Z-138 cells stably expressing pTRIPZ-EV or pTRIPZ-KLHL14 were measured without doxycycline and at one, four, eight, and eleven days under doxycycline treatment. For this, cells were incubated with BrdU to allow incorporation of the thymidine

analog into the DNA of proliferating S-phase cells and then fixed in ethanol. After treatment with a fluorescence-labeled antibody specific for BrdU and staining with Propidium Iodide, which intercalates with double-stranded DNA to separate G1 (DNA content=n2) and G2 (DNA content=n4), the samples were measured by flow cytometry. No significant changes were observed in any of the cell cycle phases (Figure 18a, b, c). The relative number of cells in the S, G1, and G2 phases remained the same between cells with doxycycline-induced KLHL14 expression and empty vector expression on all four days. Only for OCI-LY3 on day 8, a slightly significant increase of KLHL14 expressing cells in the G1 phase was observed compared to the empty vector expressing cells of that day (Figure 18c). However, since this was only observed in one cell line on one day, we concluded that this was an outlier.

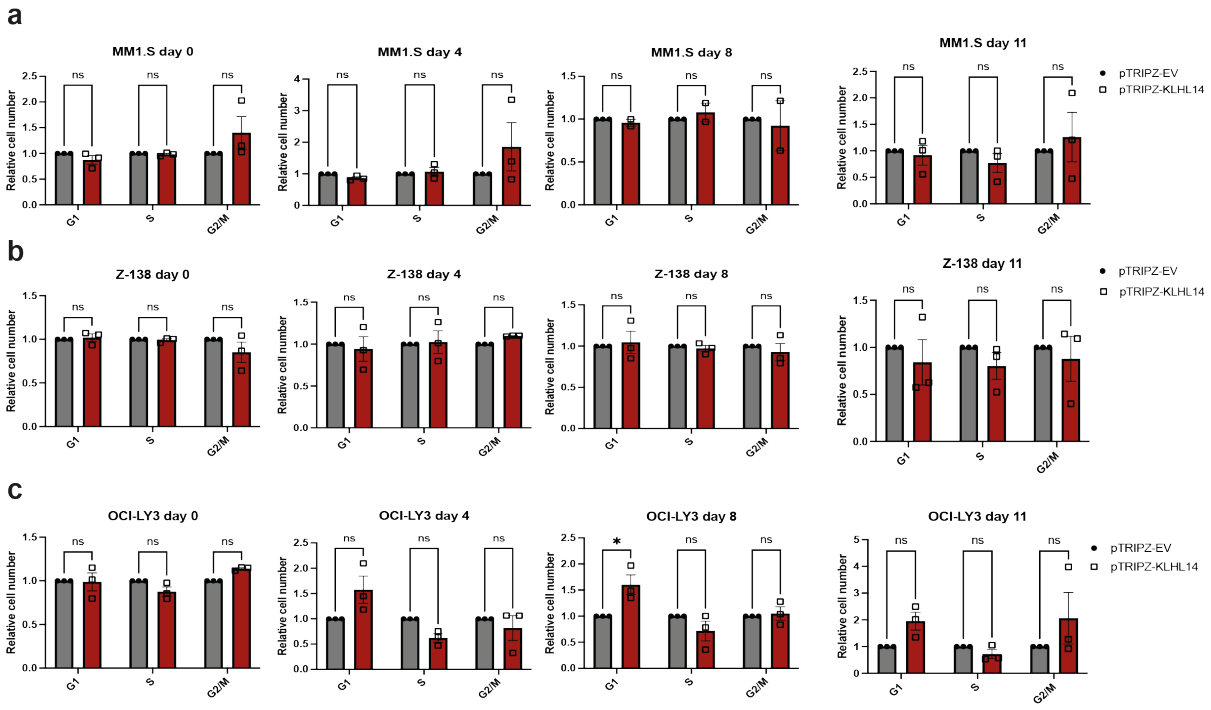

Figure 18 Changes in the cell cycle are not the cause for the dropout of cells upon KLHL14 overexpression. MM1.S, OCI-LY3, and Z-138 cells stably expressing pTRIPZ-EV or pTRIPZ-KLHL14 were treated with doxycycline (1 µg/mL) for 11 consecutive days. Cells were incubated with BrdU and the respective time points for 45 minutes, fixed in ethanol, and labeled with FITC-conjugated anti-BrdU antibody. The DNA was stained with Propidium Iodide. **(a, b, c)** Quantification of cells per cell cycle phase of corresponding cell lines analyzed by flow cytometry. Data were normalized to empty vector. Statistical tests were performed by 2way ANOVA: 0.1234 (ns), 0.0332 (*), 0,0021 (**), 0.0002(***), <0.0001(****).

Since KLHL14 expression does not seem to induce cell cycle arrest at any given phase, we analyzed whether KLHL14 expression induces a delayed and slowed cell cycle. Therefore, we performed a cell tracer assay, which is also based on an amine-reactive fluorescence-coupled dye and considered a cytoplasmic stain. The dye becomes more diluted with each cell division and changes its fluorescence signal intensity. This allows the detection of cells progressing slower through the cell cycle. Equal numbers of MM1.S, OCI-LY3, and Z-138 cells stably expressing pTRIPZ-EV or pTRIPZ-KLHL14 were treated with doxycycline for seven consecutive days. On the first day after transgene induction, they were stained with the cell-trace dye, and the APC fluorescence signal intensity was measured each day. The speed of cell division was tracked over seven days by comparing the signal intensity between cells expressing KLHL14 and the empty vector. No slowed or delayed cell cycle was observed in any of the cells after transgene induction over the time (Figure 19). An increased GM fold change of the APC signal would mean that the dye is less diluted and therefore the cells are

dividing slower, but this was not observed for any tested cell lines (Figure 19). This led to the conclusion that KLHL14 expression does not induce an altered rate of cell division.

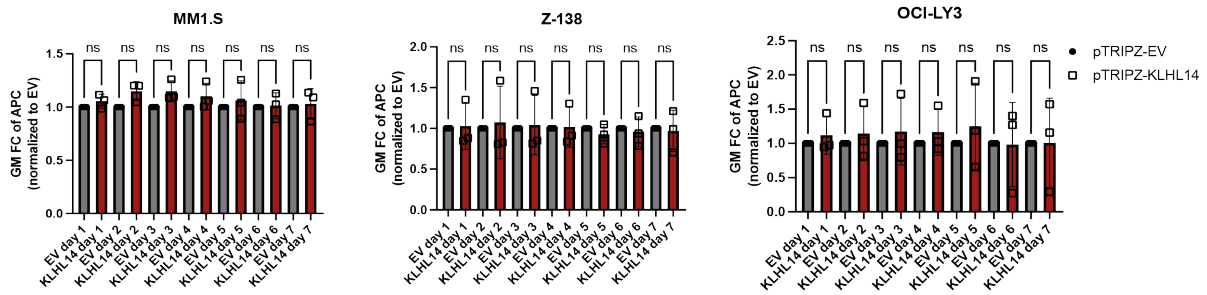

Figure 19 KLHL14 expression does not induce a lagging cell cycle. MM1.S, OCI-LY3, and Z-138 cells stably expressing pTRIPZ-EV or pTRIPZ-KLHL14 were treated with doxycycline (1 µg/mL) for seven consecutive days. Cells were counted and stained on day one post transgene induction with CellTracer APC-dye. The fluorescence signal intensity was measured daily, and the geometric mean of the APC signal fold changes were calculated and quantified. Data were normalized to empty vector. Statistical tests were performed by 2way ANOVA: 0.1234 (ns), 0.0332 (*), 0,0021 (**), 0.0002(***), <0.0001(****).

To be certain, we analyzed the protein levels of various cell cycle markers to see if we could observe consistent changes upon KLHL14 overexpression. Therefore, we conducted an immunoblot experiment on WCEs from MM1.S, OCI-LY3, and Z-138 cells stably expressing pTRIPZ-EV or pTRIPZ-KLHL14 at different time points post doxycycline induction. Similar to the previous results, no significant and consistent changes of cell cycle markers such as cyclin D, cyclin B, or p27 were observed at any time point (Figure 20). While there was a slight decrease of cyclin E and A in OCI-LY3, this observation was inconsistent for the other two cell lines (Figure 20). Taken together, these results suggest that the observed dropout phenotype is not due to changes in the cell cycle of the cells.

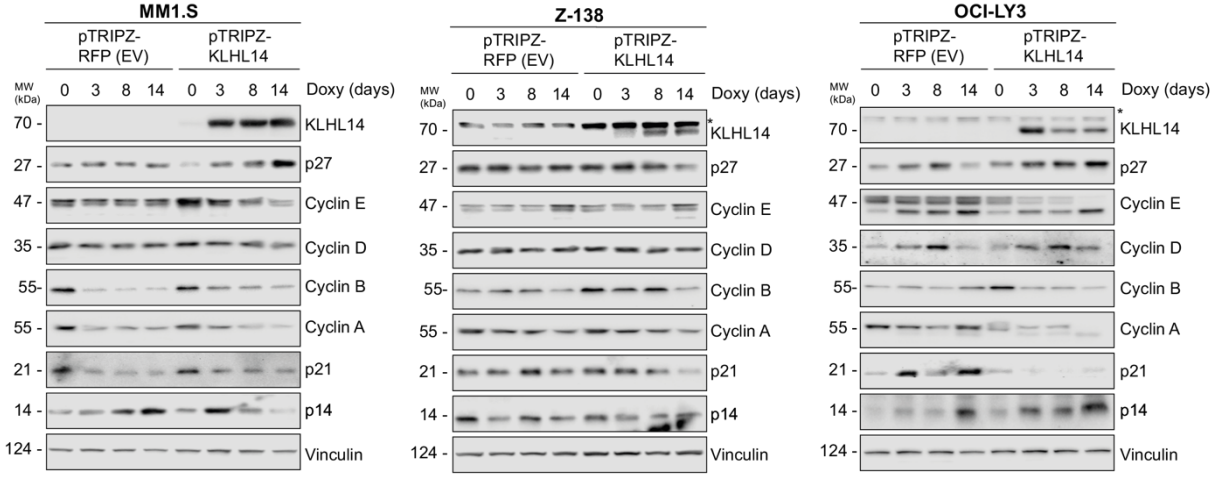

Figure 20 No increase in cell cycle marker upon KLHL14 overexpression. Immunoblot analysis of MM1.S, OCI-LY3, and Z-138 cells stably expressing pTRIPZ-EV or -KLHL14 after transgene induction by 1 µg/mL doxycycline treatment. Cells were harvested at the indicated time points and the whole cell extract was analyzed by immunoblot with the indicated antibodies. Loading control: Vinculin.

In addition to these two major molecular pathways, other cellular mechanisms may be involved in the observed dropout phenotype. Autophagy, a process that degrades and recycles damaged proteins, is particularly important under stress conditions to maintain cellular metabolism by recycling vital components. Dysregulation of this process can derail healthy

cellular homeostasis. A related cellular mechanism is the formation of aggresomes, which eliminates misfolded proteins and helps to protect the cell by isolating potentially harmful proteins. In an effort to find the underlying molecular mechanism of our observed dropout phenotype, we performed another immunoblot with the same cell lines used before. We analyze the protein levels of various cellular markers for autophagy and aggresome formation to see if we could observe changes upon KLHL14 overexpression. No significant and consistent changes in autophagy markers such as LC3A/B or p62 or aggresome formation such as XBP1, NRF2, or ATF4 were observed at any time point when cells expressing KLHL14 were compared to cells expressing empty vector (Figure 21). This result suggests that the observed dropout phenotype is not due to changes in autophagy or inhibited aggresome formation.

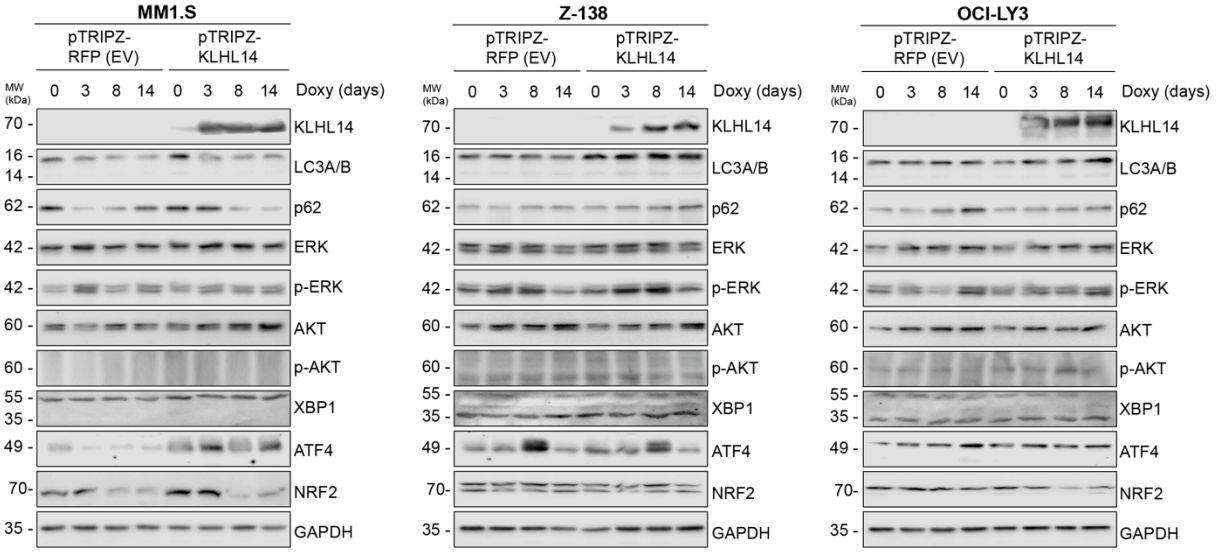

Figure 21 No increase in autophagy or aggresome formation upon KLHL14 overexpression. Immunoblot analysis of MM1.S, OCI-LY3, and Z-138 cells stably expressing pTRIPZ-EV or pTRIPZ-KLHL14 after transgene induction by 1 µg/mL doxycycline treatment. Cells were harvested at the indicated time points and the whole cell extract was analyzed by immunoblot with the indicated antibodies. Loading control: GAPDH.

5.1.8 Interactome screening for KLHL14 substrates reveals NUDCD3 as an interactor

KLHL14 functions as a subunit of the Cullin-RING ubiquitin ligase complex and is responsible for substrate recognition. Given the effects of KLHL14 overexpression leading to dropout in MM, MCL, and DLBCL cells, we conducted two interactome screens to discover potential KLHL14 substrates that could elucidate the molecular mechanism behind the observed dropout phenotype. To this end, two mass spectrometry-based interactome screens were performed, one screen with asynchronous MM1.S cells and one screen with mitotically synchronized MM1.S cells. We used the previously described doxycycline-inducible pTRIPZ system to drive the expression of FLAG-EV or FLAG-KLHL14. After 24 hours of transgene induction, the cells were harvested, subjected to FLAG immunoprecipitation using M2-FLAG affinity agarose-gel, and subsequently eluted with acidified 0.2 M glycine. For quality control, 5% of the eluate was used in a silver gel, while the remainder was precipitated with 20% trichloroacetic acid (TCA), dried, and sent to the BayBio@MRI core facility for mass spectrometric analysis. Here, the samples were resuspended, reduced, alkylated, and in-gel digested with trypsin. The resulting peptides were dissolved in 0.1% FA and 2% ACN and then analyzed by mass spectrometry.

Immunoblot analysis and silver staining revealed successful overexpression of the bait FLAG-KLHL14 and a consistent enrichment of the FLAG-tagged KLHL14 across all replicates in both screens (Figure 22a, b, c, d). In addition, the presence of other bands in the FLAG-KLHL14 samples indicates that many different proteins and potential interactors co-purify with the bait protein.

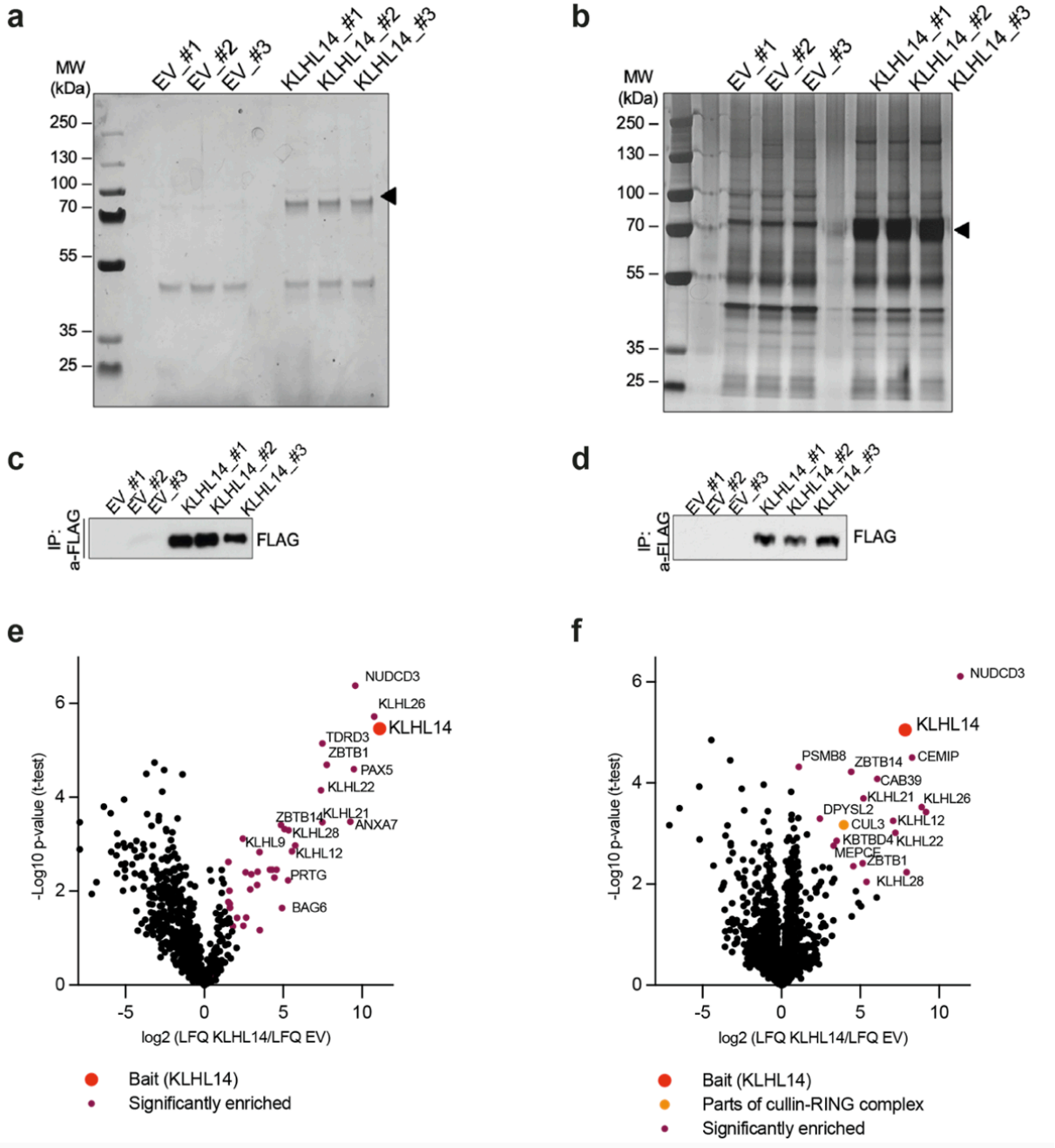

Figure 22 Mass spectrometry coupled interactome screens of asynchronous and mitotically synchronized cells identify KLHL14 substrates. MM1.S cells stably expressing pTRIPZ-EV or -KLHL14 were treated with 1 µg/mL doxycycline to induce transgene expression while for one interactome screen also being simultaneously arrested in mitosis by a sequential thymidine and nocodazole treatment for 25 hours. Left: asynchronous interactome screen **(a, c, e),** right: synchronized interactome screen **(b, d, f).** Four hours before cells were harvested, 10 µM MG132 was added to enrich for ubiquitylated proteins. After cell harvest, samples were immunoprecipitated using FLAG-M2 affinity agarose beads and eluted with acidified 0.2M glycine. 2.5% of each sample was used for SDS-PAGE followed by silver staining **(a, b)** or immunoblot **(c, d).** Arrowheads indicate the KLHL14 band. A FLAG antibody was used to show the overexpressed KLHL14 in the immunoblot. **(e, f)** The remaining 95% of the samples were analyzed by mass spectrometry. Log2 ratios of the averaged KLHL14/EV LFQ values were plotted against the negative Log10 of the corresponding p-values. Purple dots represent significantly enriched KLHL14 interactors (FDR< 0.05; S0 =0.1 by Student T-test). All experiments were set up in biological triplicates. Mass spectrometry analysis was performed at BayBioMS@MRI, and peptide and protein identification

were performed using MaxQuant software version 1.6.3.3. (Both interactome screens were performed by R. Spallek)

A total of 710 protein groups were identified in the asynchronous screen after excluding known contaminants (Figure 22e), while 1798 were detected in at least two of the three replicates in the mitotically synchronized screen (Figure 22f). Missing values for proteins not identified in a sample were imputed from a normal distribution. For the asynchronous screen, 64 proteins showed more than a twofold increase in abundance in the KLH14 samples, of which 37 reached statistical significance (FDR < 0.05; SO=0.1) and are shown as purple dots (Figure 22e). For the mitotically synchronized screen, 150 proteins showed more than a twofold increase in abundance in the KLH14 samples, of which 15 reached statistical significance (FDR < 0.05; SO=0.1) and are shown as purple dots (Figure 22f). The bait KLHL14 was among the top hits, along with some other members of the Kelch-like protein family members, which could be due to the shared BTB fold that acts as a general protein interaction domain. Interestingly, the most significant interactor in both screens was NUDCD3 (Figure 22e, f).

5.1.9 Confirmation of KLHL14 interaction with substrate NUDCD3

NUDCD3 is a poorly characterized protein that has been reported to play a role in many cellular processes by regulating the stability of the dynein intermediate chain. Aberrations in NUDCD3 protein levels can result in mis-localization or even degradation of the dynein complex, in addition to translocation of gamma-tubulin from the spindle poles and restrictions in the G1/S phase transition (Zhou et al., 2006). An affinity-pulldown assay was performed with FLAG-purified KLHL14 to confirm the interaction between KLHL14 and the potential substrate NUDCD3. HEK293T cells were transfected with either an empty vector or FLAG-tagged KLHL14. The cells were harvested the next day and subject to FLAG immunoprecipitation using M2-FLAG affinity gel. At the same time, wild type cell samples from MM, DLBCL, and MCL cell lines were harvested and lysed. The WCEs of the wild type samples were then incubated with the M2-FLAG affinity gel after the initial IP and the proteins bound to the gel were eluted and immunoblotted. For all cell lines, we observed similar levels of FLAG-KLHL14, but an increased amount of NUDCD3 protein was detected in the samples incubated with WCEs from MM, DLBCL and MCL cells, compared to samples that were not incubated with additional cell lysates (Figure 23a). This confirmed an interaction between KLHL14 and NUDCD3 in MM, MCL, and DLBCL cell lines (Figure 23a). Very long exposure would also result in a NUDCD3 band detection in the HEK293T samples without any additional cell line lysates (not shown).

To further validate these findings, we performed semi-endogenous FLAG immunoprecipitations in transfected HEK293 alone, as well as in MM1.S, OCI-LY3, and Z-138 cells stably expressing pTRIPZ-EV or pTRIPZ-KLHL14. The cells were lysed 24 hours post transfection or doxycycline-mediated transgene induction, immunoprecipitated with M2-FLAG affinity gel and immunoblotted. NUDCD3 was co-purified with KLHL14 in all four cell lines overexpressing KLHL14, but not in the cells overexpressing the empty vector (Figure 23b). This confirmed our previously observed interaction between KLHL14 and NUDCD3. Immunoblotting of the IP samples also revealed binding of KLHL14 to its E3 ligase complex component Cul3 (Figure 23b). This confirmed to some extent that overexpressed KLHL14 can form a functional E3 ligase complex in the cells.

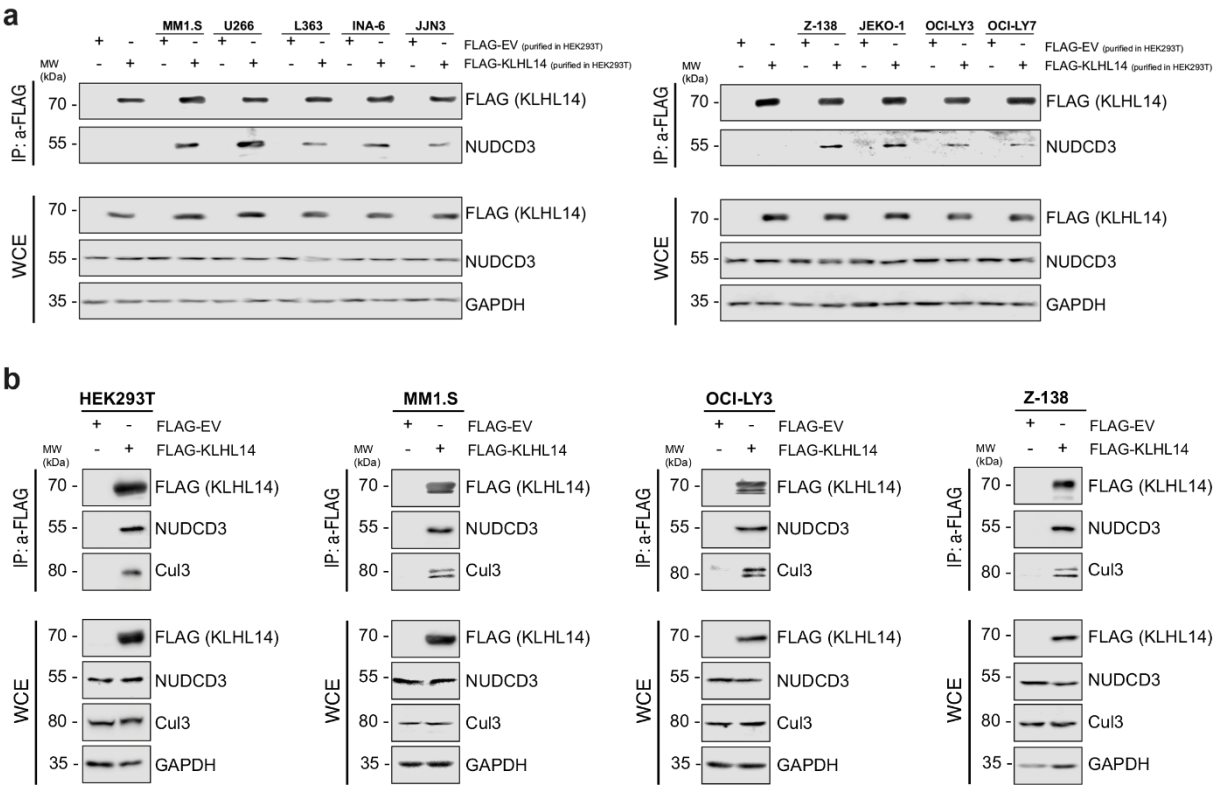

Figure 23 NUDCD3 interacts with KLHL14 in cells. (a) Affinity-pulldown assay where FLAG-tagged KLHL14 was purified from transfected HEK293T cells using M2-FLAG affinity gel and subsequently incubated overnight with WCEs from different MM, DLBCL, and MCL cell lines. The samples were analyzed by immunoblotting with the indicated antibodies. Loading control: GAPDH. **(b)** Semi-endogenous immunoprecipitation of HEK293T cells transfected with either FLAG-empty vector or FLAG-KLHL14 and MM1.S, OCI-LY3 and Z-138 cells stably expressing pTRIPZ-EV or pTRIPZ-KLHL14. Cells were harvested one day after doxycycline (1 µg/mL) transgene induction and immunoprecipitated using M2-FLAG affinity gel. Subsequently, the samples were analyzed by immunoblotting with the indicated antibodies. Loading control: GAPDH.

5.1.10 NUDCD3 overexpression or knockdown leads to a similar dropout phenotype in cells as observed with KLHL14 overexpression

We investigated the protein expression levels of NUDCD3 in different cancer entities, as it is a potential substrate of KLHL14. Therefore, we analyzed a panel of cell lines for NUDCD3 protein expression. NUDCD3 expression varied among MM, MCL, DLBCL, AML, and NSCLC cell lines, but in general almost all cell lines had some detectable level of NUDCD3 protein expression (Figure 24a, b, c, d). When the KLHL14 cell line panel was compared with the NUDCD3 panel, no correlation was found between KLHL14 and NUDCD3 protein expression levels (Figure 10, Figure 24). While some cell lines with high KLHL14 protein expression, such as TMD8 and KMS12BM, also showed a relatively high NUDCD3 protein expression, other cell lines with high KLHL14 protein expression, such as OVCAR3, had low NUDCD3 protein expression. Most of the MM cell lines with almost no KLHL14 protein expression showed moderate NUDCD3 protein expression.

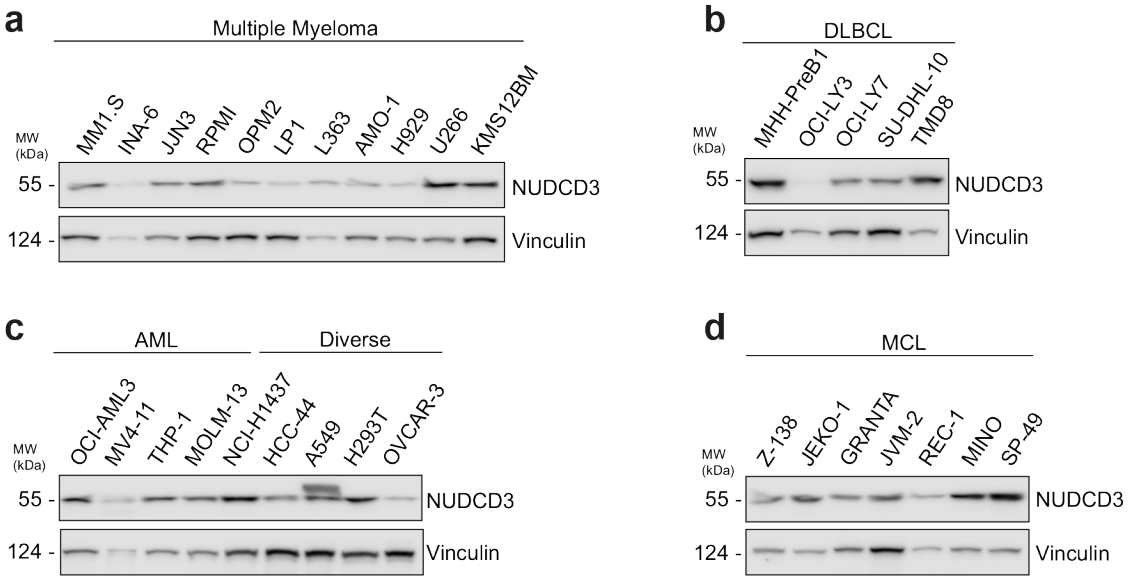

Figure 24 NUDCD3 protein expression in MM, DLBCL, AML, and MCL cell lines. Immunoblot analysis of whole cell extracts from cell lines **(a)** MM, **(b)** DLBCL, **(c)** AML/Diverse, and **(d)** MCL. The indicated antibodies were used for the immunoblots, loading control: Vinculin.

It has been published that depletion of NUDCD3 in HeLa cells inhibits cell growth and induces G1 arrest, leading to cell death (Zhou et al., 2006). Changing the abundance or localization of the suggested KLHL14 substrate NUDCD3 by ubiquitylation would also affect cell survival or proliferation. Arguing that ubiquitylation of NUDCD3 by KLHL14 would not completely reduce its protein expression levels, we chose a shRNA-based knockdown instead of a full-on CRISPR-Cas9-mediated knockout of NUDCD3. We performed a similar dropout assay as described above with KLHL14 (Figure 11), but instead, we overexpressed NUDCD3 or, in a separate dropout assay, knocked down NUDCD3 with shRNAs. The NUDCD3 overexpression dropout assay was performed similarly to the KLHL14 overexpression dropout assay described above. The overexpression constructs of FLAG-tagged NUDCD3 were validated by immunoblot analysis and showed increased NUDCD3 expression in transduced MM1.S cells (Figure 25a). For the shRNA-based NUDCD3 dropout assay, we designed shRNAs targeting NUDCD3 based on portals.broadinstitute website and also validated them. Three days after transducing the cells with lentiviral particles containing the shRNAs, the cells were harvested and immunoblotted for NUDCD3 expression. Since it was not possible to achieve a transduction efficiency close to 100% in these cells, there is not a complete knockdown of NUDCD3, but all three shRNAs resulted in a significant depletion of NUDCD3 protein levels (Figure 25b).

After confirming successful NUDCD3 overexpression and knockdown we conducted several dropout assays, as described before. Overexpression of NUDCD3 resulted in a dropout of positively transduced MM1.S and Z-138 cells (Figure 25c). No cell ratio changes were observed in OCI-LY3 overexpression NUDCD3 (Figure 25c). For the shRNA dropout screens, we transduced MM1.S, OCI-LY3, and Z-138 cells with lentiviral particles containing either a vector with the shRNAs targeting NUDCD3 or non-targeting control shRNAs, both coupled to a dsRed reporter transgene. Cell transduction efficiency ranged from 20-60% and the ratio of transduced cells (dsRed-positive) to non-transduced cells (dsRed-negative) was measured by flow cytometry. Knockdown of NUDCD3 expression by targeted shRNAs resulted in a significant dropout in the population of positively transduced cells over a 14-day period in all three cell lines (Figure 25d). This dropout was more pronounced in MM1.S and Z-138 cells

but was observed overall in all three cell lines. Interestingly, shNUDCD3_1 achieved the best dropout rates across all three cell lines, correlating to the most substantial knockdown effects as seen in the immunoblot compared to the other two shRNAs (Figure 25b, d). No dropout was observed in the non-targeting control shRNA population.

Taken together, NUDCD3 is expressed in almost all cell lines, and altering its abundance leads to a dropout phenotype similar to KLHL14 overexpression in the same cells. This suggests an important cellular role of NUDCD3 in all cell lines and a possible connection between KLHL14 and NUDCD3.

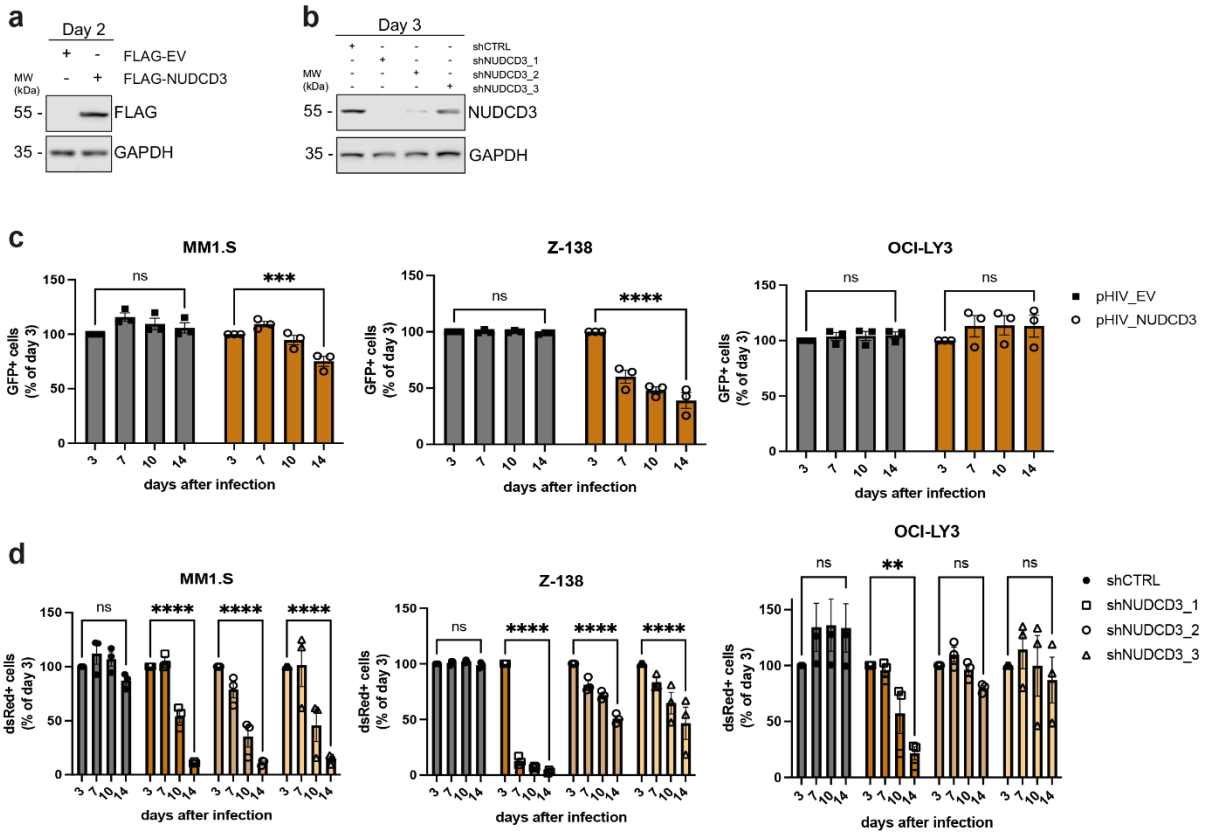

Figure 25 Altered NUDCD3 expression results in a dropout phenotype of cells. (a) Immunoblot analysis of MM1.S transduced with lentiviral particles containing FLAG-tagged NUDCD3 or FLAG-tagged empty vector. Cell pellets were harvested two days post transduction, lysed, and immunoblotted with the indicated antibodies. Loading control: GAPDH. **(b)** Immunoblot analysis of OCI-LY3 transduced with lentiviral particles containing one of three different shRNAs targeting NUDCD3 or non-targeting control shRNA. Cell pellets were harvested three days post transduction, lysed, and immunoblotted with the indicated antibodies. Loading control: GAPDH. **(c)** A competitive growth assay was performed with MM1.S, OCI-LY3, and Z-138 cells. Cells were transduced with lentiviral particles containing FLAG-NUDCD3 (in orange) or empty vector (in gray), both in combination with a GFP reporter. Transduction efficiency ranged from 20-80%. The ratio of positive (GFP+) to negative (GFP-negative) transduced cells was measured by flow cytometry over a 14-day time course. Data were normalized in relation to day 3. Statistical tests were performed by 2way ANOVA: 0.1234 (ns), 0.0332 (*), 0,0021 (**), 0.0002(***), <0.0001(****). **(d)** A competitive growth assay was performed with MM1.S, OCI-LY3, and Z-138 cells. Cells were transduced with lentiviral particles containing shRNAs targeting either NUDCD3 (NUDCD3_1/2/3 in orange) or non-targeting shRNAs (shCTRL in gray) at a transduction efficiency of 20-60%. The ratio of positive (dsRed+) to negative (dsRed-negative) transduced cells was measured by flow cytometry over a 14-day time course. Data were normalized for each shRNA in relation to day 3. Statistical tests were performed by 2way ANOVA: 0.1234 (ns), 0.0332 (*), 0,0021 (**), 0.0002(***), <0.0001(****).

5.1.11 KLHL14 ubiquitylates its substrate NUDCD3

The primary function of the Cullin-RING E3 ligase KLHL14 is to attach ubiquitin to its substrates, thereby altering the abundance, localization, or biology of the substrate protein. K-48-linkage specific ubiquitin chains are one of the most observed chain types leading to substrate degradation via the proteasome. Performing a CHX chase allows for a first assessment of substrate protein degradation via the proteasome. To analyze whether increasing KLHL14 levels affects NUDCD3 protein abundance, MM1.S and Z-138 cells stably expressing pTRIPZ-EV or pTRIPZ-KLHL14 were treated with doxycycline one day prior to the CHX chase for transgene expression. Subsequently, the cells were treated with CHX for up to eight hours at different time points. As a control, one sample was treated with the proteasome inhibitor MG132 in addition to CHX. WCEs from all conditions were analyzed by immunoblotting. Blotting for PLK1, a protein known for its rapid turnover, was used as a control to confirm inhibition of ribosomal protein synthesis and inhibited proteasomal degradation. Although both NUDCD3 protein levels decrease after inhibition of new protein synthesis with CHX treatment, the addition of KLHL14 expression did not significantly increase the turnover of NUDCD3 compared to the empty vector expression (Figure 26). Furthermore, the addition of MG132 did not recover NUDCD3 or KLHL14 protein levels in MM1.S cells. Therefore, we concluded that although NUDCD3 interacts with KLHL14, its protein stability is not affected by KLHL14 and most likely it is not K48 ubiquitylated. The missing recovery upon MG132 in MM1.S suggests that NUDCD3 is not degraded via the proteasome and, thus, most likely not K48 ubiquitylated.

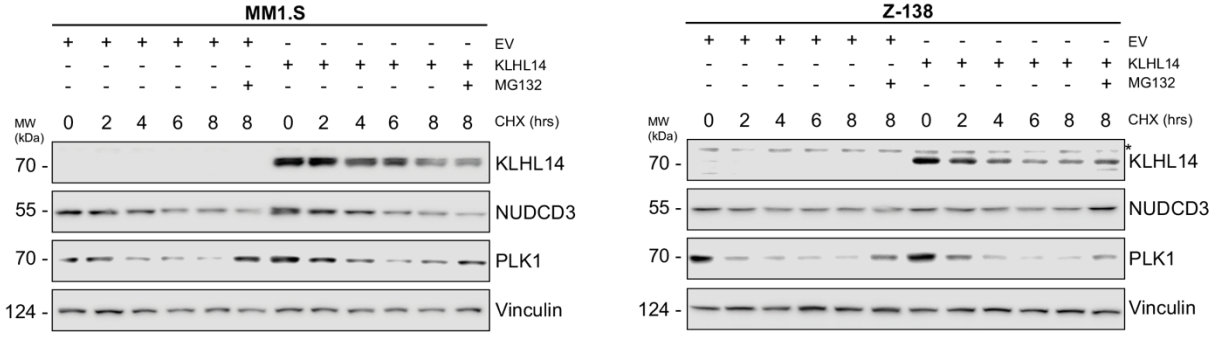

Figure 26 Destabilization of NUDCD3 is independent of KLHL14 overexpression. Immunoblot analysis of MM1.S and Z-138 cells stably expressing pTRIPZ-EV or pTRIPZ-KLHL14 after transgene induction through 1 µg/mL doxycycline treatment followed by cycloheximide (200 µg/mL) and MG132 (10 µM) treatment. Samples were harvested at the indicated time points post cycloheximide treatment. The indicated antibodies were used for immunoblotting analysis, loading control: Vinculin.

After verifying the interaction between KLHL14 and NUDCD3 and observing a dropout phenotype upon altered NUDCD3 expression but no increased degradation of NUDCD3 upon KLHL14 overexpression, we next focused on the insides of ubiquitylation of NUDCD3 by the E3 ligase KLHL14. Therefore, we performed an *in-vivo* ubiquitylation in HEK293T cells. HEK293T cells were transfected with plasmid combinations encoding HA-ubiquitin, FLAG-tagged NUDCD3 and MYC-tagged KLHL14. One day after transfection, cells were treated with MG132 for four hours to prevent proteasomal degradation of ubiquitylated proteins and subsequently harvested and lysed. FLAG immunoprecipitation was performed on the WCEs under denaturing conditions to isolate FLAG-NUDCD3 without co-isolation of other interacting proteins. The samples were analyzed by immunoblotting. This revealed a significant increase in NUDCD3 ubiquitylation upon KLHL14 overexpression compared to the ubiquitylation levels of NUDCD3 upon empty vector overexpression (Figure 27a, b). The ubiquitin bands showed

the typical smear pattern with a very prominent band at around 100 kDa. This confirmed the previously observed interaction of KLHL14 with NUDCD3 and that KLHL14 ubiquitinates NUDCD3 in HEK293T cells.

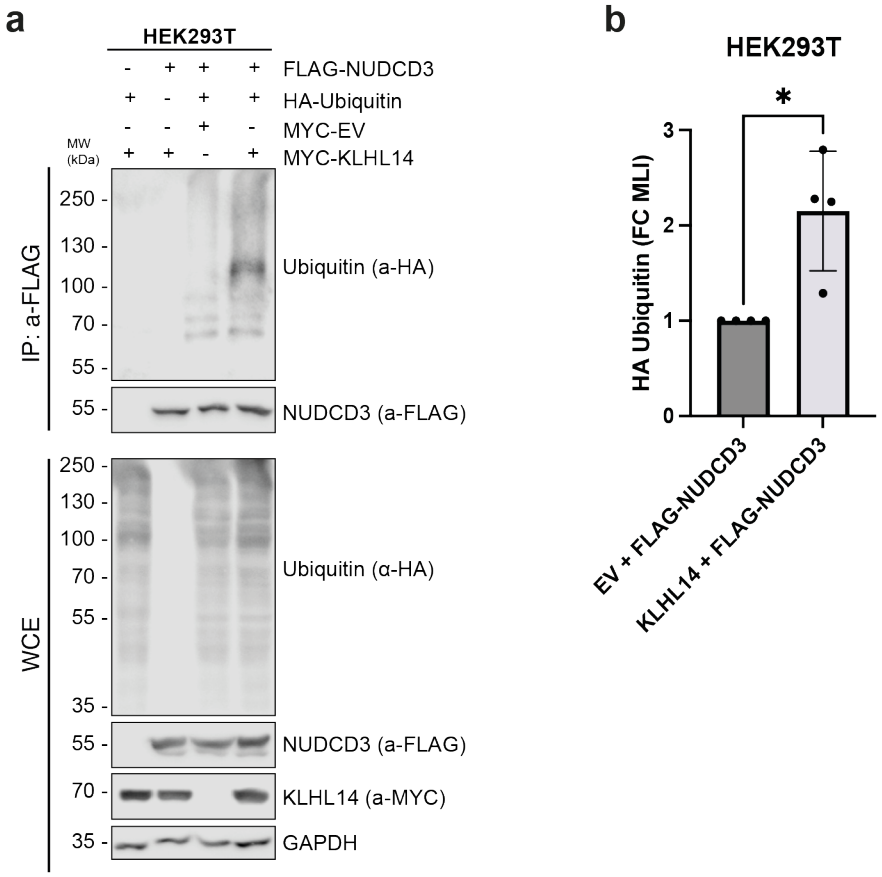

Figure 27 NUDCD3 is ubiquitylated by the E3 ligase KLHL14. *In-vivo* ubiquitylation assay of HEK293T cells transfected with the indicated plasmid combinations of HA-tagged ubiquitin, FLAG-tagged NUDCD3 and MYC-tagged KLHL14. 24 hours post transfection, the cells were treated with MG132 for four hours, then harvested and lysed. A FLAG immunoprecipitation was performed under denaturing conditions and samples were analyzed by **(a)** representative immunoblotting with the indicated antibodies. Loading control: GAPDH **(b)** Quantification of the immunoblot results from HA-Ubiquitin of MYC-EV + HA-Ubiquitin + FLAG-NUDCD3 and MYC-KLHL14 + HA-Ubiquitin + FLAG-NUDCD3 from four separate *in-vivo* ubiquitylation assays. The mean luminescence intensity (MLI) was calculated using ImageStudioLite software. Statistical tests were performed by t-test: 0.1234 (ns), 0.0332 (*), 0,0021 (**), 0.0002(***), <0.0001(****).

To determine what type of ubiquitin chains are being attached to NUDCD3 by the E3 ligase, the *in-vivo* ubiquitylation assays were repeated. The HEK293T cells were transfected with mutant ubiquitin versions instead of wild type HA-tagged ubiquitin. For this, lysine to arginine substitutions at six of the seven lysine residues of the ubiquitin were designed, leaving only one lysine available for polyubiquitin chain formation. Interestingly, the *in-vivo* ubiquitylation assays using K48-only ubiquitin revealed increased levels of ubiquitylated NUDCD3 upon KLHL14 overexpression (Figure 28a), although no increased degradation of NUDCD3 was detected in our CHX chase experiment upon KLHL14 overexpression (Figure 26). Using K63, K11, K27, K29, and K33, only ubiquitin showed a similar result, with all showing increased levels in the presence of NUDCD3 and KLHL14 compared to NUDCD3 alone and the empty vector (Figure 28b, c, d, e, f). Taken together, using chain-specific ubiquitin mutants revealed that KLHL14 polyubiquitylation of NUDCD3 is not limited to one linkage-specific polyubiquitylation.

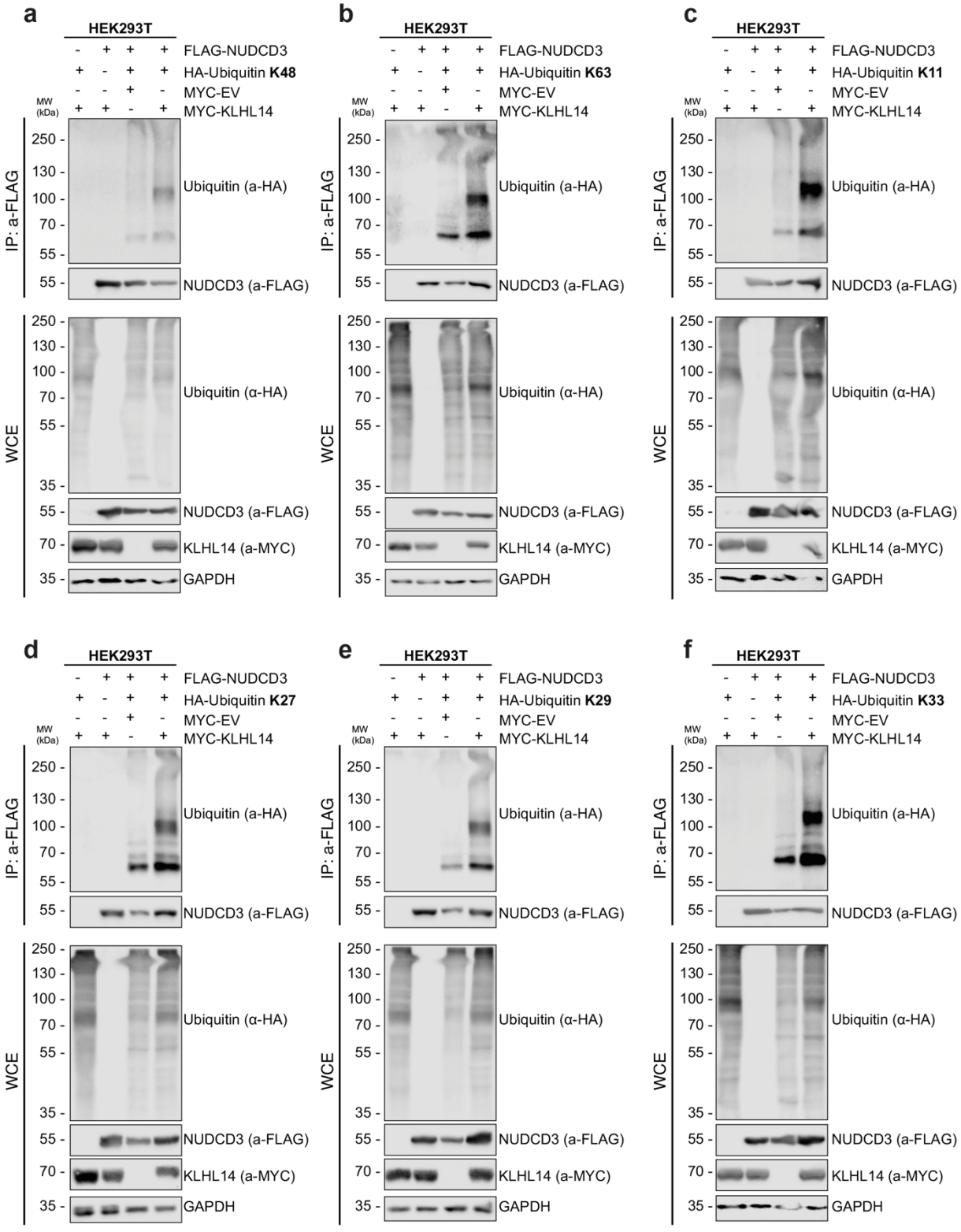

Figure 28 NUDCD3 is ubiquitylated by the E3 ligase KLHL14 forming different ubiquitin chain types. *In-vivo*-ubiquitylation assay of HEK293T cells similar to figure 27, but with mutant HA-ubiquitin (a= K48, b= K63, c= K11, d= K27, e= K29, F= K33) allowing only the indicated polyubiquitin chain types to form. At 24 hours post transfection, the cells were treated with MG132 for four hours, then harvested and lysed. A FLAG immunoprecipitation was performed on whole cell extracts under denaturing conditions and samples were analyzed by immunoblotting with the indicated antibodies. Loading control: GAPDH

5.2 Results DCAF7

5.2.1 CRISPR-Cas9-based screen identifies DCAF7 as a novel vulnerability in LuAD

Since our first goal was to find new vulnerabilities in LuAD with a focus on E3 ligases of the UPS, we used data from a previous CRISPR-Cas9-based dropout screen from our lab to find poorly characterized E3 ligase proteins that play a role in LuAD (Figure 29). The CRISPR-Cas9 screen and validation of the screen was performed by V. Wagner. Briefly, three LuAD cell lines (NCI-H1437, NCI-H23, and HCC44) were lentivirally transduced with a Cas9 expression construct, selected for expression of the construct, and tested for stable/functional Cas9 expression. The selected LuAD cell lines had wild type EGFR and ALK genes with different genetic aberrations to exclude cell line-specific effects and clinically approved drug targets. Lentiviral particles were generated from a pooled single-guide RNA (sgRNA) library described in a previous publication and provided by Mitch Weiss of the Children's Hospital in Memphis (Xu et al., 2021). The library contained 3200 sgRNAs targeting over 750 genes of the UPS. The Cas9-positive LuAD cell lines were infected with the sgRNA virus particles at a low multiplicity of infection on day zero of the screen. On the fourth day after infection, the cells were sorted using a mCherry selection marker, a cell sample was taken and the rest was cultured for an additional 14 days. Another cell sample was collected on day eighteen, and sgRNA sequences were extracted from samples of day four and eighteen and amplified for sequencing. We compared the library composition between day four and day eighteen to identify which sgRNAs decreased or increased in prevalence over time. This indicated the role of the targeted gene in either promoting or inhibiting LuAD.

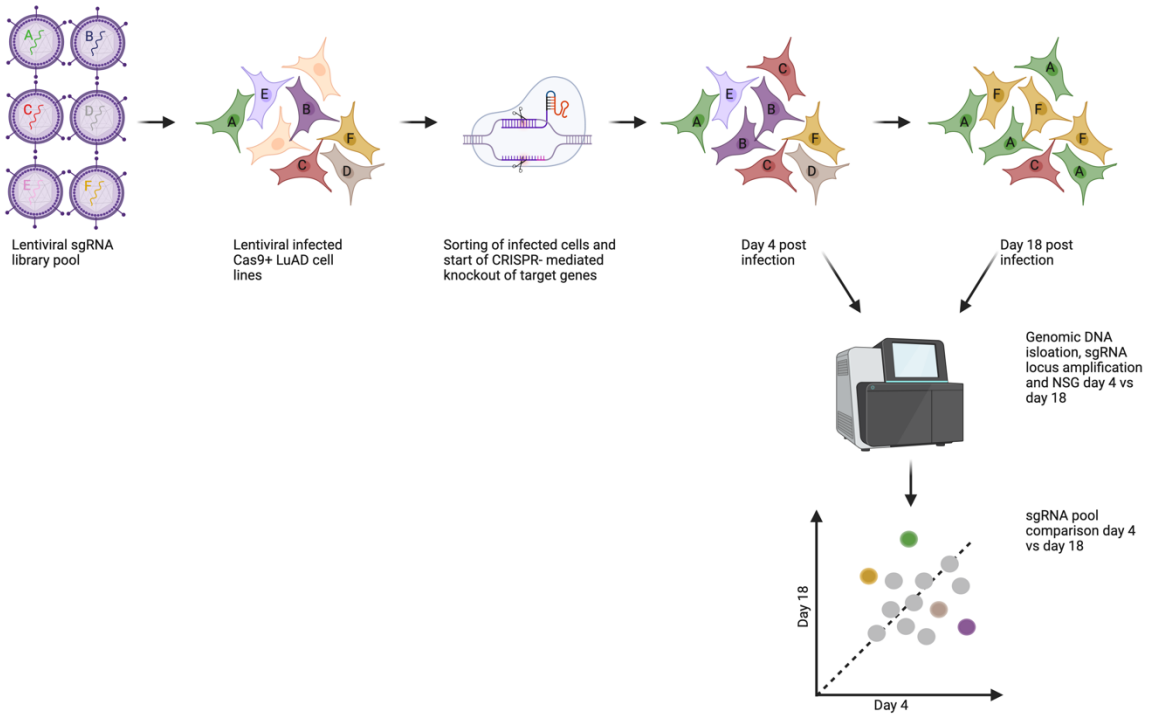

Figure 29 Schematic of the CRISPR-Cas9-based dropout screen. Lentiviral particles containing a sgRNA library were generated. Cas9+ LuAD cell lines were transduced with the sgRNA library and sorted for positive transfected cells. After CRISPR-Cas9-mediated knockout of the target genes, a cell sample was collected on day four and 18

post-transfection. Genomic DNA was isolated and the sgRNA locus was amplified and sequenced. The sgRNA abundance was compared between day four and day 18 to find genes that are essential for LuAD cell survival and therefore dropped out over the 18 days. This screen was conducted by V. Wagner. The figure was generated using Biorender.

Comparison of next-generation sequencing (NGS) results from samples collected on day 4, representing the initial library composition, and day 18, revealed DCAF7 as one of the most interesting hits in all three cell lines (Figure 30). As shown in Figure 30 in NCI-H1437, the abundance of all sgRNAs targeting DCAF7 (blue dots) decreased over time. For NCI-H23 and HCC44, most of the sgRNAs targeting DCAF7 decreased below the trash hold (dotted line) (Figure 30). This meant that over the time course of the 18 days, LuAD cells infected with sgRNAs targeting DCAF7 dropped out of the population, hinting towards a cancer cell dependency on functional DCAF7 protein expression.

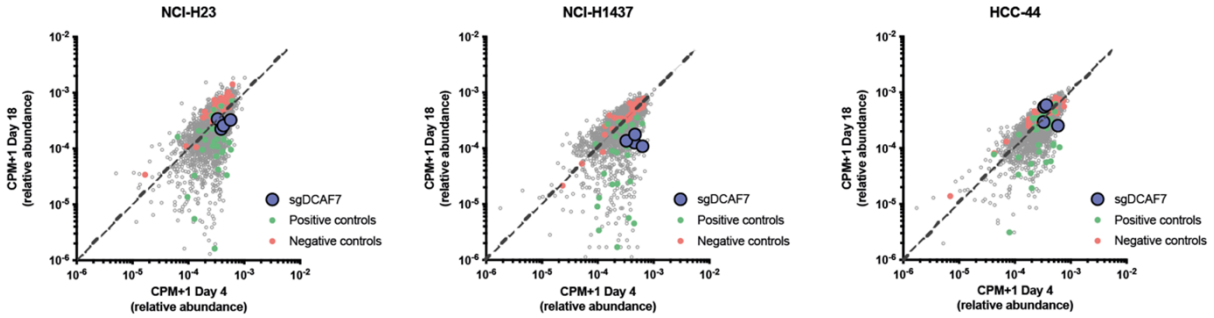

Figure 30 Results of the CRISPR-Cas9-based dropout screen. Comparison of sgRNA levels from day four to day 18 in LuAD cell lines NCI-H23, NCI-H1437, and HCC44. Points above or below the dashed line indicate an increase or decrease in sgRNA levels after 14 days. Blue dots indicate sgRNAs targeting DCAF7, red dots are non-targeting sgRNAs as negative control, and green dots are sgRNAs targeting essential genes NUP43, EIF3F, EIF3H, COPS5, COPS6, TCEB1, TCEB3, TCEB3C as positive control. The reads from the sequencing of the genomic DNA samples were mapped to the library sequence file, and the sgRNA counts were normalized to counts per million reads (CPM). For logarithmic analysis, a pseudo count of 1 was added to the CPM (CPM+1).

To confirm this initial finding, a competitive growth dropout assay was performed. The same Cas9-positive LuAD cell lines were individually transduced with the most effective sgRNAs targeting DCAF7, aiming for a transduction efficiency of 20-60%. In addition, a positive control sgRNA targeting essential polymerase 2 (sgPOLR2) and a non-targeting sgRNA (sgNT) were used for similar transduction. Over the course of 14 days, the ratio of transduced cells (GFP-positive) to non-transduced cells (GFP-negative) was measured by flow cytometry. While the non-targeting control cells maintain the same ratio over the 14 days, the sgPOLR2 transduced cells dropout over the same period (Figure 31). Similar to the CRISPR-Cas9 screen, cell-ratios with DCAF7-targeted sgRNAs were also reduced in all three cell lines over the 14 days (Figure 31).

Taken together, the data indicate that LuAD cell lines require the E3 substrate adaptor DCAF7 for cell survival, as CRISPR-Cas9-mediated knockout of DCAF7 leads to a dropout of the population of transduced cells.

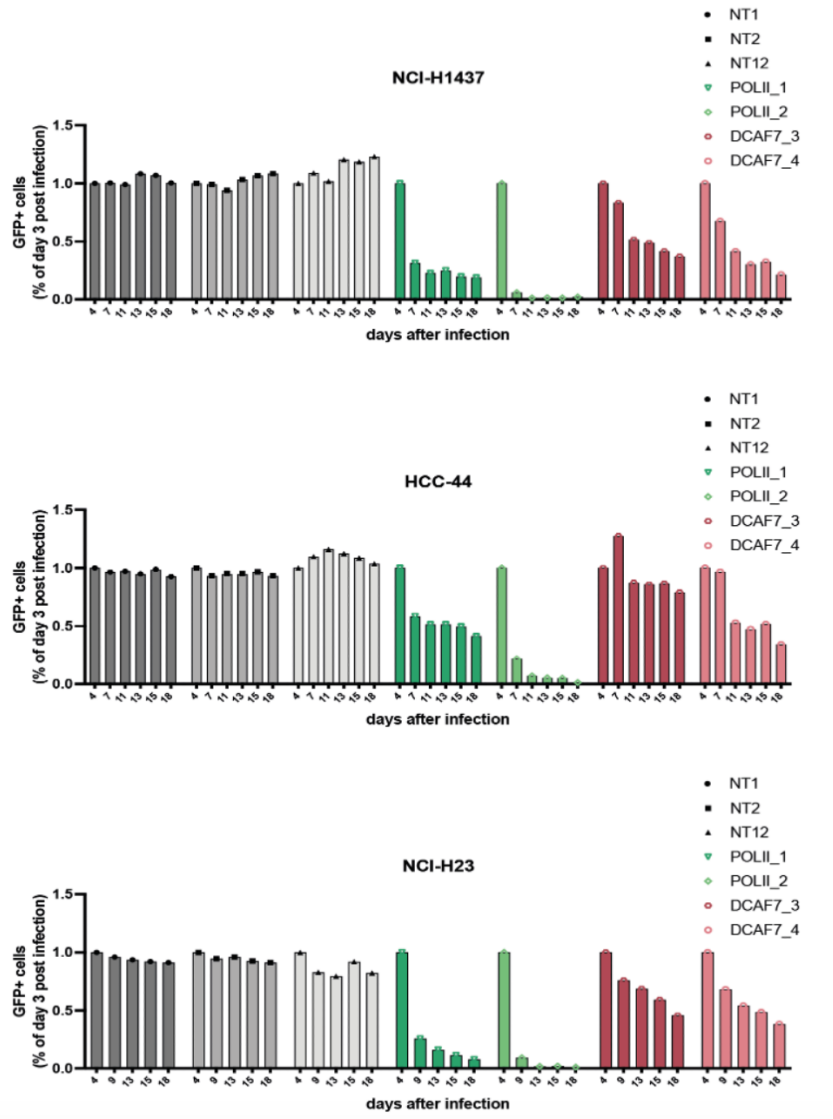

Figure 31 CRISPR-Cas9-mediated knockout of DCAF7 results in the loss of transduced cells. A competitive growth assay was performed using the Cas9-expressing LuAD cell lines NCI-H1435, NCI-H23, and HCC-44. Cells were transduced with lentiviral particles containing sgRNAs targeting either PolymeraseII (POLII_1/2 in green), DCAF7 (DCAF7_3/4 in red), or non-targeting sgRNAs (NT1/2/12 in gray) at 20-60% transduction efficiency. The ratio of positive (GFP positive) to negative (GFP negative) transduced cells was measured by flow cytometry over a 14-day time course. Data were normalized to day 4 for each sgRNA. This screen validation experiment was conducted by V.Wagner.

5.2.2 Increased DCAF7 expression in lung cancer patients

We analyzed several publicly available datasets and cross-validated the results with our screen data to further validate DCAF7 as a LuAD susceptibility at the clinical level in patient. Using the transcriptome data of the PanCancer Atlas dataset (cBioportal) on LuAD from The Cancer Genome Atlas (TCGA), we selected the ubiquitin genes found in both our CRISPR library and the TCGA dataset. We then analyzed the relative expression of these genes in the TCGA dataset, comparing tumor to normal tissue. DCAF7 was one of the upregulated ubiquitin-related genes in the dataset (Figure 32a). Comparing DCAF7 gene expression levels in patient samples of the FireHose dataset (cBioportal) showed a significant increase of DCAF7 expression in tumor patient samples compared to healthy patient samples (Figure 32b). Matching tumor to normal tissue samples of patients from the PanCancer Atlas TCGA dataset (cBioportal) also showed significantly increased DCAF7 expression in tumor

tissue (Figure 32c). Survival analysis of patients from the TCGA Firehose dataset revealed that patients with high DCAF7 mRNA levels had a worse overall survival compared to those with low DCAF7 levels (Figure 32d). A similar effect was observed when the overall survival of LuAD patients was analyzed from the KMplot database. Also here patients with high DCAF7 expression had an overall worse survival than those patients with low DCAF7 expression (Figure 32e).

Taken together, the increased expression of DCAF7 mRNA in tumor tissue and the correlation of high DCAF7 expression with worse overall survival strengthened our initial screening results and made the E3 ligase DCAF7 an interesting vulnerability in LuAD with an apparent oncogenic role.

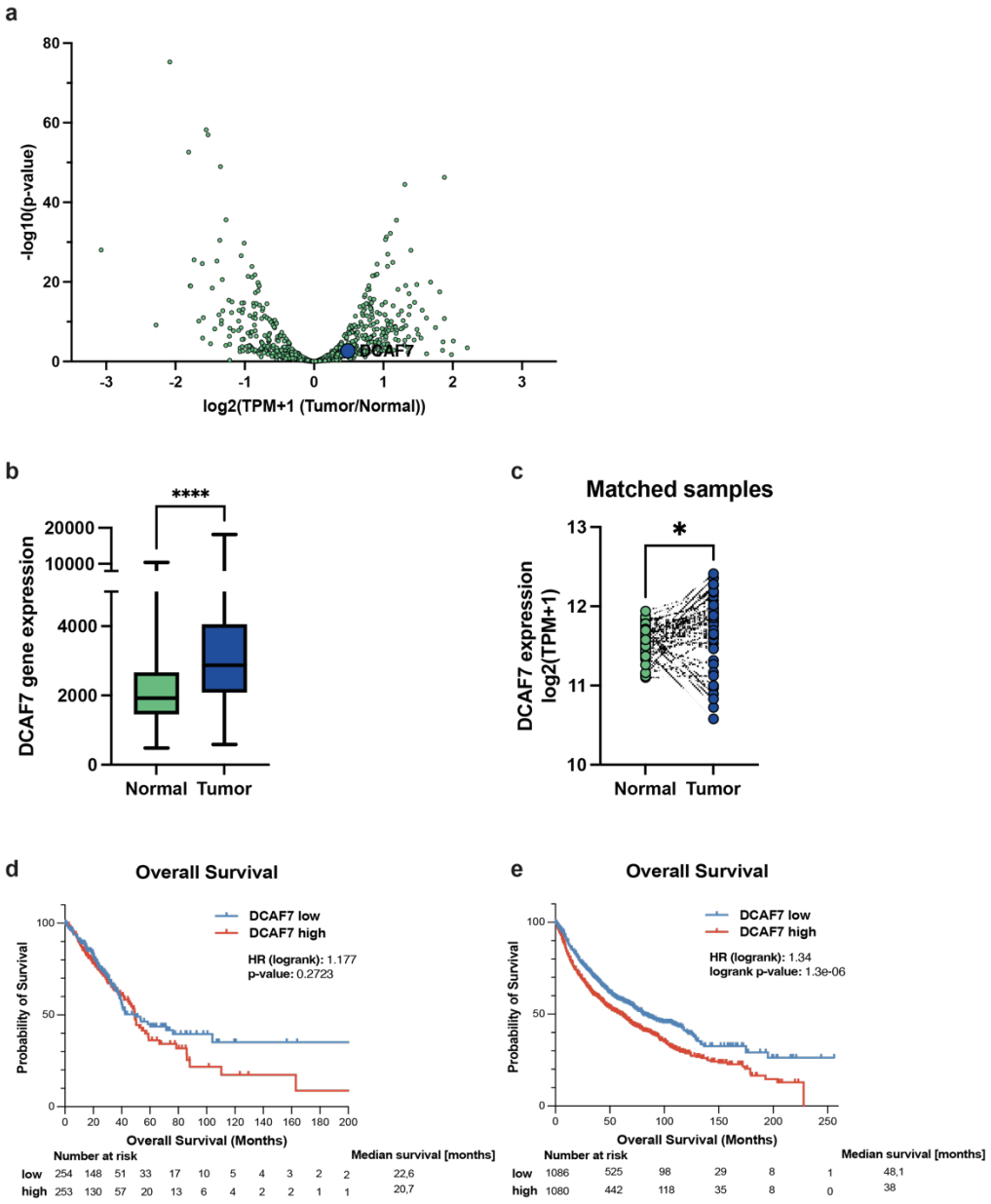

Figure 32 DCAF7 is overexpressed in LuAD patients and correlates with poorer survival. (a) Analysis of The LuAD PanCancer Atlas dataset from TCGA for expression of ubiquitin-related genes in tumor versus normal tissue. DCAF7 as a blue dot. **(b)** DCAF7 mRNA expression levels in patients from the LuAD Firehose database, normal (green) versus tumor tissue (blue). Statistical tests were performed using Welch's t-test. ****: $p < 0.001$, ***: $p < 0.001$, **: $p < 0.01$, *: $p < 0.05$. **(c)** DCAF7 mRNA expression levels in patients from The LuAD PanCancer Atlas, matched samples only, normal (green) versus tumor tissue (blue). Dashed lines connect matched samples. Statistical tests were performed using Welch's t-test. ****: $p < 0.001$, ***: $p < 0.001$, **: $p < 0.01$, *: $p < 0.05$. **(d)**

Kaplan-Meier plot of overall survival in patients with high versus low DCAF7 expression. Data from TCGA Firehose set. (**e)** Kaplan-Meier plot of overall survival in patients with high versus low DCAF7 expression. Data from KMplotter set 209592.

We used the pan-cancer analysis site TNMplot and examined DCAF7 expression levels across different cancer types, to determine if the observed overexpression of DCAF7 is a unique feature of LuAD or if it has a broader oncogenic role across different cancer entities. The database contains 56,938 samples from various databases, including GEO, GTex, TCGA, and TARGET. The comparison of normal and tumor DCAF7 expression levels revealed that almost all entities showed significantly increased DCAF7 expression in tumor tissue (Figure 33). Only in renal and adrenal cancer was DCAF7 expression not significantly increased in tumor tissue compared to normal tissue. These findings suggest that the suggested oncogenic function of a DCAF7 is not limited to LuAD.

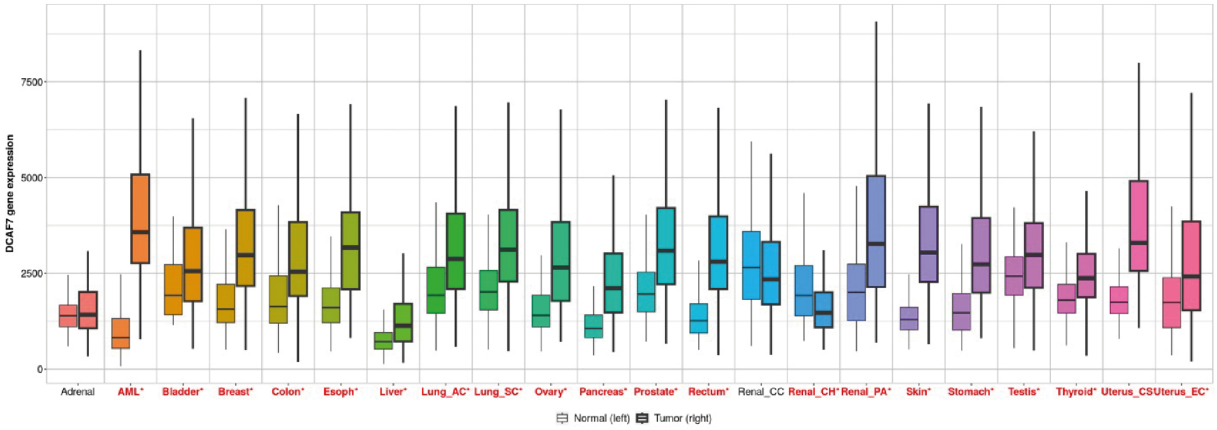

Figure 33 DCAF7 gene expression is increased in almost all cancer entities. Data from the TNMplot pan-cancer analysis page with 56,938 unique samples, including 15,648 normal, 40,442 tumor, and 848 metastasis samples from the GEO, GTex, TCGA, and TARGET databases. Normal samples on the left with thin lines, and tumor samples on the right with thick lines. Significant differences between normal and tumor DCAF7 expression levels by Mann-Whitney U test are marked with a red star.

Next, we analyzed a large panel of cell lines for DCAF7 mRNA and protein expression levels, to gain a better understanding of how DCAF7 is expressed in lung cancer cell lines and whether the previously observed overexpression of DCAF7 also applies to different lung cancer cell lines. Lung fibroblasts IMR-90 were added as a health control cell line. DCAF7 mRNA expression levels showed variability across all 18 cell lines, but most showed an increase in DCAF7 compared to the control IMR-90 cell line (Figure 34a). At the protein level, DCAF7 expression also varied from cell line to cell line (Figure 34b, c). However, the DCAF7 mRNA levels in each cell line did not directly correlate to their protein levels, suggesting a post-transcriptional or post-translational regulation of DCAF7 (Figure 34a, c). Interestingly, the non-cancerous IMR-90 cells showed the lowest DCAF7 levels at the protein level compared to the different LuAD cell lines (Figure 34b, c). In addition to the lung cancer cell lines, DCAF7 protein expression was among the highest in the embryonic kidney cell line HEK293T. Taken together, these data confirm that DCAF7 is overexpressed in most lung cancer cell lines compared to healthy lung fibroblasts.

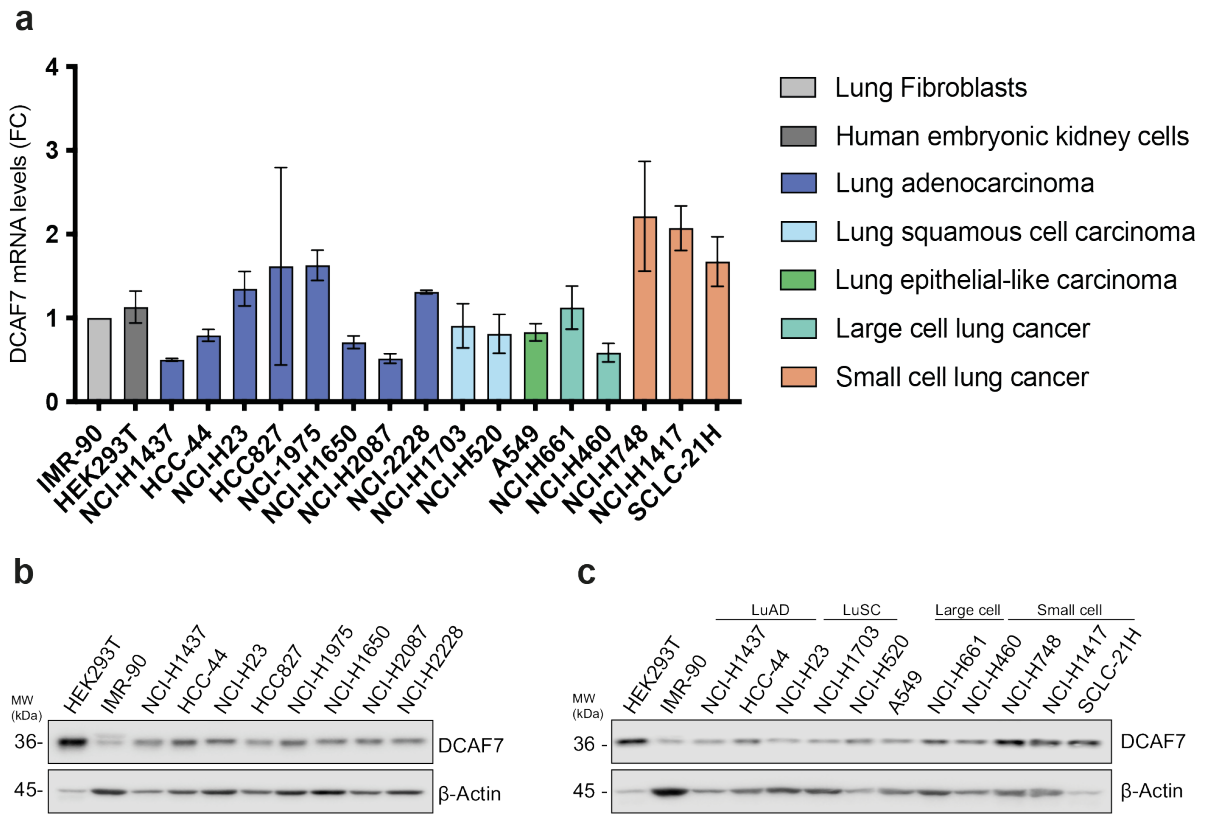

Figure 34 Most lung cancer cell lines show increased DCAF7 expression. (a) qPCR analysis, relative DCAF7 mRNA levels were quantified for each lung cancer cell line and normalized to DCAF7 mRNA expression in non-cancerous IMR-90 cells. **(b)** Immunoblot analysis of whole cell extracts from LuAD cell lines used in the qPCR experiment. Loading control: β-actin. **(c)** Immunoblot analysis of whole cell extracts from different lung cancer cell lines used in the qPCR experiment. Loading control: β-actin.

5.2.3 DCAF7 has an oncogenic function in LuAD and other cancer entities

We decided to focus on a short hairpin RNA (shRNA) knockdown system instead of sgRNA knockout to address the question of which molecular mechanisms are involved in the observed dropout phenotype. ShRNAs mediate a faster and more gradual knockdown of gene expression compared to sgRNA, making it easier to study the phenotype. Therefore, the following phenotyping experiments were mainly performed using shRNA-mediated knockdown of DCAF7 unless otherwise noted. We designed shRNAs targeting DCAF7 based on the portals.broadinstitute website and validated them in NCI-H1437 and HCC-44 cells. Three days after transducing the cells with lentiviral particles containing the shRNAs, the cells were harvested and immunoblotted for DCAF7 expression. While the third shRNA (shDCA7_3) showed the best knockdown of DCAF7, all three shRNAs showed a significant reduction in DCAF7 protein levels (Figure 35).

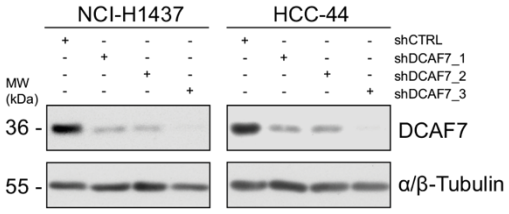

Figure 35 shRNA-mediated knockdown of DCAF7 results in reduced protein expression. Immunoblot analysis of NCI-H1437 and HCC-44 LuAD cell lines transduced with lentiviral particles containing one of three different shRNAs targeting DCAF7 or a non-targeting control shRNA. Cell pellets were harvested three days post-transduction, lysed, and immunoblotted with the indicated antibodies. Loading control: α/β-tubulin.

We confirmed the previously observed dropout phenotype following sgRNA-mediated knockout using this shRNA system. The same LuAD cell lines used in the CRISPR-Cas9 screen were transduced with lentiviral particles containing a vector carrying both the shRNA and a dsRed reporter transgene. Again, cells were transduced at an efficiency of 20-60%, and the ratio of transduced cells (dsRed+) to non-transduced cells (dsRed-negative) was measured by flow cytometry. Consistent with the sgRNA-mediated dropout assay results, the shRNA-mediated knockdown of DCAF7 also resulted in a significant dropout of positively transduced cells over 18 days (Figure 36a). Notably, a more pronounced dropout phenotype was observed in NCI-H1437 cells compared to HCC-44 and NCI-H23. Interestingly, although shDCAF7_3 showed the best knockdown in protein depletion immunoblot, in the dropout assay, shDCAF7_1 showed the best dropout rates in all cell lines, while shDCAF7_2 resulted in the lowest dropout rates (Figure 35a & Figure 36a).

Our data analysis already suggested a broader oncogenic function of DCAF7 that is not limited to LuAD (Figure 33). To confirm this, we replicated the same shRNA dropout assay in human embryonic kidney cells (HEK293T), an acute myeloid lymphoma cell line (OCI AML3), and a sarcoma cell line (U2OS). A similar dropout phenotype was observed in these non-lung related cell lines (Figure 36b). Taken together, the data confirmed that shRNA-mediated knockdown of DCAF7 also results in reduced proliferation of LuAD and other cancer cell lines, implicating a broader oncogenic function of DCAF7.

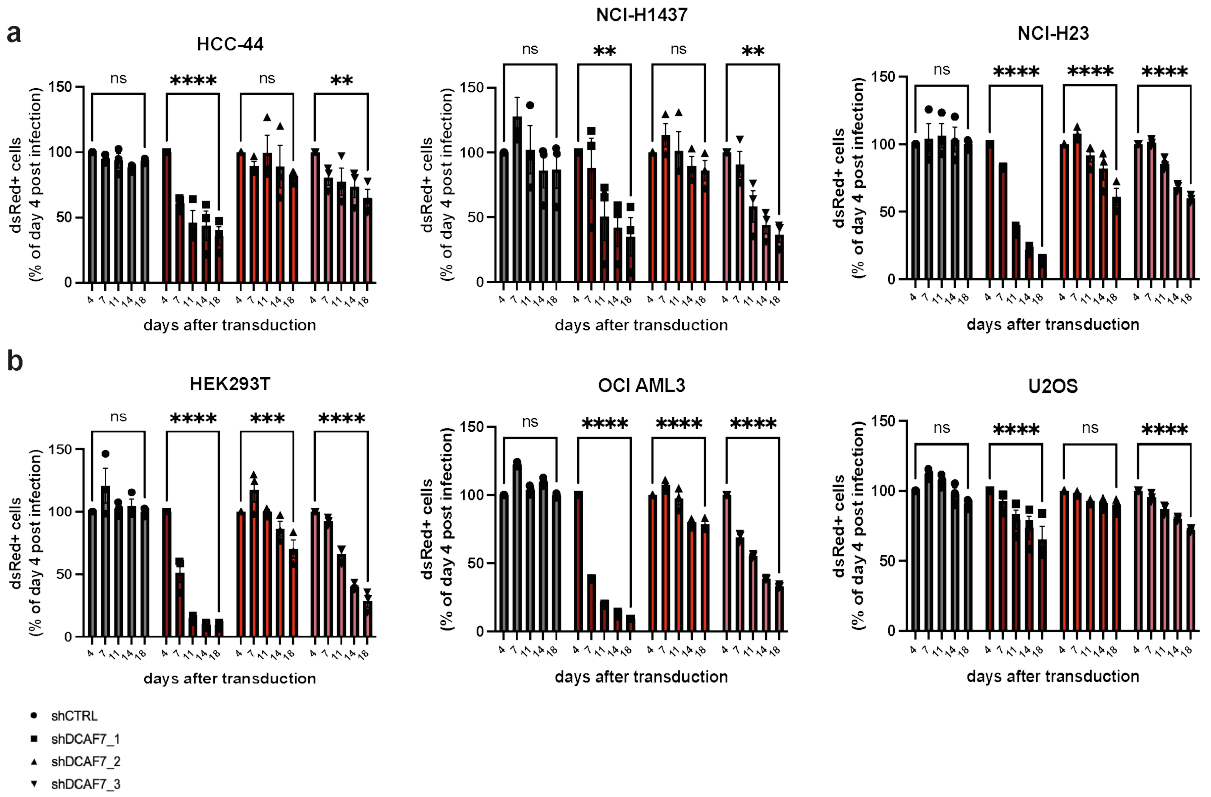

Figure 36 shRNA-mediated DCAF7 knockdown results in the dropout of transduced cells. **(a)** Competitive growth assay was performed using the LuAD cell lines NCI-H1435, NCI-H23, and HCC44 as well as **(b)** HEK293T, OCI AML3, and U2OS. Cells were transduced with lentiviral particles containing shRNAs targeting either DCAF7 (DCAF7_1/2/3 in red) or non-targeting shRNAs (shCTRL in gray) at a transduction efficiency of 20-60%. The ratio of positive (dsRed +) to negative (dsRed negative) transduced cells was measured by flow cytometry over a 14-day time course. Data were normalized to day 4 for each shRNA. Statistical tests were performed by 2way ANOVA: 0.1234 (ns), 0.0332 (*), 0,0021 (**), 0.0002(***), <0.0001(****).

5.2.4 DCAF7 knockdown does not lead to increased cell death

Next, we tried to identify the molecular mechanism behind the induced dropout phenotype of cells upon DCAF7 depletion. One potential molecular mechanism that could lead to the observed dropout of DCAF7-depleted cells is cell death. We performed a live/dead flow cytometry assay to investigate whether DCAF7 knockdown induces cell death in LuAD. This is based on an APC-coupled dye that interacts with amines on the cell surface and inside the cell, resulting in a fluorescent signal. Living cells have an intact cell membrane, so the dye can only interact with the cell surface. The dye can also interact with amines inside the cells of dying cells, resulting in increased fluorescence signals. This allowed differentiation between dead and live cells based on signal intensity measured by flow cytometry. Four and seven days after shRNA-mediated DCAF7 knockdown the number of dead cells was measured. None of the cell lines showed a significant increase in dead cells, except for HCC-44 on day seven with shDCAF7_1 (Figure 37a).

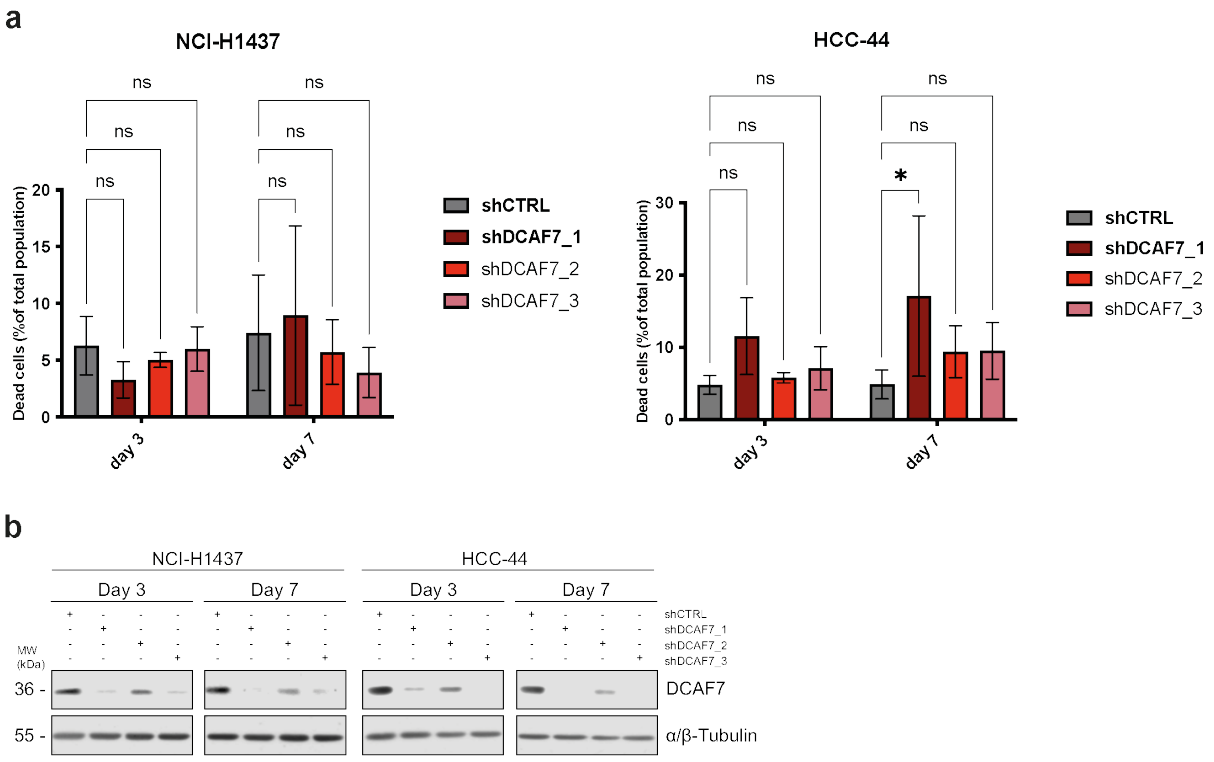

Figure 37 No increased cell death after DCAF7 knockdown in live/dead staining. HCC-44 and NCI-H1437 cells were transduced with lentiviral particles containing shRNA targeting DCAF7. Transduction efficiency was between 90-100% **(a)** Live/dead APC assay with transduced cells on day three and seven post-transduction. Cells were stained with APC-linked dye, which can only penetrate damaged membranes of dead cells, resulting in increased fluorescence signal measured by flow cytometry. Statistical tests were performed by 2way ANOVA: 0.1234 (ns), 0.0332 (*), 0,0021 (**), 0.0002(***), <0.0001(****). **(b)** Representative immunoblot analysis of HCC-44 and NCI-H1437 cells from one of the live/dead APC assays to confirm DCAF7 knockdown. Samples were harvested at the indicated time points, and whole cell extracts were analyzed by immunoblot using the indicated antibodies. Load control: α/β-tubulin.

Another method to evaluate whether DCAF7 knockdown leads to cell death is to look specifically at the expression of cell death, apoptosis, and DNA damage markers. We performed immunoblot analysis of HCC-44 and NCI-H1437 WCEs after DCAF7 depletion and looked for upregulated expression of DNA damage proteins such as γH2A.X, phosphorylated histone H3 or cleaved PARP-1 as well as increased expression of apoptosis markers such as

cleaved caspase3. Similar to the previous observation, no significant and consistent increase in DNA damage or apoptosis markers was observed after DCAF7 knockdown (Figure 38). Little increases in some markers were observed, but they were not consistent between the different shRNAs and in between the two cell lines. Therefore, we rated those observations as out layers due to off-target effects of single shRNAs.

Since we only saw increased cell death on one day and with one shRNA in the live/dead assay and no conclusive increase or decrease of any cell death or DNA damage markers, we concluded that the observed dropout phenotype was not caused by increased cell death due to DCAF7 depletion.

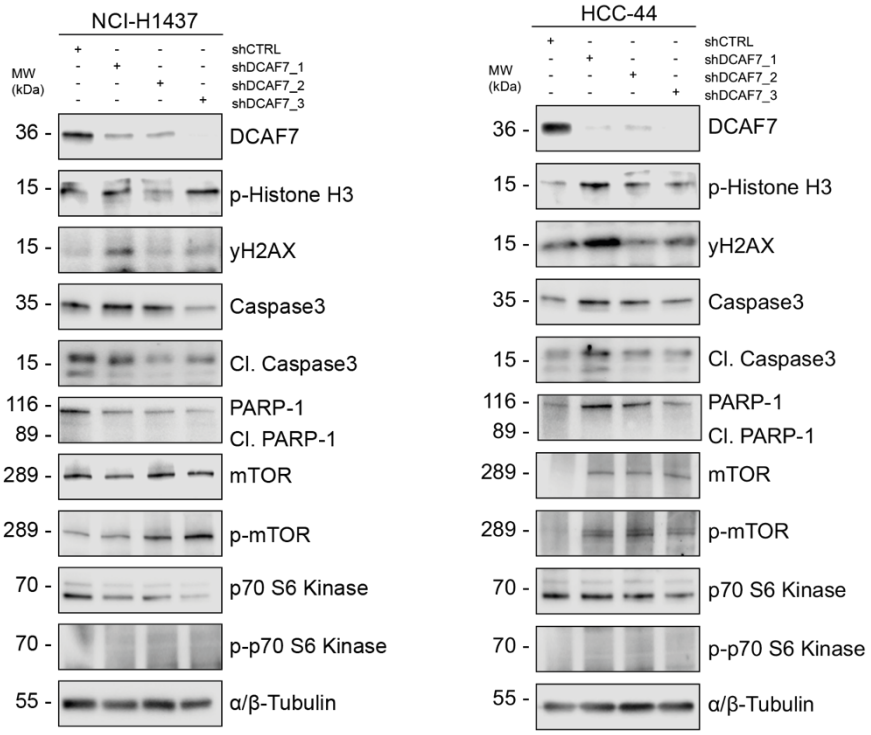

Figure 38 DNA damage or apoptosis markers remain unchanged after DCAF7 knockdown. Immunoblot analysis of HCC-44 and NCI-H1437 cells four days after DCAF7 transduction with shRNAs targeting DCAF7. Samples were harvested four days after DCAF7 depletion, and whole cell extracts were analyzed by immunoblot using the indicated antibodies. Loading control: α/β-tubulin.

5.2.5 DCAF7 knockdown does not lead to changes in cell cycle progression

Impaired cell cycle progression could be a result of DCAF7 knockdown/knockout and contribute to the dropout phenotype. Disrupted cell cycle progression can be observed as cell cycle arrest at a specific phase (G1, S, G2/M) or an extension of the overall cell cycle duration. We analyzed the cell cycle profiles of NCI-H1437 and HCC-44 LuAD cell lines after shRNA-mediated DCAF7 knockdown. Cells were fixed in ethanol and stained with Propidium Iodide, which intercalates into DNA and allows differentiation of cell cycle phases based on DNA content (G1 phase =2n, S phase ≥ 2n and ≤ 4n, G2/M phase =4n). We observed a significant decrease in S-phase for all three shRNAs targeting DCAF7 in NCI-H1437 cells (Figure 39). Interestingly, shDCAF7_1 also showed a significant increase in the G1 phase and a decrease in the G2/M phase in NCI-H1437 (Figure 39). For HCC-44, we saw a significant increase in the S phase and G2/M upon DCAF7 knockdown with shDCAF7_1 but no changes with the other shRNAs and no changes in the G1 phase (Figure 39). These inconsistent observations

may be due to off-target effects of shDCAF7_1 and were insufficient to explain the significant cell loss following DCAF7 knockdown.

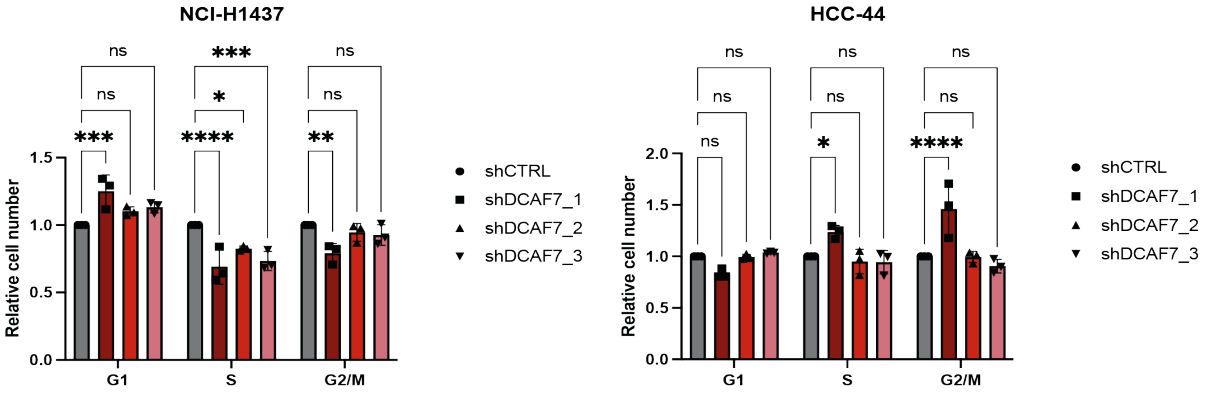

Figure 39 DCAF7 knockdown does not cause a consistent cell cycle arrest phenotype. HCC-44 and NCI-H1437 cells were transduced with lentiviral particles containing shRNA targeting DCAF7. The transduction efficiency was between 90-100%. The cell cycle analysis of LuAD cell lines took place four days after shRNA transduction. Cells were fixed in ethanol, stained with Propidium Iodide and analyzed by flow cytometry. Quantification of cells per cell cycle phase analyzed by flow cytometry. Data were normalized to shCTRL. Statistical tests were performed by 2way ANOVA: 0.1234 (ns), 0.0332 (*), 0,0021 (**), 0.0002(***), <0.0001(****).

To get a better understanding of what happens during cell cycle progression after DCAF7 knockdown, we performed an immunoblot analysis of NCI-H1437 and HCC-44 cells after DCAF7 knockdown. We analyzed the protein expression of different cell cycle markers, such as cyclin E or cyclin B, to see if we get an up- or down-regulation upon DCAF7 depletion, which would indicate a cell cycle arrest at a specific stage. Similar to the results from the Propidium Iodide assay, we were not able to detect a significant and consistent up- or downregulation of any cell cycle marker in both LuAD cell lines and with all three shRNAs (Figure 40). Taken together, this suggests that the dropout phenotype in cells is not due to cell cycle arrest but instead to a general slowing of cell proliferation.

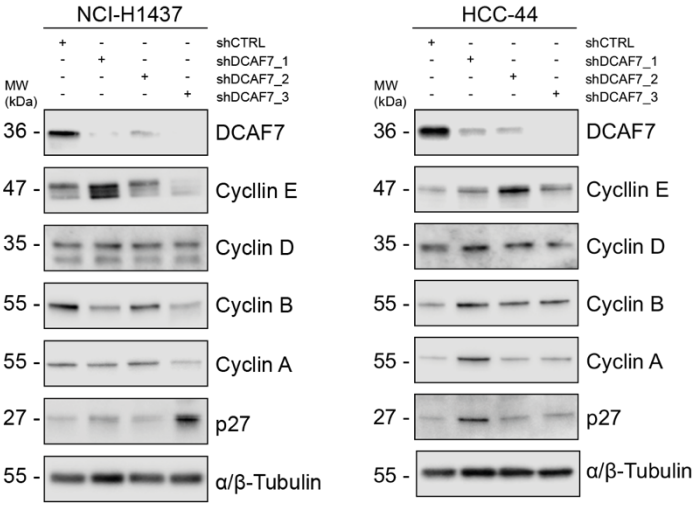

Figure 40 No up- or downregulation of cell cycle markers after DCAF7 knockdown. Immunoblot analysis of HCC-44 and NCI-H1437 cells four days after DCAF7 transduction with shRNAs targeting DCAF7. Samples were harvested and whole cell extracts were analyzed by immunoblot using the indicated antibodies. Loading control: α/β-tubulin.

5.2.6 DCAF7 localizes in the cytoplasm and nucleus of LuAD cell lines

In our aim to define the molecular mechanisms behind the dropout phenotype in cells mediated by DCAf7 knockout, we next focused on the substrate of DCAF7. However, we first validated the subcellular localization of DCAF7 within LuAD cells to better define our substrate area. This may provide information about potential functions and substrates of DCAF7 since a protein's subcellular location is often associated with its specific function. Immunofluorescence staining of NCI-H1437 and HCC-44 LuAD cells with a specific DCAF7 antibody in combination with DNA staining (Hoechst33258) and cytoskeleton staining (alpha-tubulin) followed by confocal microscopy revealed that DCAF7 appears to be localized in the nucleus as well as in the cytoplasm around the nucleus (Figure 41). While DCAF7 appeared to be localized in the nucleus, it was absent in the nucleolus and the plasma membrane of wild type NCI-H1437 and HCC-44 cells (Figure 41).

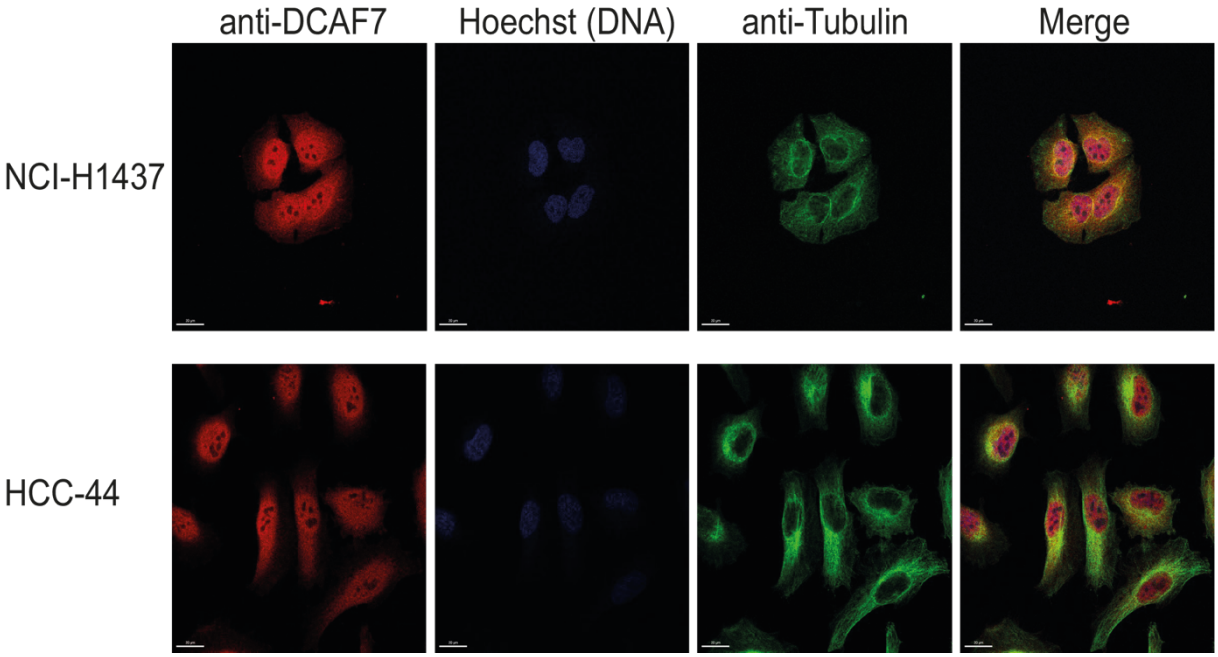

Figure 41 DCAF7 localized to both nucleus and cytoplasm in wild type LuAD cells. Representative immunofluorescence images of NCI-H1437 and HCC44 cells. Cells were mounted on chamber slides and fixed with 4% PFA. The scale bar represents 20 µm. Wild type HCC-44 and NCI-H1437 cells were stained with endogenous DCAF7 antibody (red), anti-alpha-tubulin (green), and the corresponding Alexa-Fluor-448 and -594 conjugated secondary antibodies. DNA was stained with HOECHST33258 (blue). Images were captured with a LEICA-SF8 confocal microscope.

The subcellular localization of DCAF7 was further validated by stably overexpressing FLAG-tagged DCAF7 protein in HCC-44 and staining these cells with a FLAG antibody. When comparing HCC-44 cells with FLAG-tagged DCAF7 overexpression to empty vector overexpressing cells, a similar localization of DCAF7 was detected (Figure 42a). Also here FLAG-stained DCAF7 localizes in and around the nucleus. To further confirm the subcellular localization, a complete absence of DCAF7 staining was observed after small interfering RNA (siRNA) mediated DCAF7 knockdown (Figure 42b). Taken together, we concluded that DCAF7 is predominantly localized in and around the nucleus but can also be detected in the cytoplasm of LuAD cells.

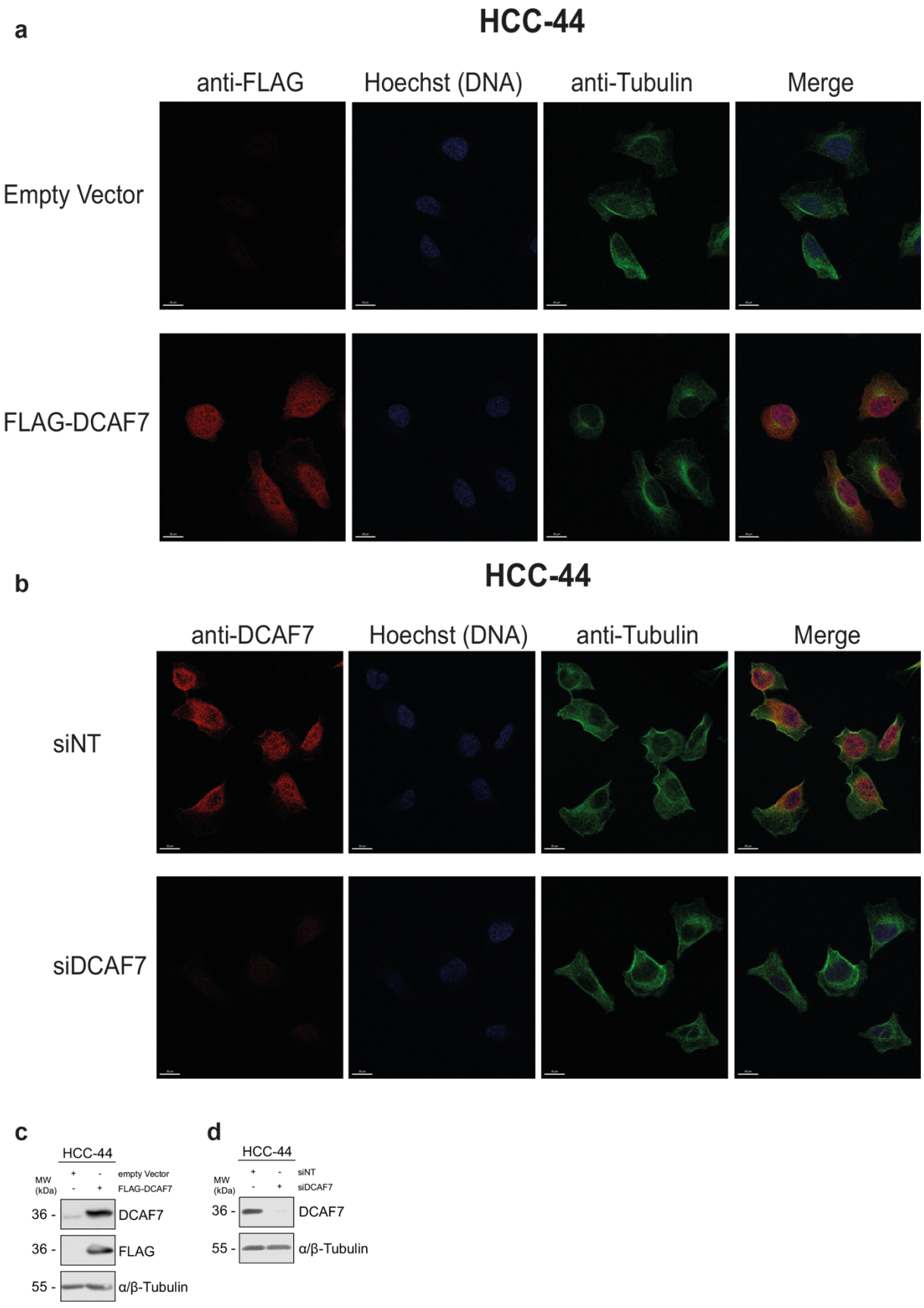

Figure 42 DCAF7 localization was confirmed with siRNAs and overexpression constructs. Representative immunofluorescence images of NCI-H1437 and HCC44 cells. Cells were mounted on chamber slides and fixed with 4% PFA. The scale bar represents 20 µm. Images were captured with a LEICA-SF8 confocal microscope. **(a)** HCC-44 cells stably overexpressing either FLAG-tagged DCAF7 or empty vector were stained with anti-FLAG (DCAF7, red), anti-alpha-tubulin (green), and the corresponding Alexa-Fluor-448 and -594 conjugated secondary antibodies. DNA was stained with HOECHST33258 (blue). **(b)** Wild type HCC-44 cells were transfected with

either non-targeting siRNA or DCAF7-targeting siRNA 48 hours before PFA fixation. Cells were stained with endogenous DCAF7 antibody (red), anti-alpha-tubulin (green), and the corresponding Alexa-Fluor-448 and -594 conjugated secondary antibodies. DNA was stained with HOECHST33258 (blue). **(c, d)** Representative immunoblot analysis of HCC-44 cells from the IF images to confirm successful DCAF7 overexpression **(c)** or knockdown **(d)**. Samples were harvested, and WCEs were analyzed by immunoblot using the indicated antibodies. Loading control: α/β-tubulin.

5.2.7 Mass spectrometry-based screening identifies ubiquitylated substrates of DCAF7

DCAF7 functions as a specific substrate adaptor protein of the DDB1-Cul4 Cullin-RING ubiquitin ligases and, as such, interacts with ubiquitylated substrate proteins. Given the previously discussed unclear phenotype of DCAF7 knockdown leading to LuAD cell dropout, another strategy was to identify DCAF7 substrates and deduce the molecular mechanism leading to the dropout phenotype in cells. We performed two screens to identify potential ubiquitylation substrates of DCAF7: An interactome screen in the form of a tandem affinity purification to identify physical interaction partners and a functional proteome screen in the form of a DiGLY purification to detect DCAF7-mediated ubiquitylated proteins.

For the interactome screen, HEK293T cells were transfected with an overexpressing Strep-FLAG-DCAF7 or an empty vector control plasmid. The dual Strep-FLAG tag (streptavidin and FLAG) allowed for increased sample purity (Figure 43a). Successful overexpression of Strep-FLAG tagged DCAF7 was confirmed by silver staining (Figure 43c). Mass spectrometry analysis of the TAP purification identified 656 proteins, including the bait DCAF7, parts of the Cullin-RING ligases such as Cul4A, Cul4B, and DDB1, and published interactors such as DYRK1A and DYRK1B (Figure 44a).

As described previously, E3 ligases facilitate the attachment of ubiquitin to lysine residues at the C-terminus of target substrate proteins. Knockdown of the substrate adaptor DCAF7 in LuAD cells should result in less ubiquitinated substrate proteins of DCAF7. To find the less ubiquitinated substrate proteins, a DiGLY purification was performed, which takes advantage of the fact that when ubiquitinated proteins are digested with trypsin, a glycine-glycine (DiGLY) motif remains where ubiquitin was attached to the lysine. This motif can be recognized by specific DiGLY antibodies to selectively enrich peptides that belong to a ubiquitinated protein (Figure 43b). Mass spectrometry analysis of the purified peptides allowed us to find less ubiquitinated proteins upon DCAF7 depletion. NCI-H1437 and HCC44 cells were harvested three days after lentiviral transduction with either one shRNA targeting DCAF7 or control non-targeting shRNA for this purification. This time point was chosen to achieve a clear DCAF7 knockdown and to minimize other ubiquitylation events. We collected samples from three biological replicates and confirmed DCAF7 knockdown by shRNA in immunoblot analysis (Figure 43d). We then split the samples and processed one part for DiGLY enrichment and the other part for full proteome analysis. The samples were given to the mass spectrometry facility in Freising led by Prof. Dr. B. Küster, who performed the measurements.

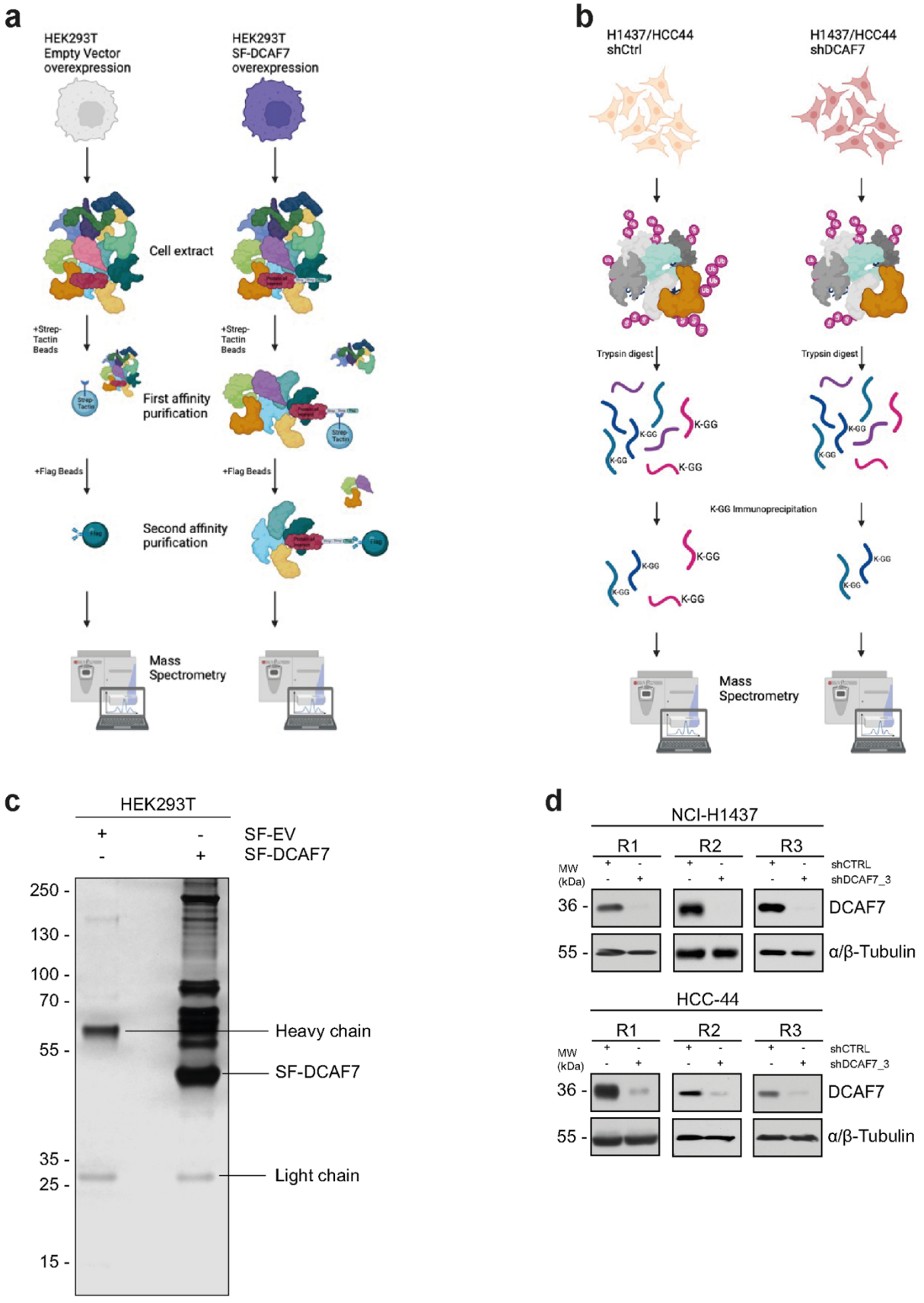

Figure 43 Mass spectrometry-based proteome and interactome screens for DCAF7 substrates. **(a)** Graphical representation of tandem affinity purification (TAP) on the left **(a)** and DiGLY purification on the right **(b)**. For TAP **(a)**, HEK293T cells were transfected with strepavidin-FLAG tagged DCAF7 (SF-DCAF7) or empty vector (SF-EV). Cell lysates were purified using Strep-tactin beads followed by Flag immunoprecipitation. After acid elution, samples were TCA precipitated and submitted for mass spectrometry analysis (TAP purification was conducted by V. Wagner). For Di-GLY **(b)**, NCI-H1437 and HCC-44 cells were transduced with either a non-targeting shRNA

(shCTRL) or a DCAF7 targeting shRNA_3 (shDCAF7_3). Cells were harvested after three days, lysed, and trypsinized. Samples were split and either DiGLY enriched and TMT labeled or directly labeled with TMT, followed by mass spectrometric analysis. **(c)** Silver staining of TAP to detect overexpression of SF-DCAF7. **(d)** Immunoblots of the three biological replicates for DiGLY analysis to check for DCAF7 knockdown. Loading control: α/β-tubulin.

Analysis of the DiGLY screen revealed peptide enrichment or depletion upon DCAF7 knockdown compared to the non-targeting shRNA, with a total of 3821 KGG peptides identified in HCC-44 and 3019 KGG peptides in NCI-H1437. To highlight significantly less ubiquitinated peptides, we set a threshold of log2FC (shCTRL/shDCAF7) ≤ -0.5 and -log10(p-value) > 1.3, shown in red (Figure 44b, c). To further identify consistent interaction partners of DCAF7, the data from both cell lines were analyzed for peptides that were less ubiquitinated in both cell lines after DCAF7 knockdown (Figure 44f) under consideration of the reference proteome to disregard peptides that were less ubiquitinated due to an overall lower abundance of the protein in the cell lines themselves (Figure 44d, e, f).

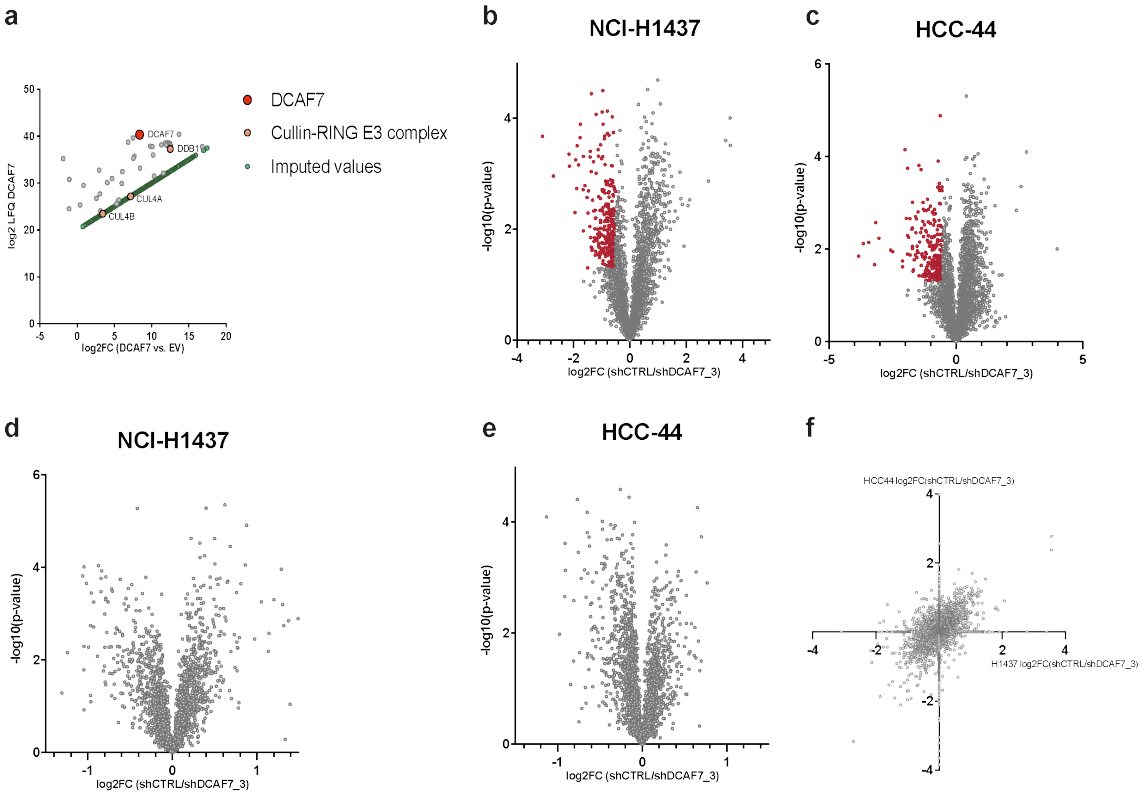

Figure 44 Mass spectrometric analysis of TAP and DiGLY screening results. (a) Mass spectrometry analysis of TAP. DCAF7 is shown as a red dot, parts of the Cullin-RING E3 ligase complex are shown as bright red dots, imputed values for proteins not detected in the empty vector are shown as bright green dots. **(b, c)** Volcano plots of mass spectrometry-based proteome analysis of DiGLY screen showing changes in ubiquitinated peptides (KGG) in NCI-H1437 and HCC-44 cells upon DCAF7 knockdown. Log2 transformed ratios of shCTRL/shDCAF7_3 reporter intensities versus negative Log10 transformed p-values calculated by Welsh's t-test. Red dots represent significantly less ubiquitinated peptides (log2FC (shCTRL/shDCAF7_3) ≤ -0.5 and -log10(p-value) > 1.3. **(d, e)** Volcano plots of mass spectrometry-based proteome analysis showing changes in protein abundance (PGs) in NCI-H1437 and HCC-44 cells upon DCAF7 knockdown. Log2 transformed ratios of shCTRL/shDCAF7_3 reporter intensities versus negative Log10 transformed p-values calculated by Welsh's t-test. **(f)** Analysis of changes in ubiquitinated peptides (KGG) in NCI-H1437 versus HCC-44 cells upon DCAF7 knockdown. NCI-H1437 Log2 transformed ratios of shCTRL/shDCAF7_3 reporter intensities versus HCC-44 Log2 transformed ratios of shCTRL/shDCAF7_3 reporter intensities. The mass spectrometric measurements were performed by Dr. Chien-Yun Lee from AG Küster.

We cross-validated the DiGLY screening results with the proteins that appeared in the TAP interactome to add another layer and select proteins for further validation as potential

substrates of DCAF7 (Figure 45a, b). From this analysis, we selected some potential substrates that were significantly less ubiquitinated in the DIGLY screen in both cell lines and also appeared in the TAP interactome, such as BUB1, as well as potential substrates that were significantly less ubiquitinated in the DiGLY screen that had known functions in pathways that could be involved in the observed dropout phenotype (Figure 45c).

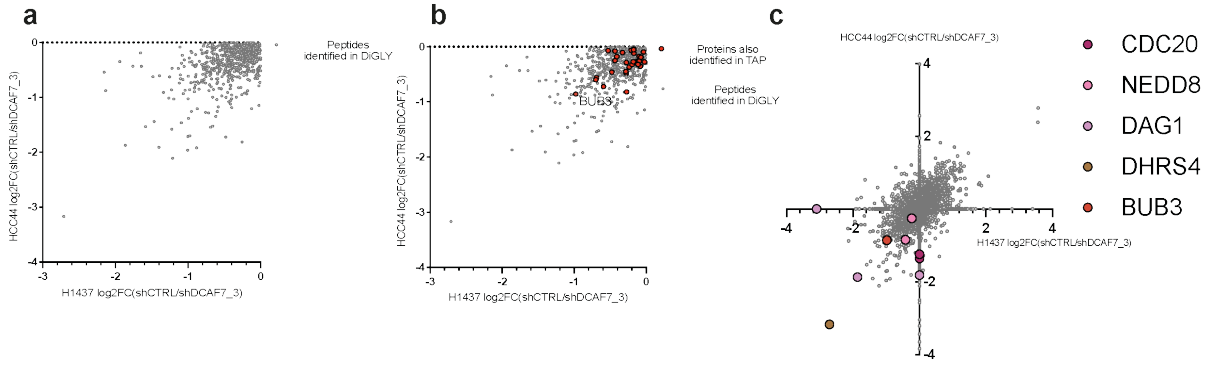

Figure 45 Cross validation of mass spectrometric results from TAP and DiGLY screening. (a) Analysis only showing less ubiquitinated peptides found in both NCI-H1437 and HCC-44 DiGLY screens after DCAF7 knockdown. NCI-H1437 Log2 transformed ratios of shCTRL/shDCAF7_3 reporter intensities versus HCC-44 Log2 transformed ratios of shCTRL/shDCAF7_3 reporter intensities. **(b)** Analysis from (a), but proteins also identified in TAP are highlighted in red. **(c)** Analysis from figure 37 (f) with interesting possible substrates of DCAF7 highlighted.

5.2.8 Mass spectrometry identified substrate candidates do not interact with DCAF7 in cells

We performed semi-endogenous FLAG immunoprecipitations to validate the interaction between DCAF7 and the potential cross-validated substrates identified in the interactome and proteome screens. For this, HEK293T cells were transfected with either FLAG-tagged DCAF7 or empty vector. NCI-H1437 and HCC-44 cells were transduced with lentiviral particles containing either empty vector or FLAG-tagged DCAF7 and the positively transduced cells were selected with puromycin. After harvesting the cells, we immunoprecipitated DCAF7 and blotted for the potential substrates. As shown in the Figure 46 the Cullin-RING ligase proteins Cul4A and DDB1 co-precipitated with FLAG-tagged DCAF7 compared to empty vector in all three cell lines. This was a positive control and suggests that DCAF7 can form an active ubiquitin ligase complex in these cell lines and interact with known interactors (Figure 46). The potential substrates picked from our cross validated screening did not co-precipitate with DCAF7 in any of the three cell lines (Figure 46). This observation contradicts the mass spectrometry screens and suggests that none of the potential substrates interact with DCAF7. Further investigation is required to find DCAF7 substrates.

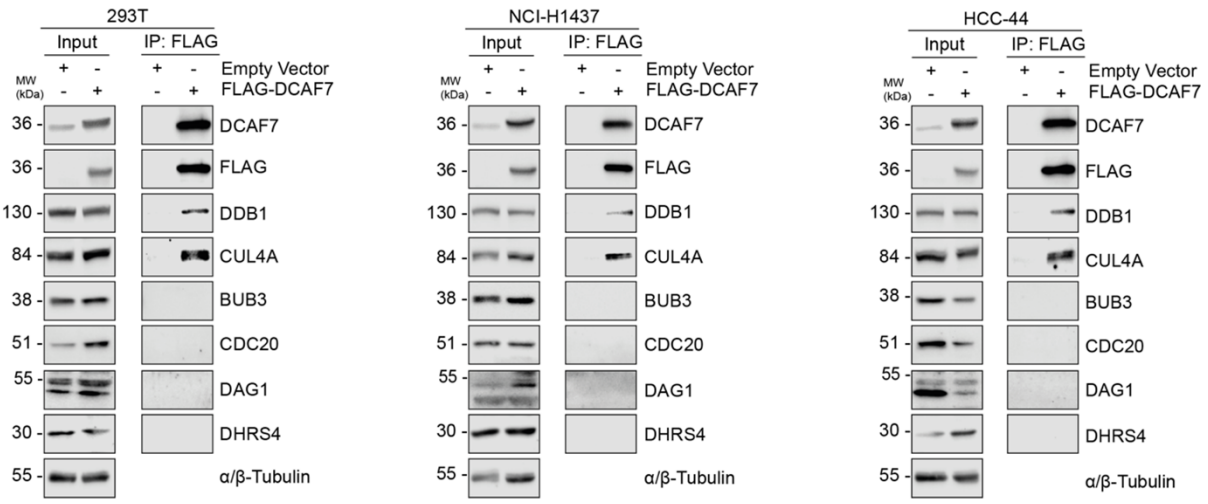

Figure 46 Potential substrates do not interact with DCAF7 in semi-endogenous FLAG-IPs. Semi-endogenous FLAG-IPs from HEK293T, NCI-H1437, and HCC-44 cells transfected with overexpressing constructs of either FLAG-tagged DCAF7 or empty vector. Interaction of Cullin-RING E3 ligase moieties and potential substrates from the mass spectrometry screens with DCAF7 were analyzed by immunoblot. Loading control: α/β-tubulin.

6 Discussion

6.1 KLHL14 acts as tumor suppressor in B-cell malignancies independent of the BCR via ubiquitylation of NUDCD3

6.1.1 KLHL14 is significantly downregulated in patient samples

Non-Hodgkin's lymphoma is one of the most common cancers in the United States, accounting for 4% of all cancers, with 95% of NHL diagnoses being B-cell related (Thandra, Barsouk, Saginala, Padala, et al., 2021). Among these, diffuse large B-cell lymphoma accounts for approximately 30% of all NHL cases, making it the most common form of lymphoma (Wang, 2023). In contrast, mantle cell lymphoma is a rarer form of NHL, accounting for only 5-7% of cases (Lynch et al., 2024). Multiple myeloma, which accounts for nearly 2% of cancer diagnoses in the United States, is also one of the most common blood cancers (Padala et al., 2021). Despite the good responsiveness of some of these blood cancers to proteasome inhibitors, most remain incurable (San-Miguel & Mateos, 2011). This highlights the potential involvement of the ubiquitin-proteasome system in these diseases, and the need for a deeper understanding of their molecular pathology to develop novel therapeutic strategies. Therefore, our first aim was to identify novel UPS components involved in the development and progression of MM, DLBCL, and MCL.

Kelch-like protein 14 was identified as one of the most significantly downregulated E3 ligases in MM and MCL patient samples (Figure 8a, b), and low expression of KLHL14 correlated with worse overall survival (Figure 9c). To independently validate the data received from T. Haferlach, we successfully confirmed that KLHL14 expression is downregulated in MM cells in other publicly available databases (Figure 9a, b). This suggests KLHL14 as a novel tumor suppressor in B-cell neoplasms and made it our main E3 ligase of interest.

6.1.2 KLHL14 tumor suppressor function is independent of the BCR

While numerous studies have focused on the role of KLHL14 in corticospinal neuron development (Sahni, Itoh, et al., 2021; Sahni, Shnider, et al., 2021; Zhang, Weinrich, et al., 2017), these publications did not address the E3 ligase function of KLHL14 and its association with the ubiquitin-proteasome system. In these studies, KLHL14 directs axons to spinal segmental levels of white matter and limits axon extension independent of its ubiquitin ligase function. More recent studies suggest a potential oncogenic role for KLHL14 in ovarian and endometrial cancer, positioning it as a promising biomarker for these diseases (Wang et al., 2022). This recent work includes the analysis of patient data from publicly available databases, which revealed significant overexpression of KLHL14 in ovarian cancer samples (Han et al., 2019). It has been shown that KLHL14 knockdown in these ovarian cancer cells reduce cell proliferation, induce G0/G1 cell cycle arrest, increase apoptosis rates, and inhibit migration (Chen et al., 2020; Nomiri et al., 2022). Further, an Encyclopedia of Genes and Genomes (KEGG) enrichment analysis suggested KLHL14 as a regulator of mTOR, WNT, and TGF-beta signaling pathways, but in these publications KLHL14 function as part of the E3 ligase complex or its role in ubiquitylation is not discussed (Nomiri et al., 2022). Another study used RNA sequencing to identify genes involved in epithelial-mesenchymal transition (EMT) (Di Lollo et al., 2020). Here, KLHL14 was discovered as one of the most up-regulated genes during EMT in amniotic epithelial cells and it was hypothesized that KLHL14 might interact with and regulate Nrf2, thereby driving EMT. However, again, this study still did not address the ubiquitylation functions of KLHL14 within the E3 ligase complex.

One of the only papers published on the E3 ligase function of KLHL14 is by Choi *et al*., where it is shown that KLHL14 ubiquitylates subunits of the B-cell receptor, therefore regulating NF-κB signaling in ABC-type DLBCL (Choi & Busino, 2019). Previous reports have shown that KLHL14 expression levels are high in DLBCL, but KLHL14 is also a hot spot for mutations that render it inactive (Schmitz et al., 2018). Choi *et al*. analyzed whole exome and genome sequencing data from patients with lymphoid malignancies and found that truncating mutations of KLHL14 are most common in ABC-type DLBCL. In this study, mutations in KLHL14 are rarely detected in patients with mantle cell lymphoma and multiple myeloma. ABC-type DLBCL, unlike GCB-type DLBCL, relies on NF-κB activation through constitutive active B-cell receptor signaling (Davis et al., 2010). A mass spectrometry screen in this study revealed that B-cell receptor subunits interact with KLHL14. This interaction increases BCR ubiquitylation and subsequent degradation through endoplasmic-reticulum-associated protein degradation (ERAD). Choi *et al*. conclude that KLHL14 acts as a tumor suppressor in ABC-type DLBCL by targeting BCR for degradation, which is why KLHL14 is frequently mutated and not functioning in this disease type.

Our study identified KLHL14 as a tumor suppressor independent of the BCR and not only in DLBCL but also in MM and MCL cell lines (Figure 8 & Figure 9 &Figure 11). For the DLBCL cell lines, we selected OCI-LY7 (GCB type DLBCL cell line that does not dependent on NF-κB signaling through constitutive active BCR (Young et al., 2015)), OCI-LY3 (ABC type DLBCL cell line reported to be independent of BCR signaling (Davis et al., 2010)), and MHH-PREB-1 (which does not belong to either subtype). We observed a dropout phenotype upon KLHL14 expression in all three DLBCL cell lines (Figure 11a), suggesting a BCR-independent mechanism for the tumor suppressor function of KLHL14. Similarly, we observed the same dropout phenotype in MM cells, where NF-κB activation is essential for tumor proliferation and survival but primarily signaled through APRIL and BAFF binding to TACI and BCMA pathways (Figure 11a)(Tai et al., 2016, Laurent et al 2015). In addition, it has been reported that MM cells lack a functional BCR (Demchenko & Kuehl, 2010; Yoshida et al., 2010), further suggesting a BCR-independent tumor suppressor function of KLHL14. MCLs continue to express their BCR throughout and following their transformation into cancer cells. This signaling pathway is often deregulated due to mutations (Merolle et al., 2018). We were also able to confirm this dropout phenotype upon KLHL14 overexpression in three MCL cell lines (Figure 11) Additionally, we could not detect BCR subunits in our interactome screen upon KLHL14 overexpression (Figure 22e, f). Taken together, this strongly suggests an additional role for KLHL14 as a tumor suppressor, independent of its published substrate BCR. This is highly likely since E3 ubiquitin ligases can have more than one substrate and interact with and ubiquitinate multiple proteins.

6.1.3 The tumor suppressor function of KLHL14 is limited to B-cell malignancies *in-vitro*

Following the identification of KLHL14 as a tumor suppressor in patients with multiple myeloma and mantle cell lymphoma, we demonstrated that overexpression of KLHL14 in *in vitro* cell line models of MM, MCL, and DLBCL inhibited cell growth in competition-based dropout assays (Figure 11a). This tumor suppressor function of KLHL14 occurred only in B-cell malignancies, while other cancer entities, including AML and lung cancer, stayed unaffected (Figure 11a). This suggests a unique role of KLHL14 in these diseases and proposes KLHL14 as a therapeutic target specifically for B-cell malignancies. However, a dropout assay would need to be performed in healthy plasma cells to confirm that the tumor

suppressive function of KLHL14 is only affecting malignant B-cells and ensure limited off-target effects for healthy cells. Nevertheless, since our initial patient data samples from T.Haferlach were received five years ago and have changed over time, this *in vitro* dropout assay further confirmed our initial hypothesis that KLHL14 is a downregulated tumor suppressor specific in B-cell malignancies. Notably, we were able to show that in order to act as a tumor suppressor full length KLHL14 is required (Figure 12). Mutations in the Kelch or BTB domain of KLHL14 result in inhibition of this specific tumor suppressive function, which highlight that the dropout phenotype is based on KLHL14 function.

In the future, to confirm KLHL14 as a therapeutic target for B-cell malignancies, we first would have to validate its tumor suppressor function in preclinical mouse models. For these *in vivo* experiments the same cell lines used in the *in vitro* dropout assays could be used in a xenograft mouse model. Here a mixed population of cells encoding either the EV or KLHL14 could be injected subcutaneously or orthotropic into immunocompromised mice. After tumor engraftment, KLHL14 transgene expression ($dsRED^-$) or EV expression ($dsRED^+$) can be induced using doxycycline-containing food. Tumor burden could then be assessed in an endpoint study via flow cytometry analysis using entity-specific cell surface markers (e.g., CD20, BCMA, CD138, CD38). The percentage of $dsRED^+$ (EV) / $dsRED^-$ would again allow us to assess the dropout of the KLHL14 transgene-expressing cells. This provides us with initial insights into whether KLHL14 also exerts a tumor suppressing function *in vivo*.

6.1.4 KLHL14 overexpression results in a significant dropout phenotype of cells with an unclear underlying molecular mechanism

Understanding the precise molecular mechanisms behind KLHL14-mediated dropout of malignant B-cell is essential for understanding its tumor suppressive functions. In the conducted phenotypic experiments, KLHL14 overexpression had a limited effect on cell cycle progression as well as cell death (Figure 17 &Figure 18). Although minor changes in the expression of cell cycle or apoptosis markers were detected in some cell lines, these findings were inconsistent and mostly found in one cell line (Figure 17b & Figure 20 & Figure 21). Given the significant dropout observed in all B-cell malignancies, we hypothesize that the underlying effects would be consistent across the three cell lines and manifest as significant changes in the molecular pathways involved. In addition, the distinct foci-like subcellular localization of KLHL14 in and around the nucleus, has not yet been linked to a specific molecular mechanism (Figure 14 & Figure 15a, b). Additional research is required to determine whether the foci-like dot structures observed in this study can be consistently observed across various cell lines and if those KLHL14 foci's are co-localizing with potential KLHL14 interactors or substrates.

It may be necessary to introduce a stimulus such as DNA damage to achieve a more pronounced phenotype in these phenotype assays. Treating cells with Doxorubicin or Etoposide during KLHL14 overexpression may provide a clearer phenotype and allow for a better understanding of the effects of KLHL14. Synchronizing the cells with Palbociclib and Nocodazole, followed by cell cycle phenotype experiments, may reveal hidden phenotypic changes that were previously undetectable.

Notably, numerous other pathways could be involved in the observed dropout phenotype and could be triggered by KLHL14 overexpression, such as changes in cellular metabolism, which we have not investigated yet. A relatively simple method to investigate this is Single Cell Energetic Metabolism by Profiling Translation inhibition (SCENITH), which determines the protein synthesis levels as a measure of metabolic activity through measuring

puromycin uptake with a specific antibody in flow cytometry (Arguello et al., 2020). A more complex assay to conduct would be the Seahorse assay, which quantifies oxygen consumption rate and extracellular acidification rate, allowing to determine mitochondrial respiration and glycolytic activity. This allows measuring cellular metabolism in real-time but needs optimization due to the assay's complexity/sensitivity and a specialized instrument. Interestingly, Choi et al. have shown that KLHL14 ubiquitylation is involved in ERAD. In our CHX chase experiments, KLHL14 was not recovered after MG132 inhibition of the proteasome in MM1.S (Figure 26) (Choi et al., 2020). Therefore, potential degradation by other pathways, such as the lysosome, needs to be investigated in the future.

We performed all phenotypic experiments using the doxycycline-inducible system pTRIPZ, because we never achieved close to 100% efficiency with lentiviral transduction. This system is widely used for inducible gene expression in many studies, but it comes with some potential drawbacks. Not only can the pTRIPZ vector exhibit leaky expression of the transgenes in the absence of doxycycline, but also the degree of induced transgene expression can vary between different cell lines. While we did not observe leakiness, there were significant changes in KLHL14 protein expression levels between our cell lines present. Furthermore, doxycycline can have a toxic effect on cells under prolonged exposure, altering cell behavior and health and therefore interfering with experimental results. In addition, our cell lines have undergone several selection steps to obtain a pure population. During this selection process only the healthiest and most resistant cells survived and are present in our transgene cell lines. This could mean that these transgene pTRIPZ cell lines are already more resistant to KLHL14 expression than unselected wild type cells and therefore not show significant changes in our phenotype assays.

A somewhat related topic is protein complex stoichiometry, which is the ratio of proteins within a protein complex (Marsh & Teichmann, 2015). E3 ubiquitin ligases such as KLHL14 consist of many subunits to form a functional complex. In our pTRIPZ overexpression system, we only induced the expression of KLHL14, but not all the other subunits within the E3 ligase complex. Stoichiometry can influence the activity, stability, and interaction of the protein complex with other proteins .Reports show that insufficient or excess amounts of any single subunit can potentially limit complex assembly or biological functions (Taggart et al., 2020). While we observed a significant dropout with our doxycycline-inducible KLHL14 system, not considering the stoichiometry of the other subunits may not be sufficient to uncover the molecular mechanisms underlying the observed dropout phenotype.

As the experiments to this point did not reveal a clear molecular effect of KLHL14 overexpression in our phenotype experiments, we conducted a transcriptomic analysis by RNA sequencing. Therefore, MM1.S, OCI-LY3, and Z-138 cells stably overexpressing KLHL14 or an empty vector after doxycycline-induced transgene expression were harvested four and seven days post-induction for RNA isolation and sequencing. The sequencing process is still ongoing, however once we receive the results, we plan to use gene set enrichment analysis (GSEA) to identify the most significantly altered gene sets per condition and cross-validate these sets across cell lines to uncover common patterns. This approach is expected to provide insight into which molecular pathways are activated or regulated in these cell lines during KLHL14 overexpression.

A general consideration is that we worked with three different cell entities (MM = MM1.S, MCL = Z-138, DLBCL = OCI-LY3) during our phenotypic experiments. While all three showed a clear dropout phenotype upon KLHL14 overexpression, different expression levels of the different markers were observed in the cell cycle or cell death assays (Figure 17 & Figure

20 & Figure 21). It is possible that KLHL14 exerts different molecular mechanisms within these entities and also interacts with different substrates depending on the cell line or entity. DLBCL, MM, and MCL are all highly heterogenic disease with different molecular mechanisms even within the same entity depending on the patient/cell line. Especially MM shows a high grade of genetic instability with significant differences even within these cells. Showing a dropout in all B-cell neoplasms confirms the KLHL14 tumor suppressive phenotype in these different entities but the underlying differences in molecular mechanism could explain the observed inconsistent results in the phenotype experiments and could make it very difficult to find a consistent molecular mechanism in all three entities. Therefore, an option for the future would be to focus on one cancer entity such as MM, establish a phenotype and validate this phenotype in the other entities.

In summary, we found that KLHL14s function as tumor suppressor can neither be linked to cell death nor to impairments in cell cycle. We were not able to identify the specific molecular mechanism of KLHL14 most likely due to the molecular distances between three investigated entities.

6.1.5 Identification of NUDCD3 as a potential ubiquitylated substrate of KLHL14

KLHL14 is a component of the Cullin-RING ubiquitin ligase complex and carries substrate specificity. After confirming KLHL14 as a tumor suppressor, one of the main aims of this study was to identify KLHL14 interactors and ubiquitinated substrates. This approach could improve our understanding of the molecular pathways regulated by KLHL14 and thus may shed light on the molecular mechanisms driving the observed dropout phenotype in cells. To this end, we performed two mass spectrometry-based interactome screens in MM: one with mitotically synchronized MM1.S cells (Figure 22a, c, e) and one with asynchronous MM1.S cells (Figure 22b, d, f). This two-way approach was motivated by preliminary evidence suggesting that KLHL14 overexpression leads to G1 cell cycle arrest. The most significant interactor found in this screen was NUDCD3 (Figure 22e, f), a protein involved in dynein intermediate chain stabilization and mitosis. As this protein was found to interact with KLHL14 in our MCL and DLBCL cell line models as well (Figure 23a, b), we followed up on characterizing this KLHL14-NUDCD3 interaction.

Notably, the BioGRID database (www.thebiogridd.org) of protein, genetic and chemical interactions reports three papers that have also identified NUDCD3 as a potential interactor of KLHL14. This database contains over 80,000 publications for more than 2.5 million protein and gene interactions. Here, the paper by Huttlin et al., who performed high-throughput affinity purification mass spectrometry in HEK293T cells for interacting partners, identified KLHL14 as an interactor with NUDCD3 (Huttlin et al., 2021; Huttlin et al., 2017; Huttlin et al., 2015).

We also discovered interactions between KLHL14 and PAX5 and ZBTB14 in our initial interactome screens (Figure 22e, f). Both could be interesting interactors since PAX5 is a key regulator of B-cell differentiation and is expressed during early B-cell development, whereas ZBTB14 is a transcription factor. However, our cross-validation with semi-endogenous immunoprecipitation did not confirm any interaction between these proteins and KLHL14 (data not shown). Therefore, we did not follow up on these hits. Notably, KLHL9/13, another Kelch family member, emerged as a prominent hit in the interactome screen (Figure 22e) and showed interaction with KLHL14 in semi-endogenous immunoprecipitation experiments in cells (data not shown). This observed interaction between the two E3 ligase complexes may be due to the shared BTB domain. One Kelch E3 ligase may be regulating the other Kelch E3 ligase by

ubiquitylation, changing its function, localization, or abundance. This needs further investigation in the future.

Although we successfully identified potential substrates of KLHL14 with the affinity-based flag-purification, conformation and cross-validation of these candidates using different approaches is essential for this study as this approach has its limitations. FLAG-based affinity purification coupled with mass spectrometry is a widely used technique to detect protein-protein interactions and gain insight into dynamic cellular processes. E3 ligand-substrate interactions are typically transient and occur at low abundance, therefore they may not be detected by this screening method. While the bait protein (KLHL14) must be FLAG-tagged, this tag can inhibit protein folding and function, thus altering KLHL14s natural behavior within the cell. Furthermore, the binding process of FLAG-tagged KLHL14 to the M2-FLAG affinity gel occurs after cell lysis, resulting in the loss of KLHL14s natural subcellular localization, which seems to be very specific for KLHL14, and can lead to false-positive interactions. Furthermore, the bait-substrate interactions detected do not provide any clues as to what this interaction does on a functional level.

There is the possibility that despite our two affinity-based screenings coupled with mass spectrometric analysis, some KLHL14 interactors were not detected with these approaches. Alternative screening methods that mimic more physiological conditions are based on in-cell proximity labeling of interaction partners, such as BioID or TurboID purification. Here, a biotin ligase is fused to the bait protein, which biotinylates nearby proteins upon the addition of biotin. The biotinylated proteins are subsequently purified with streptavidin and analyzed by mass spectrometry to identify potential interactors (Roux et al., 2018). An improved method based on the same principle is TurboID, in which smaller biotin ligases are fused to the bait, resulting in reduced interference with bait protein function and localization, as well as higher biotinylating activity (Cho et al., 2020). APEX (Engineered Ascorbate Peroxidase) screening is even more advanced, where the bait protein is tagged with the APEX enzyme, which generates biotin-phenol radicals that rapidly attach biotin to proximal proteins within milliseconds (Martell et al., 2012). The main challenge with these methods is background labeling, as all proteins in the proximity of the bait are biotinylated, resulting in numerous hits, including non-specific background labeled proteins after mass spectrometric analysis. Optimization of the biotinylating process is critical, such as an optimal incubation time with biotin, but these methods significantly increase the likelihood of detecting transient interactors of KLHL14.

Our first interactome screens were affinity-based and could thus only detect interactions between proteins, not the function and modifications of these interactors. Therefore, a functional proteomic screening approach would be beneficial to study changes in potential KLHL14 substrates upon KLHL14 overexpression. Since KLHL14 is a ubiquitin E3 ligase, we expect potential substrates to become more ubiquitylated upon KLHL14 overexpression and, in the case of K48 ubiquitylation, less abundant due to proteasomal degradation. Cross-validation of such a functional proteomic screen with the interactome candidates could help to identify KLHL14 substrates of interest. A more functional mass spectrometry-based screen would be a His-tagged ubiquitin purification. Here, cells expressing His-tagged ubiquitin in addition to KLHL14 would be purified by histidine pull-down with nickel-NTA-agarose, and subsequently more or less ubiquitinated proteins could be quantified by mass spectrometry to reveal changes in ubiquitylation upon KLHL14 expression. While this method can result in non-physiological ubiquitylation and potential artifacts, another more advanced method would be DiGLY purification (Also see discussion DCAF7 project below). This affinity-based method uses specific antibodies that recognize the Lys-ε-Gly-Gly motifs left behind after trypsin digestion of ubiquitinated proteins. These peptides can then be enriched

and identified/quantified by mass spectrometry analysis. We would look for peptides that become more ubiquitylated upon KLHL14 overexpression compared to an empty vector, allowing us to study changes in ubiquitylation on a proteome-wide scale. In addition, this technique allows the enrichment of Di-GLY-modified peptides, enabling the identification of low-abundant ubiquitinated proteins.

In conclusion, we detected several potential interaction substrates of KLHL14 including other Kelch family members, but the most significant hit in our interactome screen was NUDCD3. It is likely to find multiple interactors of an E3 ligase since they typically have multiple substrates and can interact with and ubiquitinate various proteins. For a more extended screening, an interactome approach using TurboID or APEX combined with a functional proteomic approach using DiGLY enrichment followed by mass spectrometry would likely yield even more KLHL14 interactors. In addition, screening for interactors not only in MM1.S but also in cell lines from other B-cell entities and cross-validating the identified interactors would provide the best chance of identifying more potent substrates of KLHL14 that may affect different entities.

6.1.6 NUDCD3 as an interaction partner of KLHL14

Following the two interactome screens, we decided to further investigate NUDCD3 as a potential interactor of KLHL14, given its significant presence in both screens and its documented role in cell proliferation. A 2006 study reported that NUDCD3 is essential for cell viability by stabilizing dynein (Zhou et al., 2006). Here, it is reported that NUDCD3 expression increases during mitosis, and NUDCD3 depletion induces mitotic arrest through loss of dynein function in combination with failure to recruit γ-tubulin to the spindle poles. Interestingly, NUDCD3 depletion resulted in dynein aggregation, and immunofluorescence imaging of NUDCD3 in this study revealed aggregation in foci-like structures similar to those observed in our KLHL14 IFs (Figure 15b). This similarity suggests a role for KLHL14 in dynein intermediate chain biology and supports our finding of NUDCD3 as a KLHL14 interactor (Zhou et al., 2006). We confirmed this interaction by affinity pull-down assays and semi-endogenous immunoprecipitation in several cell lines across the three entities of interest (Figure 23a, b). Cul3, a component of the functional KLHL14 ligase complex, was also detected in these semi-endogenous immunoprecipitations, confirming the functionality of the E3 ligase complex. Further verification of this protein-protein interaction could be achieved by endogenous immunoprecipitation, particularly in MCL cell lines, given the low levels of endogenous KLHL14 in most MM cells. Conducting immunofluorescence microscopy and stain for NUDCD3 and KLHL14 could further confirm a co-localization within the cell and, therefore the likelihood of interaction on a subcellular level.

Not only depletion but also overexpression of NUDCD3 has been reported to inhibit cell proliferation by regulating cytokinesis (Cai et al., 2009). This study also shows that NUDCD3 localizes to punctate structures during telophase of cell division, which is similar to the IF localization of KLHL14 (Figure 15b). These findings underscore the importance of maintaining optimal NUDCD3 levels for cell proliferation and are consistent with the results of our NUDCD3 overexpression and shRNA-mediated knockdown dropout assays (Figure 25c, d). Interestingly, in our NUDCD3 dropout assays, OCI-LY3 seems to be the most resistant cell line, and no dropout was observed upon overexpression of NUDCD3, while only one shRNA induced moderate dropout upon depletion of NUDCD3 in this cell line (Figure 25c, d). This suggests that NUDCD3 may be involved in different molecular pathways in the cell lines tested. However, it needs to be generally noted that all cell lines were less susceptible to the NUDCD3

overexpression than to the shRNA-mediated knockdown (Figure 25c, d). Since we could not identify the underlying processes that caused the dropout of cells overexpressing KLHL14, another approach would be to repeat phenotypic assays, such as live/dead staining or Propidium Iodide/BrdU cell cycle analysis, but with NUDCD3 overexpression or knockdown to potentially elucidate the molecular pathways involved.

We confirmed NUDCD3 as an interaction partner of the KLHL14 in all three disease entities. Furthermore, cells were susceptible to knockdown and overexpression of NUDCD3. Therefore, it is possible that KLHL14 and NUDCD3 are involved in similar molecular pathways.

6.1.7 KLHL14 induces poly-ubiquitylation of NUDCD3

The interaction of NUDCD3 does not necessarily mean that NUDCD3 interacts with the whole KLHL14/Cul3-ligase complex. Therefore, we next confirmed that NUDCD3 ubiquitylation increases upon KLHL14 expression in HEK293T cells (Figure 27 & Figure 28). This suggests that binding of KLHL14 to the substrate NUDCD3 leads to its ploy-ubiquitylation and that various linkage-specific ubiquitin chains are attached to NUDCD3. However, this assay was insufficient to reveal the regulatory function of KLHL14-mediated NUDCD3 ubiquitylation.

A CHX chase revealed no changes in NUDCD3 stability (Figure 26) upon KLHL14 overexpression and only a small recovery with MG132. However, *in-vivo*-ubiquitylation assays showed increased K48 chains on NUDCD3 following KLHL14 overexpression (Figure 28a). It appears that KLHL14 can attach different linkage-specific chain types to NUDCD3 (Figure 28a-f). To attach multiple different ubiquitin chains to its substrate would be an unusual characteristic of a E3 ubiquitin ligase and the possibility exists, that the observed effect may be a HEK293T cell related artifact. Therefore, performing these *in-vivo*-ubiquitylation assays in MM, MCL, and DLBCL cell lines would be more physiological. A tandem ubiquitin-binding entities (TUBEs) assay could be conducted to ensure NUDCD3 ubiquitylation by KLHL14. TUBEs consist of ubiquitin-binding domains arranged in tandems that allow the simultaneous binding of multiple ubiquitin moieties with higher affinity than ubiquitin-associated domains found in native proteins. These TUBEs are coupled to either magnetic beads or normal agarose beads. We would be able to determine whether more ubiquitylated NUDCD3 is bound to the TUBEs upon KLHL14 expression by overexpressing KLHL14 in our B-cell malignancy cell lines and performing a TUBE-immunoprecipitation on the samples followed by immunoblotting for NUDCD3. This could confirm the ubiquitylation of NUDCD3 by KLHL14 in B-cell malignancies.

To identify the types of chains attached to NUDCD3, a simple mass spectrometry analysis of ubiquitylated NUDCD3 could reveal different ubiquitin chains. In addition, chain-specific antibodies are available, but obtaining detectable signals has been challenging due to their sensitivity and susceptibility to background noise. Another strategy to distinguish chain type is to conduct TUBE assays with K48- or K63-specific TUBEs that only bind to these chain types.

In conclusion, we have shown that NUDCD3 is a potential ubiquitylation substrate of KLHL14 in HEK293T cells. However, further studies are needed to confirm this observation in different cancer cell lines and determine the types of ubiquitin chains attached to NUDCD3. Next, we would need to establish the exact function of KLHL14-mediated NUDCD3 ubiquitylation.

6.1.8 Exploiting KLHL14 therapeutically as a treatment option for B-cell malignancies in relapsed/refractory patients

Our goal was to identify UPS-related vulnerabilities in B-cell malignancies that could be analyzed and provide the basis for novel therapeutic approaches. Despite the fact that we confirmed KLHL14 as tumor suppressor specifically in B-cell lymphomas, it is not feasible to directly exploit this function in patients. This would require reintroduction of KLHL14 in patients since its expression is downregulated or KLHL14 is mutated in most B-cell lymphoma. However, instead of targeting KLHL14, we propose to focus on its interactor NUDCD3. Our data shows that changing NUDCD3 abundance through overexpression or knockdown result in the inhibition of cancer cell growth. Developing specific NUDCD3 PROTACs or molecular glues that disrupt NUDCD3 function specifically, might have the same inhibitory effect in patients. While we still need to show that the observed NUDCD3 dropout phenotype is B-cell malignancy specific, the KLHL14-NUDCD3 axis is a potential new target in B-cell malignancies.

6.2 Identification of DCAF7 as a novel vulnerability in LuAD and other entities

6.2.1 CRISPR-Cas9-based dropout screen leads to the discovery of DCAF7 as vulnerability in LuAD

Lung adenocarcinoma (LuAD) is one of the most commonly diagnosed and deadly cancers worldwide, and the number of cases is expected to increase in the coming years (Thandra, Barsouk, Saginala, Aluru, & Barsouk, 2021). The reliance on surgery combined with chemotherapy as current treatment options underscores the urgent need for new therapeutic targets that reveal actionable vulnerabilities in lung adenocarcinoma. Since aberrations in the ubiquitin-proteasome system have been implicated in several cancers, investigating the role of the UPS in LuAD may reveal new vulnerabilities. Therefore, V. Wagner specifically targeted the UPS in LuAD by performing a CRISPR-Cas9-based dropout screen using a sgRNA library targeting only UPS related genes (Figure 29). This screen revealed relatively uncharacterized E3 ubiquitin ligases with potentially oncogenic functions, such as the substrate adaptor of the E3 ligase DCAF7 (Figure 30). To fully understand this potential vulnerability in LuAD, a thorough molecular characterization of DCAF7 and the associated substrates and pathways involved was necessary and carried out as part of the presented work.

Since the discovery of CRISPR-Cas9 gene editing, whole genome screens have become a standard tool in several areas of cancer research. These large-scale screens based on competitive growth have led to the discovery of many important and now well-characterized oncogenes. However, since most of these genes have been extensively studied or were not ideal for developing new therapeutics, we decided to perform a more targeted CRISPR-Cas9 screen. By focusing our guide library exclusively on UPS genes, we aimed to uncover potentially overlooked critical cancer dependencies in LuAD. This approach led us to identify UPS-related genes that show a dependency in LuAD, and although DCAF7 was not the top-ranked hit, it was among the top genes identified in the screen (Figure 30). While this screen was already a targeted approach, another layer could be added to future CRISPR-Cas9 screens. For example, future screens could be modified to specifically look for ligases that are involved in specific molecular mechanisms, such as differentiation or sensitizing cells to certain

drugs, or focus on already known drug targets or mutations such as EGFR or KRAS in LuAD. This would make finding the corresponding phenotype for identified novel E3 ligases easier.

6.2.2 DCAF7 depletion leads to dropout phenotype in cells

The discovery of DCAF7 as a potential LuAD oncogene is an important step, but more is needed to achieve the goal of identifying a new and potent therapeutic target. After identifying DCAF7 as a novel susceptibility in LuAD through a CRISPR-Cas9 screen, we validated its oncogenic function using patient data. Here, DCAF7 gene expression was significantly higher in tumor tissues, and elevated DCAF7 expression correlated with poorer overall survival (Figure 32a-e).

In vitro cell culture experiments further confirmed these findings, where DCAF7 depletion resulted in growth disadvantage and dropout in a competition assay (Figure 36a, b). This phenotype, observed with both sgRNA-mediated knockout and shRNA-mediated knockdown of DCAF7, occurred regardless of the genetic background of the cell lines and was also observed in other cancer entities (Figure 31 &Figure 36b). This suggested a broader oncogenic role for DCAF7, not limited to LuAD. Notably, the dropout rates varied depending on the cell line and the specific sgRNA/shRNA used, all cell lines tested showed a dropout over time upon DCAF7 depletion (Figure 31 & Figure 36a, b). Extending the dropout assay to other LuAD cell lines with varying DCAF7 protein levels and different genetic backgrounds know to meditated resistance to current LuAD treatments, could help determine if there is a correlation between dropout rate and DCAF7 protein expression. Furthermore, this could shed light on whether different genetic backgrounds impact the dropout phenotype in LuAD cells. In addition, including normal lung fibroblasts, such as IMR-90, and performing similar dropout assays targeting DCAF7 could further validate the cancer-specific dependence on high DCAF7 expression.

Our observations of cellular dropout following DCAF7 depletion in LuAD and other cancers underscore the potential of DCAF7 as a therapeutic target. The next step in validating the oncogenic function of DCAF7 for clinical application in LuAD patients will be preclinical studies in tumor mouse models. Using an approach similar to the dropout assays but in patient-derived xenograft mouse models could provide initial insights. Injecting immunocompromised mice with human LuAD cells after DCAF7 knockdown and monitoring tumor growth could clarify whether the oncogenic role of DCAF7 is reflected *in vivo*.

Although we observed increased DCAF7 protein expression in almost all lung cancer cell lines compared to normal lung fibroblasts, these levels did not correlate with the qPCR results of the corresponding cell lines (Figure 33a-c). This discrepancy suggests the possibility of post-transcriptional or post-translational modifications of DCAF7, which warrants further investigation.

In conclusion, we identified DCAF7 in a UPS-targeted CRISPR-Cas9 dropout screen and showed a cancer-specific dependence on high DCAF7 expression across multiple entities. This suggests a broad oncogenic role of DCAF7.

6.2.3 The underlying molecular mechanisms of DCAF7 remain unknown

Understanding the molecular mechanism behind the dropout observed in DCAF7-depleted LuAD cells is critical to fully characterize the mechanistic means of DCAF7 and

potentially develop new therapies targeting DCAF7. Our investigations into whether DCAF7 depletion induces increased cell death or inhibits cell cycle progression in LuAD cell lines revealed only modest effects (Figure 37a & Figure 39). There was little change in cell death following DCAF7 knockdown, and while slight changes in cell cycle progression were observed, these were inconsistent across the different shRNAs and cell lines (Figure 38 & Figure 40). We also examined cell death and cell cycle progression at later time points after DCAF7 knockdown (data not shown) but discovered a similar picture of no significant contribution to increased cell death or slowed cell cycle progression by DCAF7 depletion.

We used the NCI-H1437 and HCC-44 LuAD cell lines for all phenotypic experiments because the original CRISPR-Cas9 screen was performed in the same cell lines (Figure 30). However, considering LuAD cell lines with higher DCAF7 protein expression may yield a more distinct phenotype, as NCI-H1437 and HCC-44 have lower DCAF7 levels than other LuAD cell lines (Figure 34b, c). We decided to use shRNA-mediated knockdown of DCAF7 because of the advantages over sgRNAs already discussed, but since we were not able to detect a specific phenotype induced by DCAF7 knockdown, sgRNA-mediated knockout of DCAF7 is another option.

In addition, we aim to explore other molecular mechanisms and pathways that may explain the growth deficit, such as alterations in metabolism and ferroptosis in the future. In a genome wide CRISPR screen DCAF7 was published as an mTORC1 regulator. Here, DCAF7 knockout reduced rpS6 phosphorylation, positioning it as an upstream regulator of mTORC1 signaling (Condon et al., 2021). Although we did not observe increased levels of mTOR phosphorylation or cell death (Figure 38), we did not thoroughly investigate different forms of cell death. Ferroptosis is an oxidative and iron-dependent type of necrotic cell death that plays a critical role in the development and progression of many different cancers (Jiang et al., 2021). Using publicly available gene expression profiles, DCAF7 was identified as a ferroptosis-related diagnostic biomarker in hepatocellular carcinoma (Yi et al., 2023). Another study confirmed DCAF7 as a potential key modulator of ferroptosis in a bioinformatic analysis (Tian et al., 2023). The investigation of ferroptosis by Annexin V staining combined with live/dead dye and the use of the ferroptosis inhibitor Lip-1 could determine whether DCAF7 depletion induces ferroptosis in our LuAD setting and is the cause of our dropout phenotype.

Another study performed a phenotypic CRISPR-Cas9 screen coupled with chemical inhibition of numerous molecular pathways to identify and characterize E3 ubiquitin ligase functions. Here, DCAF7 knockout resulted in cells that were more sensitive to Palbociclib and Ribociclib treatment, suggesting a role for DCAF7 in the G1 to S transition (Hundley et al., 2021).

We showed that the subcellular localization of DCAF7 was predominantly in the nucleus and around the nucleus in the cytoplasm (Figure 41 & Figure 42a, b). This specific localization of DCAF7 was also observed in a publication where DCAF7 was found to interact with DYRK1A and HIPK2 (Glenewinkel et al., 2016). Although our observations were limited to LuAD cell lines, given the broader oncogenic role of DCAF7 in various cancers, it would be interesting to investigate whether this specific localization persists in other cancer cell lines or even healthy lung fibroblasts. The investigation of the subcellular localization of DCAF7 clearly showed that its function and potential substrates exclude proteins on the plasma membrane.

Performing proteomic or transcriptomic analyses after DCAF7 knockdown in NCI-H1437 and HCC-44 cells represents another strategy to uncover molecular pathways involved in the observed dropout phenotype. Observations from the dropout assay, particularly the significant decrease between days four and seven post-transduction with shRNA targeting

DCAF7, suggest that comparing cells from these time points could provide valuable insights. RNA sequencing to identify differentially expressed genes may give insight into the cellular responses and networks affected by DCAF7 knockdown. Advanced proteomic studies, such as protein microarrays, could also elucidate changes in protein expression and post-translational modifications resulting from DCAF7 depletion and help find the underlying phenotype the DCAF7 depletion.

In summary, our results indicate that the oncogenic function of DCAF7 is not associated with altered cell cycle progression or increased cell death. Nevertheless, there are many other potential molecular pathways that we have yet to investigate and that could play a role in DCAF7 biology.

6.2.4 DCAF7 interactors and substrates identified by TAP and DiGLY assays

One of the main functions of ubiquitin ligases is the post-translationally modification of substrate proteins by attaching ubiquitin to their lysine residues. DCAF7 acts as a specific substrate adaptor for the DDB1-Cul4 Cullin-RING E3 ligases. Due to the ambiguous phenotype observed upon DCAF7 depletion, we adopted an alternative strategy to identify DCAF7 substrates and thereby elucidate the molecular mechanisms behind the dropout phenotype in cells. Therefore, two mass spectrometry-based screens were performed: an affinity-based interactome screen (Figure 43a) and a ubiquitin-specific DiGLY functional proteomics screen (Figure 43b). Cross-validation of these screens provided a comprehensive list of potential DCAF7 substrates (Figure 45). Of these, the most significant hits were selected for further analysis, but most hits still need to be investigated.

The two-step purification process of the TAP interactome screen allowed the detection of DCAF7 interacting proteins while significantly reducing non-specific interactions (background) at a high purity level. Our setup of the experiment was to conduct only a single TAP to identify interactors due to the massive amounts of cells needed, but this is insufficient for statistical analysis. Repeating the TAP in biological triplicates would provide more reliable results. Additionally, the dual-affinity tags used to achieve the high purity levels could affect protein expression levels, localization, or obscure binding sites for interactors, potentially interfering with protein function and complex formation. Another challenge in finding ubiquitin ligase interactors is the transient nature of E3 ligase interaction with its ubiquitylated substrates. These interactions are brief and can lead to substrate degradation depending on the type of ubiquitin chains attached. In addition, the purification process requires multiple wash steps that risk the loss of these transient interactions.

A simpler method commonly used to detect protein-protein interactions are FLAG-IPs followed by mass spectrometry analysis. While simple, this technique provides a viable alternative for interactor identification and could complement the more complex TAP strategy. This could provide a broader understanding of the role and interactions of DCAF7.

While DiGLY purification coupled to mass spectrometry allows the purification of peptides with a high degree of specificity because it is based on the di-glycine residue left on lysine residues after trypsin digestion, which is a unique marker of ubiquitylation, there are notable drawbacks to this technique (Kim et al., 2011). One significant challenge is the trypsin-based digestion process required to expose the diglycine residue for detection by specific antibodies. Incomplete cleavage by trypsin at arginine residues within ubiquitin can result in unrecognizable residues, causing ubiquitylated peptides to be missed in the analysis. In addition, protein domains with high concentrations of lysine and arginine may be cleaved into

peptides that are too small to be detected by mass spectrometry. Furthermore, trypsin digestion may also affect ubiquitin-like proteins such as NEDD8, leaving an identical DiGLY motif on these lysin residue. This similarity makes it impossible to distinguish between neddylated and ubiquitylated peptides and both can appear in the mass spectrometry analysis (Sun & Zhang, 2022). Notably, NEDD8 was amongst the top hits in our DiGLY screen (Figure 45c). To overcome the problem of small, undetectable peptides and the limitations of mass spectrometry detection, sample fractionation can be used. For example, liquid chromatography fractionation increases the detection depth of ubiquitylation sites and peptides. The combination of pre-fractionation and anti-K-ε-GG antibody enrichment can significantly increase the sensitivity of protein ubiquitylation identification (Kim et al., 2011).

Another methodological consideration is the timing of cell harvest after DCAF7 knockdown. We chose an early timepoint, three days post-knockdown, based on the significant reduction in DCAF7 protein observed by immunoblotting. However, this timing may have been too early to detect all substrates affected by DCAF7 depletion and needs optimization.

Given these challenges, alternative screening methods such as TUBE, BioID, or APEX (Discussed above) may provide better results. These methods could circumvent some of the limitations associated with the discussed purification methods. They could provide broader and more accurate identification of substrates of DCAF7.

6.2.5 The substrate of DCAF7 remains unknown

After cross-validating the two screens, we selected four potential substrates of DCAF7 based on their reduced ubiquitylation in both NCI-H1437 and HCC-44 cells in the DiGLY screen, some of these potential substrates were also co-purified in the TAP screen (Figure 45c). Many identified candidate substrates that exhibited decreased ubiquitylation upon DCAF7 depletion are integral to vital cellular processes such as cell cycle progression and DNA damage response. Given the lack of clear direction from our phenotypic experiments, we selected substrate candidates known to play a role in these essential mechanisms, as well as candidates beyond these recognized pathways (Figure 45c). Although we observed no effect on cell cycle progression in our Propidium Iodide cell cycle assay and immunoblot analysis of cell cycle markers upon DCAF7 depletion, two cell cycle-related hits emerged from our substrate screening.

Cell division cycle protein 20 (CDC20) is a regulatory protein essential for the progression of the cell cycle from metaphase to anaphase by activating the anaphase-promoting complex (APC/C). This can lead to the degradation of other cell cycle proteins and the separation of sister chromosomes. Notably, CDC20 expression is often elevated in several cancer types, including lung cancer (He & Meng, 2023).

The mitotic checkpoint protein BUB3 is involved in cell cycle progression by regulating the spindle assembly checkpoint to ensure proper chromosome attachment to spindle microtubules prior to anaphase. Furthermore, BUB3 works with other proteins to inhibit APC/C, thereby preventing aneuploidy and maintaining genomic stability (Silva & Bousbaa, 2022).

Unrelated to the cell cycle are the functions of Dystroglycan 1 (DAG1) and Dehydrogenase/Reductase (SDR family) Member 4 (DHRS4), which were among the top hits in the DiGLY screen and showed the most pronounced reduction in ubiquitylation levels in both cell lines upon DCAF7 depletion. DAG1 is critical for maintaining cell integrity by linking the extracellular matrix to the cytoskeleton and mediating cellular adhesion and signal transduction

(Quereda et al., 2022). DHRS4 affects proliferation and cellular differentiation by converting retinal to retinol during vitamin A metabolism.

We could not show any interaction between DCAF7 and candidate substrates by semi-endogenous immunoprecipitation in LuAD or HEK293T cell lines (Figure 46). It is possible that despite our double screening approach some DCAF7 interactors may have remained undetected. Therefore, more sensitive and accurate substrate screening techniques may be required to identify interacting substrates of DCAF7. Alternatively, a clearer phenotype involving a specific molecular mechanism may facilitate better cross-validation of the screens, increasing the likelihood of identifying substrates related to the molecular pathway of the observed phenotype.

6.2.6 Already published DCAF7 substrates

DCAF7-mediated ubiquitylation substrates have not been well characterized in recent publications, and only a few interactors have been found so far. One of the best-studied interactors of DCAF7 is DYRK1A, which plays a central role in regulating the transcription of genes critical for development and tissue homeostasis. DYRK1A interacts with DCAF7 in a ubiquitin-independent manner, forming a complex that not only stabilizes DYRK1A but also anchors it to RNA polymerase II, thereby regulating the kinase activity of DYRK1A on Pol II (Ananthapadmanabhan et al., 2023; Yu et al., 2019).

Another published interaction partner of DCAF7 is IRS1, which is involved in the regulation of cell proliferation. In this study, a BioID screen identified DCAF7 as an interactor of IRS1. Following up on this interaction, it is shown that DCAF7 knockdown resulted in cell cycle arrest at G2 and inhibited cell proliferation. But similar to the DYRK1A interaction, the authors are uncertain whether this is a ubiquitin-mediated effect or just an effect of the interaction between DCAF7 and IRS1 (Frendo-Cumbo et al., 2022).

Like the interactions described above, DCAF7 is also required to maintain normal levels of ERCC1-XPF, which is critical for DNA repair pathways, in a ubiquitin-proteasome-independent manner (Kawara et al., 2019).

Interestingly, our tandem affinity purification screen identified DYRK1A, DYRK1B, and IRS1 as interactors of DCAF7, while none were detected in our DiGLY screen (Figure 44a & Figure 45a), suggesting a ubiquitin independent role of DCAF7 with these proteins.

MEN1, a tumor suppressor in pancreatic neuroendocrine tumors of unknown function, represents the only published interactor of DCAF7 identified as a ubiquitylated substrate in cancer research (Xu et al., 2023). The study found elevated levels of DCAF7 in tumor tissue that correlated with poor prognosis and showed that DCAF7 controls MEN1 protein abundance through ubiquitylation. While DCAF7 facilitated the degradation of MEN1 and activated mTOR signaling, DCAF7 knockout resulted in inhibition of cancer cell proliferation.

Although MEN1 is proposed to be a ubiquitinated substrate of DCAF7, it was not detected in our DiGLY screen. This discrepancy may be because our screen was performed in LuAD cell lines, where DCAF7 may interact with different ubiquitinated substrates than in pancreatic neuroendocrine cancer.

6.2.7 DCAF7 as a potential target in patients with LuAD and other cancers

Similar to our KLHL14 project, the primary goal was to find targetable vulnerabilities within the UPS in LuAD for new innovative therapeutic approaches. We identified DCAF7 as a potential oncogene in LuAD and other cancers. Depletion of this E3 ligase causes inhibition of cancer cell growth in a wide range of cancer entities. PROTACs or specific molecular antibodies that target and degrade DCAF7 are potential therapeutic approaches that could offer patients a better alternative to systemic chemotherapy with fewer side effects. However, to advance such therapies and fully exploit this novel vulnerability, it is critical to better understand the molecular function of DCAF7 in these cancer entities and to find its ubiquitylated substrates.

Despite our efforts to determine the underlying phenotype of DCAF7 depletion in cells, the involved molecular mechanisms remain unknown. In addition, no DCAF7 interactor was detected despite cross validation of an affinity based interactome and a functional proteome screen. Taken together we decided to hold off with the DCAF7 project and put all our resources and time into the KLHL14 project.

7 Publications

7.1 Published Article in peer-review journal

Adam Wahida, Christoph Schmaderer, Maike Büttner-Herold, Caterina Branca, Sainitin Donakonda, Flora Haberfellner, Carlos Torrez, Jessica Schmitz, **Tobias Schulze**, Tobias Seibt, Rupert Öllinger, Thomas Engleitner, Bernhard Haller, Katja Steiger, Roman Günthner, Georg Lorenz, Monica Yabal, Quirin Bachmann, Matthias C. Braunisch, Philipp Moog, Edouard Matevossian, Volker Aßfalg, Stefan Thorban, Lutz Renders, Martin R. Späth, Roman-Ulrich Müller, Dirk L. Stippel, Wilko Weichert, Julia Slotta-Huspenina, Sibylle von Vietinghoff, Ondrej Viklicky, Douglas R. Green, Roland Rad, Kerstin Amann, Andreas Linkermann, Jan Hinrich Bräsen, Uwe Heemann, and Stephan Kemmner. “High RIPK3 expression is associated with a higher risk of early kidney transplant failure”. iScience. 2023 Sep 17;26(10):107879. doi: 10.1016/j.isci.2023.107879. eCollection 2023 Oct 20.

7.2 Conference contributions

Tobias Schulze, Ria Spallek, Rupert Öllinger, Thomas Engleitner, Jana Zecha, Roland Rad, Bernhard Küster, Leonie Rieger, Florian Bassermann. „Identification and characterization of KLHL14 as a novel tumor suppressor in in B cell malignancies”. Jahrestagung der Deutschen, Österreichischen und Schweizerischen Gesellschaften für Hämatologie und Medizinische Onkologie, Hamburg, 2023. Poster

8 Acknowledgments

My dissertation would not have been possible without the support of many people, so I would like to take this opportunity to thank everyone who has contributed in any way to this work.

First and foremost, I would like to thank Prof. Dr. Florian Bassermann for giving me the opportunity to do my Ph.D. in his excellent research group. His knowledge, expertise, and motivation always provided helpful input and guided me throughout my time in his lab. He shaped me into a hardworking scientist and a better thinker through his constant support, meaningful feedback, and patience. I would also like to thank Prof. Dr. Daniel Krappmann and Prof. Dr. Robert Oostendorp, who were part of my thesis advisory committee and through countless scientific discussions always gave me valuable scientific feedback and pushed the projects forward.

A special thanks goes to all the great people at AG Bassermann, who made even long lab days fun and were always willing to help me. Thank you all for all the input, moral support and fun activities outside the lab. I would like to thank Ria Spallek and Vinona Wagner, who started the KLHL14 and DCAF7 project that I took over, and who always took the time to discuss project progress and help with specific lab assays. A special thanks goes to Leonie Rieger for all the constructive talks and feedback and especially for always staying positive and helping me during the last phase of my work. A thanks goes out my two medicine boys Nico and Kilian for their moral support especially outside the lab and to Marlene and Jacob for spending countless evenings with me working in the lab.

Furthermore, I would like to thank all my collaborators for their contribution to the project, especially Dr. T. Haferlach, who provided us with most of the patient data, and Dr. Piero Giansanti and Dr. Yun-Chien Chang for their support with the mass spectrometry analysis.

The biggest thank goes to my family, my girlfriend Giuliana and all my friends for their endless support and interest in the success of my work. You all encouraged me constantly and you all where at my side even on the difficult days. Without you all this work would not have been possible, thank you for believing in me.

9 References

Allman, D., Wilmore, J. R., & Gaudette, B. T. (2019). The continuing story of T-cell independent antibodies. *Immunol Rev*, *288*(1), 128-135. https://doi.org/10.1111/imr.12754

An, S., & Fu, L. (2018). Small-molecule PROTACs: An emerging and promising approach for the development of targeted therapy drugs. *EBioMedicine*, *36*, 553-562. https://doi.org/10.1016/j.ebiom.2018.09.005

Ananthapadmanabhan, V., Shows, K. H., Dickinson, A. J., & Litovchick, L. (2023). Insights from the protein interaction Universe of the multifunctional "Goldilocks" kinase DYRK1A. *Front Cell Dev Biol*, *11*, 1277537. https://doi.org/10.3389/fcell.2023.1277537

Angers, S., Li, T., Yi, X., MacCoss, M. J., Moon, R. T., & Zheng, N. (2006). Molecular architecture and assembly of the DDB1-CUL4A ubiquitin ligase machinery. *Nature*, *443*(7111), 590-593. https://doi.org/10.1038/nature05175

Arguello, R. J., Combes, A. J., Char, R., Gigan, J. P., Baaziz, A. I., Bousiquot, E., Camosseto, V., Samad, B., Tsui, J., Yan, P., Boissonneau, S., Figarella-Branger, D., Gatti, E., Tabouret, E., Krummel, M. F., & Pierre, P. (2020). SCENITH: A Flow Cytometry-Based Method to Functionally Profile Energy Metabolism with Single-Cell Resolution. *Cell Metab*, *32*(6), 1063-1075 e1067. https://doi.org/10.1016/j.cmet.2020.11.007

Armitage, J. O., & Longo, D. L. (2022). Mantle-Cell Lymphoma. *N Engl J Med*, *386*(26), 2495-2506. https://doi.org/10.1056/NEJMra2202672

Ashrafi, A., Akter, Z., Modareszadeh, P., Modareszadeh, P., Berisha, E., Alemi, P. S., Chacon Castro, M. D. C., Deese, A. R., & Zhang, L. (2022). Current Landscape of Therapeutic Resistance in Lung Cancer and Promising Strategies to Overcome Resistance. *Cancers (Basel)*, *14*(19). https://doi.org/10.3390/cancers14194562

Bard, J. A. M., Goodall, E. A., Greene, E. R., Jonsson, E., Dong, K. C., & Martin, A. (2018). Structure and Function of the 26S Proteasome. *Annu Rev Biochem*, *87*, 697-724. https://doi.org/10.1146/annurev-biochem-062917-011931

Bartha, A., & Gyorffy, B. (2021). TNMplot.com: A Web Tool for the Comparison of Gene Expression in Normal, Tumor and Metastatic Tissues. *Int J Mol Sci*, *22*(5). https://doi.org/10.3390/ijms22052622

Bassermann, F., Eichner, R., & Pagano, M. (2014). The ubiquitin proteasome system - implications for cell cycle control and the targeted treatment of cancer. *Biochim Biophys Acta*, *1843*(1), 150-162. https://doi.org/10.1016/j.bbamcr.2013.02.028

Bassermann, F., & Pagano, M. (2010). Dissecting the role of ubiquitylation in the DNA damage response checkpoint in G2. *Cell Death Differ*, *17*(1), 78-85. https://doi.org/10.1038/cdd.2009.104

Beguelin, W., Popovic, R., Teater, M., Jiang, Y., Bunting, K. L., Rosen, M., Shen, H., Yang, S. N., Wang, L., Ezponda, T., Martinez-Garcia, E., Zhang, H., Zheng, Y., Verma, S. K., McCabe, M. T., Ott, H. M., Van Aller, G. S., Kruger, R. G., Liu, Y., . . . Melnick, A. M. (2013). EZH2 is required for germinal center formation and somatic EZH2 mutations promote lymphoid transformation. *Cancer Cell*, *23*(5), 677-692. https://doi.org/10.1016/j.ccr.2013.04.011

Bekes, M., Langley, D. R., & Crews, C. M. (2022). PROTAC targeted protein degraders: the past is prologue. *Nat Rev Drug Discov*, *21*(3), 181-200. https://doi.org/10.1038/s41573-021-00371-6

Berndsen, C. E., & Wolberger, C. (2014). New insights into ubiquitin E3 ligase mechanism. *Nat Struct Mol Biol*, *21*(4), 301-307. https://doi.org/10.1038/nsmb.2780

Bertoni, F., & Ponzoni, M. (2007). The cellular origin of mantle cell lymphoma. *Int J Biochem Cell Biol*, *39*(10), 1747-1753. https://doi.org/10.1016/j.biocel.2007.04.026

Bethune, G., Bethune, D., Ridgway, N., & Xu, Z. (2010). Epidermal growth factor receptor (EGFR) in lung cancer: an overview and update. *J Thorac Dis*, *2*(1), 48-51. https://www.ncbi.nlm.nih.gov/pubmed/22263017

Bodor, J. N., Kasireddy, V., & Borghaei, H. (2018). First-Line Therapies for Metastatic Lung Adenocarcinoma Without a Driver Mutation. *J Oncol Pract*, *14*(9), 529-535. https://doi.org/10.1200/JOP.18.00250

Budhidarmo, R., Nakatani, Y., & Day, C. L. (2012). RINGs hold the key to ubiquitin transfer. *Trends Biochem Sci*, *37*(2), 58-65. https://doi.org/10.1016/j.tibs.2011.11.001

Cabanillas, F., & Shah, B. (2017). Advances in Diagnosis and Management of Diffuse Large B-cell Lymphoma. *Clin Lymphoma Myeloma Leuk*, *17*(12), 783-796. https://doi.org/10.1016/j.clml.2017.10.007

Cai, Y., Yang, Y., Shen, M., & Zhou, T. (2009). Inhibition of cytokinesis by overexpression of NudCL that is localized to the centrosome and midbody. *Cell Res*, *19*(11), 1305-1308. https://doi.org/10.1038/cr.2009.118

Cai, Z., Moten, A., Peng, D., Hsu, C. C., Pan, B. S., Manne, R., Li, H. Y., & Lin, H. K. (2020). The Skp2 Pathway: A Critical Target for Cancer Therapy. *Semin Cancer Biol*, *67*(Pt 2), 16-33. https://doi.org/10.1016/j.semcancer.2020.01.013

Calame, K. L. (2001). Plasma cells: finding new light at the end of B cell development. *Nat Immunol*, *2*(12), 1103-1108. https://doi.org/10.1038/ni1201-1103

Cascio, P., Hilton, C., Kisselev, A. F., Rock, K. L., & Goldberg, A. L. (2001). 26S proteasomes and immunoproteasomes produce mainly N-extended versions of an antigenic peptide. *EMBO J*, *20*(10), 2357-2366. https://doi.org/10.1093/emboj/20.10.2357

Chapuy, B., Stewart, C., Dunford, A. J., Kim, J., Kamburov, A., Redd, R. A., Lawrence, M. S., Roemer, M. G. M., Li, A. J., Ziepert, M., Staiger, A. M., Wala, J. A., Ducar, M. D., Leshchiner, I., Rheinbay, E., Taylor-Weiner, A., Coughlin, C. A., Hess, J. M., Pedamallu, C. S., . . . Shipp, M. A. (2018). Molecular subtypes of diffuse large B cell lymphoma are associated with distinct pathogenic mechanisms and outcomes. *Nat Med*, *24*(5), 679-690. https://doi.org/10.1038/s41591-018-0016-8

Chaudhuri, J., Tian, M., Khuong, C., Chua, K., Pinaud, E., & Alt, F. W. (2003). Transcription-targeted DNA deamination by the AID antibody diversification enzyme. *Nature*, *422*(6933), 726-730. https://doi.org/10.1038/nature01574

Chen, J. W., & Dhahbi, J. (2021). Lung adenocarcinoma and lung squamous cell carcinoma cancer classification, biomarker identification, and gene expression analysis using overlapping feature selection methods. *Sci Rep*, *11*(1), 13323. https://doi.org/10.1038/s41598-021-92725-8

Chen, S., Wu, J., Lu, Y., Ma, Y. B., Lee, B. H., Yu, Z., Ouyang, Q., Finley, D. J., Kirschner, M. W., & Mao, Y. (2016). Structural basis for dynamic regulation of the human 26S proteasome. *Proc Natl Acad Sci U S A*, *113*(46), 12991-12996. https://doi.org/10.1073/pnas.1614614113

Chen, Y., Ren, W., Wang, Q., He, Y., Ma, D., & Cai, Z. (2022). The regulation of necroptosis by ubiquitylation. *Apoptosis*, *27*(9-10), 668-684. https://doi.org/10.1007/s10495-022-01755-8

Chen, Z., Wu, M., & Liu, J. (2020). Kelch-like protein 14 promotes proliferation and migration of ovarian cancer cells. *Int J Clin Exp Pathol*, *13*(12), 2950-2961. https://www.ncbi.nlm.nih.gov/pubmed/33425096

Cheung, W. K., & Nguyen, D. X. (2015). Lineage factors and differentiation states in lung cancer progression. *Oncogene*, *34*(47), 5771-5780. https://doi.org/10.1038/onc.2015.85

Chihara, D., Johnston, K., Bolatova, T., Szabo, S., Kalsekar, A., Mutebi, A., Yang, H., Liu, Y., Attinson, D., & Hutchings, M. (2022). An Epidemiological Model to Estimate the Prevalence of Diffuse Large B-Cell Lymphoma in the United States. *Clin Lymphoma Myeloma Leuk*, *22*(12), e1092-e1099. https://doi.org/10.1016/j.clml.2022.08.008

Cho, K. F., Branon, T. C., Udeshi, N. D., Myers, S. A., Carr, S. A., & Ting, A. Y. (2020). Proximity labeling in mammalian cells with TurboID and split-TurboID. *Nat Protoc*, *15*(12), 3971-3999. https://doi.org/10.1038/s41596-020-0399-0

Choi, J., & Busino, L. (2019). E3 ubiquitin ligases in B-cell malignancies. *Cell Immunol*, *340*, 103905. https://doi.org/10.1016/j.cellimm.2019.02.004

Choi, J., Lee, K., Ingvarsdottir, K., Bonasio, R., Saraf, A., Florens, L., Washburn, M. P., Tadros, S., Green, M. R., & Busino, L. (2018). Loss of KLHL6 promotes diffuse large B-cell lymphoma growth and survival by stabilizing the mRNA decay factor roquin2. *Nat Cell Biol*, *20*(5), 586-596. https://doi.org/10.1038/s41556-018-0084-5

Choi, J., Phelan, J. D., Wright, G. W., Haupl, B., Huang, D. W., Shaffer, A. L., 3rd, Young, R. M., Wang, Z., Zhao, H., Yu, X., Oellerich, T., & Staudt, L. M. (2020). Regulation of B cell receptor-dependent NF-kappaB signaling by the tumor suppressor KLHL14. *Proc Natl Acad Sci U S A*, *117*(11), 6092-6102. https://doi.org/10.1073/pnas.1921187117

Choi, J., Zhou, N., & Busino, L. (2019). KLHL6 is a tumor suppressor gene in diffuse large B-cell lymphoma. *Cell Cycle*, *18*(3), 249-256. https://doi.org/10.1080/15384101.2019.1568765

Chuang, J. C., & Neal, J. W. (2015). Crizotinib as first line therapy for advanced ALK-positive non-small cell lung cancers. *Transl Lung Cancer Res*, *4*(5), 639-641. https://doi.org/10.3978/j.issn.2218-6751.2015.03.06

Clipson, A., Barrans, S., Zeng, N., Crouch, S., Grigoropoulos, N. F., Liu, H., Kocialkowski, S., Wang, M., Huang, Y., Worrillow, L., Goodlad, J., Buxton, J., Neat, M., Fields, P., Wilkins, B., Grant, J. W., Wright, P., Ei-Daly, H., Follows, G. A., . . . Du, M. Q. (2015). The prognosis of MYC translocation positive diffuse large B-cell lymphoma depends on the second hit. *J Pathol Clin Res*, *1*(3), 125-133. https://doi.org/10.1002/cjp2.10

Cobaleda, C., Schebesta, A., Delogu, A., & Busslinger, M. (2007). Pax5: the guardian of B cell identity and function. *Nat Immunol*, *8*(5), 463-470. https://doi.org/10.1038/ni1454

Condon, K. J., Orozco, J. M., Adelmann, C. H., Spinelli, J. B., van der Helm, P. W., Roberts, J. M., Kunchok, T., & Sabatini, D. M. (2021). Genome-wide CRISPR screens reveal multitiered mechanisms through which mTORC1 senses mitochondrial dysfunction. *Proc Natl Acad Sci U S A*, *118*(4). https://doi.org/10.1073/pnas.2022120118

Cook, L., & Macdonald, D. H. (2007). Management of paraproteinaemia. *Postgrad Med J*, *83*(978), 217-223. https://doi.org/10.1136/pgmj.2006.054627

Cooper, M. D. (2015). The early history of B cells. *Nat Rev Immunol*, *15*(3), 191-197. https://doi.org/10.1038/nri3801

Cornall, R. J., Cheng, A. M., Pawson, T., & Goodnow, C. C. (2000). Role of Syk in B-cell development and antigen-receptor signaling. *Proc Natl Acad Sci U S A*, *97*(4), 1713-1718. https://doi.org/10.1073/pnas.97.4.1713

Costa, L. J., & Usmani, S. Z. (2020). Defining and Managing High-Risk Multiple Myeloma: Current Concepts. *J Natl Compr Canc Netw*, *18*(12), 1730-1737. https://doi.org/10.6004/jnccn.2020.7673

Cotto-Rios, X. M., Bekes, M., Chapman, J., Ueberheide, B., & Huang, T. T. (2012). Deubiquitinases as a signaling target of oxidative stress. *Cell Rep*, *2*(6), 1475-1484. https://doi.org/10.1016/j.celrep.2012.11.011

Curry, J. D., Geier, J. K., & Schlissel, M. S. (2005). Single-strand recombination signal sequence nicks in vivo: evidence for a capture model of synapsis. *Nat Immunol*, *6*(12), 1272-1279. https://doi.org/10.1038/ni1270

Dammer, E. B., Na, C. H., Xu, P., Seyfried, N. T., Duong, D. M., Cheng, D., Gearing, M., Rees, H., Lah, J. J., Levey, A. I., Rush, J., & Peng, J. (2011). Polyubiquitin linkage profiles in three models of proteolytic stress suggest the etiology of Alzheimer disease. *J Biol Chem*, *286*(12), 10457-10465. https://doi.org/10.1074/jbc.M110.149633

Davis, R. E., Ngo, V. N., Lenz, G., Tolar, P., Young, R. M., Romesser, P. B., Kohlhammer, H., Lamy, L., Zhao, H., Yang, Y., Xu, W., Shaffer, A. L., Wright, G., Xiao, W., Powell, J., Jiang, J. K., Thomas, C. J., Rosenwald, A., Ott, G., . . . Staudt, L. M. (2010). Chronic active B-cell-receptor signalling in diffuse large B-cell lymphoma. *Nature*, *463*(7277), 88-92. https://doi.org/10.1038/nature08638

de Sousa, V. M. L., & Carvalho, L. (2018). Heterogeneity in Lung Cancer. *Pathobiology*, *85*(1-2), 96-107. https://doi.org/10.1159/000487440

Demchenko, Y. N., & Kuehl, W. M. (2010). A critical role for the NFkB pathway in multiple myeloma. *Oncotarget*, *1*(1), 59-68. https://doi.org/10.18632/oncotarget.109

Deng, L., Meng, T., Chen, L., Wei, W., & Wang, P. (2020). The role of ubiquitination in tumorigenesis and targeted drug discovery. *Signal Transduct Target Ther*, *5*(1), 11. https://doi.org/10.1038/s41392-020-0107-0

Dhanoa, B. S., Cogliati, T., Satish, A. G., Bruford, E. A., & Friedman, J. S. (2013). Update on the Kelch-like (KLHL) gene family. *Hum Genomics*, *7*(1), 13. https://doi.org/10.1186/1479-7364-7-13

Di Costanzo, A., Del Gaudio, N., Conte, L., & Altucci, L. (2020). The Ubiquitin Proteasome System in Hematological Malignancies: New Insight into Its Functional Role and Therapeutic Options. *Cancers (Basel)*, *12*(7). https://doi.org/10.3390/cancers12071898

Di Lollo, V., Canciello, A., Orsini, M., Bernabo, N., Ancora, M., Di Federico, M., Curini, V., Mattioli, M., Russo, V., Mauro, A., Camma, C., & Barboni, B. (2020). Transcriptomic and computational analysis identified LPA metabolism, KLHL14 and KCNE3 as novel regulators of Epithelial-Mesenchymal Transition. *Sci Rep*, *10*(1), 4180. https://doi.org/10.1038/s41598-020-61017-y

Diaz, S., Wang, K., Sjogren, B., & Liu, X. (2022). Roles of Cullin-RING Ubiquitin Ligases in Cardiovascular Diseases. *Biomolecules*, *12*(3). https://doi.org/10.3390/biom12030416

Dong, Y., Zhang, S., Wu, Z., Li, X., Wang, W. L., Zhu, Y., Stoilova-McPhie, S., Lu, Y., Finley, D., & Mao, Y. (2019). Cryo-EM structures and dynamics of substrate-engaged human 26S proteasome. *Nature*, *565*(7737), 49-55. https://doi.org/10.1038/s41586-018-0736-4

Duan, S., & Pagano, M. (2021). Ubiquitin ligases in cancer: Functions and clinical potentials. *Cell Chem Biol*, *28*(7), 918-933. https://doi.org/10.1016/j.chembiol.2021.04.008

Ducker, C., & Shaw, P. E. (2021). USP17-mediated de-ubiquitination and cancer: Clients cluster around the cell cycle. *Int J Biochem Cell Biol*, *130*, 105886. https://doi.org/10.1016/j.biocel.2020.105886

Dunleavy, K., Pittaluga, S., Czuczman, M. S., Dave, S. S., Wright, G., Grant, N., Shovlin, M., Jaffe, E. S., Janik, J. E., Staudt, L. M., & Wilson, W. H. (2009). Differential efficacy of bortezomib plus chemotherapy within molecular subtypes of diffuse large B-cell lymphoma. *Blood*, *113*(24), 6069-6076. https://doi.org/10.1182/blood-2009-01-199679

Enchev, R. I., Schulman, B. A., & Peter, M. (2015). Protein neddylation: beyond cullin-RING ligases. *Nat Rev Mol Cell Biol*, *16*(1), 30-44. https://doi.org/10.1038/nrm3919

Ferlay, J., Colombet, M., Soerjomataram, I., Parkin, D. M., Pineros, M., Znaor, A., & Bray, F. (2021). Cancer statistics for the year 2020: An overview. *Int J Cancer*. https://doi.org/10.1002/ijc.33588

Fernandez-Quintero, M. L., Pomarici, N. D., Math, B. A., Kroell, K. B., Waibl, F., Bujotzek, A., Georges, G., & Liedl, K. R. (2020). Antibodies exhibit multiple paratope states influencing V(H)-V(L) domain orientations. *Commun Biol*, *3*(1), 589. https://doi.org/10.1038/s42003-020-01319-z

Fhu, C. W., & Ali, A. (2021). Dysregulation of the Ubiquitin Proteasome System in Human Malignancies: A Window for Therapeutic Intervention. *Cancers (Basel)*, *13*(7). https://doi.org/10.3390/cancers13071513

Fonseca, R., Blood, E., Rue, M., Harrington, D., Oken, M. M., Kyle, R. A., Dewald, G. W., Van Ness, B., Van Wier, S. A., Henderson, K. J., Bailey, R. J., & Greipp, P. R. (2003). Clinical and biologic implications of recurrent genomic aberrations in myeloma. *Blood*, *101*(11), 4569-4575. https://doi.org/10.1182/blood-2002-10-3017

Frauwirth, K. A., & Thompson, C. B. (2002). Activation and inhibition of lymphocytes by costimulation. *J Clin Invest*, *109*(3), 295-299. https://doi.org/10.1172/JCI14941

French, M. E., Koehler, C. F., & Hunter, T. (2021). Emerging functions of branched ubiquitin chains. *Cell Discov*, *7*(1), 6. https://doi.org/10.1038/s41421-020-00237-y

Frendo-Cumbo, S., Li, T., Ammendolia, D. A., Coyaud, E., Laurent, E. M. N., Liu, Y., Bilan, P. J., Polevoy, G., Raught, B., Brill, J. A., Klip, A., & Brumell, J. H. (2022). DCAF7 regulates cell proliferation through IRS1-FOXO1 signaling. *iScience*, *25*(10), 105188. https://doi.org/10.1016/j.isci.2022.105188

Frick, M., Dorken, B., & Lenz, G. (2011). The molecular biology of diffuse large B-cell lymphoma. *Ther Adv Hematol*, *2*(6), 369-379. https://doi.org/10.1177/2040620711419001

Gandhi, L., Rodriguez-Abreu, D., Gadgeel, S., Esteban, E., Felip, E., De Angelis, F., Domine, M., Clingan, P., Hochmair, M. J., Powell, S. F., Cheng, S. Y., Bischoff, H. G., Peled, N., Grossi, F., Jennens, R. R., Reck, M., Hui, R., Garon, E. B., Boyer, M., . . . Investigators, K.-. (2018). Pembrolizumab plus Chemotherapy in Metastatic

Non-Small-Cell Lung Cancer. *N Engl J Med*, *378*(22), 2078-2092. https://doi.org/10.1056/NEJMoa1801005

Garcia-Ortiz, A., Rodriguez-Garcia, Y., Encinas, J., Maroto-Martin, E., Castellano, E., Teixido, J., & Martinez-Lopez, J. (2021). The Role of Tumor Microenvironment in Multiple Myeloma Development and Progression. *Cancers (Basel)*, *13*(2). https://doi.org/10.3390/cancers13020217

Giles, J. (2004). Chemistry Nobel for trio who revealed molecular death-tag. *Nature*, *431*(7010), 729. https://doi.org/10.1038/431729a

Giles, L. M., Li, L., & Chin, L. S. (2009). Printor, a novel torsinA-interacting protein implicated in dystonia pathogenesis. *J Biol Chem*, *284*(32), 21765-21775. https://doi.org/10.1074/jbc.M109.004838

Girardini, M., Maniaci, C., Hughes, S. J., Testa, A., & Ciulli, A. (2019). Cereblon versus VHL: Hijacking E3 ligases against each other using PROTACs. *Bioorg Med Chem*, *27*(12), 2466-2479. https://doi.org/10.1016/j.bmc.2019.02.048

Glenewinkel, F., Cohen, M. J., King, C. R., Kaspar, S., Bamberg-Lemper, S., Mymryk, J. S., & Becker, W. (2016). The adaptor protein DCAF7 mediates the interaction of the adenovirus E1A oncoprotein with the protein kinases DYRK1A and HIPK2. *Sci Rep*, *6*, 28241. https://doi.org/10.1038/srep28241

Gstaiger, M., Jordan, R., Lim, M., Catzavelos, C., Mestan, J., Slingerland, J., & Krek, W. (2001). Skp2 is oncogenic and overexpressed in human cancers. *Proc Natl Acad Sci U S A*, *98*(9), 5043-5048. https://doi.org/10.1073/pnas.081474898

Gyorffy, B. (2024). Transcriptome-level discovery of survival-associated biomarkers and therapy targets in non-small-cell lung cancer. *Br J Pharmacol*, *181*(3), 362-374. https://doi.org/10.1111/bph.16257

Haglund, K., & Dikic, I. (2005). Ubiquitylation and cell signaling. *EMBO J*, *24*(19), 3353-3359. https://doi.org/10.1038/sj.emboj.7600808

Han, M., Yang, H. J., & Lin, Q. (2019). KLHL14, an ovarian and endometrial-specific gene, is over-expressed in ovarian and endometrial cancer. *Math Biosci Eng*, *17*(2), 1702-1717. https://doi.org/10.3934/mbe.2020089

Hanahan, D., & Weinberg, R. A. (2000). The hallmarks of cancer. *Cell*, *100*(1), 57-70. https://doi.org/10.1016/s0092-8674(00)81683-9

Hatakeyama, S., & Nakayama, K. I. (2003). U-box proteins as a new family of ubiquitin ligases. *Biochem Biophys Res Commun*, *302*(4), 635-645. https://doi.org/10.1016/s0006-291x(03)00245-6

He, M., Cao, C., Ni, Z., Liu, Y., Song, P., Hao, S., He, Y., Sun, X., & Rao, Y. (2022). PROTACs: great opportunities for academia and industry (an update from 2020 to 2021). *Signal Transduct Target Ther*, *7*(1), 181. https://doi.org/10.1038/s41392-022-00999-9

He, M., Lv, W., & Rao, Y. (2021). Opportunities and Challenges of Small Molecule Induced Targeted Protein Degradation. *Front Cell Dev Biol*, *9*, 685106. https://doi.org/10.3389/fcell.2021.685106

He, W., & Meng, J. (2023). CDC20: a novel therapeutic target in cancer. *Am J Transl Res*, *15*(2), 678-693. https://www.ncbi.nlm.nih.gov/pubmed/36915766

Heider, M., Nickel, K., Hogner, M., & Bassermann, F. (2021). Multiple Myeloma: Molecular Pathogenesis and Disease Evolution. *Oncol Res Treat*, *44*(12), 672-681. https://doi.org/10.1159/000520312

Helmink, B. A., & Sleckman, B. P. (2012). The response to and repair of RAG-mediated DNA double-strand breaks. *Annu Rev Immunol*, *30*, 175-202. https://doi.org/10.1146/annurev-immunol-030409-101320

Herbst, R. S., Morgensztern, D., & Boshoff, C. (2018). The biology and management of non-small cell lung cancer. *Nature*, *553*(7689), 446-454. https://doi.org/10.1038/nature25183

Hershko, A., & Ciechanover, A. (1998). The ubiquitin system. *Annu Rev Biochem*, *67*, 425-479. https://doi.org/10.1146/annurev.biochem.67.1.425

Hicke, L. (2001). Protein regulation by monoubiquitin. *Nat Rev Mol Cell Biol*, *2*(3), 195-201. https://doi.org/10.1038/35056583

Hill, H. A., Qi, X., Jain, P., Nomie, K., Wang, Y., Zhou, S., & Wang, M. L. (2020). Genetic mutations and features of mantle cell lymphoma: a systematic review and meta-analysis. *Blood Adv*, *4*(13), 2927-2938. https://doi.org/10.1182/bloodadvances.2019001350

Hoffman, W., Lakkis, F. G., & Chalasani, G. (2016). B Cells, Antibodies, and More. *Clin J Am Soc Nephrol*, *11*(1), 137-154. https://doi.org/10.2215/CJN.09430915

Holstein, S. A. (2023). Ciltacabtagene autoleucel for the treatment of multiple myeloma. *Drugs Today (Barc)*, *59*(1), 1-16. https://doi.org/10.1358/dot.2023.59.1.3509751

Hoyer, B. F., Moser, K., Hauser, A. E., Peddinghaus, A., Voigt, C., Eilat, D., Radbruch, A., Hiepe, F., & Manz, R. A. (2004). Short-lived plasmablasts and long-lived plasma cells contribute to chronic humoral autoimmunity in NZB/W mice. *J Exp Med*, *199*(11), 1577-1584. https://doi.org/10.1084/jem.20040168

Huang, X., & Dixit, V. M. (2016). Drugging the undruggables: exploring the ubiquitin system for drug development. *Cell Res*, *26*(4), 484-498. https://doi.org/10.1038/cr.2016.31

Hundley, F. V., Sanvisens Delgado, N., Marin, H. C., Carr, K. L., Tian, R., & Toczyski, D. P. (2021). A comprehensive phenotypic CRISPR-Cas9 screen of the ubiquitin pathway uncovers roles of ubiquitin ligases in mitosis. *Mol Cell*, *81*(6), 1319-1336 e1319. https://doi.org/10.1016/j.molcel.2021.01.014

Huttlin, E. L., Bruckner, R. J., Navarrete-Perea, J., Cannon, J. R., Baltier, K., Gebreab, F., Gygi, M. P., Thornock, A., Zarraga, G., Tam, S., Szpyt, J., Gassaway, B. M., Panov, A., Parzen, H., Fu, S., Golbazi, A., Maenpaa, E., Stricker, K., Guha Thakurta, S., . . . Gygi, S. P. (2021). Dual proteome-scale networks reveal cell-specific remodeling of the human interactome. *Cell*, *184*(11), 3022-3040 e3028. https://doi.org/10.1016/j.cell.2021.04.011

Huttlin, E. L., Bruckner, R. J., Paulo, J. A., Cannon, J. R., Ting, L., Baltier, K., Colby, G., Gebreab, F., Gygi, M. P., Parzen, H., Szpyt, J., Tam, S., Zarraga, G., Pontano-Vaites, L., Swarup, S., White, A. E., Schweppe, D. K., Rad, R., Erickson, B. K., . . . Harper, J. W. (2017). Architecture of the human interactome defines protein communities and disease networks. *Nature*, *545*(7655), 505-509. https://doi.org/10.1038/nature22366

Huttlin, E. L., Ting, L., Bruckner, R. J., Gebreab, F., Gygi, M. P., Szpyt, J., Tam, S., Zarraga, G., Colby, G., Baltier, K., Dong, R., Guarani, V., Vaites, L. P., Ordureau, A., Rad, R., Erickson, B. K., Wuhr, M., Chick, J., Zhai, B., . . . Gygi, S. P. (2015). The BioPlex Network: A Systematic Exploration of the Human Interactome. *Cell*, *162*(2), 425-440. https://doi.org/10.1016/j.cell.2015.06.043

Issaeva, N., Bozko, P., Enge, M., Protopopova, M., Verhoef, L. G., Masucci, M., Pramanik, A., & Selivanova, G. (2004). Small molecule RITA binds to p53, blocks p53-HDM-2 interaction and activates p53 function in tumors. *Nat Med*, *10*(12), 1321-1328. https://doi.org/10.1038/nm1146

Jackson, S., & Xiong, Y. (2009). CRL4s: the CUL4-RING E3 ubiquitin ligases. *Trends Biochem Sci*, *34*(11), 562-570. https://doi.org/10.1016/j.tibs.2009.07.002

Jiang, M., Hu, R., Yu, R., Tang, Y., & Li, J. (2021). A narrative review of mechanisms of ferroptosis in cancer: new challenges and opportunities. *Ann Transl Med*, *9*(20), 1599. https://doi.org/10.21037/atm-21-4863

Jin, J., Arias, E. E., Chen, J., Harper, J. W., & Walter, J. C. (2006). A family of diverse Cul4-Ddb1-interacting proteins includes Cdt2, which is required for S phase destruction of the replication factor Cdt1. *Mol Cell*, *23*(5), 709-721. https://doi.org/10.1016/j.molcel.2006.08.010

Jin, J., Cardozo, T., Lovering, R. C., Elledge, S. J., Pagano, M., & Harper, J. W. (2004). Systematic analysis and nomenclature of mammalian F-box proteins. *Genes Dev*, *18*(21), 2573-2580. https://doi.org/10.1101/gad.1255304

Johnson, M., Garassino, M. C., Mok, T., & Mitsudomi, T. (2022). Treatment strategies and outcomes for patients with EGFR-mutant non-small cell lung cancer resistant to EGFR tyrosine kinase inhibitors: Focus on novel therapies. *Lung Cancer*, *170*, 41-51. https://doi.org/10.1016/j.lungcan.2022.05.011

Kales, S. C., Ryan, P. E., Nau, M. M., & Lipkowitz, S. (2010). Cbl and human myeloid neoplasms: the Cbl oncogene comes of age. *Cancer Res*, *70*(12), 4789-4794. https://doi.org/10.1158/0008-5472.CAN-10-0610

Kapadia, B. B., & Gartenhaus, R. B. (2019). DUBbing Down Translation: The Functional Interaction of Deubiquitinases with the Translational Machinery. *Mol Cancer Ther*, *18*(9), 1475-1483. https://doi.org/10.1158/1535-7163.MCT-19-0307

Kawara, H., Akahori, R., Wakasugi, M., Sancar, A., & Matsunaga, T. (2019). DCAF7 is required for maintaining the cellular levels of ERCC1-XPF and nucleotide excision repair. *Biochem Biophys Res Commun*, *519*(1), 204-210. https://doi.org/10.1016/j.bbrc.2019.08.147

Khodabakhshi, A. H., Morin, R. D., Fejes, A. P., Mungall, A. J., Mungall, K. L., Bolger-Munro, M., Johnson, N. A., Connors, J. M., Gascoyne, R. D., Marra, M. A., Birol, I., & Jones, S. J. (2012). Recurrent targets of aberrant somatic hypermutation in lymphoma. *Oncotarget*, *3*(11), 1308-1319. https://doi.org/10.18632/oncotarget.653

Khoronenkova, S. V., Dianova, II, Ternette, N., Kessler, B. M., Parsons, J. L., & Dianov, G. L. (2012). ATM-dependent downregulation of USP7/HAUSP by PPM1G activates p53 response to DNA damage. *Mol Cell*, *45*(6), 801-813. https://doi.org/10.1016/j.molcel.2012.01.021

Kim, J. Y., Lee, R., Xiao, G., Forbes, D., & Bargonetti, J. (2020). MDM2-C Functions as an E3 Ubiquitin Ligase. *Cancer Manag Res*, *12*, 7715-7724. https://doi.org/10.2147/CMAR.S260943

Kim, W., Bennett, E. J., Huttlin, E. L., Guo, A., Li, J., Possemato, A., Sowa, M. E., Rad, R., Rush, J., Comb, M. J., Harper, J. W., & Gygi, S. P. (2011). Systematic and quantitative assessment of the ubiquitin-modified proteome. *Mol Cell*, *44*(2), 325-340. https://doi.org/10.1016/j.molcel.2011.08.025

Komander, D. (2009). The emerging complexity of protein ubiquitination. *Biochem Soc Trans*, *37*(Pt 5), 937-953. https://doi.org/10.1042/BST0370937

Komander, D., & Rape, M. (2012). The ubiquitin code. *Annu Rev Biochem*, *81*, 203-229. https://doi.org/10.1146/annurev-biochem-060310-170328

Koues, O. I., Oltz, E. M., & Payton, J. E. (2015). Short-Circuiting Gene Regulatory Networks: Origins of B Cell Lymphoma. *Trends Genet*, *31*(12), 720-731. https://doi.org/10.1016/j.tig.2015.09.006

Kraan, W., Horlings, H. M., van Keimpema, M., Schilder-Tol, E. J., Oud, M. E., Scheepstra, C., Kluin, P. M., Kersten, M. J., Spaargaren, M., & Pals, S. T. (2013). High

prevalence of oncogenic MYD88 and CD79B mutations in diffuse large B-cell lymphomas presenting at immune-privileged sites. *Blood Cancer J*, *3*(9), e139. https://doi.org/10.1038/bcj.2013.28
Kuehl, W. M., & Bergsagel, P. L. (2002). Multiple myeloma: evolving genetic events and host interactions. *Nat Rev Cancer*, *2*(3), 175-187. https://doi.org/10.1038/nrc746
Kumar, A., Eyre, T. A., Lewis, K. L., Thompson, M. C., & Cheah, C. Y. (2022). New Directions for Mantle Cell Lymphoma in 2022. *Am Soc Clin Oncol Educ Book*, *42*, 1-15. https://doi.org/10.1200/EDBK_349509
Kumar, S. K., Rajkumar, V., Kyle, R. A., van Duin, M., Sonneveld, P., Mateos, M. V., Gay, F., & Anderson, K. C. (2017). Multiple myeloma. *Nat Rev Dis Primers*, *3*, 17046. https://doi.org/10.1038/nrdp.2017.46
Kunjappu, M. J., & Hochstrasser, M. (2014). Assembly of the 20S proteasome. *Biochim Biophys Acta*, *1843*(1), 2-12. https://doi.org/10.1016/j.bbamcr.2013.03.008
Kuppers, R. (2005). Mechanisms of B-cell lymphoma pathogenesis. *Nat Rev Cancer*, *5*(4), 251-262. https://doi.org/10.1038/nrc1589
Kuppers, R., & Dalla-Favera, R. (2001). Mechanisms of chromosomal translocations in B cell lymphomas. *Oncogene*, *20*(40), 5580-5594. https://doi.org/10.1038/sj.onc.1204640
Kurosaki, T., Kometani, K., & Ise, W. (2015). Memory B cells. *Nat Rev Immunol*, *15*(3), 149-159. https://doi.org/10.1038/nri3802
Kyle, R. A., & Rajkumar, S. V. (2009). Criteria for diagnosis, staging, risk stratification and response assessment of multiple myeloma. *Leukemia*, *23*(1), 3-9. https://doi.org/10.1038/leu.2008.291
Lababede, O., & Meziane, M. A. (2018). The Eighth Edition of TNM Staging of Lung Cancer: Reference Chart and Diagrams. *Oncologist*, *23*(7), 844-848. https://doi.org/10.1634/theoncologist.2017-0659
Lai, K. P., Chen, J., & Tse, W. K. F. (2020). Role of Deubiquitinases in Human Cancers: Potential Targeted Therapy. *Int J Mol Sci*, *21*(7). https://doi.org/10.3390/ijms21072548
Lane, D. P. (1992). Cancer. p53, guardian of the genome. *Nature*, *358*(6381), 15-16. https://doi.org/10.1038/358015a0
LaPlante, G., & Zhang, W. (2021). Targeting the Ubiquitin-Proteasome System for Cancer Therapeutics by Small-Molecule Inhibitors. *Cancers (Basel)*, *13*(12). https://doi.org/10.3390/cancers13123079
Lee, J., & Zhou, P. (2007). DCAFs, the missing link of the CUL4-DDB1 ubiquitin ligase. *Mol Cell*, *26*(6), 775-780. https://doi.org/10.1016/j.molcel.2007.06.001
Lemaire, M., Deleu, S., De Bruyne, E., Van Valckenborgh, E., Menu, E., & Vanderkerken, K. (2011). The microenvironment and molecular biology of the multiple myeloma tumor. *Adv Cancer Res*, *110*, 19-42. https://doi.org/10.1016/B978-0-12-386469-7.00002-5
Lenz, G., Davis, R. E., Ngo, V. N., Lam, L., George, T. C., Wright, G. W., Dave, S. S., Zhao, H., Xu, W., Rosenwald, A., Ott, G., Muller-Hermelink, H. K., Gascoyne, R. D., Connors, J. M., Rimsza, L. M., Campo, E., Jaffe, E. S., Delabie, J., Smeland, E. B., . . . Staudt, L. M. (2008). Oncogenic CARD11 mutations in human diffuse large B cell lymphoma. *Science*, *319*(5870), 1676-1679. https://doi.org/10.1126/science.1153629
Li, F., Aljahdali, I. A. M., & Ling, X. (2022). Molecular Glues: Capable Protein-Binding Small Molecules That Can Change Protein-Protein Interactions and Interactomes

for the Potential Treatment of Human Cancer and Neurodegenerative Diseases. *Int J Mol Sci*, *23*(11). https://doi.org/10.3390/ijms23116206

Li, J. Y., Gaillard, F., Moreau, A., Harousseau, J. L., Laboisse, C., Milpied, N., Bataille, R., & Avet-Loiseau, H. (1999). Detection of translocation t(11;14)(q13;q32) in mantle cell lymphoma by fluorescence in situ hybridization. *Am J Pathol*, *154*(5), 1449-1452. https://doi.org/10.1016/S0002-9440(10)65399-0

Li, S., Liu, J., Min, Q., Ikawa, T., Yasuda, S., Yang, Y., Wang, Y. Q., Tsubata, T., Zhao, Y., & Wang, J. Y. (2018). Kelch-like protein 14 promotes B-1a but suppresses B-1b cell development. *Int Immunol*, *30*(7), 311-318. https://doi.org/10.1093/intimm/dxy033

Liu, B., Ruan, J., Chen, M., Li, Z., Manjengwa, G., Schluter, D., Song, W., & Wang, X. (2022). Deubiquitinating enzymes (DUBs): decipher underlying basis of neurodegenerative diseases. *Mol Psychiatry*, *27*(1), 259-268. https://doi.org/10.1038/s41380-021-01233-8

Liu, J., Leung, C. T., Liang, L., Wang, Y., Chen, J., Lai, K. P., & Tse, W. K. F. (2022). Deubiquitinases in Cancers: Aspects of Proliferation, Metastasis, and Apoptosis. *Cancers (Basel)*, *14*(14). https://doi.org/10.3390/cancers14143547

Livneh, I., Cohen-Kaplan, V., Cohen-Rosenzweig, C., Avni, N., & Ciechanover, A. (2016). The life cycle of the 26S proteasome: from birth, through regulation and function, and onto its death. *Cell Res*, *26*(8), 869-885. https://doi.org/10.1038/cr.2016.86

Lynch, D. T., Koya, S., Acharya, U., & Kumar, A. (2024). Mantle Cell Lymphoma. In *StatPearls*. https://www.ncbi.nlm.nih.gov/pubmed/30725670

Marsh, J. A., & Teichmann, S. A. (2015). Structure, dynamics, assembly, and evolution of protein complexes. *Annu Rev Biochem*, *84*, 551-575. https://doi.org/10.1146/annurev-biochem-060614-034142

Martell, J. D., Deerinck, T. J., Sancak, Y., Poulos, T. L., Mootha, V. K., Sosinsky, G. E., Ellisman, M. H., & Ting, A. Y. (2012). Engineered ascorbate peroxidase as a genetically encoded reporter for electron microscopy. *Nat Biotechnol*, *30*(11), 1143-1148. https://doi.org/10.1038/nbt.2375

Martin-Romano, P., Baldini, C., & Postel-Vinay, S. (2020). How Much Can We Bet on Activity of BET Inhibitors Beyond NUT-Midline Carcinoma? *JNCI Cancer Spectr*, *4*(2), pkz092. https://doi.org/10.1093/jncics/pkz092

Merolle, M. I., Ahmed, M., Nomie, K., & Wang, M. L. (2018). The B cell receptor signaling pathway in mantle cell lymphoma. *Oncotarget*, *9*(38), 25332-25341. https://doi.org/10.18632/oncotarget.25011

Metzger, M. B., Hristova, V. A., & Weissman, A. M. (2012). HECT and RING finger families of E3 ubiquitin ligases at a glance. *J Cell Sci*, *125*(Pt 3), 531-537. https://doi.org/10.1242/jcs.091777

Metzger, M. B., Pruneda, J. N., Klevit, R. E., & Weissman, A. M. (2014). RING-type E3 ligases: master manipulators of E2 ubiquitin-conjugating enzymes and ubiquitination. *Biochim Biophys Acta*, *1843*(1), 47-60. https://doi.org/10.1016/j.bbamcr.2013.05.026

Mevissen, T. E., Hospenthal, M. K., Geurink, P. P., Elliott, P. R., Akutsu, M., Arnaudo, N., Ekkebus, R., Kulathu, Y., Wauer, T., El Oualid, F., Freund, S. M., Ovaa, H., & Komander, D. (2013). OTU deubiquitinases reveal mechanisms of linkage specificity and enable ubiquitin chain restriction analysis. *Cell*, *154*(1), 169-184. https://doi.org/10.1016/j.cell.2013.05.046

Mevissen, T. E. T., & Komander, D. (2017). Mechanisms of Deubiquitinase Specificity and Regulation. *Annu Rev Biochem*, *86*, 159-192. https://doi.org/10.1146/annurev-biochem-061516-044916

Miyata, Y., & Nishida, E. (2023). Identification of FAM53C as a cytosolic-anchoring inhibitory binding protein of the kinase DYRK1A. *Life Sci Alliance*, *6*(12). https://doi.org/10.26508/lsa.202302129

Myers, D. J., & Wallen, J. M. (2024). Lung Adenocarcinoma. In *StatPearls*. https://www.ncbi.nlm.nih.gov/pubmed/30137862

Nakayama, K. I., & Nakayama, K. (2006). Ubiquitin ligases: cell-cycle control and cancer. *Nat Rev Cancer*, *6*(5), 369-381. https://doi.org/10.1038/nrc1881

Nandi, D., Tahiliani, P., Kumar, A., & Chandu, D. (2006). The ubiquitin-proteasome system. *J Biosci*, *31*(1), 137-155. https://doi.org/10.1007/BF02705243

Nemazee, D. (2017). Mechanisms of central tolerance for B cells. *Nat Rev Immunol*, *17*(5), 281-294. https://doi.org/10.1038/nri.2017.19

Nguyen, K. T., Ju, S., Kim, S. Y., Lee, C. S., Lee, C., & Hwang, C. S. (2022). N-Terminal Modifications of Ubiquitin via Methionine Excision, Deamination, and Arginylation Expand the Ubiquitin Code. *Mol Cells*, *45*(3), 158-167. https://doi.org/10.14348/molcells.2022.2027

Nguyen, T. T., Kim, J. W., Choi, H. I., Maeng, H. J., & Koo, T. S. (2022). Development of an LC-MS/MS Method for ARV-110, a PROTAC Molecule, and Applications to Pharmacokinetic Studies. *Molecules*, *27*(6). https://doi.org/10.3390/molecules27061977

Niemann, C. U., & Wiestner, A. (2013). B-cell receptor signaling as a driver of lymphoma development and evolution. *Semin Cancer Biol*, *23*(6), 410-421. https://doi.org/10.1016/j.semcancer.2013.09.001

Nijman, S. M., Luna-Vargas, M. P., Velds, A., Brummelkamp, T. R., Dirac, A. M., Sixma, T. K., & Bernards, R. (2005). A genomic and functional inventory of deubiquitinating enzymes. *Cell*, *123*(5), 773-786. https://doi.org/10.1016/j.cell.2005.11.007

Nomiri, S., Karami, H., Baradaran, B., Javadrashid, D., Derakhshani, A., Nourbakhsh, N. S., Shadbad, M. A., Solimando, A. G., Tabrizi, N. J., Brunetti, O., Nasseri, S., Racanelli, V., Safarpour, H., & Silvestris, N. (2022). Exploiting systems biology to investigate the gene modules and drugs in ovarian cancer: A hypothesis based on the weighted gene co-expression network analysis. *Biomed Pharmacother*, *146*, 112537. https://doi.org/10.1016/j.biopha.2021.112537

Nunes, A. T., & Annunziata, C. M. (2017). Proteasome inhibitors: structure and function. *Semin Oncol*, *44*(6), 377-380. https://doi.org/10.1053/j.seminoncol.2018.01.004

Odogwu, L., Mathieu, L., Blumenthal, G., Larkins, E., Goldberg, K. B., Griffin, N., Bijwaard, K., Lee, E. Y., Philip, R., Jiang, X., Rodriguez, L., McKee, A. E., Keegan, P., & Pazdur, R. (2018). FDA Approval Summary: Dabrafenib and Trametinib for the Treatment of Metastatic Non-Small Cell Lung Cancers Harboring BRAF V600E Mutations. *Oncologist*, *23*(6), 740-745. https://doi.org/10.1634/theoncologist.2017-0642

Oki, Y., Kelly, K. R., Flinn, I., Patel, M. R., Gharavi, R., Ma, A., Parker, J., Hafeez, A., Tuck, D., & Younes, A. (2017). CUDC-907 in relapsed/refractory diffuse large B-cell lymphoma, including patients with MYC-alterations: results from an expanded phase I trial. *Haematologica*, *102*(11), 1923-1930. https://doi.org/10.3324/haematol.2017.172882

Oranger, A., Carbone, C., Izzo, M., & Grano, M. (2013). Cellular mechanisms of multiple myeloma bone disease. *Clin Dev Immunol*, *2013*, 289458. https://doi.org/10.1155/2013/289458

Oyajobi, B. O. (2007). Multiple myeloma/hypercalcemia. *Arthritis Res Ther*, *9 Suppl 1*(Suppl 1), S4. https://doi.org/10.1186/ar2168

Padala, S. A., Barsouk, A., Barsouk, A., Rawla, P., Vakiti, A., Kolhe, R., Kota, V., & Ajebo, G. H. (2021). Epidemiology, Staging, and Management of Multiple Myeloma. *Med Sci (Basel)*, *9*(1). https://doi.org/10.3390/medsci9010003

Palumbo, A., Avet-Loiseau, H., Oliva, S., Lokhorst, H. M., Goldschmidt, H., Rosinol, L., Richardson, P., Caltagirone, S., Lahuerta, J. J., Facon, T., Bringhen, S., Gay, F., Attal, M., Passera, R., Spencer, A., Offidani, M., Kumar, S., Musto, P., Lonial, S., . . . Moreau, P. (2015). Revised International Staging System for Multiple Myeloma: A Report From International Myeloma Working Group. *J Clin Oncol*, *33*(26), 2863-2869. https://doi.org/10.1200/JCO.2015.61.2267

Parker, D. C. (1993). The functions of antigen recognition in T cell-dependent B cell activation. *Semin Immunol*, *5*(6), 413-420. https://doi.org/10.1006/smim.1993.1047

Parrondo, R. D., Ailawadhi, S., Sher, T., Chanan-Khan, A. A., & Roy, V. (2020). Autologous Stem-Cell Transplantation for Multiple Myeloma in the Era of Novel Therapies. *JCO Oncol Pract*, *16*(2), 56-66. https://doi.org/10.1200/JOP.19.00335

Paulmann, C., Spallek, R., Karpiuk, O., Heider, M., Schaffer, I., Zecha, J., Klaeger, S., Walzik, M., Ollinger, R., Engleitner, T., Wirth, M., Keller, U., Kronke, J., Rudelius, M., Kossatz, S., Rad, R., Kuster, B., & Bassermann, F. (2022). The OTUD6B-LIN28B-MYC axis determines the proliferative state in multiple myeloma. *EMBO J*, *41*(20), e110871. https://doi.org/10.15252/embj.2022110871

Peng, J., Jiang, K., Sun, X., Wu, L., Wang, J., Xi, X., Tan, X., Liang, T., Tan, C., & Zhang, P. (2022). Identification of a class of potent USP25/28 inhibitors with broad-spectrum anti-cancer activity. *Signal Transduct Target Ther*, *7*(1), 393. https://doi.org/10.1038/s41392-022-01209-2

Peng, Z., Liao, Z., Matsumoto, Y., Yang, A., & Tomkinson, A. E. (2016). Human DNA Ligase I Interacts with and Is Targeted for Degradation by the DCAF7 Specificity Factor of the Cul4-DDB1 Ubiquitin Ligase Complex. *J Biol Chem*, *291*(42), 21893-21902. https://doi.org/10.1074/jbc.M116.746198

Peschard, P., & Park, M. (2003). Escape from Cbl-mediated downregulation: a recurrent theme for oncogenic deregulation of receptor tyrosine kinases. *Cancer Cell*, *3*(6), 519-523. https://doi.org/10.1016/s1535-6108(03)00136-3

Poletto, S., Novo, M., Paruzzo, L., Frascione, P. M. M., & Vitolo, U. (2022). Treatment strategies for patients with diffuse large B-cell lymphoma. *Cancer Treat Rev*, *110*, 102443. https://doi.org/10.1016/j.ctrv.2022.102443

Pu, J. J., Savani, M., Huang, N., & Epner, E. M. (2022). Mantle cell lymphoma management trends and novel agents: where are we going? *Ther Adv Hematol*, *13*, 20406207221080743. https://doi.org/10.1177/20406207221080743

Puertas, B., Gonzalez-Calle, V., Sobejano-Fuertes, E., Escalante, F., Rey-Bua, B., Padilla, I., Garcia-Sanz, R., Puig, N., Gutierrez, N. C., & Mateos, M. V. (2023). Multiple myeloma with t(11;14): impact of novel agents on outcome. *Blood Cancer J*, *13*(1), 40. https://doi.org/10.1038/s41408-023-00807-9

Quereda, C., Pastor, A., & Martin-Nieto, J. (2022). Involvement of abnormal dystroglycan expression and matriglycan levels in cancer pathogenesis. *Cancer Cell Int*, *22*(1), 395. https://doi.org/10.1186/s12935-022-02812-7

Rabkin, C. S., Hirt, C., Janz, S., & Dolken, G. (2008). t(14;18) Translocations and risk of follicular lymphoma. *J Natl Cancer Inst Monogr*(39), 48-51. https://doi.org/10.1093/jncimonographs/lgn002

Rajkumar, S. V. (2012). Doublets, triplets, or quadruplets of novel agents in newly diagnosed myeloma? *Hematology Am Soc Hematol Educ Program*, *2012*, 354-361. https://doi.org/10.1182/asheducation-2012.1.354

Rajkumar, S. V., Gupta, V., Fonseca, R., Dispenzieri, A., Gonsalves, W. I., Larson, D., Ketterling, R. P., Lust, J. A., Kyle, R. A., & Kumar, S. K. (2013). Impact of primary molecular cytogenetic abnormalities and risk of progression in smoldering multiple myeloma. *Leukemia*, *27*(8), 1738-1744. https://doi.org/10.1038/leu.2013.86

Rajkumar, S. V., & Kumar, S. (2016). Multiple Myeloma: Diagnosis and Treatment. *Mayo Clin Proc*, *91*(1), 101-119. https://doi.org/10.1016/j.mayocp.2015.11.007

Rastogi, I., Jeon, D., Moseman, J. E., Muralidhar, A., Potluri, H. K., & McNeel, D. G. (2022). Role of B cells as antigen presenting cells. *Front Immunol*, *13*, 954936. https://doi.org/10.3389/fimmu.2022.954936

Ravid, T., & Hochstrasser, M. (2008). Diversity of degradation signals in the ubiquitin-proteasome system. *Nat Rev Mol Cell Biol*, *9*(9), 679-690. https://doi.org/10.1038/nrm2468

Reck, M., Carbone, D. P., Garassino, M., & Barlesi, F. (2021). Targeting KRAS in non-small-cell lung cancer: recent progress and new approaches. *Ann Oncol*, *32*(9), 1101-1110. https://doi.org/10.1016/j.annonc.2021.06.001

Rodriguez, S., Abundis, C., Boccalatte, F., Mehrotra, P., Chiang, M. Y., Yui, M. A., Wang, L., Zhang, H., Zollman, A., Bonfim-Silva, R., Kloetgen, A., Palmer, J., Sandusky, G., Wunderlich, M., Kaplan, M. H., Mulloy, J. C., Marcucci, G., Aifantis, I., Cardoso, A. A., & Carlesso, N. (2020). Therapeutic targeting of the E3 ubiquitin ligase SKP2 in T-ALL. *Leukemia*, *34*(5), 1241-1252. https://doi.org/10.1038/s41375-019-0653-z

Roex, G., Timmers, M., Wouters, K., Campillo-Davo, D., Flumens, D., Schroyens, W., Chu, Y., Berneman, Z. N., Lion, E., Luo, F., & Anguille, S. (2020). Safety and clinical efficacy of BCMA CAR-T-cell therapy in multiple myeloma. *J Hematol Oncol*, *13*(1), 164. https://doi.org/10.1186/s13045-020-01001-1

Rohondia, S. O., Ahmed, Z. S. O., & Dou, Q. P. (2020). Updated Review and Perspective on 20S Proteasome Inhibitors in the Treatment of Lung Cancer. *Curr Cancer Drug Targets*, *20*(6), 392-409. https://doi.org/10.2174/1568009620666200226094000

Ronau, J. A., Beckmann, J. F., & Hochstrasser, M. (2016). Substrate specificity of the ubiquitin and Ubl proteases. *Cell Res*, *26*(4), 441-456. https://doi.org/10.1038/cr.2016.38

Rosenwald, A., & Staudt, L. M. (2003). Gene expression profiling of diffuse large B-cell lymphoma. *Leuk Lymphoma*, *44 Suppl 3*, S41-47. https://doi.org/10.1080/10428190310001623775

Roth, D. B. (2014). V(D)J Recombination: Mechanism, Errors, and Fidelity. *Microbiol Spectr*, *2*(6). https://doi.org/10.1128/microbiolspec.MDNA3-0041-2014

Rotin, D., & Kumar, S. (2009). Physiological functions of the HECT family of ubiquitin ligases. *Nat Rev Mol Cell Biol*, *10*(6), 398-409. https://doi.org/10.1038/nrm2690

Roux, K. J., Kim, D. I., Burke, B., & May, D. G. (2018). BioID: A Screen for Protein-Protein Interactions. *Curr Protoc Protein Sci*, *91*, 19 23 11-19 23 15. https://doi.org/10.1002/cpps.51

Ruano-Ravina, A., Provencio, M., Calvo de Juan, V., Carcereny, E., Moran, T., Rodriguez-Abreu, D., Lopez-Castro, R., Cuadrado Albite, E., Guirado, M., Gomez Gonzalez,

L., Massuti, B., Ortega Granados, A. L., Blasco, A., Cobo, M., Garcia-Campelo, R., Bosch, J., Trigo, J., Juan, O., Aguado de la Rosa, C., . . . Cerezo, S. (2020). Lung cancer symptoms at diagnosis: results of a nationwide registry study. *ESMO Open*, *5*(6), e001021. https://doi.org/10.1136/esmoopen-2020-001021

Sahni, V., Itoh, Y., Shnider, S. J., & Macklis, J. D. (2021). Crim1 and Kelch-like 14 exert complementary dual-directional developmental control over segmentally specific corticospinal axon projection targeting. *Cell Rep*, *37*(3), 109842. https://doi.org/10.1016/j.celrep.2021.109842

Sahni, V., Shnider, S. J., Jabaudon, D., Song, J. H. T., Itoh, Y., Greig, L. C., & Macklis, J. D. (2021). Corticospinal neuron subpopulation-specific developmental genes prospectively indicate mature segmentally specific axon projection targeting. *Cell Rep*, *37*(3), 109843. https://doi.org/10.1016/j.celrep.2021.109843

Sahtoe, D. D., & Sixma, T. K. (2015). Layers of DUB regulation. *Trends Biochem Sci*, *40*(8), 456-467. https://doi.org/10.1016/j.tibs.2015.05.002

San-Miguel, J., Dhakal, B., Yong, K., Spencer, A., Anguille, S., Mateos, M. V., Fernandez de Larrea, C., Martinez-Lopez, J., Moreau, P., Touzeau, C., Leleu, X., Avivi, I., Cavo, M., Ishida, T., Kim, S. J., Roeloffzen, W., van de Donk, N., Dytfeld, D., Sidana, S., . . . Einsele, H. (2023). Cilta-cel or Standard Care in Lenalidomide-Refractory Multiple Myeloma. *N Engl J Med*, *389*(4), 335-347. https://doi.org/10.1056/NEJMoa2303379

San-Miguel, J. F., & Mateos, M. V. (2011). Can multiple myeloma become a curable disease? *Haematologica*, *96*(9), 1246-1248. https://doi.org/10.3324/haematol.2011.051169

Sandel, P. C., & Monroe, J. G. (1999). Negative selection of immature B cells by receptor editing or deletion is determined by site of antigen encounter. *Immunity*, *10*(3), 289-299. https://doi.org/10.1016/s1074-7613(00)80029-1

Sasso, J. M., Tenchov, R., Wang, D., Johnson, L. S., Wang, X., & Zhou, Q. A. (2023). Molecular Glues: The Adhesive Connecting Targeted Protein Degradation to the Clinic. *Biochemistry*, *62*(3), 601-623. https://doi.org/10.1021/acs.biochem.2c00245

Schabath, M. B., & Cote, M. L. (2019). Cancer Progress and Priorities: Lung Cancer. *Cancer Epidemiol Biomarkers Prev*, *28*(10), 1563-1579. https://doi.org/10.1158/1055-9965.EPI-19-0221

Schatz, D. G., & Ji, Y. (2011). Recombination centres and the orchestration of V(D)J recombination. *Nat Rev Immunol*, *11*(4), 251-263. https://doi.org/10.1038/nri2941

Schatz, D. G., & Swanson, P. C. (2011). V(D)J recombination: mechanisms of initiation. *Annu Rev Genet*, *45*, 167-202. https://doi.org/10.1146/annurev-genet-110410-132552

Schauer, N. J., Magin, R. S., Liu, X., Doherty, L. M., & Buhrlage, S. J. (2020). Advances in Discovering Deubiquitinating Enzyme (DUB) Inhibitors. *J Med Chem*, *63*(6), 2731-2750. https://doi.org/10.1021/acs.jmedchem.9b01138

Schmidt, M. F., Gan, Z. Y., Komander, D., & Dewson, G. (2021). Ubiquitin signalling in neurodegeneration: mechanisms and therapeutic opportunities. *Cell Death Differ*, *28*(2), 570-590. https://doi.org/10.1038/s41418-020-00706-7

Schmitz, R., Wright, G. W., Huang, D. W., Johnson, C. A., Phelan, J. D., Wang, J. Q., Roulland, S., Kasbekar, M., Young, R. M., Shaffer, A. L., Hodson, D. J., Xiao, W., Yu, X., Yang, Y., Zhao, H., Xu, W., Liu, X., Zhou, B., Du, W., . . . Staudt, L. M. (2018).

Genetics and Pathogenesis of Diffuse Large B-Cell Lymphoma. *N Engl J Med*, *378*(15), 1396-1407. https://doi.org/10.1056/NEJMoa1801445
Schreiber, S. L. (2021). The Rise of Molecular Glues. *Cell*, *184*(1), 3-9. https://doi.org/10.1016/j.cell.2020.12.020
Schulman, B. A., & Harper, J. W. (2009). Ubiquitin-like protein activation by E1 enzymes: the apex for downstream signalling pathways. *Nat Rev Mol Cell Biol*, *10*(5), 319-331. https://doi.org/10.1038/nrm2673
Senft, D., Qi, J., & Ronai, Z. A. (2018). Ubiquitin ligases in oncogenic transformation and cancer therapy. *Nat Rev Cancer*, *18*(2), 69-88. https://doi.org/10.1038/nrc.2017.105
Sethi, A. K., & Haq, B. (2021). A Patient With Regressed Diffuse Large B-Cell Lymphoma and Aggressive Follicular Lymphoma. *Cureus*, *13*(5), e15275. https://doi.org/10.7759/cureus.15275
Sharma, P., Kanapuru, B., George, B., Lin, X., Xu, Z., Bryan, W. W., Pazdur, R., & Theoret, M. R. (2022). FDA Approval Summary: Idecabtagene Vicleucel for Relapsed or Refractory Multiple Myeloma. *Clin Cancer Res*, *28*(9), 1759-1764. https://doi.org/10.1158/1078-0432.CCR-21-3803
Shen, H., & Maki, C. G. (2011). Pharmacologic activation of p53 by small-molecule MDM2 antagonists. *Curr Pharm Des*, *17*(6), 560-568. https://doi.org/10.2174/138161211795222603
Sheppard, E. C., Morrish, R. B., Dillon, M. J., Leyland, R., & Chahwan, R. (2018). Epigenomic Modifications Mediating Antibody Maturation. *Front Immunol*, *9*, 355. https://doi.org/10.3389/fimmu.2018.00355
Shi, D., & Grossman, S. R. (2010). Ubiquitin becomes ubiquitous in cancer: emerging roles of ubiquitin ligases and deubiquitinases in tumorigenesis and as therapeutic targets. *Cancer Biol Ther*, *10*(8), 737-747. https://doi.org/10.4161/cbt.10.8.13417
Shi, H., Seegobin, K., Heng, F., Zhou, K., Chen, R., Qin, H., Manochakian, R., Zhao, Y., & Lou, Y. (2022). Genomic landscape of lung adenocarcinomas in different races. *Front Oncol*, *12*, 946625. https://doi.org/10.3389/fonc.2022.946625
Shi, X., Xiang, S., Cao, J., Zhu, H., Yang, B., He, Q., & Ying, M. (2019). Kelch-like proteins: Physiological functions and relationships with diseases. *Pharmacol Res*, *148*, 104404. https://doi.org/10.1016/j.phrs.2019.104404
Silva, P. M. A., & Bousbaa, H. (2022). BUB3, beyond the Simple Role of Partner. *Pharmaceutics*, *14*(5). https://doi.org/10.3390/pharmaceutics14051084
Sluimer, J., & Distel, B. (2018). Regulating the human HECT E3 ligases. *Cell Mol Life Sci*, *75*(17), 3121-3141. https://doi.org/10.1007/s00018-018-2848-2
Snyder, N. A., & Silva, G. M. (2021). Deubiquitinating enzymes (DUBs): Regulation, homeostasis, and oxidative stress response. *J Biol Chem*, *297*(3), 101077. https://doi.org/10.1016/j.jbc.2021.101077
Song, Z., Zheng, Y., Wang, X., Su, H., Zhang, Y., & Song, Y. (2017). ALK and ROS1 rearrangements, coexistence and treatment in epidermal growth factor receptor-wild type lung adenocarcinoma: a multicenter study of 732 cases. *J Thorac Dis*, *9*(10), 3919-3926. https://doi.org/10.21037/jtd.2017.09.79
Spratt, D. E., Walden, H., & Shaw, G. S. (2014). RBR E3 ubiquitin ligases: new structures, new insights, new questions. *Biochem J*, *458*(3), 421-437. https://doi.org/10.1042/BJ20140006

Stalker, M. E., & Mark, T. M. (2022). Clinical Management of Triple-Class Refractory Multiple Myeloma: A Review of Current Strategies and Emerging Therapies. *Curr Oncol*, *29*(7), 4464-4477. https://doi.org/10.3390/curroncol29070355

Stewart, M. D., Ritterhoff, T., Klevit, R. E., & Brzovic, P. S. (2016). E2 enzymes: more than just middle men. *Cell Res*, *26*(4), 423-440. https://doi.org/10.1038/cr.2016.35

Stirnimann, C. U., Petsalaki, E., Russell, R. B., & Muller, C. W. (2010). WD40 proteins propel cellular networks. *Trends Biochem Sci*, *35*(10), 565-574. https://doi.org/10.1016/j.tibs.2010.04.003

Suda, K., Tomizawa, K., & Mitsudomi, T. (2010). Biological and clinical significance of KRAS mutations in lung cancer: an oncogenic driver that contrasts with EGFR mutation. *Cancer Metastasis Rev*, *29*(1), 49-60. https://doi.org/10.1007/s10555-010-9209-4

Suh, K. S., Tanaka, T., Sarojini, S., Nightingale, G., Gharbaran, R., Pecora, A., & Goy, A. (2013). The role of the ubiquitin proteasome system in lymphoma. *Crit Rev Oncol Hematol*, *87*(3), 306-322. https://doi.org/10.1016/j.critrevonc.2013.02.005

Sun, M., & Zhang, X. (2022). Current methodologies in protein ubiquitination characterization: from ubiquitinated protein to ubiquitin chain architecture. *Cell Biosci*, *12*(1), 126. https://doi.org/10.1186/s13578-022-00870-y

Swatek, K. N., & Komander, D. (2016). Ubiquitin modifications. *Cell Res*, *26*(4), 399-422. https://doi.org/10.1038/cr.2016.39

Swerdlow, S. H., Campo, E., Pileri, S. A., Harris, N. L., Stein, H., Siebert, R., Advani, R., Ghielmini, M., Salles, G. A., Zelenetz, A. D., & Jaffe, E. S. (2016). The 2016 revision of the World Health Organization classification of lymphoid neoplasms. *Blood*, *127*(20), 2375-2390. https://doi.org/10.1182/blood-2016-01-643569

Taggart, J. C., Zauber, H., Selbach, M., Li, G. W., & McShane, E. (2020). Keeping the Proportions of Protein Complex Components in Check. *Cell Syst*, *10*(2), 125-132. https://doi.org/10.1016/j.cels.2020.01.004

Takahashi, K., Inukai, T., Imamura, T., Yano, M., Tomoyasu, C., Lucas, D. M., Nemoto, A., Sato, H., Huang, M., Abe, M., Kagami, K., Shinohara, T., Watanabe, A., Somazu, S., Oshiro, H., Akahane, K., Goi, K., Kikuchi, J., Furukawa, Y., . . . Sugita, K. (2017). Anti-leukemic activity of bortezomib and carfilzomib on B-cell precursor ALL cell lines. *PLoS One*, *12*(12), e0188680. https://doi.org/10.1371/journal.pone.0188680

Testoni, M., Zucca, E., Young, K. H., & Bertoni, F. (2015). Genetic lesions in diffuse large B-cell lymphomas. *Ann Oncol*, *26*(6), 1069-1080. https://doi.org/10.1093/annonc/mdv019

Thai, A. A., Solomon, B. J., Sequist, L. V., Gainor, J. F., & Heist, R. S. (2021). Lung cancer. *Lancet*, *398*(10299), 535-554. https://doi.org/10.1016/S0140-6736(21)00312-3

Thandra, K. C., Barsouk, A., Saginala, K., Aluru, J. S., & Barsouk, A. (2021). Epidemiology of lung cancer. *Contemp Oncol (Pozn)*, *25*(1), 45-52. https://doi.org/10.5114/wo.2021.103829

Thandra, K. C., Barsouk, A., Saginala, K., Padala, S. A., Barsouk, A., & Rawla, P. (2021). Epidemiology of Non-Hodgkin's Lymphoma. *Med Sci (Basel)*, *9*(1). https://doi.org/10.3390/medsci9010005

Tian, M., Zhi, J. Y., Pan, F., Chen, Y. Z., Wang, A. Z., Jia, H. Y., Huang, R., & Zhong, W. H. (2023). Bioinformatics analysis identifies potential ferroptosis key genes in the pathogenesis of diabetic peripheral neuropathy. *Front Endocrinol (Lausanne)*, *14*, 1048856. https://doi.org/10.3389/fendo.2023.1048856

Timms, R. T., Mena, E. L., Leng, Y., Li, M. Z., Tchasovnikarova, I. A., Koren, I., & Elledge, S. J. (2023). Defining E3 ligase-substrate relationships through multiplex CRISPR screening. *Nat Cell Biol*, *25*(10), 1535-1545. https://doi.org/10.1038/s41556-023-01229-2

Tracz, M., & Bialek, W. (2021). Beyond K48 and K63: non-canonical protein ubiquitination. *Cell Mol Biol Lett*, *26*(1), 1. https://doi.org/10.1186/s11658-020-00245-6

Valimberti, I., Tiberti, M., Lambrughi, M., Sarcevic, B., & Papaleo, E. (2015). E2 superfamily of ubiquitin-conjugating enzymes: constitutively active or activated through phosphorylation in the catalytic cleft. *Sci Rep*, *5*, 14849. https://doi.org/10.1038/srep14849

van Gent, D. C., & van der Burg, M. (2007). Non-homologous end-joining, a sticky affair. *Oncogene*, *26*(56), 7731-7740. https://doi.org/10.1038/sj.onc.1210871

Verschueren, M. V., Peters, B. J., Bloem, L. T., Kruik, V. R., Uitvlugt, E. B., Bijsmans, A. R., Egberts, A. C., & van de Garde, E. M. (2023). Pembrolizumab Plus Chemotherapy Per PD-L1 Stratum In Patients With Metastatic Non-Small Cell Lung Cancer: Real-World Effectiveness Versus Trial Efficacy. *Clin Lung Cancer*. https://doi.org/10.1016/j.cllc.2023.12.011

Voges, D., Zwickl, P., & Baumeister, W. (1999). The 26S proteasome: a molecular machine designed for controlled proteolysis. *Annu Rev Biochem*, *68*, 1015-1068. https://doi.org/10.1146/annurev.biochem.68.1.1015

Vos, Q., Lees, A., Wu, Z. Q., Snapper, C. M., & Mond, J. J. (2000). B-cell activation by T-cell-independent type 2 antigens as an integral part of the humoral immune response to pathogenic microorganisms. *Immunol Rev*, *176*, 154-170. https://doi.org/10.1034/j.1600-065x.2000.00607.x

Walden, H., & Rittinger, K. (2018). RBR ligase-mediated ubiquitin transfer: a tale with many twists and turns. *Nat Struct Mol Biol*, *25*(6), 440-445. https://doi.org/10.1038/s41594-018-0063-3

Walser, T., Cui, X., Yanagawa, J., Lee, J. M., Heinrich, E., Lee, G., Sharma, S., & Dubinett, S. M. (2008). Smoking and lung cancer: the role of inflammation. *Proc Am Thorac Soc*, *5*(8), 811-815. https://doi.org/10.1513/pats.200809-100TH

Wang, S. S. (2023). Epidemiology and etiology of diffuse large B-cell lymphoma. *Semin Hematol*. https://doi.org/10.1053/j.seminhematol.2023.11.004

Wang, X., Sun, R., Hong, X., Chen, C., & Ding, Y. (2022). KLHL14: A Novel Prognostic Biomarker and Therapeutic Target for Ovarian Cancer. *J Oncol*, *2022*, 9799346. https://doi.org/10.1155/2022/9799346

Wardemann, H., Yurasov, S., Schaefer, A., Young, J. W., Meffre, E., & Nussenzweig, M. C. (2003). Predominant autoantibody production by early human B cell precursors. *Science*, *301*(5638), 1374-1377. https://doi.org/10.1126/science.1086907

Weaver, C. J., & Tariman, J. D. (2017). Multiple Myeloma Genomics: A Systematic Review. *Semin Oncol Nurs*, *33*(3), 237-253. https://doi.org/10.1016/j.soncn.2017.05.001

Weber, J., Polo, S., & Maspero, E. (2019). HECT E3 Ligases: A Tale With Multiple Facets. *Front Physiol*, *10*, 370. https://doi.org/10.3389/fphys.2019.00370

Wing, S. S. (2003). Deubiquitinating enzymes--the importance of driving in reverse along the ubiquitin-proteasome pathway. *Int J Biochem Cell Biol*, *35*(5), 590-605. https://doi.org/10.1016/s1357-2725(02)00392-8

Wu, H. Q., Baker, D., & Ovaa, H. (2020). Small molecules that target the ubiquitin system. *Biochem Soc Trans*, *48*(2), 479-497. https://doi.org/10.1042/BST20190535

Wu, X., Miao, J., Jiang, J., & Liu, F. (2017). Analysis of methylation profiling data of hyperplasia and primary and metastatic endometrial cancers. *Eur J Obstet Gynecol Reprod Biol*, *217*, 161-166. https://doi.org/10.1016/j.ejogrb.2017.08.036

Xing, P. Y., Zhu, Y. X., Wang, L., Hui, Z. G., Liu, S. M., Ren, J. S., Zhang, Y., Song, Y., Liu, C. C., Huang, Y. C., Liao, X. Z., Xing, X. J., Wang, D. B., Yang, L., Du, L. B., Liu, Y. Q., Zhang, Y. Z., Liu, Y. Y., Wei, D. H., . . . Lu, C. G. (2019). What are the clinical symptoms and physical signs for non-small cell lung cancer before diagnosis is made? A nation-wide multicenter 10-year retrospective study in China. *Cancer Med*, *8*(8), 4055-4069. https://doi.org/10.1002/cam4.2256

Xu, J., Ye, Z., Zhuo, Q., Gao, H., Qin, Y., Lou, X., Zhang, W., Wang, F., Wang, Y., Jing, D., Fan, G., Zhang, Y., Chen, X., Chen, J., Xu, X., Yu, X., & Ji, S. (2023). MEN1 Degradation Induced by Neddylation and the CUL4B-DCAF7 Axis Promotes Pancreatic Neuroendocrine Tumor Progression. *Cancer Res*, *83*(13), 2226-2247. https://doi.org/10.1158/0008-5472.CAN-22-3599

Xu, P., Scott, D. C., Xu, B., Yao, Y., Feng, R., Cheng, L., Mayberry, K., Wang, Y. D., Bi, W., Palmer, L. E., King, M. T., Wang, H., Li, Y., Fan, Y., Alpi, A. F., Li, C., Peng, J., Papizan, J., Pruett-Miller, S. M., . . . Weiss, M. J. (2021). FBXO11-mediated proteolysis of BAHD1 relieves PRC2-dependent transcriptional repression in erythropoiesis. *Blood*, *137*(2), 155-167. https://doi.org/10.1182/blood.2020007809

Yang, P., Cerhan, J. R., Vierkant, R. A., Olson, J. E., Vachon, C. M., Limburg, P. J., Parker, A. S., Anderson, K. E., & Sellers, T. A. (2002). Adenocarcinoma of the lung is strongly associated with cigarette smoking: further evidence from a prospective study of women. *Am J Epidemiol*, *156*(12), 1114-1122. https://doi.org/10.1093/aje/kwf153

Yang, Q., Zhao, J., Chen, D., & Wang, Y. (2021). E3 ubiquitin ligases: styles, structures and functions. *Mol Biomed*, *2*(1), 23. https://doi.org/10.1186/s43556-021-00043-2

Yi, S., Zhang, C., Li, M., & Wang, J. (2023). Construction of a Novel Diagnostic Model Based on Ferroptosis-Related Genes for Hepatocellular Carcinoma Using Machine and Deep Learning Methods. *J Oncol*, *2023*, 1624580. https://doi.org/10.1155/2023/1624580

Yin, C. C., & Luthra, R. (2013). Molecular detection of t(11;14)(q13;q32) in mantle cell lymphoma. *Methods Mol Biol*, *999*, 211-216. https://doi.org/10.1007/978-1-62703-357-2_14

Yoshida, T., Mei, H., Dorner, T., Hiepe, F., Radbruch, A., Fillatreau, S., & Hoyer, B. F. (2010). Memory B and memory plasma cells. *Immunol Rev*, *237*(1), 117-139. https://doi.org/10.1111/j.1600-065X.2010.00938.x

Younes, A., Sehn, L. H., Johnson, P., Zinzani, P. L., Hong, X., Zhu, J., Patti, C., Belada, D., Samoilova, O., Suh, C., Leppa, S., Rai, S., Turgut, M., Jurczak, W., Cheung, M. C., Gurion, R., Yeh, S. P., Lopez-Hernandez, A., Duhrsen, U., . . . investigators, P. (2019). Randomized Phase III Trial of Ibrutinib and Rituximab Plus Cyclophosphamide, Doxorubicin, Vincristine, and Prednisone in Non-Germinal Center B-Cell Diffuse Large B-Cell Lymphoma. *J Clin Oncol*, *37*(15), 1285-1295. https://doi.org/10.1200/JCO.18.02403

Young, R. M., Shaffer, A. L., 3rd, Phelan, J. D., & Staudt, L. M. (2015). B-cell receptor signaling in diffuse large B-cell lymphoma. *Semin Hematol*, *52*(2), 77-85. https://doi.org/10.1053/j.seminhematol.2015.01.008

Yousefelahiyeh, M., Xu, J., Alvarado, E., Yu, Y., Salven, D., & Nissen, R. M. (2018). DCAF7/WDR68 is required for normal levels of DYRK1A and DYRK1B. *PLoS One*, *13*(11), e0207779. https://doi.org/10.1371/journal.pone.0207779

Yu, D., Cattoglio, C., Xue, Y., & Zhou, Q. (2019). A complex between DYRK1A and DCAF7 phosphorylates the C-terminal domain of RNA polymerase II to promote myogenesis. *Nucleic Acids Res*, *47*(9), 4462-4475. https://doi.org/10.1093/nar/gkz162

Zhang, J., Weinrich, J. A. P., Russ, J. B., Comer, J. D., Bommareddy, P. K., DiCasoli, R. J., Wright, C. V. E., Li, Y., van Roessel, P. J., & Kaltschmidt, J. A. (2017). A Role for Dystonia-Associated Genes in Spinal GABAergic Interneuron Circuitry. *Cell Rep*, *21*(3), 666-678. https://doi.org/10.1016/j.celrep.2017.09.079

Zhang, J., Yang, Z., Ou, J., Xia, X., Zhi, F., & Cui, J. (2017). The F-box protein FBXL18 promotes glioma progression by promoting K63-linked ubiquitination of Akt. *FEBS Lett*, *591*(1), 145-154. https://doi.org/10.1002/1873-3468.12521

Zhang, X., He, Y., Zhang, P., Budamagunta, V., Lv, D., Thummuri, D., Yang, Y., Pei, J., Yuan, Y., Zhou, D., & Zheng, G. (2020). Discovery of IAP-recruiting BCL-X(L) PROTACs as potent degraders across multiple cancer cell lines. *Eur J Med Chem*, *199*, 112397. https://doi.org/10.1016/j.ejmech.2020.112397

Zheng, M., Yang, J., Xu, X., Sebolt, J. T., Wang, S., & Sun, Y. (2010). Efficacy of MDM2 inhibitor MI-219 against lung cancer cells alone or in combination with MDM2 knockdown, a XIAP inhibitor or etoposide. *Anticancer Res*, *30*(9), 3321-3331. https://www.ncbi.nlm.nih.gov/pubmed/20944104

Zhou, T., Zimmerman, W., Liu, X., & Erikson, R. L. (2006). A mammalian NudC-like protein essential for dynein stability and cell viability. *Proc Natl Acad Sci U S A*, *103*(24), 9039-9044. https://doi.org/10.1073/pnas.0602916103

Zhu, F., Crombie, J. L., Ni, W., Hoang, N. M., Garg, S., Hackett, L., Chong, S. J. F., Collins, M. C., Rui, L., Griffin, J., & Davids, M. S. (2024). Hypomethylating agent decitabine sensitizes diffuse large B-cell lymphoma to venetoclax. *Haematologica*, *109*(1), 186-199. https://doi.org/10.3324/haematol.2023.283245

Zuin, A., Isasa, M., & Crosas, B. (2014). Ubiquitin signaling: extreme conservation as a source of diversity. *Cells*, *3*(3), 690-701. https://doi.org/10.3390/cells3030690